

THE DISCOVERY AND CHARACTERIZATION OF SMALL MOLECULE 20S  
PROTEASOME ACTIVATORS: IMPLICATIONS IN PROTEOSTASIS DISORDERS

By

Evert Njomen

A DISSERTATION

Submitted to  
Michigan State University  
in partial fulfillment of the requirements  
for the degree of

Chemistry-Doctor of Philosophy  
Pharmacology and Toxicology-Dual Major

2019

## ABSTRACT

### THE DISCOVERY AND CHARACTERIZATION OF SMALL MOLECULE 20S PROTEASOME ACTIVATORS: IMPLICATIONS IN PROTEOSTASIS DISORDERS

By

Evert Nijomen

Maintenance of proteome fidelity is required to preserve the health of an organism in defiance of developmental fluxes, environmental insults, infectious diseases, and the challenges of aging. This crucial role is the responsibility of the proteostasis (protein homeostasis) network, a multicomponent and unified system involving protein synthesis, folding, and degradation. The degradation system is regulated by the proteasome and the autophagy pathways. These proteolytic systems have thus emerged as therapeutic targets for numerous proteostasis disorders. However, their therapeutic regulation is only feasible if there is a fine understanding of how they function, and the mechanisms of crosstalk underlying their cooperative nature. After more than three decades since the discovery of the proteasome, there is still so much to be known about this exquisite enzyme. Proteolysis by the proteasome could be 20S- or 26S-mediated and may or may not be ubiquitin-dependent. The goal of this dissertation was to discover and characterize small molecules that allow for the decoding of 20S-mediated proteolysis and its role in the regulation of autophagy, with the hope of finding new vulnerabilities for proteostasis drug discovery.

In this endeavor, two classes of 20S proteasome activators; imidazolines and phenothiazines were identified via high throughput screening (HTS). In a mechanistic study consisting of cellular, biochemical, biophysical and computational approaches, the imidazoline, TCH-165, was found to stabilize the open-gate active conformation of the human 20S proteasome. This translated into enhanced degradation of cancer-driving intrinsically disordered proteins (IDPs) such as c-Myc, and sensitization of both established and primary cancer cells to this

molecule. TCH-165 was also found to enhance 20S-mediated clearance of two key SNARE proteins; SNAP29 and STX17, with subsequent inhibition of autolysosome formation. These observations implicate the 20S proteasome as a key regulator of autophagic flux. The clearance of ubiquitinated proteins was not affected at concentrations required to boost 20S-mediated degradation of these IDPs. Thus, the 20S-ubiquitin-independent pathway could be enhanced without significantly affecting the 26S-ubiquitin-dependent pathway. These findings provide a new targetable vulnerability for IDP-driven cancers and autophagy-associated chemoresistance.

In a proof-of-concept approach, the phenothiazine, chlorpromazine was modified to diminish its dopamine D2 receptor (D2R) activity while retaining its ability to enhance 20S-mediated proteolysis of IDPs associated with neurodegenerative disorders. Using these molecules as controls, the AlphaLISA technology was applied in a proteasome-protein degradation system thereby allowing for the development of an assay that allows for the measurement of 20S activation at the cellular and protein levels. These small molecule 20S agonists can therefore serve as leads to further explore the therapeutic potential of 20S activation in proteostasis disorders or as new tools to provide insight into the ambiguous mechanics of 20S-gate regulation and signaling.

In an expanded exploration to cover infectious diseases, some imidazolines were found to inhibit the growth of *Mycobacterium tuberculosis* (*Mtb*), the causative agent for tuberculosis (TB). Given the structural differences between human and *Mtb* proteasome, CRISPRi/dCas9 system was used to validate the *Mtb* proteasome as a target for this anti-mycobacterium activity.

Dedicated in loving memory of my father, Wanda Elias, and the numerous family members who departed while I was on this journey. I miss you all.



## ACKNOWLEDGEMENTS

This dissertation would not have been possible without the supports and encouragements from many people, and I would like to extend my deepest appreciation to each one of them. First, I would like to express my sincere gratitude to my mentor Prof. Jetze Tepe for giving me the wonderful opportunity to work with him. Thank you for being patient even when I complained or didn't want to listen, for the immense knowledge and for being there when things were tougher. Writing together and having the autonomy to drive a project forward are my best memories. I highly appreciate your guidance and encouragement in overcoming the numerous obstacles I faced in the past five years. Next, I would like to thank my wonderful committee members for their enormous supports. Dr. Robert Abramovitch, you opened your lab to me, gave me feedbacks on my work and sent out numerous reference letters for me. Thank you for your mentorship. Dr. Anne Dorrance, I learnt a lot from you especially during our IPSTP workshops. You were also very supportive in moving my dual major processing forward. I want to thank you for all the help, the opportunity to learn from you, and of course the Thanksgiving dinners. Dr. Kevin Walker, I would like to start by apologizing for all the early morning sonication noise coming from the back of your office. Thank you for letting me use your lab, and for your constructive inputs in my research. Next, I would like to thank Dr. Xuefei Huang for your inputs and for serving on my committee. Finally, thank you to Dr. Richard Neubig for making the time to answer my numerous questions despite your huge departmental responsibilities, and for being part of my dissertation committee.

To my former mentor, Dr. Hedeel Evans, thank you for instilling the habit of independent thinking in me. I first heard about the autophagy and proteasome pathways in your cell signaling class. Today, I am honored to have contributed to the understanding of these proteolytic systems.

I would like to appreciate supports and training provided by the T32/IPSTP program. It was a tremendous privilege learning from one of the best group of professors and fellow graduate students. Special appreciation to the Magdalina Nzekwo Ngeyi Endowment (MNNE) for giving me the privilege to higher education. Thank you to Dr. Stanley-Pierre Ngeyi for moral and financial support. I would not be here, nor could I have done this without these support systems. I am forever indebted.

I would also like to thank Dr. Tom Dexheimer for all the help with assay development, and Dr. Melinda Frame for technical support and training with confocal microscopy. I highly appreciate the supports from past and current members of the Tepe research group. Special thanks to Dr. Travis Bethel, Dr. Matthew Gilletto and Dr. Corey Jones for helping with transition into graduate school and for their critical inputs in preparing for my comprehensive exams. Thank you to Dr. Theresa Lansdell for initial assistant with cell culture work and for sharing protocols with me. Thank you to Katarina Keel, Shafaat Mehedi, Taylor Fiolek and Grace Hubbell for your critical insights during presentations and group meetings. I would also like to thank Dr. Tyler Walter for helping with my cloning questions.

My sincere gratitude to Dr. Gary Blanchard for helping with fellowship applications and my training in the chemistry program. I highly appreciate the supports from Anna, Heidi, Tiphani, Dawn, Marvey, Bob and Eric for helping me keep up with departmental requirements and for assisting in timely purchase of research needs. Thank you to the Pharmacology and Toxicology graduate office for all the support.

Finally, I am grateful to my family; the list is too long so I will only mention a few. I want to thank my mom, Anna Nfaluk for letting me go this far from home and for believing in my strength. Thank you to my sister Jacqueline Mbakwi and my brother Wanda Michael for playing

the role of parents in my life. To my other family members and friends; Pierrette, Elian, Elvis, Gladys, Cilolen, Syvester, Cyprien (my bestie), Ahinsa (my graduate school sister), Noura and Katayoon thank you for being there and for believing in me.

## TABLE OF CONTENTS

LIST OF TABLES .....	xii
LIST OF FIGURES .....	xiii
KEY TO ABBREVIATIONS .....	xvi
CHAPTER ONE .....	1
Protein Homeostasis in Pathophysiology.....	1
1.1 Introduction.....	2
1.2 The ubiquitin proteasome system (UPS) .....	5
1.2.1 Structure of the proteasome .....	5
1.2.2 Defining intrinsic disorder and substrates of the proteasome degradation systems .....	9
1.2.3 The 26S proteasome and ubiquitin- ATP-dependent proteolysis .....	10
1.2.4 The 20S proteasome and ubiquitin-ATP-independent proteolysis .....	11
1.3 Drugging the 20S proteasome degradation system.....	12
1.3.1 Drugging the 20S proteasome in cancer .....	12
1.3.2 Drugging the 20S proteasome in neurodegenerative diseases .....	15
1.4 Approaches toward enhancement of proteasome-mediated proteolysis .....	16
1.4.1 Proteasome activation by agonist induced conformational modification .....	16
1.4.1.1 Peptide-based proteasome agonists.....	16
1.4.1.2 Small molecule proteasome agonists .....	17
1.4.2 Proteasome activation by regulation of post-translational modifications.....	19
1.4.2.1 Small molecule kinase modulators .....	19
1.4.2.2 Small molecule deubiquitinase inhibitors .....	21
1.4.3 Proteasome activation by genetic manipulation .....	23
1.4.3.1 Upregulation of proteasome activity through subunit overexpression .....	23
1.4.3.2 Upregulation of proteasome activity through Nrf2 activation .....	23
1.4.3.3 Upregulation of proteasome activating caps and generation of open-gate 20S mutants.....	24
1.4.4 Proteasome activation via unknown mechanisms.....	25
1.5 Conclusion .....	27
CHAPTER TWO .....	29
Deciphering the Mechanism of Proteasome Modulation by Imidazolines .....	29
2.1 Introduction.....	30
2.1.1 Background.....	30
2.1.2 Objective .....	33
2.2 Results and Discussion .....	33
2.2.1 TCH-165 enhances 20S-mediated but not 26S-mediated degradation of peptides .....	33
2.2.2 Imidazolines do not denature the 20S proteasome .....	34
2.2.3 TCH-165 enhances 20S-mediated degradation of tau and $\alpha$ -synuclein.....	36
2.2.4 TCH-165 stabilizes the open-gate conformation of 20S proteasome .....	37
2.2.5 Stabilization of open-gate 20S by TCH-165 may involve interaction with the $\alpha$ -ring....	38

2.2.6 TCH-165 enhances the degradation of cancer-associated IDPs in cell culture .....	42
2.2.7 TCH-165 inhibits 26S assembly in cell culture .....	46
2.2.8 TCH-165 forms a hybrid with single capped 20S proteasome .....	49
2.2.9 Imidazolines do not induce oxidative stress in cells .....	51
2.2.10 TCH-165 is effective against established and primary cancer cells .....	52
2.3 Conclusions .....	54
CHAPTER THREE .....	55
The Role of 20S Proteasome in Autophagy Regulation: A Small Molecule-Driven Mechanistic Investigation.....	55
3.1 Introduction.....	56
3.1.1 Background.....	56
3.1.2 Objective .....	58
3.2 Results and Discussion .....	60
3.2.1 TCH-165 inhibits autophagy flux .....	60
3.2.2 TCH-165 interferes with autolysosome formation .....	65
3.2.3 TCH-165 links the 20S proteasome as a negative regulator of autophagy flux .....	68
3.2.4 The 20S proteasome regulates autophagy via the proteolysis of SNAP29 and STX17 ..	72
3.2.5 The proteolysis of SNAP29 and STX17 are ubiquitin-independent.....	73
3.2.6 SNAP29 is a substrate of the 20S proteasome.....	76
3.2.7 SNAP29 and STX17 interact with the 20S proteasome .....	76
3.2.8 Proteasome activation by imidazolines parallel autophagy inhibition .....	77
3.2.9 Oxidative stress does not mimic the effect of TCH-165 on autophagy .....	78
3.3 Conclusions.....	81
CHAPTER FOUR.....	82
The Identification of New Scaffolds for Proteasome Activation and the Development of Assays for Hit Validation.....	82
4.1 Introduction.....	83
4.1.1 Background.....	83
4.1.2 Objective .....	85
4.2 Results and Discussion .....	85
4.2.1 Phenothiazines are small molecule activators of 20S proteasome.....	85
4.2.2 The D2R antagonist, chlorpromazine can be repurposed as 20S agonist .....	88
4.2.3 Quantification of 20S proteasome activity by alpha synuclein AlphaLISA technology .	91
4.2.4 Quantification of 20S proteasome activity by GFPspark-ODC AlphaLISA in cells.....	93
4.3 Conclusions.....	97
CHAPTER FIVE .....	98
Imidazolines as Anti-Mycobacterial Agent: CRISPRi/dCas9-Driven Target Validation .....	98
5.1 Introduction.....	99
5.1.1 Background.....	99
5.1.2 Objective .....	105
5.2 Results and Discussion .....	106
5.2.1 Imidazolines inhibit <i>Mycobacterium tuberculosis</i> growth .....	106

5.2. Imidazolines inhibit the proteasome of <i>Mycobacterium tuberculosis</i> in the presence of sodium dodecyl sulfate .....	106
5.2.3 CRISPRi/dcas9 knockdown of proteasome-related genes decreases proteasome activity in <i>Mycobacterium smegmatis</i> .....	109
5.2.4 CRISPRi/dcas9 knockdown of proteasome-related genes does not sensitize <i>Mycobacterium smegmatis</i> to imidazolines .....	111
5.3 Conclusions .....	113
CHAPTER SIX .....	115
Summary and Overall Conclusion .....	115
6.1 Summary .....	116
6.2 Overall conclusion .....	118
CHAPTER SEVEN .....	119
Materials and Methods .....	119
7.1 Materials .....	120
7.1.1 Key resource tables .....	120
7.2 Methods .....	125
7.2.1 Cell culture .....	125
7.2.2 Isolation and culture of primary multiple myeloma cells .....	125
7.2.3 Cell viability assay .....	125
7.2.4 Transient and stable transfections .....	125
7.2.5 Immunoprecipitation .....	127
7.2.6 Immunoblot .....	128
7.2.7 Oxyblot: Protein carbonyl quantification .....	129
7.2.8 siRNA gene knockdown .....	130
7.2.9 Quantitative real time polymerase chain reaction (qRT-PCR) .....	130
7.2.10 Purified 20S proteasome activity assay and high throughput screening .....	130
7.2.11 Proteasome activity in cell lysates from treated cells .....	131
7.2.12 Cathepsin D and E activity .....	132
7.2.13 Proteasome-mediated degradation of IDPs in biochemical assays .....	132
7.2.14 Proteasome-mediated degradation of IDPs in cells .....	133
7.2.15 Proteasome AlphaLISA assays .....	134
7.2.16 Proteasome native gel and in-gel activity assays .....	137
7.2.17 Confocal immunofluorescence .....	138
7.2.18 Confocal live imaging .....	139
7.2.19 Bacterial culture .....	140
7.2.20 Affinity purification of <i>Mtb</i> 20S proteasome .....	140
7.2.21 Affinity purification of mycobacterium proteasome-associated ATPase (Mpa) .....	141
7.2.22 Design of single guide RNA (sgRNA) .....	142
7.2.23 Plasmid construction and cloning .....	145
7.2.24 Bacterial mRNA isolation and quantification .....	147
7.2.25 Proteasome activity in <i>Mycobacterium smegmatis</i> cell lysate .....	147
7.2.26 <i>Mycobacterium smegmatis</i> growth inhibition .....	148
7.2.27 Quantification and statistical analysis .....	148

APPENDICES .....	149
APPENDIX A: Copyright permission letter for chapter 1 .....	150
APPENDIX B: Copyright permission letter for chapter 2.....	151
APPENDIX C: Copyright permission letter for chapter 3.....	152
APPENDIX D: Copyright permission letter for chapter 4 .....	153
REFERENCES .....	154

## LIST OF TABLES

Table 1: PONDR VSL2 prediction of disorder in autophagosome-lysosome fusion proteins .....	69
Table 2: SAR of chlorpromazine analogues for proteasome activation and antagonism of D2R.	89
Table 3: Antibodies .....	120
Table 4: Peptides and recombinant proteins .....	121
Table 5: Cell lines, cell culture and transfection reagents .....	121
Table 6: Oligonucleotides and recombinant DNA.....	122
Table 7: Bacterial strains .....	123
Table 8: Critical commercial assay kits .....	123
Table 9: Other chemicals and reagents .....	124
Table 10: Proteasome native gel composition .....	137
Table 11: sgRNAs for mycobacterium proteasome and proteasome-related genes. Fold repression (FR) for the PAMs indicated are based on Rock et al's study. <sup>337</sup> The sgRNAs corresponding to the yellow highlighted FR were the ones used in this study. ....	143



## LIST OF FIGURES

Figure 1.1: An overview of the proteostasis network. ....	4
Figure 1.2: Structure of proteasome subcomplexes .....	6
Figure 1.3: Simplified arrangement of the 19S subunits .....	8
Figure 1.4: Schematic of protein ubiquitinylation. ....	12
Figure 1.5: Selected examples of small molecule proteasome activators.....	20
Figure 1.6: Examples of small molecules that enhance proteasome activity through regulation of post-translational modifications.....	22
Figure 1.7: Genetic upregulation of proteasome activity.....	26
Figure 2.1: Structures of proteasome modulators used in this chapter .....	32
Figure 2.2: TCH-165 enhances 20S-mediated degradation of peptide substrates .....	34
Figure 2.3: Imidazolines do not denature the 20S proteasome .....	35
Figure 2.4: TCH-165 enhances 20S-mediated degradation of tau and $\alpha$ -synuclein .....	37
Figure 2.5: TCH-165 stabilizes the open-gate conformation of 20S proteasome.....	38
Figure 2.6: Stabilization of open-gate 20S by TCH-165 may involve interaction with the $\alpha$ -ring. ....	40
Figure 2.7: The activity of TCH-165 requires specific interaction with the $\alpha$ -ring of the human 20S proteasome.....	41
Figure 2.8: TCH-165 increases proteasome activity in cell culture.....	43
Figure 2.9: TCH-165 enhances 20S-mediated degradation of c-Fos in a glioblastoma cell line .	44
Figure 2.10: TCH-165 enhances 20S-mediated degradation of c-Myc in a multiple myeloma (RPMI-8226) and an acute lymphoblastic leukemia (CCRF-CEM) cell lines .....	46
Figure 2.11: TCH-165 inhibits the assembly of 26S proteasome in cell culture .....	48
Figure 2.12: In-gel activation of single capped 20S proteasome.....	50
Figure 2.13: Imidazolines do not induce oxidative stress in cells .....	51
Figure 2.14: TCH-165 is effective against established and primary cancer cells.....	53

Figure 3.1: A simplified overview of the autophagy pathway.....	57
Figure 3.2: The proteolytic arms of the proteostasis machinery.....	58
Figure 3.3: TCH-165 induces the accumulation of LC3B-II and autophagic vacuoles.....	61
Figure 3.4: TCH-165 inhibits autophagic flux.....	62
Figure 3.5: TCH-165 induces the accumulation of p62.....	64
Figure 3.6: TCH-165 interferes with autolysosome formation.....	65
Figure 3.7: TCH-165 does not affect lysosomal pH.....	67
Figure 3.8: TCH-165 inhibits autophagosome-lysosome fusion.....	68
Figure 3.9: TCH-165 stimulates proteasomal degradation of SNAP29 and STX17.....	70
Figure 3.10: Regulation of autophagy genes by TCH-165.....	71
Figure 3.11: The 20S proteasome regulates autophagy via the proteolysis of SNAP29 and STX17.....	72
Figure 3.12: The proteolysis of SNAP29 and STX17 are ubiquitin-independent.....	75
Figure 3.13: SNAP29 is a substrate of the 20S proteasome.....	76
Figure 3.14: SNAP29 and STX17 interact with the 20S proteasome.....	77
Figure 3.15: Autophagy inhibition parallels proteasome activation by imidazolines.....	78
Figure 3.16: Activity of TCH-165 under condition of oxidative stress.....	79
Figure 3.17: 20S proteasome mediated regulation of autophagic flux.....	80
Figure 4.1: Principle of proteasome AlphaLISA assay.....	85
Figure 4.2: Phenothiazines are small molecule activators of the 20S proteasome.....	87
Figure 4.3: The D2R antagonist, chlorpromazine can be repurposed as 20S agonist.....	90
Figure 4.4: Quantification of 20S proteasome activity by alpha synuclein AlphaLISA technology.....	92
Figure 4.5: Quantification of 20S proteasome activity by GFPspark-ODC AlphaLISA in cell culture.....	94
Figure 4.6: Optimization of GFPspark-ODC assay.....	96

Figure 5.1: The granuloma of <i>Mycobacterium tuberculosis</i> .....	101
Figure 5.2: The <i>Mycobacterium tuberculosis</i> pup-proteasome system .....	102
Figure 5.3: CRISPR interference system .....	103
Figure 5.4: SAR of imidazolines against human 20S proteasome and growth of <i>Mycobacterium tuberculosis</i> .....	107
Figure 5.5: In vitro activity of imidazolines in purified <i>Mycobacterium tuberculosis</i> proteasome assay .....	108
Figure 5.6: CRISPRi/dcas9 system under the control of anhydrotetracycline (ATC)-inducible promoter (P <sub>Tet</sub> ) .....	109
Figure 5.7: CRISPRi/dcas9 knockdown of proteasomal genes in <i>Mycobacterium smegmatis</i> ..	111
Figure 5.8: Effect of CRISPRi/dcas9 knockdown of pup-proteasome genes on the growth of <i>Mycobacterium smegmatis</i> .....	112

## KEY TO ABBREVIATIONS

AD	Alzheimer's disease
AFM	Atomic force microscopy
ALS	Amyotrophic lateral sclerosis
APS	Ammonium persulfate
Blm 10	Bleomycin-sensitive
Boc-LRR-AMC	Tert-butoxyl-leucyl-arginyl-arginyl- 7-amino-4-methylcoumarin
Cas9	CRISPR associated protein 9
CD	Circular dichroism
CDC	Center for disease control and prevention
Cdk1	Cyclin dependent kinase 1
CP	Core particle
CRISPRi	Clustered regularly interspaced short palindromic repeats interference
D3T	3H-1,2-dithiole-3-thione
Dsk2	Dual-specificity protein kinase 2
Hb-Y-X	Hydrophobic-tyrosine-any amino acid
HD	Huntington's disease
HEPES	4-(2-hydroxyethyl)-1-piperazineethanesulfonic acid
HIV	Human immunodeficiency virus
HL60	Peripheral blood promyeloblast
IDP	Intrinsically disordered proteins
IMR90	Lung fibroblast
IPTG	Isopropyl $\beta$ -D-1-thiogalactopyranoside
LB	Lauria-Bertani <sup>[LSEP]</sup>

LMP2	Low molecular mass polypeptide 2
LMP7	Low molecular mass polypeptide 7
MAPK	Mitogen-activated protein kinase
MECL-1	Multicatalytic endopeptidase complex subunit 1
MHC	Major histocompatibility complex
MS	Mass spectrometry
Msmeg	<i>Mycobacterium smegmatis</i>
Mtb 20S	<i>Mycobacterium tuberculosis</i> 20S proteasome
Mtb	<i>Mycobacterium tuberculosis</i>
NCC	NIH (National institute of health) clinical collection
Nrf2	Nuclear factor (erythroid-derived 2)-like 2
PA200	Proteasome activator 200 kDa
PA26	Proteasome activator 26 subunit
PA28	Proteasome activator 28 subunit
PA700	Proteasome activator 700 kDa
PAGE	Poly acrylamide gel electrophoresis <sup>[11]</sup> <sub>SEP</sub>
PAM	Protospacer adjacent motif
PAP1	Proteasome-activating peptide 1
PBS	Phosphate-buffered saline
PCR	Polymerase chain reaction
PD	Parkinson's disease
PDE4	Phosphodiesterase type 4
PKA	Protein kinase A
Pten	Phosphatase and tensin homolog
Rad23	Radiation sensitivity abnormal 23

Rpn	Non-ATPase regulatory particle
Rpt	ATPase regulatory particle
SDS	Sodium dodecyl sulfate <sup>[11]</sup> <sub>[SEP]</sub>
sgRNA	Single guide RNA
SOD1	Superoxide dismutase 1
Suc-LLVY-AMC	Succinyl-leucyl-leucyl-valyl-tyrosyl-7-amido-4-methylcoumarin
t-BHQ	Tert-butylhydroquinone
TEMED	<i>N, N, N', N'</i> -tetramethylethylenediamine
UCH37	Ubiquitin C-terminal hydrolase 37
USP14	Ubiquitin specific peptidase 14
W138/T	Lung fibroblast
WHO	World health organization
WT	Wild type
Z-LLE-AMC	Carboxylbenzyl-leucyl-leucyl-glutamyl-7-amido-4-methylcoumarin

# **CHAPTER ONE**

## **Protein Homeostasis in Pathophysiology**

## 1.1 Introduction

The credence of protein homeostasis (proteostasis) proposes the existence of different and unified biological pathways within the cell which control protein synthesis, folding, and degradation in a synchronized manner.<sup>1,2</sup> Understanding of this protein quality control network is crucial in depicting the underlying causes of human diseases associated with imbalance in protein homeostasis. Unremitting flux of the cellular proteome, each protein at its own rate, must be sustained during successful development, healthy aging, environmental or xenobiotic stresses, and to minimize homeostasis perturbations and disorders.<sup>3-5</sup> The cellular concentration and functional state of all proteins must be continuously evaluated to uphold the required balance. The ability for a cell to progress through basic cellular functions such as life cycle (cell growth and proliferation), differentiation, cell signaling and self-renewal or to acclimate to cellular fluctuations necessitates a continuous flux in its proteome.<sup>1</sup> This continuous flux and proteome fidelity are maintained by the protein homeostasis (proteostasis) network. This network comprises the protein synthesis machinery (the ribosomes), protein folding complexes (the chaperones), and two proteolytic systems; the proteasomal and the autophagy (lysosomal) systems (Fig. 1.1).<sup>6</sup>

Eukaryotic cells avoid nonproductive interactions and aggregation of proteins through molecular chaperone-mediated co-translational folding of nascent polypeptides attached to the ribosome.<sup>7</sup> Additionally, chaperones recognize unfolded and/or aberrant proteins and assist them in regaining stability. Redundant proteins or those with damage beyond repair are promptly discarded through the proteolytic pathways to avoid proteotoxicity due to aggregation or undesirable signaling.<sup>3,8</sup> The flexibility and crosstalk among components of the quality control network sustain proteostasis under different pathophysiological conditions such as cellular growth, differentiation, xenobiotic, and oxidative stress. These proteostasis components are functionally



coupled, and compensatory strategies are in place to evade proteostasis failure if the activity of one or more of the network components deteriorates.<sup>9–11</sup> However, the high variability in structural complexity, half-life, vulnerability to damage, function and cellular localization of proteins make cellular proteolysis and proteostasis a complex affair. Due to this complexity, malfunctioning of the protein homeostasis network is inevitable and affects critical signaling pathways.<sup>5,12,13</sup> The majority of non-infectious diseases are thus a consequence of failure in the human proteostasis system.<sup>1</sup> Modulation of intracellular protein concentration via regulation of the proteolytic machineries has long been validated as promising milieu for the development of treatments for different human diseases such as neurodegeneration, cancer, and autoimmunity.<sup>12,14–19</sup>

The degradation scheme of the proteostasis network is maintained by both the ubiquitin-proteasome system (UPS) and the lysosome-autophagy system (autophagy).<sup>9,20</sup> The autophagy pathway enables cellular degradation of protein complexes, protein aggregates and damaged organelles in a lysosome-dependent mechanism. The UPS on the other hand targets the degradation of mostly soluble, nuclear, cytosolic and some membrane proteins. Some intracellular proteins are relatively stable (half-life >1day), but others are rapidly degraded (half-life < 30 minutes) to initiate or terminate specific cellular functions and/or signaling. The UPS has been found to be an exquisitely regulated system, working with great specificity and selectivity when interacting with substrates and directing their degradations.

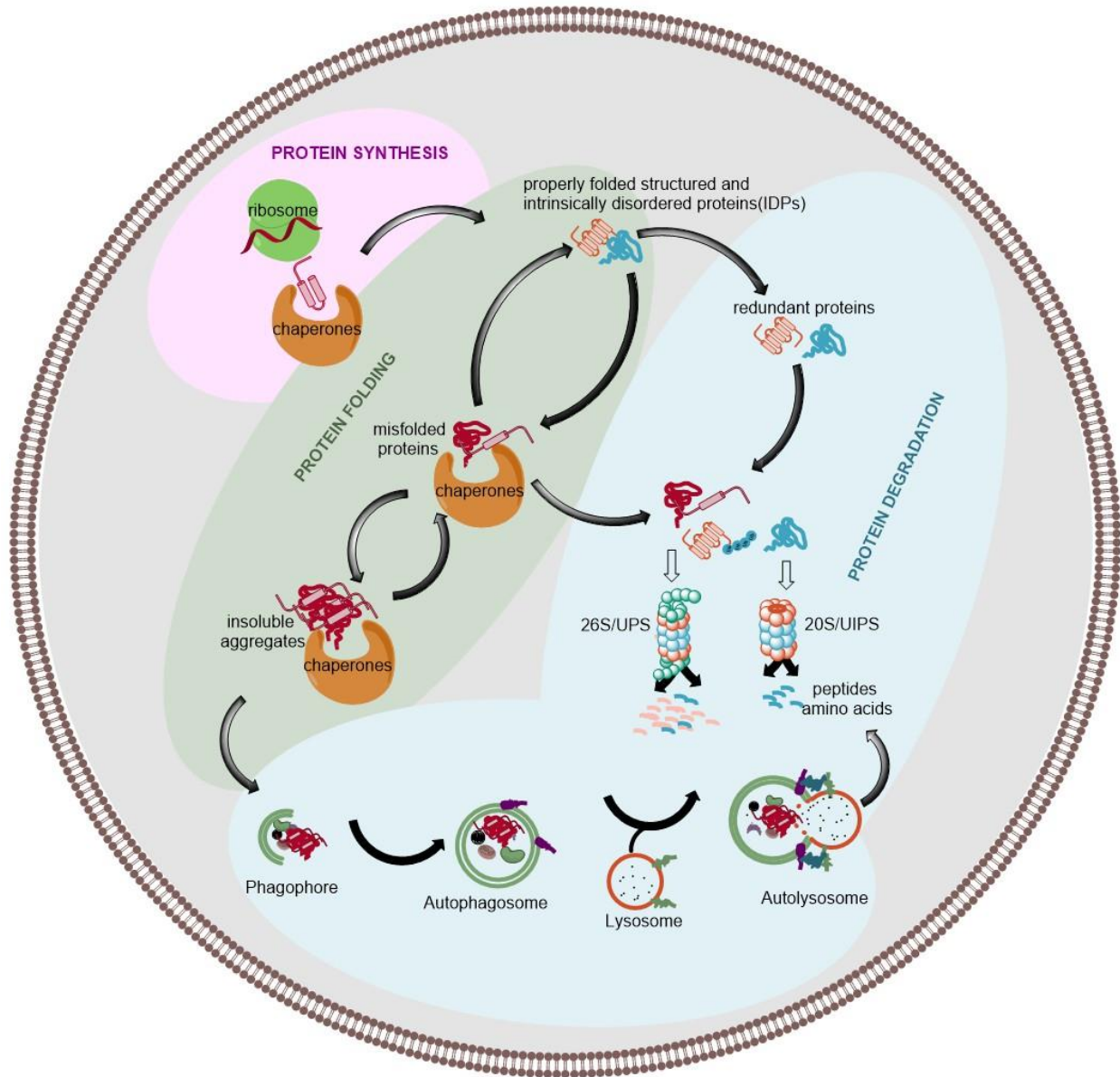


**Figure 1.1: An overview of the proteostasis network.** Nascently synthesized proteins at the ribosomes are assisted into a folded and functional state by molecular chaperones. Misfolded proteins or protein aggregates that cannot regain stability are directed to the proteasome or autophagy system for degradation. The interplay of these systems maintains proteome fidelity and proper cellular function.

## 1.2 The ubiquitin proteasome system (UPS)

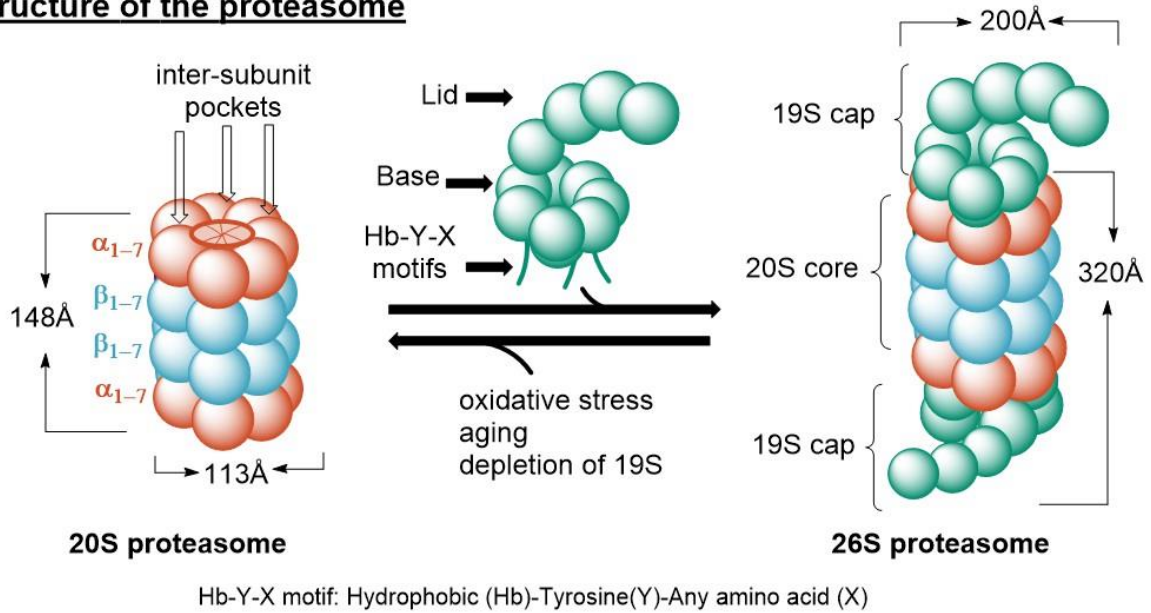
### 1.2.1 Structure of the proteasome

In eukaryotic cells, important biological processes such as cell growth and differentiation, cell signaling and self-renewal are controlled by the main selective proteolytic pathway called the ubiquitin proteasome system (UPS).<sup>15,21</sup> At the focus of the UPS is the proteasome. The 26S proteasome is a multi-catalytic proteinase complex of about 2,000 kDa. The 26S consists of two subcomplexes; the 750 kDa 20S catalytic core particle (CP) and the 19S regulatory particle (RP) or PA700 of about 700 kDa. The 26S proteasome is formed when the latent cylindrical-shaped 20S CP is capped by one or two 19S RP. The names 19S, 20S and 26S proteasomes refer to the apparent sedimentation coefficient of the different complexes as determined by density-gradient centrifugation analysis. Although single and double capped 20S proteasomes have sedimentation coefficients of 26S and 30S, respectively,<sup>22</sup> in this dissertation and in most literatures, 26S refers to the protease component (both single and double capped 20S) of the ubiquitin-dependent proteasome pathway (section 1.2.3 ).

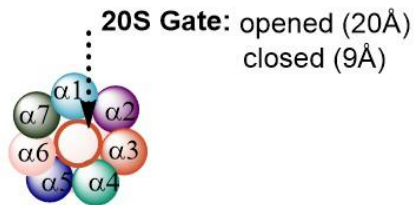
The 20S CP is a 28-subunit threonine protease with six catalytic sites and three types of enzymatic activities. The 20S proteasome (Fig. 1.2A) consists of four stacked rings; two inner  $\beta$ -rings and two outer  $\alpha$ -rings. The  $\alpha$  and  $\beta$ -rings are each composed of hetero-heptameric subunits;  $\alpha 1$ - $\alpha 7$  (Fig. 1.2B) and  $\beta 1$ - $\beta 7$  (Fig. 1.2C), respectively.<sup>23-25</sup> Each  $\beta$ -ring contains three catalytic subunits ( $\beta 5$ ,  $\beta 2$  and  $\beta 1$ ) that exhibition chymotrypsin-like (CT-L), trypsin-like (Tryp-L) and caspase-like (Casp-L) activity, respectively.<sup>26-29</sup> The outer  $\alpha$ -rings serve as gated channels that regulate substrate entry and product exit from the inner catalytic chambers. These outer rings also act as docking surfaces for the 19S RP (Fig. 1.2A). A number of other non-ATPase regulatory

particles such as the 11S complex (PA28) and PA200 (Blm10 in yeast) also reversibly associate with the 20S CP by docking onto the  $\alpha$ -rings.<sup>30–33</sup>

### A Structure of the proteasome



### B Cross section of an $\alpha$ -ring



### C Cross section of a $\beta$ -ring

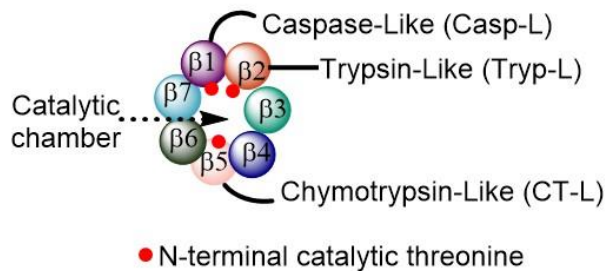


**Figure 1.2: Structure of proteasome subcomplexes.** (A) Structure of the 20S proteasome in equilibrium with the 26S proteasome. Also shown are the dimensions of the 20S core particle (~15 nm x 11 nm) and that of a single capped 20S (~20 nm x 32 nm).<sup>34</sup> (B) Cross-section of the 20S alpha ring showing entrance into the catalytic chamber with pore size at 0.9 nm when closed and 2 nm when opened. (C) Cross-section of the beta ring showing the three catalytically active subunits with N-terminal nucleophilic threonine.

The 19S RP (Fig. 1.3) is responsible for 20S gate opening, recruitment, unfolding and threading of ubiquitinated substrates into the 20S CP.<sup>25,35–37</sup> The 19S RP is a protein complex of about 19 subunits and is divided into two subcomplexes; the base that interacts directly with the 20S and a peripheral lid. The base is comprised of hexameric AAA-ATPase subunits, Rpt1–Rpt6, and tetrameric non-ATPase subunits, Rpn1, Rpn2, Rpn10, and Rpn13. The ATPase activity in the base is essential for protein substrate unfolding, gate opening and translocation of substrate into the 20S core. Unlike the other 19S subunits, the Rpn4 subunit is not a stable (half-life of ~2 minutes; also, a proteasome substrate) module of the 19S cap.<sup>38,39</sup> Rpn4 interacts with the Rpn2 subunit and functions as a ligand and transcriptional regulator of cellular proteasome concentration. The lid is made of nine non-ATPase subunits; Rpn3, Rpn5–Rpn9, Rpn11, Rpn12, and Sem1. The lid, specifically the Rpn11 subunit functions as a deubiquitinase.<sup>40,41</sup> Rpn10 and other reversibly associated proteins such as radiation sensitivity abnormal 23 (Rad23) and dual-specificity protein kinase 2 (Dsk2) serve as ubiquitin receptors that direct polyubiquitinated proteins to the proteasome. The Rpn subunits also create docking site(s) for other proteins including the proteasome associated deubiquitinating enzymes; ubiquitin specific peptidase 14 (USP14) and ubiquitin C-terminal hydrolase 37 (UCH37).<sup>42–44</sup> The 19S and other endogenous protein activators such as the PA200 and PAN (from archaeal species) contain a conserved C-terminal hydrophobic-tyrosine-any amino acid (Hb-Y-X) motif that triggers 20S gate opening upon ATP binding (Fig. 1.2A). These Hb-Y-X motifs are inserted into inter-subunit pockets created by neighboring  $\alpha$  subunits. In these pockets, interaction with conserved residues is believed to result in a rotation in the  $\alpha$  subunits and a displacement of a reverse-turn loop that maintains the open-gate conformer.<sup>27,31</sup>

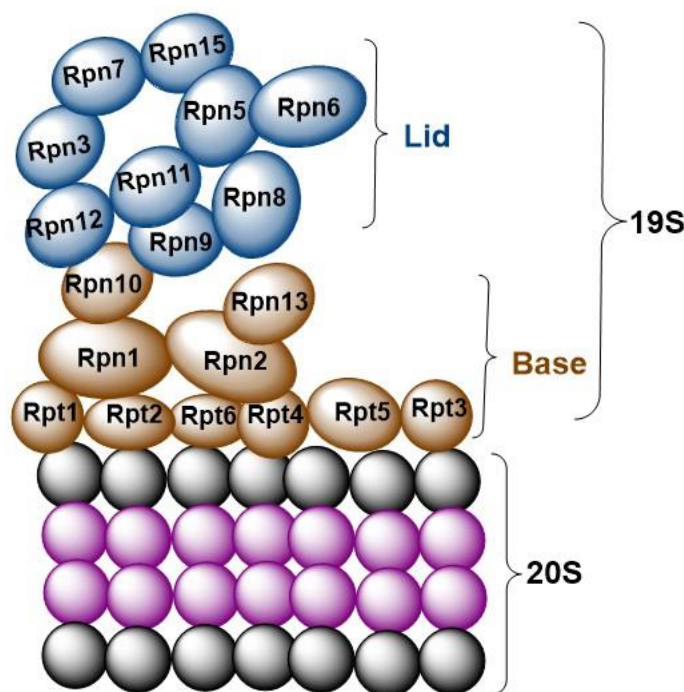


**Figure 1.3:** Simplified arrangement of the 19S subunits.

In immune cells and during an immune response, or in response to treatments with cytokines such as interferon- $\gamma$  (IFN- $\gamma$ ) or tumor necrosis factor- $\alpha$  (TNF- $\alpha$ ), the constitutive catalytic 20S proteasome subunits  $\beta$ 1,  $\beta$ 2, and  $\beta$ 5 are replaced by the inducible subunits LMP2 ( $\beta$ 1i), MECL-1 ( $\beta$ 2i), and LMP7 ( $\beta$ 5i), respectively, forming the immunoproteasome (i20S).<sup>45–49</sup> The immunoproteasome has an altered substrate binding pocket which results in cleavage pattern optimized for generating peptides for presentation on the major histocompatibility complex (MHC) class I molecules. The i20S can also associate with the IFN- $\gamma$ -inducible 11S (PA28) regulatory complex on one end and 19S on the other end to form a hybrid proteasome, or it can associate with the 11S on both ends.<sup>50</sup> The so called thymoproteasome (t20S) has also been identified in cortical epithelial cells of the thymus. The t20S consist of  $\beta$ 1i,  $\beta$ 2i, and  $\beta$ 5t catalytic subunits, and it is believed to play a role in positive selection of CD8+ cells.<sup>51</sup>

### 1.2.2 Defining intrinsic disorder and substrates of the proteasome degradation systems

Proteins degraded by the proteasome fall into two main classes; misfolded/damaged proteins and redundant proteins.<sup>52–54</sup> The latter is further divided into structured and intrinsically disordered proteins. It is a well-established paradigm that proteins' functions are dependent on their abilities to fold into well-defined 3-dimensional (3D) structures.<sup>55</sup> However, a plethora of data suggest that protein function is not exclusively dependent on a defined 3D conformation,<sup>56–59</sup> but that, there are regions of some polypeptide chains which are unable to fold into fixed 3D structures. These regions, typically > 30 amino acid residues are called intrinsically disordered regions (IDRs), and proteins are named intrinsically disordered proteins (IDPs) if they are mostly composed of such polypeptides. These IDPs/IDPRs are significantly enriched in disorder-promoting amino acid residues, such as Ala, Arg, Gly, Gln, Ser, Glu, Lys, and Pro<sup>60,61</sup> and are deficient in order-promoting amino acids (Trp, Tyr, Phe, Ile, Leu, Val, Cys, and Asn).<sup>62,63</sup> These amino acid sequence compositions have allowed for the development of *in silico* software for disorder prediction in proteins. Examples of such tools are PONDR,<sup>64</sup> IUPred<sup>65</sup> and SPOT-Disorder-Single.<sup>66</sup> More accurate confirmation of protein disorder is commonly achieved with biophysical techniques such as nuclear magnetic resonance (NMR)<sup>67</sup> and circular dichroism (CD).<sup>68</sup>

About 30% of the proteome are IDPs or have significant IDRs.<sup>69</sup> Among these IDPs, about 75% constitute the bulk of signaling proteins. IDPs are typically, but not exclusively low abundance proteins that function through interaction with other proteins or as hubs in protein-protein interaction networks involve in driving transcription, cell signaling, cell growth and proliferation.<sup>70–72</sup> Thus, deregulation of IDPs are associated with the onset of several human diseases including cancer,<sup>73</sup> neurodegeneration,<sup>74</sup> cardiovascular diseases<sup>57</sup> and diabetes.<sup>58</sup> This

protein class is generally thought of as “undruggable”. The lack of druggability of IDPs is due to significant flexibility in the protein 3-D structure that makes it difficult to map canonical drug pockets, as well as the lack of crystal structures.<sup>81</sup> IDPs are primarily degraded by the 20S proteasome.<sup>54,73,75,76</sup> It should be noted that the presence of IDRs in proteins does not necessarily dictate protein half-life or imply proteasomal degradation by default. In cells, IDPs are typically protected from default proteolysis by ‘nanny’ chaperones or through interaction with other proteins that restrict accessibility to their protease sensitive sites.<sup>54,77,78</sup> Since IDPs are mostly low abundance proteins, deregulations that promote their accumulation are often associated with numerous diseases.<sup>57,59,74</sup> Thus, targeting IDPs through enhanced proteasomal degradation may present a new therapeutic approach for IDP- associated disorders.

### **1.2.3 The 26S proteasome and ubiquitin- ATP-dependent proteolysis**

The 26S proteasome mainly targets structured proteins for degradation; although a certain fraction of misfolded and intrinsically disordered proteins (IDPs) are also degraded by the 26S in a ubiquitin-independent manner.<sup>79–82</sup> Structured proteins due for degradation are tagged with chains of polyubiquitin which serve as a degron for their turnover. Polyubiquitinated proteins are recognized by the ubiquitin receptors, Rpn10 and Rpn13. The ubiquitin tag is then removed by deubiquitinases such as the Rpn11, USP14 or UCH37.<sup>44</sup> The ATPase activities of the 19S base then unfolds and directs proteins into the catalytic chamber for degradation.<sup>79,83,84</sup>

Ubiquitin is a small protein (~8 kDa) of 76 amino-acids, consisting of seven lysine (K) residues at positions 6, 11, 27, 29, 33, 48 and 63 through which it can be attached to protein substrates.<sup>85,86</sup> Polyubiquitination of substrate proteins at K-48 of ubiquitin serves as the primary degron for 26S-mediated proteolysis.<sup>87</sup> Ubiquitin ligation at other lysine residues has been shown to be involved in DNA repair (K-6),<sup>88</sup> cell cycle regulation (K-11),<sup>89</sup> mitochondrial transport,<sup>90</sup>



protein trafficking (K-33),<sup>91</sup> and in directing of proteins towards autophagy-mediated proteolysis (K-63 and K-29).<sup>92</sup> A series of enzymes, ubiquitin ligases (E1, E2 and E3) coordinate the attachment of mono- and polyubiquitin to proteins. Ubiquitin is first activated in an ATP-dependent reaction by an E1 ubiquitin-activating enzyme, to which it becomes attached by a thioester bond. Subsequently, the activated ubiquitin is transferred to the active site cysteine of the E2 ubiquitin-conjugating enzyme. E3 or ubiquitin-protein ligase, together with E2 catalyze the transfer of ubiquitin onto the protein that is destined for degradation (Fig. 1.4).<sup>85,93–95</sup>

#### **1.2.4 The 20S proteasome and ubiquitin-ATP-independent proteolysis**

The 20S proteasome directly degrades misfolded, oxidatively damaged and intrinsically disordered proteins which do not require the unfoldase activity of the 19S base. Furthermore, 20S-mediated proteolysis does not require polyubiquitination of its substrates.<sup>82,96,97</sup> The 20S proteasome exists mainly in its closed-gate/latent conformation in which access to the catalytic chamber is obstructed by converging N-terminal residues of the alpha subunits.<sup>98</sup> The 20S-mediated proteolysis is thought to involve a direct interaction of the protein substrate with the  $\alpha$ 3 subunit, which brings about a conformational change and subsequent degradation of the target protein.<sup>73</sup>

A number of non-ATPase regulatory particles such as the 11S complex (PA28) and Bim10 (PA200) also reversibly associate with the 20S CP by docking onto the  $\alpha$ -rings, thereby inducing an open-gate conformation that promotes ubiquitin/ATP-independent proteolysis.<sup>31–33</sup> Therefore, small molecules that induce open-gate conformation (s) of the 20S proteasome can thus mimic ATP- and ubiquitin-independent proteolysis seen with non-ATPase caps.

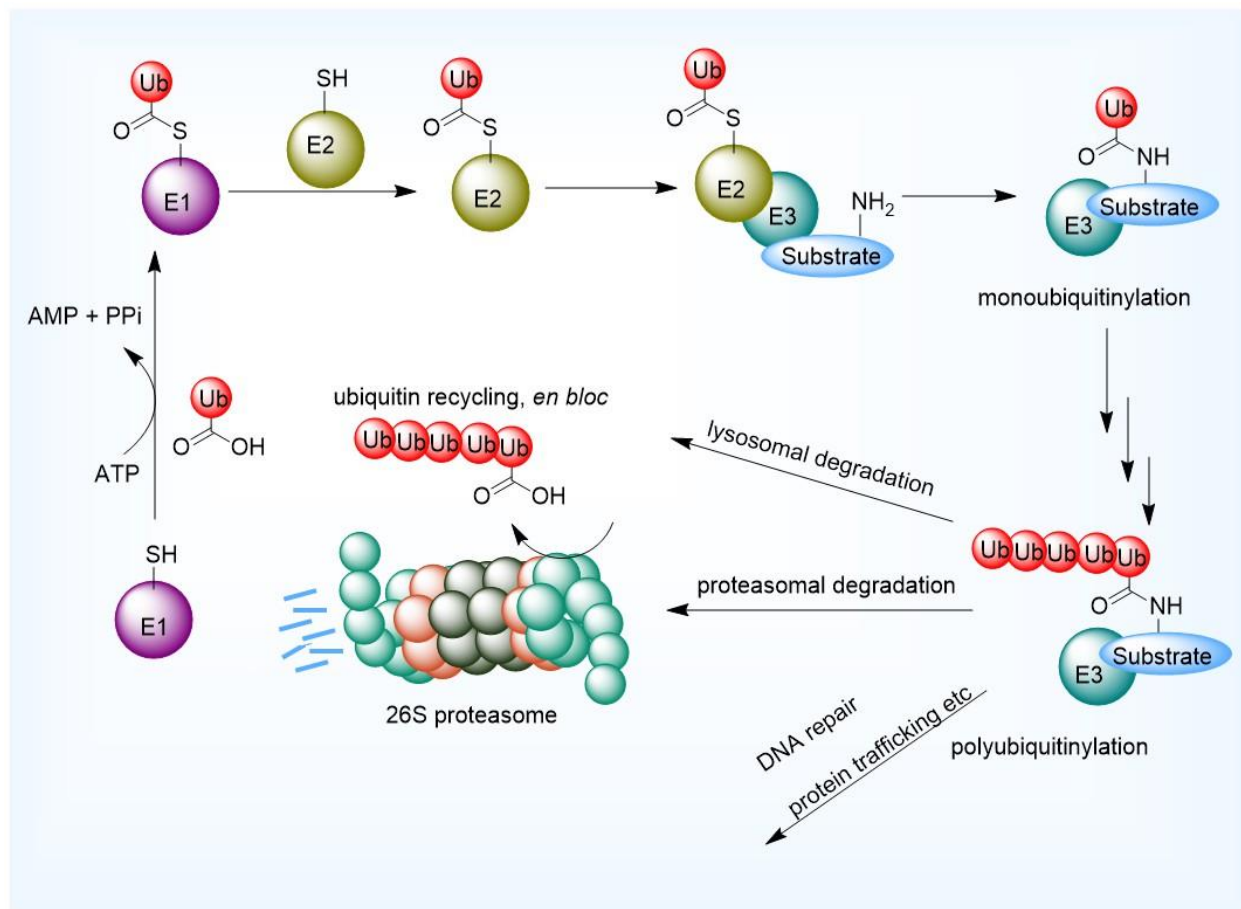


**Figure 1.4: Schematic of protein ubiquitinylation.** Ubiquitin is activated upon binding to the E1 activating enzyme with its C-terminus. The activated ubiquitin is transferred from E1 to the cysteine residue of the E2 conjugating enzyme. The E3 ligase associates with E2 to form a complex of E2-E3-protein substrate. The ubiquitin is then transferred to a lysine residue on the substrate protein. This process is repeated until the desired polyubiquitin chain is formed.

### 1.3 Drugging the 20S proteasome degradation system

#### 1.3.1 Drugging the 20S proteasome in cancer

Proteasome-mediated degradation is a crucial post-translational mechanism that exerts spatiotemporal control on effector proteins essential for proper functioning of cellular pathways and regulatory networks.<sup>15,19</sup> The proteasome degradation system plays an important role in cell

proliferation and survival, through its involvement in regulating transcription factors such as c-Myc, c-Fos, p53 and NF- $\kappa$ B.<sup>99</sup> Thus, proteasome-regulated signaling plays a crucial role in the onset and progress of cancer.<sup>100</sup> Among these cancers are blood cancers such as multiple myeloma (MM). Multiple myeloma is a malignant tumor of transformed B-lymphocytes,<sup>101–103</sup> in which mutated B cells differentiate into multiple myeloma cells (instead of plasma cells). These myeloma cells eventually take over the bone marrow microenvironment and continuously produce immature antibodies called monoclonal proteins (M proteins). The accumulation of M-proteins and leaching of calcium into soft tissues lead to bone fracture and kidney failure in MM patients.

The M-proteins produced by MM cells are degraded by the proteasome via the endoplasmic reticulum (ER) associated protein degradation pathway. Secretion of unusually high levels of M-proteins by MM cells places a high burden on the proteasome, making the proteasomal system a key to the survival of MM cells.<sup>100</sup> Proteasome inhibition interferes with crucial signaling pathways as a result of a halt in this “house cleaning” role as well as fatal amino acid shortage and disruption of protein homeostasis.<sup>104</sup> Proteasome inhibition therefore serves as a means of inducing the accumulation of toxic proteins, cell cycle arrest, inhibition of angiogenesis, and subsequent induction of programmed cell death (apoptosis).<sup>73,74</sup> This therapeutic approach forms the basis for clinically used anticancer agents such as bortezomib (Velcade®), carfilzomib (Kyprolis®) and ixazomib (Ninlaro®). These drugs are electrophilic molecules which form covalent bond with the N-terminal catalytic threonine in the proteasome active sites. The studies presented in subsequent chapters are focused on regulating proteasome activity in a manner to promote the degradation of dysregulated proteins. As such, proteasome inhibitors will not be discussed in detail.

Dysregulation of intrinsically disordered proteins (IDPs) is associated with the onset of several human diseases including cancer,<sup>73</sup> neurodegeneration,<sup>74</sup> cardiovascular diseases<sup>57</sup> and

diabetes.<sup>58</sup> A good example of dysregulated IDP in cancer is c-Myc. C-Myc is an IDP that is dysregulated in more than 50% of human cancers.<sup>105</sup> Dysregulation in c-Myc driven genes is more prevalent in cancers of hematopoietic origin such as multiple myeloma, Burkitt lymphoma and B cell lymphoma. In multiple myeloma for example, translocation of the MYC locus or mutation in upstream regulators such as K-RAS<sup>106,107</sup> drives the overexpression of c-Myc, which in turn drive MM growth and progression. A plethora of data<sup>105,108–110</sup> has been used to validate c-Myc as a drug target in MM and other blood cancers. Thus, proteasome activation presents a new therapeutic vulnerability for c-Myc addicted cancers.

c-Fos is another IDP that is dysregulated in glioblastoma multiforme.<sup>111,112</sup> Glioblastoma is an aggressive, fast-growing brain tumor that develops from star-shape glial cells (oligodendrocytes and astrocytes).<sup>113–115</sup> These cells normally support nerve cells within the central nervous system. Treatment of glioblastoma presents a lot of challenges due to localization of tumor in the brain, inherent resistance to traditional chemotherapies, neurotoxicity, and more.<sup>116,117</sup> Overexpression of c-Fos in glioblastoma has been found to be a driver in activating key enzymes in lipid biosynthesis pathways,<sup>118</sup> thereby promoting membrane biogenesis, tumor growth and progression. Thus, targeting c-Fos through enhanced proteasomal degradation may present a new therapeutic approach for glioblastoma and related cancers.

c-Myc and c-Fos are only a drop from the pool of dysregulated signaling and cancer-associated IDPs. The concept of targeting cancer through proteasome activation has not yet been validated. Thus, part of my dissertation presents preliminary data supporting the premise of this new therapeutic approach.

### 1.3.2 Drugging the 20S proteasome in neurodegenerative diseases

The proteasome is the cell's first defense mechanism against accumulating proteotoxic stresses induced by oxidative damage.<sup>4,21,119</sup> The 20S proteasome complex is capable of directly targeting oxidatively damaged proteins to detoxify the cell.<sup>120–122</sup> Reactive oxygen species, from exogenous sources, the mitochondrial respiratory chain and other cellular metabolic processes accumulate as we age, causing substantial damage to proteins and other macromolecules.<sup>119,123</sup> Upon oxidative damage, proteins unfold and expose hydrophobic regions which makes them aggregation-prone. Thus, in order to combat increasing levels of oxidatively damaged proteins, an increase in the 20S proteasome complex is generated by disassembly of the 26S proteasome.<sup>124,125</sup> Yet, accumulation of damaged proteins beyond proteasome degradation capacity is inevitable. When this happens, dysregulation of proteostasis and proteotoxic stress occurs, and are the hallmarks of several neurodegenerative diseases, including Parkinson's disease (PD), Alzheimer's disease (AD), Huntington's disease (HD) and amyotrophic lateral sclerosis (ALS, also called Lou Gehrig's disease).<sup>12,126–131</sup>

Genetic manipulation of the proteasome proteolytic systems in animal models of different neurodegenerative disorders suggests that stimulating the activities of the proteolytic systems could be an effective strategy to treat these disorders.<sup>132,133</sup> In aged individuals, who are the major victims of this disease class, the proteasome exists mainly as the latent 20S,<sup>119,134–136</sup> thus making 20S a better target for these diseases.<sup>137,138</sup> Furthermore, proteins such as tau,  $\alpha$ -synuclein, amyloid-beta and many others prion-like proteins which contribute to this class of diseases are intrinsically disordered,<sup>74</sup> further supporting the importance of 20S proteasome activation as a therapeutic approach in neurodegeneration. However, decreased 26S proteasome activity and

accumulation of ubiquitinated proteins has been observed in postmortem brains of AD patients.<sup>139</sup> This suggests that both 20S and 26S are essential in targeting this class of disorder.

## **1.4 Approaches toward enhancement of proteasome-mediated proteolysis**

It is well established that aging is associated with the accumulation of damaged and misfolded proteins. This phenomenon is paralleled by decreased proteasome activity. Enhancement of proteasome activity has many therapeutic potentials, yet, it is still a relatively unexplored field. In this chapter, a comprehensive review of the different approaches used to increase proteasome activity is presented. Chapters 2 and 4 in this dissertation are focused on the discovery and characterization of small molecule 20S proteasome activators. Therefore, a more comprehensive covering of this topic requires summaries of both current literatures, as well as findings from my own studies. Furthermore, emphasis will be placed on activation of the 20S proteasome, since this is the main latent form, and the core protease essential for the degradation of IDPs.

### **1.4.1 Proteasome activation by agonist induced conformational modification**

#### **1.4.1.1 Peptide-based proteasome agonists**

In cells, 20S gate opening is triggered by a conserved C-terminal hydrophobic-tyrosine-any amino acid (Hb-Y-X) motif present in endogenous protein activators such as the 19S, PA200 and PAN (from archaeal species).<sup>35</sup> These Hb-Y-X motifs are inserted into inter-subunit pockets created by neighboring  $\alpha$  subunits. In these pockets, interactions with conserved residues result in a rotation in the  $\alpha$  subunits and a displacement of a reverse-turn loop that maintains the open-gate conformation. As anticipated, C-terminal peptides derived from the Hb-X-Y motifs of Rpt2 and Rpt5 subunits of the 19S proteasome are capable of boosting 20S-mediated degradation of peptides and proteins in biochemical assays.<sup>36,140</sup> More recently, proline- and arginine-rich (PR) peptides

previously reported as allosteric proteasome inhibitors<sup>141,142</sup> were converted into proteasome activators through modifications with C-terminal Hb-X-Y residues.<sup>143</sup> The PA26 and PA28 protein activators lacking the Hb-Y-X motif activate the 20S proteasome through a mechanism distinct from that of ATPase activators and it does not involve  $\alpha$  subunit rotation.<sup>35</sup> This diversity in structure and mechanism of proteasome activation by endogenous proteins suggest the presence of different allosteric pockets that can be targeted pharmacologically for the enhancement of proteasome activities.

A synthetic peptide called proteasome-activating peptide 1 (PAP1) has also been reported to increase the CT-L proteasome activity via a gate opening mechanism in the  $\alpha$ -ring of the 20S CP.<sup>144</sup> This peptide protected fibroblasts from hydrogen peroxide-induced oxidative stress, as well as prevented the aggregation of superoxide dismutase 1 (SOD1) in a cellular model of amyotrophic lateral sclerosis (ALS). Likewise, Kisselev *et al.*<sup>145</sup> reported evidence of hydrophobic peptide-induced gate opening in the  $\alpha$ -ring of the 20S CP.

Although clinically used proteasome inhibitors are peptide-based,<sup>146</sup> peptide drugs and peptide-based proteasome activators are limited by intrinsic peptide properties such as poor membrane permeability and susceptibility to proteolytic inactivation.<sup>147</sup> Furthermore, peptide activators bearing the Hb-Y-X motifs may also compete with endogenous proteasome activators (19S, 11S), with possibilities of intricate cellular outcomes.

#### **1.4.1.2 Small molecule proteasome agonists**

In 1988, Tanaka *et al.*<sup>148</sup> demonstrated that the eukaryotic 20S proteasome was mainly latent (closed-gate conformation) and could be activated in biochemical assays with low concentrations of sodium dodecyl sulfate (0.02-0.08% SDS) or with poly-lysine. SDS is believed to act via partial denaturation of the 20S and is characterized by inhibition at concentrations greater

than 0.08 %, <sup>98</sup> most likely due to destabilization of the enzyme's 3D confirmation. "SDS-like" proteasome activation has also been observed with lipids, <sup>149</sup> fatty acids, <sup>150</sup> and the natural product oleuropein. <sup>151</sup> Although the activity-response of these molecules impedes their use in physiologically relevant systems, they remain invaluable *in vitro* tools.

Progress toward the discovery of drug-like proteasome agonists has been slow, but a few have been identified. Molecules that interact with either the 20S or both the 20S and 26S proteasome function through two main mechanisms; (1) *Gate-openers*: Molecules that promote substrate entry into the catalytic pocket through allosteric interactions necessary for gate-opening in the alpha ring of the 20S proteasome. (2) *Stimulators*: Molecules that promote 20S and/or 26S-mediated degradation through allosteric interactions required for enhanced substrate binding and/or degradation in one or more catalytic sites. Among the first reported 20S agonists is the triterpenoid, betulinic acid (Fig. 1.5, **1**), <sup>152</sup> which specifically enhances the CT-L activity of the 20S proteasome. Unfortunately, chemical modifications to improve activity resulted in proteasome inhibitors with complicated structure activity relationships (SAR).

In a search for novel activators, we screened the NIH clinical collection (NCC) and Prestwick library and identified chlorpromazine (**2**) and other phenothiazines as 20S agonists that specifically enhanced 20S CT-L activity, while promoting the degradation of IDPs in biochemical and cellular assays (see chapter 4 for details). <sup>153</sup> Chemical modification of chlorpromazine abolished its dopamine D2 activity while maintaining significant proteasome stimulating properties. Coincidentally, methylene blue, a structural analogue of chlorpromazine has been demonstrated to reduce the levels of amyloid beta (A $\beta$ ) and rescues early cognitive deficits by increasing proteasome activity in a mouse model of AD. <sup>154</sup> These data, thus, support the robustness of phenothiazines as proteasome activators in AD therapy.



In a more mechanistic endeavor, we identified the imidazoline TCH-165 (**3**) and its analogues as 20S activators that induce gate-opening in the alpha ring of the 20S proteasome, as observed by atomic force microscopy (AFM).<sup>81</sup> TCH-165 was found to enhance the degradation of IDPs in biochemical and cellular assays. In cells, TCH-165 also shifted the 20S-26S equilibrium in favor of the 20S, presumably by competing with the 19S cap for 20S binding. Interestingly, the degradation of ubiquitinated proteins was largely maintained by single capped 20S (see chapter 2 for details).

In an attempt to establish secondary assays for validation of “true” activators, Trader *et al.*<sup>155</sup> screened a small library of the NCC and discovered MK-886 (**4**) and AM-404 as new classes of 20S activators capable of enhancing the degradation of  $\alpha$ -synuclein in cell culture. In a parallel effort, Coleman & Trader<sup>156</sup> identified two 20S activators, and a cytosine derivative (**5**) as stimulator of both 20S and 26S proteasomes. Among the 20S activators was the natural product, ursolic acid (**6**), another triterpenoid and an analogue of betulinic acid. The mechanism of proteasome activation by ursolic acid<sup>156</sup> appears to be distinct from that of betulinic acid,<sup>152</sup> further supporting the complexity associated with this class of molecules and proteasome activators, in general.

Although some of these molecules have already been classified in literature<sup>35</sup> as stimulators and gate-openers,<sup>138</sup> it should be noted that imidazolines are the only class of 20S agonist with biophysical data (AFM)<sup>81</sup> supporting their gate-opening activity.

## **1.4.2 Proteasome activation by regulation of post-translational modifications**

### **1.4.2.1 Small molecule kinase modulators**

Proteasome activation has also been realized through upstream modulation of kinases, with resultant post-translational modification of proteasome subunits. The human 26S proteasome

undergoes reversible phosphorylation in response to the ever-changing pathophysiological state of the cells.<sup>157</sup> More than 455 phosphorylation sites have been identified in the human 26S proteasome and they play different roles ranging from modulation of 26S assembly, stability, and activity. For example, osmotic stress inhibits proteasome activity via p38-MAPK-dependent phosphorylation of the 19S Rpn2 subunit.<sup>158</sup>

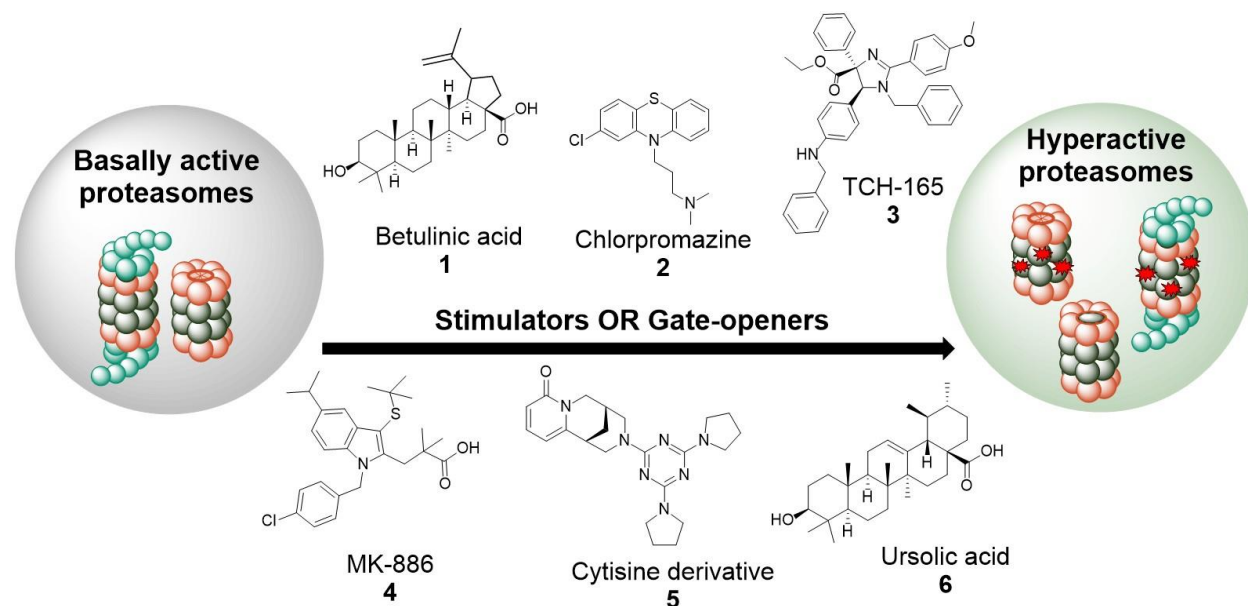


**Figure 1.5: Selected examples of small molecule proteasome activators.** These molecules activate the proteasome through gate-opening (e.g **3**) in the alpha ring and/or through enhancement of substrate binding in the catalytic pocket of the proteasome.

Phosphorylation of the 19S proteasome Rpt6 subunit by cAMP-dependent protein kinase A (PKA) was found to upregulate 26S assembly and proteasome activity *in vitro* and *in vivo*.<sup>159,160</sup> Rolipram (Fig. 1.6, **8**), a small molecule inhibitor of phosphodiesterase type 4 (PDE4),<sup>161</sup> was demonstrated to raise the level of cAMP in the brain of mice, activated PKA and presumably increased proteasome activity through subunit (Rpt6) phosphorylation. Most importantly, rolipram

promoted the clearance of abnormal tau and improved cognition in mouse model of Alzheimer's disease.<sup>162</sup>

PKA-mediated phosphorylation of the non-ATPase 19S subunit Rpn6 has also been shown to increase the degradation of ubiquitinated and aggregation-prone proteins such as tau in different cell lines.<sup>163</sup> These studies validated the involvement of the 26S proteasome in the degradation of IDPs, further supporting the significance of targeting either the 20S and/or 26S in the quest for increasing proteasome-mediated IDP clearance.

#### **1.4.2.2 Small molecule deubiquitinase inhibitors**

The 19S proteasome subunit Rpn11 has deubiquitinase activity that recycles polyubiquitin by removing them *en bloc* from protein substrates that are committed for degradation.<sup>42</sup> Additional deubiquitinases, USP14 and UCH37 reversibly interact with the proteasome and can trim ubiquitin chains independent of substrate commitment to degradation.<sup>43,44,164</sup>

Lee *et al.*<sup>165</sup> demonstrated that ubiquitin chain trimming by USP14 inhibits substrate degradation by the proteasome. In the same study, a small molecule inhibitor of USP14, IU1 (Fig. 1.6, 7), was found to promote the degradation of different proteasome substrates, including tau. IU1 also promoted the degradation of oxidized proteins, thereby conferring a cytoprotective effect towards oxidative stress in HEK cells.

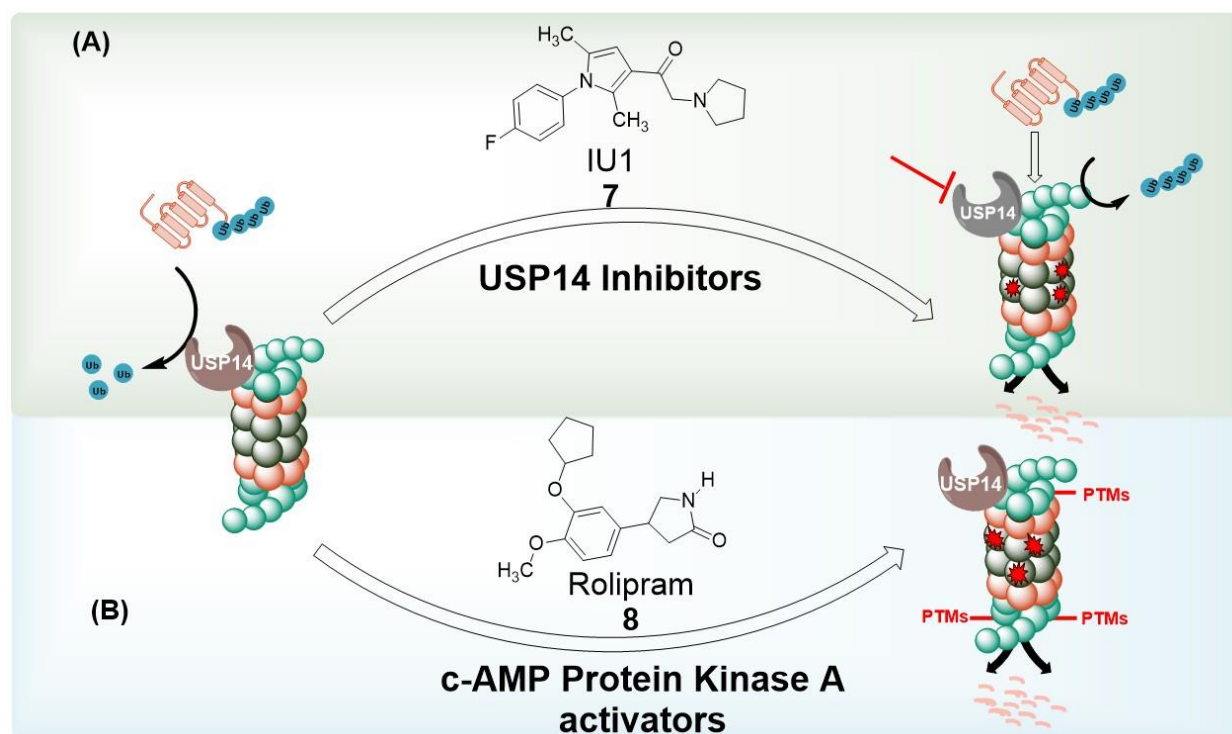


**Figure 1.6: Examples of small molecules that enhance proteasome activity through regulation of post-translational modifications. (A)** Inhibition of USP14 prevents ubiquitin chain trimming, thereby promoting 26S-mediated protein degradation. **(B)** Phosphorylation of 19S Rpn6 subunit through activation of c-AMP PKA enhances 26S-mediated proteolysis.

Interestingly, inhibition of USP14 by siRNA knockdown or use of its small molecule inhibitor led to accumulation of polyubiquitinated proteins with increased apoptosis of multiple myeloma cells.<sup>166</sup> This translated to extended survival in xenograft models of multiple myeloma. In a parallel study, the small molecule inhibitor of USP14 and UCH37, b-AP15, also promoted the accumulation of polyubiquitin, and delayed tumor progression in a mouse model of multiple myeloma<sup>167</sup> as well as four different models of solid tumors.<sup>168</sup> These complex outcomes seen with USP14 inhibition might be a result of its numerous diverse cellular functions. However, targeting

USP14 represents an exciting approach that may effectively translates in combating multiple types of cancers.

### **1.4.3 Proteasome activation by genetic manipulation**

#### **1.4.3.1 Upregulation of proteasome activity through subunit overexpression**

Pioneering work involving upregulation of proteasome activity through genetic manipulation were first illustrated by Gaczynska *et al.*<sup>169,170</sup> In these studies, overexpression of the 20S  $\beta 5i$  (LMP7) subunit in lymphoblasts and HeLa cells resulted in increased CT-L and Tryp-L activities, while overexpression of  $\beta 1i$  (LMP2) only elevated the Tryp-L like activity. In 2005, Chondogianni and coworkers<sup>171</sup> published a more in-depth study on proteasome activation via subunit upregulation: Stable overexpression of the 20S  $\beta 5$  catalytic subunit in two established (WI38/T and HL60) and primary (IMR90) human fibroblast cell lines resulted in elevated levels of other  $\beta$ -subunits, increased level of assembled proteasome, with a concomitant increase in all three proteasome proteolytic activities. Consistent with the role of the proteasome,  $\beta 5$ -overexpressing cell lines conferred protection against several oxidation-induced proteotoxic stresses, via enhanced degradation of oxidized proteins. A few parallel studies have also found  $\beta 5$ -overexpression to protect against oxidative stress in human lens epithelial cells<sup>172</sup> and to prevent replicative senescence of human bone marrow stromal cells.<sup>173</sup> These findings further corroborate the role of the proteasome in combating diverse classes of proteotoxic disorders.

#### **1.4.3.2 Upregulation of proteasome activity through Nrf2 activation**

The transcription factor, Nrf2 (Nuclear factor (erythroid-derived 2)-like 2), is a basic leucine zipper<sup>174</sup> that controls the expression of antioxidant enzymes including glutathione S-transferase, NADPH quinone oxidoreductase 1,<sup>175</sup> as well as proteasome subunits.<sup>176</sup> Accordingly, overexpression of the proteasome has also been achieved through small molecule activators of

Nrf2. Kwak *et al.*<sup>176</sup> demonstrated that the indirect antioxidant 3H-1,2-dithiole-3-thione (D3T, Fig. 1.7) upregulated both 20S and 19S proteasome subunits as well as proteasome activity only in Nrf2 positive fibroblast. A more recent article showed that activation of Nrf2 with D3T significantly improved cognitive deficits in a mouse model of Alzheimer's disease and dramatically reduced the level of insoluble amyloid beta (A $\beta$ ), as well as oxidative stress.<sup>177</sup> The triterpenoid, 18 $\alpha$ -glycyrrhetic acid (18 $\alpha$ -GA), has also been shown to delay replicative senescence in human fibroblast through Nrf2-mediated upregulation of proteasome subunit and activity.<sup>178</sup> In *Caenorhabditis elegans*, 18 $\alpha$ -GA also decreased A $\beta$  deposition and delayed the progress of AD, while promoting proteasome-dependent life span extension.<sup>179</sup> The food additive tert-butylhydroquinone (t-BHQ) and food supplement sulforaphane also increase proteasome activity through activation of Nrf2.<sup>180</sup> The increase in proteasome activity with t-BHQ and sulforaphane was accompanied by delayed differentiation, increase self-renewal and pluripotency in human embryonic stem cells (hESCs) and in induced pluripotent stem cell (iPS-IMR90). Similar activities have been observed by others in neuroblastoma cells,<sup>181</sup> where sulforaphane-Nrf2-mediated upregulation of proteasome activity protected against oxidative stress.

#### **1.4.3.3 Upregulation of proteasome activating caps and generation of open-gate 20S mutants**

The 20S proteasome exists mainly in its latent state conformation in which entrance into the catalytic chamber is occluded by converging N-terminal of the  $\alpha$ -subunits.<sup>28,148,182</sup> Proteins must access these gated channels to be degraded by the 20S core particle. Reasonably, one approach to increase proteasome activity has been aimed at genetically increasing accessibility through these gated channels. Accordingly, overexpression of the 19S Rpn6 subunit led to enrichment of assembled 26S and increased proteasome activity in embryonic stem cells.<sup>183</sup> Meanwhile, enhancement of proteasome activity via overexpression of PA28 $\alpha$  was found to

protect against proteinopathy and ischemia/reperfusion injury in mice.<sup>184</sup> These findings further highlight the importance of proteasome activation beyond neurodegenerative diseases and aging. In a more recent study, Choi *et al.*<sup>185</sup>, took a unique approach towards genetic upregulation of proteasome activity. Choi *et al.* showed that deleting the N-terminal of  $\alpha$ -3 subunit generates an  $\alpha$ -3 $\Delta$ N mutant that is incorporated into fully assembled 20S and 26S proteasomes in cells. These  $\alpha$ -3 $\Delta$ N mutant proteasomes showed increased degradation of about two hundred 20S and 26S protein substrates, including tau and  $\alpha$ -synuclein. Furthermore, the enhanced degradation of  $\alpha$ -synuclein significantly delayed the formation of  $\alpha$ -synuclein aggregates. Significant resistance against oxidative stress was also observed with cells carrying the open-gate mutant.

Most of these genetic approaches have only been explored at the *in vitro* levels (Fig. 1.7), with little or no supporting animal data. However, one could envision the delivery of proteasome  $\beta$ 5 subunit, 19S Rpn6, and/or  $\alpha$ -3 $\Delta$ N as gene therapy for the treatment of several diseases.

#### **1.4.4 Proteasome activation via unknown mechanisms**

Pyrazolones were previously reported to have neuroprotective function in a cellular model of ALS, with a significant increase in the median survival time of an ALS transgenic mouse model.<sup>186–188</sup> More recently, the activities of pyrazolones in ALS model have been linked to proteasome activation.<sup>189</sup> This conclusion was based on enhanced degradation of model proteasome substrates in cells, as well as affinity pull-down of Rpt2 and Rpt3 as interacting partners of pyrazolones. However, given that the activities of these compounds were not assayed with purified proteasome, it is not clear if they are direct proteasome agonists, modulators of endogenous proteasome activators (based on the pull-down assay with 19S subunits) or upstream modulators of proteasome post-translational modifiers. Thus, in this chapter, and based on my

classification, pyrazolones are categorized as enhancers of proteasome activity with unknown mechanism of action.

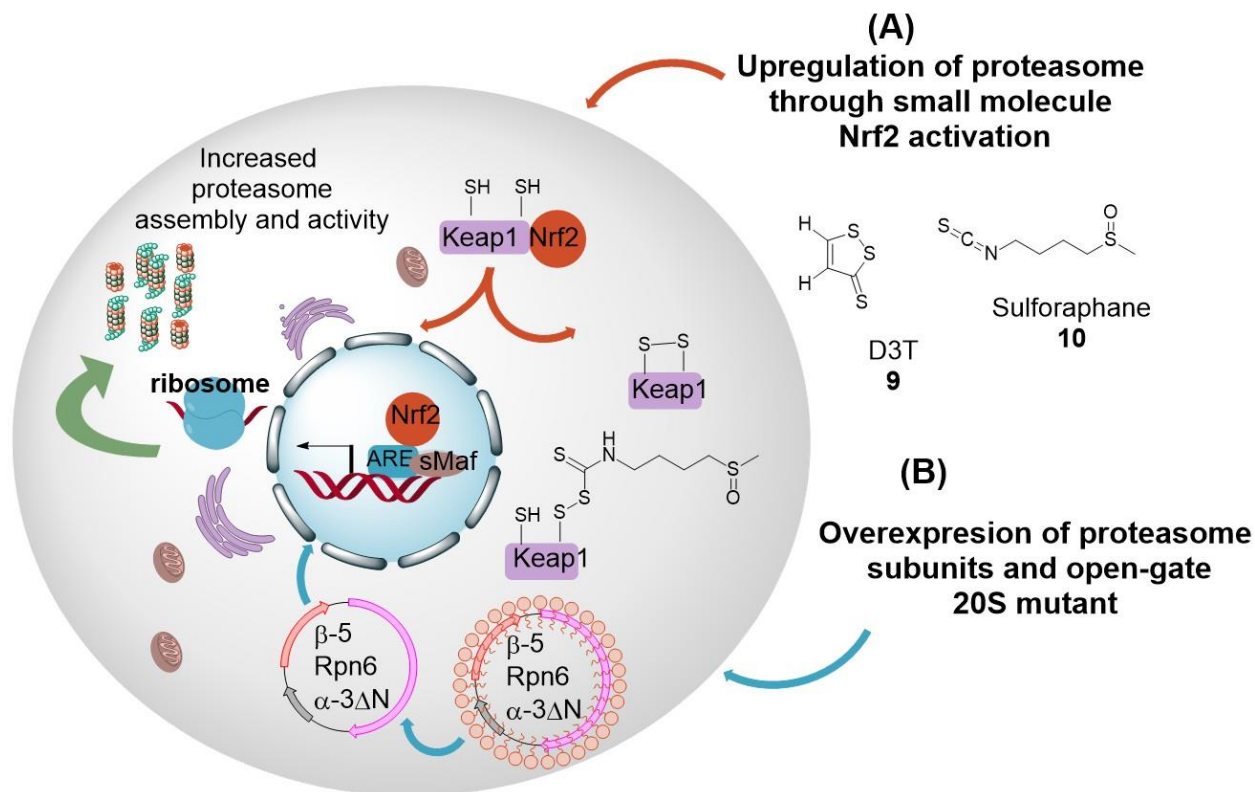


**Figure 1.7: Genetic upregulation of proteasome activity.** (A) Through small molecule activators of Nrf2 and (B) through overexpression of proteasome subunits.

By means of a chemical genetic screen, Leestemaker *et al.*<sup>190</sup> identified PD169316, a p38 MAPK inhibitor, as enhancer of 26S proteasome activity. Though the exact mechanism behind 26S activation by the p38 MAPK inhibitor could not be deciphered, the authors also demonstrated a decrease in the level of  $\alpha$ -synuclein as well as protection against toxic  $\alpha$ -synuclein in primary mouse neurons. Furthermore, activity-based probes that bind to the proteasome catalytic sites in activity-dependent manner were developed to further the effort of discovering new proteasome modulators.<sup>190</sup>



## 1.5 Conclusion

Enhancing proteasome activity reduces the proteotoxic burden cells experience upon aging. In humans,<sup>191,192</sup> rodents,<sup>154,193,194</sup> and cells,<sup>52,178,195–199</sup> increased proteasome activity delays ageing<sup>196,200–202</sup> and results in longer lifespan,<sup>203–205</sup> by reducing proteotoxic pathologies. Supporting this idea, cells from human centenarians exhibit enhanced proteasome activity compared to cells from adults of different ages.<sup>191</sup>

Cellular studies using short term exposure to proteasome agonists have thus far not illustrated inherent toxicity, however no studies have yet defined any long-term effects.<sup>85</sup> The lack of initial toxicity may be due to the protective roles of “nanny” chaperones or other protein complexes, which greatly limit the access of the 20S proteasome to its targets, thus yielding proteolytic selectivity.<sup>77,97,137,206</sup> In addition, the rate of proteasomal degradation of disordered regions is also dependent on the composition and length of specific disordered initiation sequences.<sup>207</sup> Stimulation of proteasome activity is therefore anticipated to have a differential effect on the clearance of different proteins.

Proteasome inhibition is the mechanism of action of most chemotherapeutics targeting blood cancer such as multiple myeloma.<sup>208</sup> Thus, a question that has become of concern is whether proteasome activators can cause cancer. Indeed, enhanced degradation of misfolded proteins through Nrf2-mediated upregulation of proteasome activity has been demonstrated to promote tumorigenesis.<sup>209</sup> Other studies demonstrated that deletion of Keap1, a negative regulator of Nrf2, and Pten drive the progress of non-small-cell lung cancer<sup>210,211</sup>. It should however be noted that Nrf2 activation drives the expression of many genes, including cyclin B and cyclin-dependent kinase 1(CDK1)<sup>212</sup> which are involved in driving mitotic division.<sup>213</sup> As discussed in chapter 2, proteasome activation with small molecule 20S agonists induce anti-tumor efficacy most

likely through enhanced degradation of cancer associated-IDPs. Thus, the effect of proteasome activation on tumorigenesis must be examined on a case by case basis.

In terms of 20S proteasome target selectivity, the relative susceptibility of disordered proteins to 20S-mediated proteolysis is far more limited than perhaps anticipated. 20S-mediated degradation is dictated by the level of substrate disorder, protein sequence, cellular compartmentalization and proteolytic accessibility.<sup>54,73,77,214,215</sup> Moreover, small molecule 20S activation involves the induction of conformational changes that may be unique for each agonist, with the possibility of disparate pool of select target proteins for proteolytic degradation.<sup>216</sup> Therefore, it is possible or perhaps likely, that different classes of 20S agonists may exert different substrate selectivity amongst proteolytically susceptible IDPs.

## **CHAPTER TWO**

### **Deciphering the Mechanism of Proteasome Modulation by Imidazolines**

Reproduced in part with permission from **Njomen Evert** and Tepe J. Jetze. Small Molecule Modulation of Proteasome Assembly. *Biochemistry*. **2018**, 57 (28), 4214–4224. Copyright 2018 American Chemical Society

## 2.1 Introduction

### 2.1.1 Background

The discovery of the proteasome<sup>26,79</sup> and its role in maintaining proteome fidelity and cellular functions<sup>6,52</sup> has unlocked different areas of research targeting this multi-catalytic threonine protease, in proteostasis disorders. These include cancer,<sup>168,208,217</sup> neurodegeneration<sup>18,132,218</sup> and age-related diseases.<sup>196,202,219</sup> Pioneering this field is the area of proteasome inhibition.<sup>217,220–222</sup>

Proteasome inhibition interferes with crucial signaling pathways as a result of fatal amino acid shortage,<sup>223</sup> and disruption of protein homeostasis. Thus, proteasome inhibition serves as a means of inducing cell cycle arrest, inhibition of angiogenesis, and subsequent induction of programmed cell death (apoptosis).<sup>208</sup> This concept is fully taken advantage of in the design of chemotherapeutic agents, especially in the area of multiple myeloma (MM),<sup>220</sup> a malignant tumor of differentiated B-cells.<sup>102,103</sup> Excessive production of immature/non-functional immunoglobulin by myeloma cells makes them exquisitely reliant on the proteasome to clear these redundant proteins (waste).<sup>222</sup> Consequently, partial inhibition of the proteasome selectively kills MM cells over normal cells, forming the basis for the design and synthesis of small molecules targeting MM via the proteasome.<sup>221,222,224</sup>

The druggability of this multi-catalytic protease, the proteasome, was endorsed by the 2003 FDA approval of bortezomib (Fig. 2.1A),<sup>225</sup> a boronate peptide-based competitive proteasome inhibitor, for the treatment of MM and related cancers. This cutting edge drug and its second generation analogues<sup>226,227</sup> are electrophilic traps that form a covalent bond with the active site threonine, thereby interfering with substrate binding.<sup>220</sup> Many patients are inherently resistant to bortezomib or may develop resistance in the course of treatment.<sup>228</sup> Although the actual mechanism of resistance is not clear, acquired resistance to bortezomib in multiple myeloma cell

lines has been partly attributed to mutation(s) and upregulation in the  $\beta$ -5 subunit of the proteasome.<sup>229,230</sup> Unlike the mutations, upregulation of  $\beta$ -5 subunit has been observed in both cell cultures and in MM patients. In addition, peripheral neuropathy resulting from off-target toxicity is another problem posed by competitive proteasome inhibitors such as bortezomib.<sup>231</sup>

While bortezomib and its analogues remain first-line therapy for MM patients, the inherent drug resistance<sup>229</sup> and toxicity<sup>231</sup> have led to the search for non-competitive proteasome inhibitors with the hope of overcoming these challenges. A number of these non-competitive proteasome modulators with poorly characterized mechanism of action have been published.<sup>141,232,233</sup> Among these were the imidazoline-based proteasome modulators discovered by the Tepe lab.<sup>234</sup>

Imidazolines or TCH-compounds were previously reported by the Tepe lab as non-competitive modulators of the proteasome that were effective in overcoming bortezomib resistance *in vitro*, and translated in blocking tumor growth *in vivo*.<sup>234</sup> The parent compound of that study (TCH-013) was found not to interact with the catalytic sites of the proteasome but allosterically modulate 20S proteolysis. Subsequent optimization of the scaffold generated TCH-165.<sup>235</sup>

TCH-165 and analogues were identified as non-competitive inhibitors of the 20S proteasome<sup>235</sup> in an assay that utilizes sodium dodecyl sulfate (SDS) buffer. The 20S proteasome is mainly latent, due to its closed-gate conformation which obstructs the access to the catalytic chamber.<sup>236</sup> As such, canonical proteasome biochemical assay (which before 2014 all focused on proteasome inhibition) is preceded by treatment with low concentrations of detergents such as SDS (0.01-0.03%)<sup>98</sup> to generate an active conformation before treatment with test compounds. Exclusion of SDS from this assay system resulted in reversal of activity for imidazolines. That is, imidazolines act as 20S proteasome activators in SDS free buffer. These intricate observations

warranted a detailed mechanistic investigation on how these molecules modulate the proteasome and how their unique activities could be harnessed therapeutically.

In an effort to elucidate the mechanism of action of imidazolines,<sup>234,235,237</sup> TCH-165 (Fig. 2.1B) was utilized because of its potency (proteasome activation), *in vivo* efficacy (anti-tumor activity), as well as its availability. Experimental controls included the parent compound TCH-013 (moderately active analogue), the inactive analogue TCH-023 (Fig. 2.1B) and the proteasome inhibitors bortezomib and epoxomicin (Fig. 2.1A)

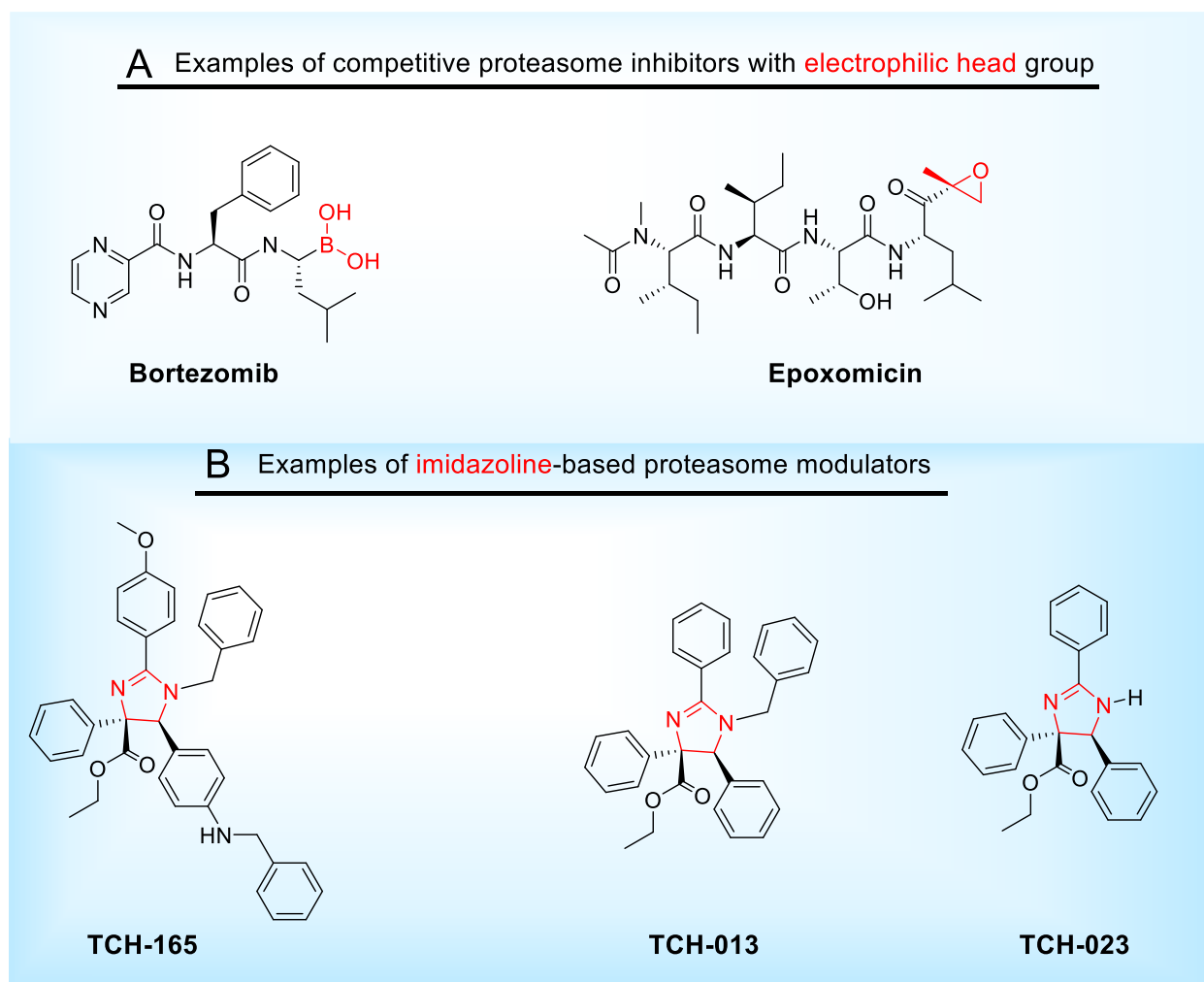


**Figure 2.1:** Structures of proteasome modulators used in this chapter

### 2.1.2 Objective

The goals of this chapter were (1) to understand the cellular mechanism of proteasome regulation by imidazolines and (2) to investigate how allosteric ligandability of this multi-catalytic protease perturbs 20S proteasome-regulated signaling.

## 2.2 Results and Discussion

### 2.2.1 TCH-165 enhances 20S-mediated but not 26S-mediated degradation of peptides

The activity of the proteasome can be measured in biochemical assays by quantifying the fluorescence of free 7-amino-4-methylcoumarin (AMC)<sup>238</sup> released upon cleavage of amide bonds in peptides designed for each proteasome catalytic sites.<sup>239</sup> Proteolysis of the peptide substrate is boosted following stabilization of the open-gate 20S conformation. Human 20S proteasome was pretreated with various concentrations of TCH-165 and proteasome activity quantified by measuring the release of AMC from the fluorogenic chymotrypsin-like (CT-L) peptide substrate (Suc-LLVY-AMC) over time. The concentration of drug required for induction of 50% maximum activity ( $EC_{50}$ ) was determined by fitting the relative fluorescence units and concentrations into a four-parameter dose-response curve. No fluorescence was detected in the absence of the AMC-labeled substrate, indicating that TCH-165 does not have intrinsic fluorescence at the AMC wavelength. Using AMC-labelled peptide substrates tailored to each of the catalytic site,<sup>238,239</sup> TCH-165 was found to enhance all three proteasome catalytic activities (Fig. 2.2A). The  $EC_{50}$  of TCH-165 was found to be 4.2  $\mu$ M for the chymotrypsin-like (CT-L), 3.2  $\mu$ M for the trypsin-like (Tryp-L) and 4.7  $\mu$ M for the caspase-like (Casp-L) catalytic sites (Fig. 2.2B). This observation suggests enrichment in the open-gate 20S conformation that allows the access of each of the substrates into the catalytic chamber.<sup>144,185</sup> The concentrations of TCH-165 required to double 20S activity (Active Concentration at 200% activity,  $AC_{200}$ ) were also in the low single digit

micromolar range (1-3  $\mu$ M) for all three catalytic sites (Fig. 2.2B). Under similar assay conditions, TCH-165 had no effects on the proteolytic activity of doubled capped 20S (26S proteasome, Fig. 2.2C).

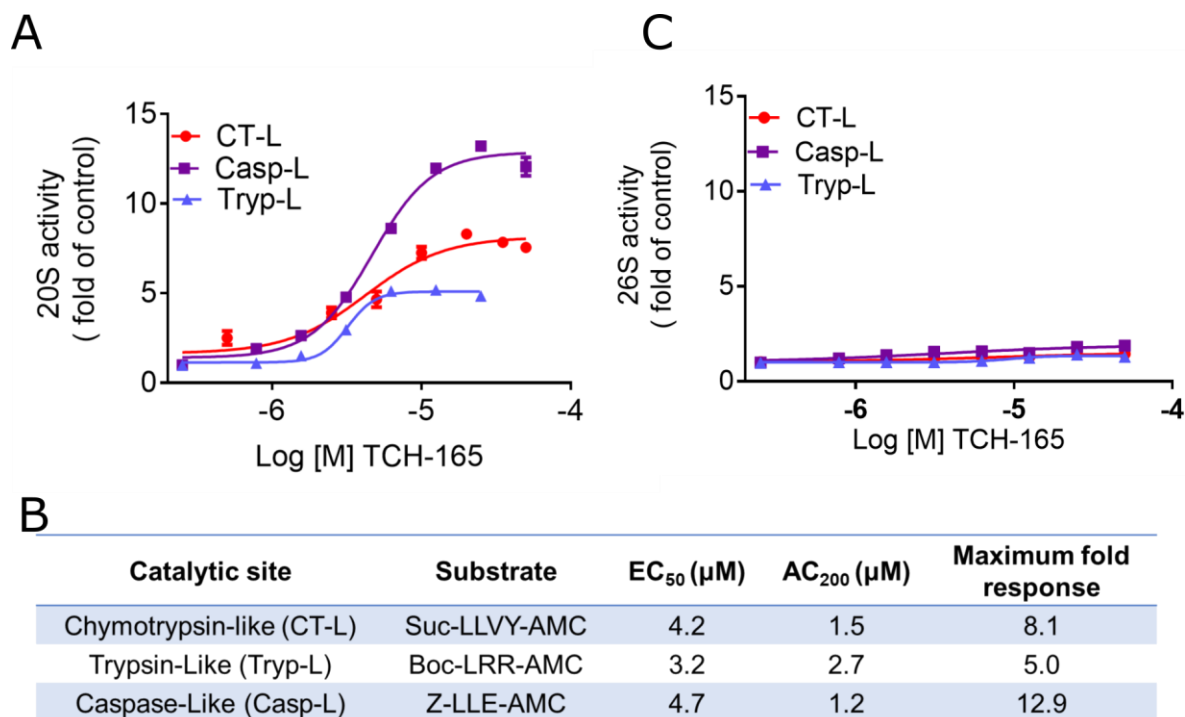


**Figure 2.2: TCH-165 enhances 20S-mediated degradation of peptide substrates.** (A) Concentration–response curve of TCH-165 for 20S. 20S proteasome-mediated proteolysis of the fluorogenic substrates Suc-LLVY-AMC for chymotrypsin-like (CT-L), Boc-LRR-AMC for trypsin-like (Tryp-L), and Z-LLE-AMC for caspase-like (Casp-L) activities. (B) EC<sub>50</sub> values of TCH-165 and maximum fold enhancement of 20S activities. (C) Same as A for 26S proteasome.

### 2.2.2 Imidazolines do not denature the 20S proteasome

The majority of previously reported direct pharmacological activators of the 20S proteasome turned out to have “detergent-like” behavior such as with SDS.<sup>216</sup> In addition to the



standard drug-response saturation curve (Fig. 2.2A, usually bimodal for “SDS-like” molecules), native gel electrophoresis was used to differentiate imidazolines from “SDS-like” proteasome activators. Unlike SDS which activates the proteasome via partial denaturation of the enzyme (Fig. 2.3A), exposure of the 20S proteasome to imidazolines (illustrated with TCH-013) was found not to induce denaturation of the 20S. Denaturation of the 20S is indicated by streaking of the native gel, as the 20S subunits fall apart. Although TCH-013 does not induce partial denaturation on its own (Fig. 2.3A, last 3), combination with SDS (Fig. 2.3A, last lane) appears to boost SDS-induced streaking (a more denatured state of the enzyme). This could explain why combining other imidazolines<sup>234,235</sup> or TCH-013 with SDS results in 20S inhibition (Fig. 2.3B). These data illustrate that imidazolines are different from the SDS-like scaffolds.

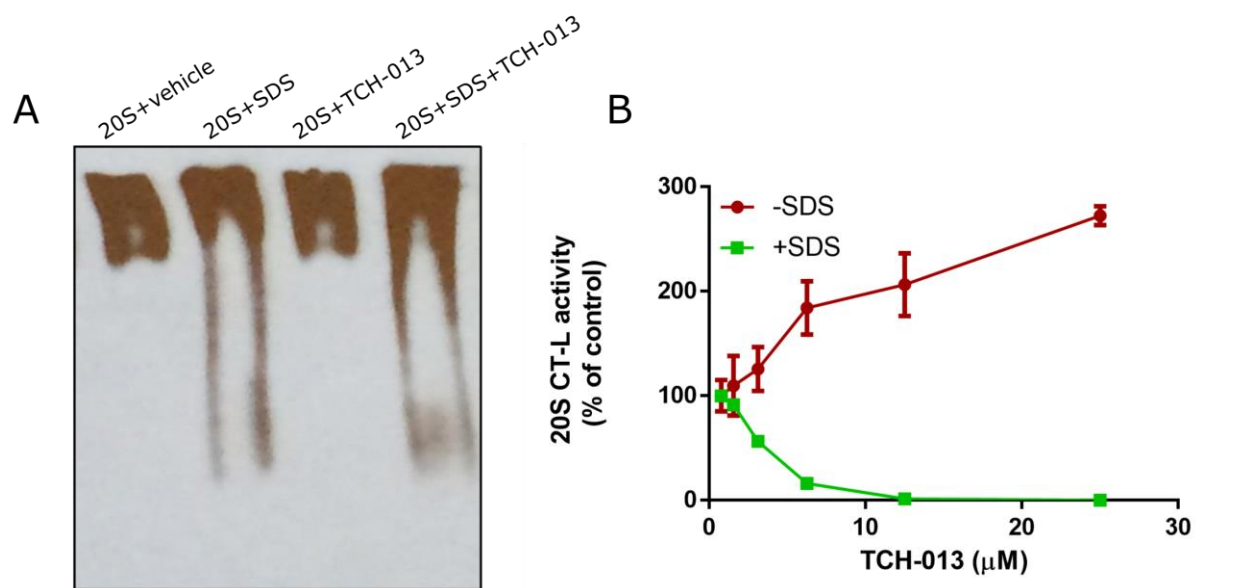


**Figure 2.3: Imidazolines do not denature the 20S proteasome.** (A) Native gel/immunoblot of purified 20S proteasome exposed to vehicle, TCH-013 (10 μM), 0.02 % SDS or combinations for 1h at 37°C. (B) Concentration–response curve of TCH-013 for 20S proteasome-mediated proteolysis of the fluorogenic substrates, Suc-LLVY-AMC, with or without 0.02% SDS.

### 2.2.3 TCH-165 enhances 20S-mediated degradation of tau and $\alpha$ -synuclein

At the start of this project, in 2014, drug discovery in the field of proteasome regulation was more focused on proteasome inhibition. There were no literature guidelines on how to go about validating proteasome activators. My approach was to look at those proteins that have been labelled as ubiquitin-independent 20S proteasome substrates, and study how their degradations were influenced by what we anticipated to be proteasome activators.

Thus, to determine whether the enhanced 20S activity translated to more relevant targets, the ability of TCH-165 to enhance 20S-mediated degradation of the intrinsically disordered 20S proteasome substrates,  $\alpha$ -synuclein ( $\alpha$ -syn)<sup>75,240,241</sup> and tau (tau441)<sup>242,243</sup> were investigated. For these studies, the disordered proteins  $\alpha$ -syn (Fig. 2.4A) or tau (Fig.2.4C) were mixed with the structured protein, GAPDH (non 20S substrate), and treated with purified 20S proteasome in the presence of various concentrations of TCH-165 or bortezomib (BTZ, proteasome inhibitor as negative control)<sup>225</sup> for 1h. The mixture was analyzed for protein degradation by western blot. Figures 2.4B and 2.4D clearly demonstrate that TCH-165 enhanced the degradation of both  $\alpha$ -syn and tau, over vehicle control. Importantly, TCH-165 did not induce the degradation of GAPDH, which is normally not degraded by the 20S (Fig. 2.4A and C, lower panels).

These data demonstrate two important findings; (1) TCH-165 enhances 20S-mediated degradation of IDPs,  $\alpha$ -syn and tau *in vitro*, and (2) TCH-165 does not induce the degradation of structured proteins, such as GAPDH. Furthermore, TCH-165 failed to enhance 26S-mediated degradation of  $\alpha$ -synuclein (Fig. 2.4A, right panel) and tau (Fig. 2.4C, right panel), suggesting a mechanism that is consistent with gate-opening.

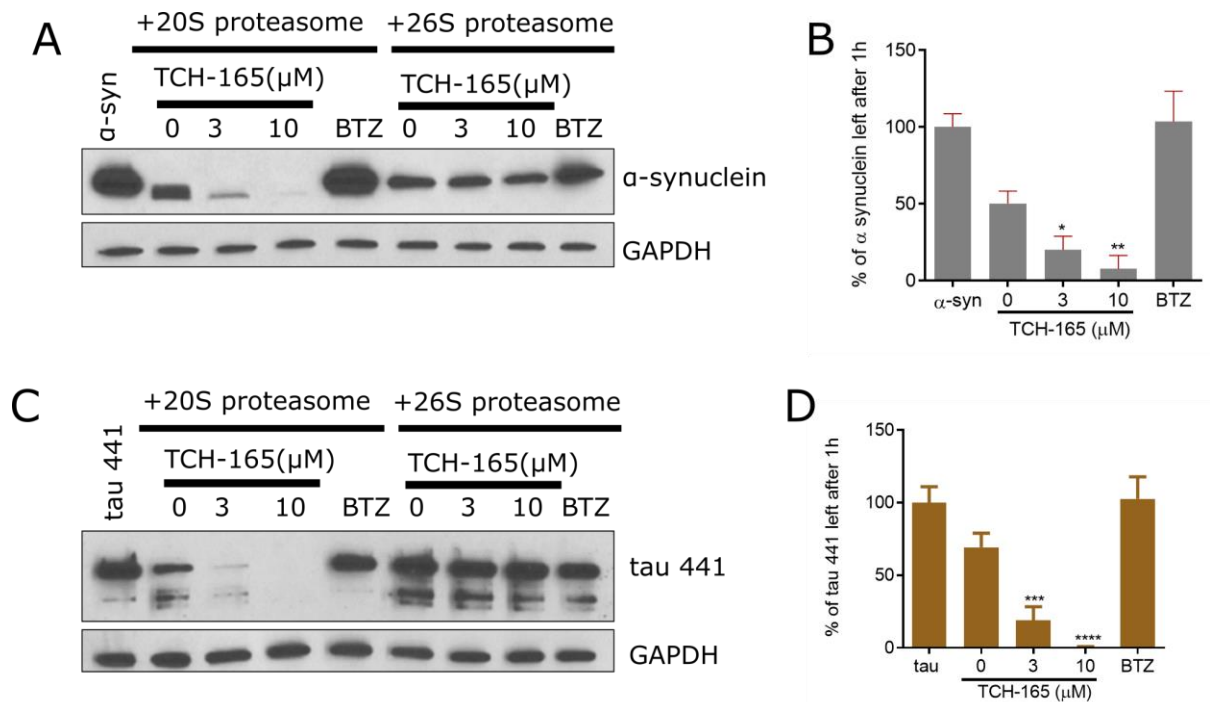


**Figure 2.4: TCH-165 enhances 20S-mediated degradation of tau and  $\alpha$ -synuclein.** (A) Immunoblot of GAPDH and  $\alpha$ -synuclein digestion with the 20S or 26S proteasome pretreated with TCH-165 or the proteasome inhibitor bortezomib (BTZ, 2  $\mu$ M). (B) Quantification of A for 20S-mediated proteolysis (n=4). (C) Same as A but with tau441. (D) Quantification of C for 20S-mediated proteolysis (n=4). Data are presented as mean  $\pm$  SD. (one-way ANOVA; ns, not significant; \* $p < 0.05$ ; \*\* $p < 0.01$ ; \*\*\* $p < 0.001$ , \*\*\*\* $p < 0.0001$ ).

## 2.2.4 TCH-165 stabilizes the open-gate conformation of 20S proteasome

To gain insight into the mechanism of imidazoline-mediated activation of 20S in a single molecule fashion, our collaborator, Prof. Maria Gaczynska used atomic force microscopy (AFM) to study TCH-165 mediated gate-switching dynamics of 20S proteasome. Gently isolated eukaryotic proteasome particles repeatedly scanned and imaged by oscillating (tapping) mode AFM in liquid constantly change between open (pore size of  $\sim 2$  nm in diameter) and closed ( $\sim 0.9$  nm in diameter) forms, with the more stable closed-gate form in about 3:1 molar excess (Fig.

2.5A).<sup>244,245</sup> Examination of more than a hundred single 20S particles in the top-view position revealed a concentration-dependent increase in the open-gate conformers upon treatment with TCH-165, from 28% with vehicle to 59% at 2  $\mu$ M TCH-165 (Fig. 2.5B,  $p < 0.001$  for  $\geq 400$  nM). Like the control, TCH-165 treated particles continuously switched between open and closed conformations. However, unlike the control, the open-gate conformation was more stable in the presence of TCH-165. Since the open-gate conformation is more receptive to substrates, it was anticipated that the enhancement of 20S proteasome activity by TCH-165 was due to stabilization of the open-gate 20S conformation.

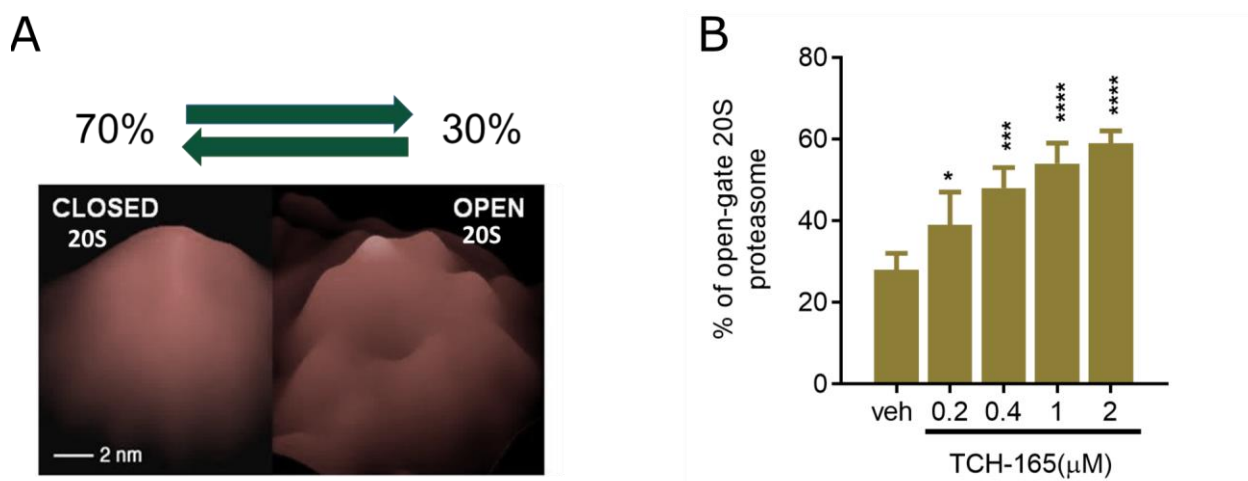


**Figure 2.5: TCH-165 stabilizes the open-gate conformation of 20S proteasome.** (A) AFM images of closed- and open-gate 20S proteasome shown as tilted top-view of standing particles. (B) Ratio of open-gate conformers in populations of the 20S proteasome treated with TCH-165. Data are mean  $\pm$  SD of at least four fields with 120–260 particles per field (one-way ANOVA; \* $p < 0.05$ , \*\* $p < 0.01$ , \*\*\* $p < 0.001$ ).

### 2.2.5 Stabilization of open-gate 20S by TCH-165 may involve interaction with the $\alpha$ -ring

*In silico* docking studies (by Dr. Corey Jones, a former MSU graduate student) were performed to find possible binding sites of TCH-165 that may explain its gate regulation seen in

the AFM studies. Autodock Vina<sup>246</sup> run through PyRx<sup>247</sup> was used to manage the workflow. For these studies, TCH-165 was found to preferentially bind in the  $\alpha 1/\alpha 2$  inter-subunit pocket (Fig. 2.6A). Interestingly, this pocket was also primarily targeted by the phenothiazine-based 20S agonists,<sup>153</sup> which we will find in chapter four to be mechanistically distinct from imidazolines.

The  $\alpha 1/\alpha 2$  inter-subunit pocket is known to bind the C-terminal Hb-Y-X-motif of the Rpt3 peptide of the 19S cap (Fig. 2.6B).<sup>248,249</sup> In a competition experiment by Prof. Maria Gaczynska, the Rpt3 peptide, which normally binds to the  $\alpha$ -ring without activating the proteasome on its own,<sup>249</sup> was found to inhibit TCH-165 enhancement of 20S activity by approximately 30% (Fig. 2.6C). Although these data indicate that the interaction of the Rpt3 peptide with the  $\alpha$ -ring prevents 20S activation by TCH-165, it does not necessarily dictate pocket selectivity as higher concentrations of Rpt3 could not overcome TCH-165 activity any further. Consistent with the possibility of more than one binding pocket, I also observed that the Rpt5 peptide which normally binds in the  $\alpha 5/\alpha 6$  inter-subunit pocket significantly reduced the ability of TCH-165 to enhance 20S activity (Fig. 2.6D). While this observation is consistent with competition, it does not necessarily preclude negative allosteric modulation. To further examine the role of the  $\alpha$ -ring, the immunoproteasome (i20S), the yeast proteasome and the *Mycobacterium tuberculosis* proteasome (*Mtb*20S) were evaluated for activation by TCH-165. The i20S has an identical  $\alpha$ -ring to the constitutive 20S CP, but incorporates the structurally distinct catalytic subunits LMP7, MECL1 and LMP2, instead of  $\beta 5$ ,  $\beta 2$  and  $\beta 1$ , in its core.<sup>45,46</sup> The yeast proteasome is very similar to the human 20S proteasome but has significant topological differences in the subunits of the  $\alpha$ -ring.<sup>250,251</sup> In contrast, the *Mtb*20S proteasome has an  $\alpha$ -ring comprised of 7 identical subunits ( $\alpha 1$ - $\alpha 7$ ) and exhibits a very different  $\alpha$ -ring topology.<sup>252</sup>

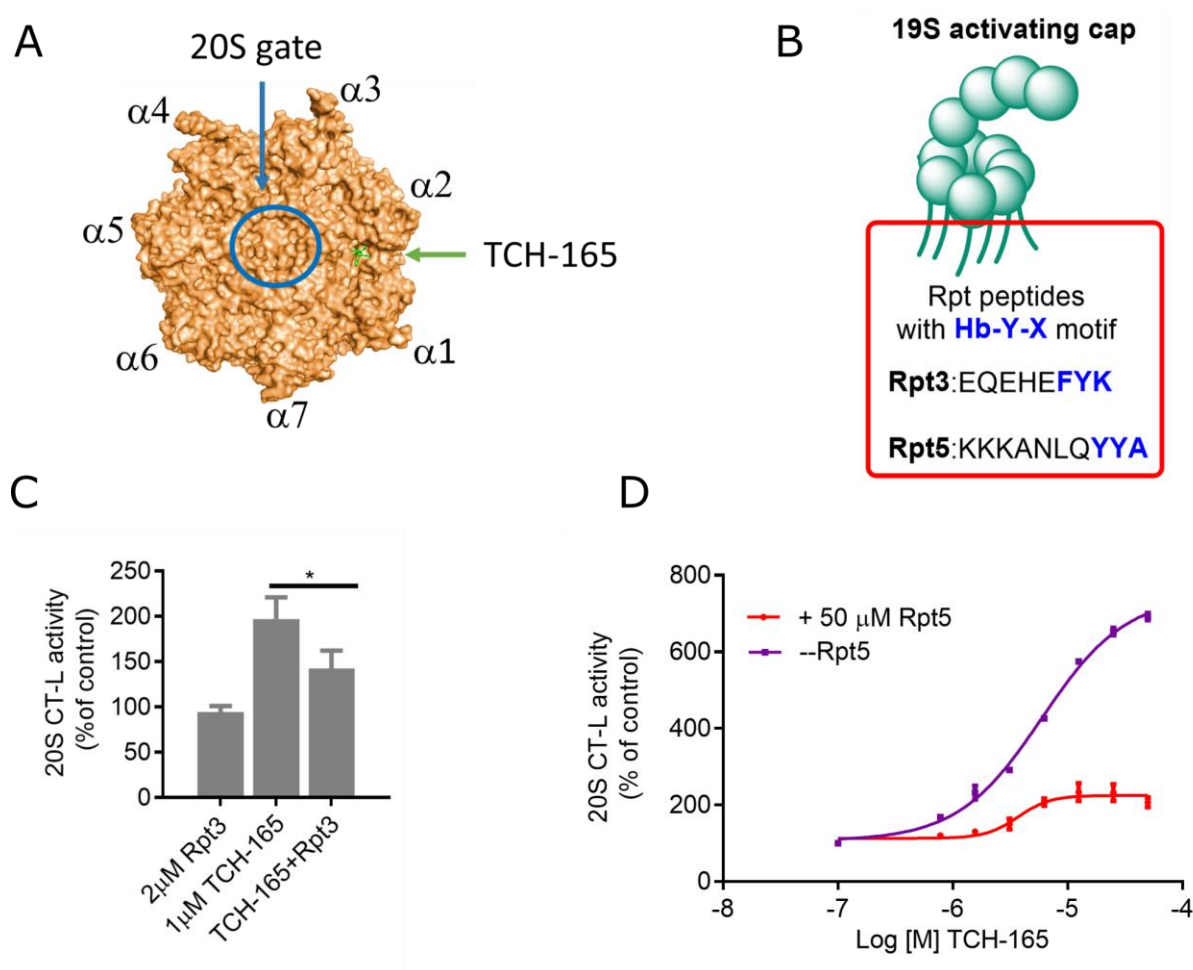
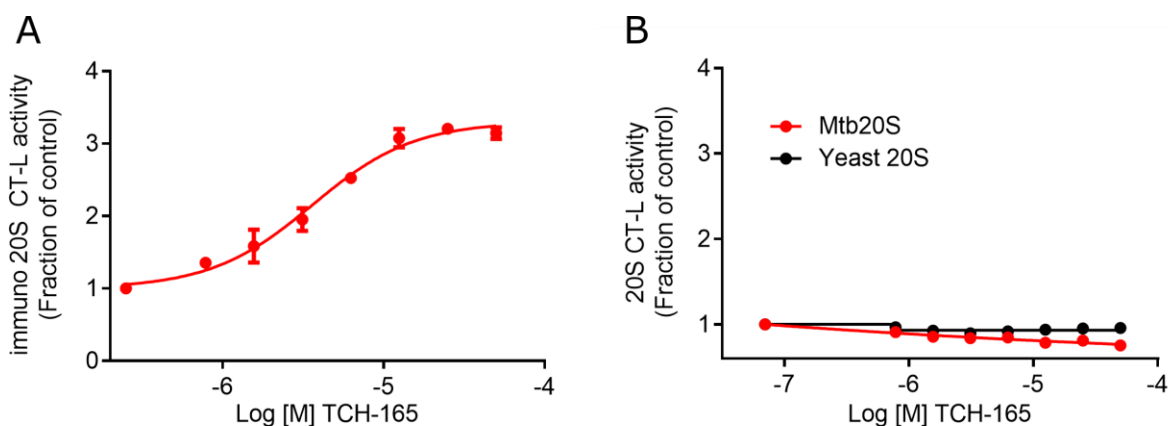


**Figure 2.6: Stabilization of open-gate 20S by TCH-165 may involve interaction with the  $\alpha$ -ring.** (A) Top view of the  $\alpha$ -ring showing the preferred docking site utilizing Autodock Vina, with TCH-165 in the  $\alpha1/\alpha2$  inter-subunit binding pocket of the 20S proteasome. (B) Cartoon of the 19S regulatory particle (RP) showing the Rpt peptides with Hb-Y-X motif. (C) TCH-165 competition experiment with the Rpt3 peptide (which normally binds in the  $\alpha1/\alpha2$  pocket) for 20S proteolysis ( $n = 3$ ,  $*p < 0.05$ ). (D) TCH-165 competition experiment with the Rpt5 peptide (which normally binds in the  $\alpha5/\alpha6$  pocket and enhances 20S-mediated proteolysis) for 20S proteolysis.

Analogous to the constitutive 20S, TCH-165 was capable of enhancing the proteolytic activity of the i20S by more than 3-fold (Fig. 2.7A). However, TCH-165 was unable to enhance

the activity of the yeast or *Mtb*20S proteasome (Fig. 2.7B). These data confirm the significance of  $\alpha$ -ring topology in the mechanism of action of TCH-165. Consistent with these observations, TCH-165 was unable to enhance 26S proteasome mediated-proteolysis of fluorescent peptides (Fig. 2.2C) or disordered proteins (Fig. 2.4A and C; right panel).

This suggests that blocking the  $\alpha$ -rings with two 19S RP as in the fully assembled 26S proteasome prevented TCH-165 from binding on the  $\alpha$ -ring and enhancing proteolysis. The activity of TCH-165-treated 20S was higher than that of equimolar 26S proteasome in these assays. This suggest that the lack of enhancement of 26S activity by TCH-165 was not due to maximum activity of the core enzyme of 26S, but likely a consequence of the TCH-165 binding site being occupied by the 19S caps. Collectively, these data are consistent with interaction of TCH-165 with the  $\alpha$ -ring of the 20S proteasome.




---

**Figure 2.7: The activity of TCH-165 requires specific interaction with the  $\alpha$ -ring of the human 20S proteasome. (A) Concentration–response curve of TCH-165 for the hydrolysis of Suc-LLVY-AMC by the human immunoproteasome (i20S) and (B) by the yeast and *Mtb*20S.**

---

### 2.2.6 TCH-165 enhances the degradation of cancer-associated IDPs in cell culture

To be more useful, the activity of these molecules must translate in a more complex system. Using AMC-labelled peptide substrate, the ability of TCH-165 to enhance cellular proteasome activity was first evaluated in cell lysates from cells treated with either vehicle, TCH-165 or the proteasome inhibitor, epoxomicin, for 12h. In this study, TCH-165 increased cellular proteasome activity by more than 50%, at 10  $\mu$ M (Fig. 2.8A). Given the anti-tumor efficacy of the parent imidazoline (TCH-013),<sup>234</sup> attention was paid to IDPs that are often overexpressed in certain cancers. For these studies, TCH-165 was tested in HEK-293T cells expressing ornithine decarboxylase1 (ODC), tagged with the green fluorescent protein spark (GFPSpark) on its N-terminal. GFPSpark is a structured protein of ~25 kDa. It folds faster than GFP and is not degraded by the 20S. Meanwhile, the disordered C-terminal of ODC is a well-known 20S substrate,<sup>76</sup> and the most studied, before the recent identification of numerous IDPs regulated by the 20S proteasome. Thus, 20S agonists would enhance the C-terminal degradation of the GFPSpark-ODC fusion protein (75 kDa), but not GFP, resulting in a band-shift that can be detected by western blot using an anti-GFP antibody (Fig. 2.8B). Cells were cultured with TCH-165 for 24h after which the lysates were immunoblotted with anti-GFP (Fig. 2.8C and D). Cycloheximide was used to ensure changes were occurring at the post-translational level. Fig. 2.8C shows that TCH-165 enhanced the cleavage of ODC, but not the structured GFP, resulting in free GFPSpark (25 kDa) and the GFPSpark-ODC fragments (~50kDa). Importantly, the TCH-165-enhanced proteolytic degradation was blocked by bortezomib (Fig. 2.8D). This suggested that the proteasome is likely



the main enzyme responsible for TCH-165 enhancement of ODC degradation.

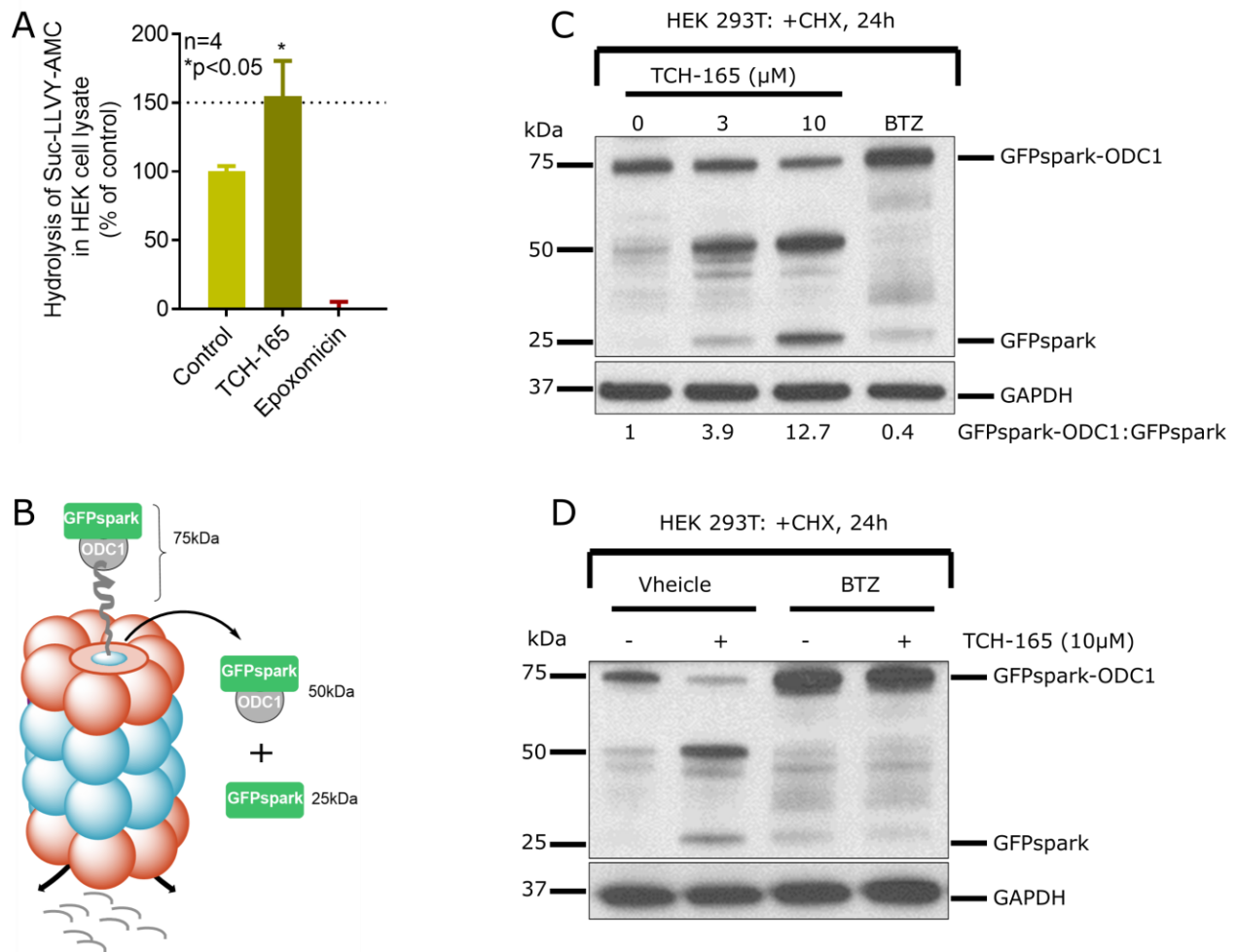


**Figure 2.8: TCH-165 increases proteasome activity in cell culture.** (A) Hydrolysis of Suc-LLVY-AMC peptide in HEK cell lysates from cells treated with vehicle (DMSO), TCH-165 (10  $\mu$ M), or epoxomicin (1  $\mu$ M) for 12h. (B) Predictive schematic of ODC-GFPspark degradation by the 20S proteasome. (C) HEK cells stably expressing GFPspark-ODC were treated with TCH-165 (0, 3, and 10  $\mu$ M) or bortezomib (BTZ, 3  $\mu$ M) with cycloheximide (50  $\mu$ g/mL) for 24h, and cell lysates immunoblotted with anti-GFP. (D) Immunoblot of cell lysates from HEK cells (stably expressing GFPspark-ODC) treated with cycloheximide (50  $\mu$ g/mL) and either vehicle, TCH-165 (10  $\mu$ M), BTZ (3  $\mu$ M), or a combination of TCH-165 and BTZ for 24h.

The proto-oncoprotein c-Fos is mostly disordered (Fig. 2.9A).<sup>253</sup> Similar to ODC, c-Fos is targeted for degradation by the 26S proteasome in a ubiquitin-dependent manner, but the bulk of its degradation is mediated by the ubiquitin-independent 20S proteasome.<sup>254–256</sup>

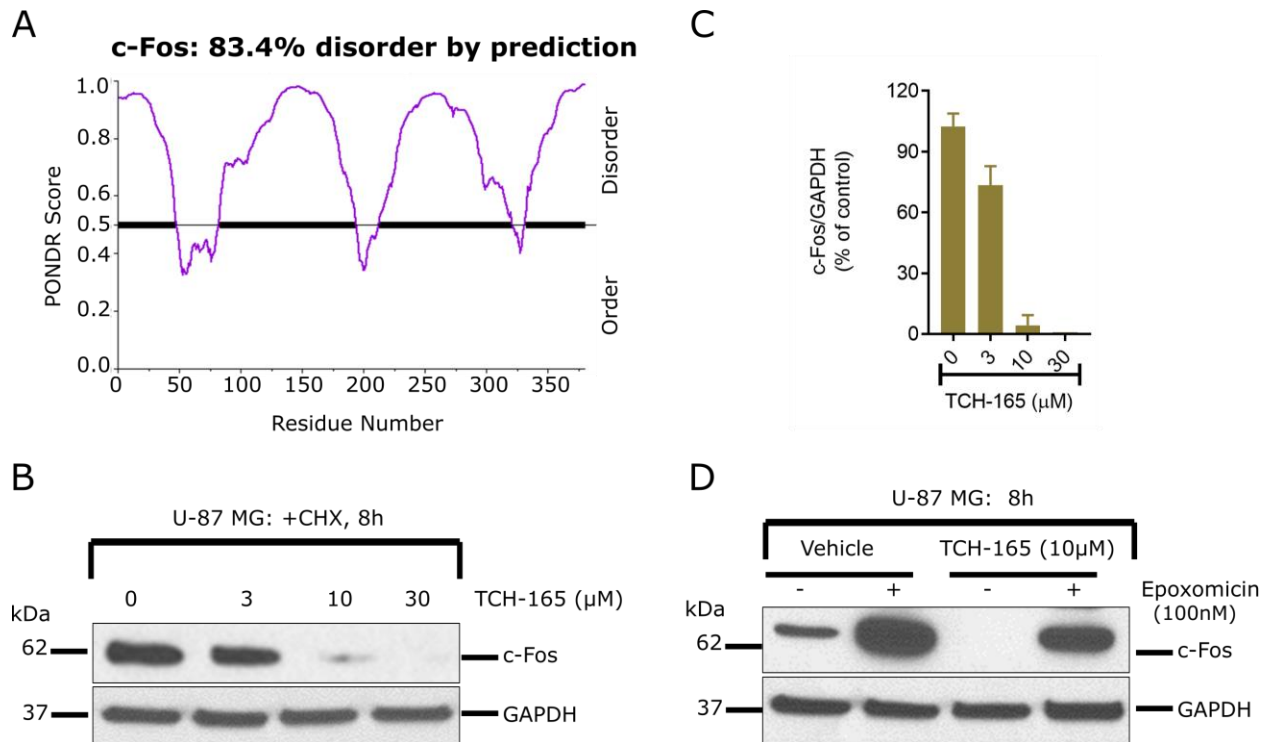


**Figure 2.9: TCH-165 enhances 20S-mediated degradation of c-Fos in a glioblastoma cell line.**

(A) Intrinsic disorder in c-Fos as predicted with POND VSL2 software. (B) Glioblastoma cells (U-87 MG) were treated with TCH-165 (0, 3, 10, or 30 μM) for 8h (with 50 μg/mL) and immunoblotted with anti-c-Fos or anti-GAPDH. (C) Densitometry of F using image J software (n=2). (D) Glioblastoma cells (U-87 MG) were treated with the vehicle or TCH-165 (10 μM) in combination with or without epoxomicin (100 nM) for 8 h and immunoblotted with anti c-Fos and GAPDH as loading control.

Overexpression of c-Fos is associated with increased membrane biogenesis and poor prognosis in glioblastoma multiforme,<sup>111,118,257</sup> a malignant tumor of glial (brain supporting)

cells.<sup>115</sup> Furthermore, due to its involvement in c-Fos/c-Jun AP-1 mediated expression of pro-inflammatory cytokines, the pharmacological regulation of c-Fos may have therapeutic implications in the treatment of intervertebral disk degeneration and rheumatoid arthritis.<sup>258,259</sup> Considering the role of c-Fos in glioblastoma,<sup>111,118,257</sup> the effects of TCH-165 on c-Fos degradation was evaluated in the glioblastoma cell line, U-87 MG. Treatment of U-87 MG cells with TCH-165 for 8h resulted in a significant concentration dependent reduction of c-Fos levels (Fig. 2.9B and C). The reduction in c-Fos protein levels in cycloheximide treated cells confirms that the c-Fos reduction is at the post-translation level and not due to changes in protein synthesis. Furthermore, the enhanced degradation of c-Fos by TCH-165 was blocked by the selective proteasome inhibitor epoxomicin (100 nM), confirming the proteasome as the main enzyme involved in TCH-165-enhanced degradation of c-Fos (Fig. 2.9D).

c-Myc is a short-lived (half-life of ~30 minutes)<sup>260</sup> intrinsically disorder protein (Fig. 2.10A) known to drive poor prognosis in blood cancers such as multiple myeloma<sup>106,109</sup> and acute lymphoblastic leukemia.<sup>110</sup> Thus, targeting c-Myc through enhanced proteasomal degradation could be of therapeutic benefit in these cancers. As such, the ability of TCH-165 to enhance c-Myc degradation was also evaluated in an acute lymphoblastic leukemia cell line (CCRF-CEM) and in a multiple myeloma cell line (RPMI 8226). After 4h of treatment, TCH-165 was found to rapidly enhance the degradation of c-Myc in both cell lines (Fig. 2.10B). Again, this degradation was blocked by the proteasome inhibitor, bortezomib (BTZ). Furthermore, the effect of TCH-165 on c-Myc degradation in CEM cells was found to be concentration dependent (Fig. 2.10C and D). These data show that TCH-165 enhances the proteasomal degradation of cancer-driving IDPs; ODC1, c-Fos and c-Myc over structured proteins in cell culture.

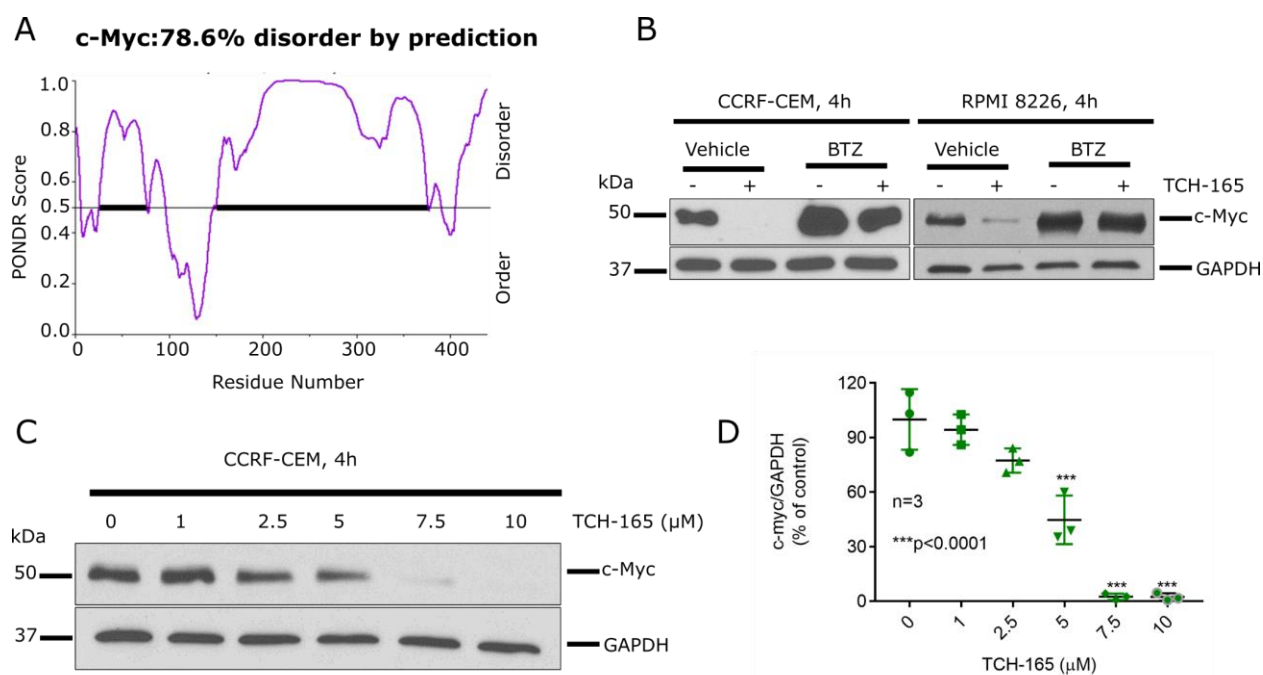


**Figure 2.10: TCH-165 enhances 20S-mediated degradation of c-Myc in a multiple myeloma (RPMI-8226) and an acute lymphoblastic leukemia (CCRF-CEM) cell lines. (A)** Intrinsic disorder in c-Myc as predicted with PONDR VSL2 software. **(B)** CEM (10μM TCH-165) and RPMI (5μM TCH-165) cells were treated with either vehicle, TCH-165, Bortezomib (BTZ, 5μM) or combinations for 4h. Cell lysate were immunoblotted for c-Myc and GAPDH. **(C)** CEM cells were treated with different concentrations of TCH-165 and lysates immunoblotted for c-Myc and GAPDH. **(L)** Densitometry of C using image J software.

## 2.2.7 TCH-165 inhibits 26S assembly in cell culture

Endogenous proteasome activators, including PA28αβ, PA28γ and Bln10, compete with the 19S RP for binding to the 20S CP.<sup>32,33,41</sup> Enhanced degradation of intrinsically disordered proteins by TCH-165 can be a result of increased enzymatic activity of the 20S, increased amount of free 20S through competition with the 19S caps or a combination of both effects. To examine the role of small molecule 20S activator in 19S-20S binding, changes in the distribution of

proteasome sub-complexes were examined. HEK293T cells were treated with vehicle and various concentrations of TCH-165 for 24h after which cell lysates were resolved on a native gel and immunoblotted for proteasome sub-complexes using anti- $\beta 5$  or anti-Rpt1. Remarkably, the immunoblot revealed a concentration-dependent decrease in the amount of fully assembled 26S proteasome (19S-20S-19S) and single capped proteasome (19S-20S, Fig. 2.11A and B). This was accompanied by a concentration-dependent increase in the levels of free 19S and 20S proteasomes. No changes were observed in the levels of individual subunits ( $\beta 5$  of the 20S core and Rpt1 of the 19S cap, Fig. 2.11A, lower panel). This suggests that changes in the level of 26S and 20S were not occurring at the transcriptional/translational levels but are likely due to a shift in the equilibrium between free 20S CP and assembled 26S proteasome particles.

Considering the decrease in the amount of fully assembled 26S proteasome, clearance of ubiquitinated proteins was also evaluated. Fig. 2.11A, middle panel shows that the level of K-48 ubiquitinated proteins remains largely the same at  $\leq 10 \mu\text{M}$  TCH-165. As anticipated, only when there are no 19S capped proteasome present (i.e. 19S-20S-19S and 19S-20S), do ubiquitinated substrates start to accumulate. These data illustrate that the single capped 20S proteasome (i.e. 19S-20S) is still fully capable of processing ubiquitinated proteins, and perhaps even more efficiently than double capped. Thus, at low or intermediate concentrations ( $\leq 10 \mu\text{M}$ ), TCH-165 does not induce the accumulation of ubiquitinated proteins. This implies that as long as single capped proteasome complexes (19S-20S) remain present in the cells, the ubiquitin-independent 20S proteasome pathway could be active without significantly affecting the processing of ubiquitinated substrates.

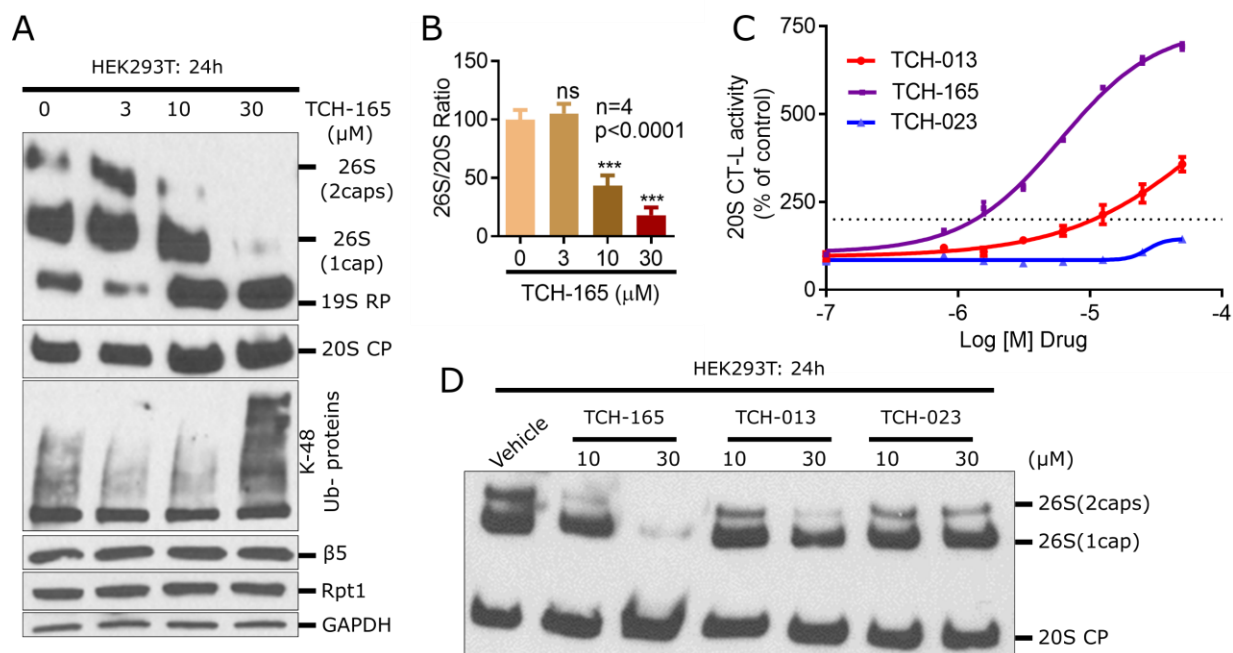


**Figure 2.11: TCH-165 inhibits the assembly of 26S proteasome in cell culture.** (A) HEK293T cells treated with the vehicle or TCH-165 (3, 10, and 30 μM) for 24h were immunoblotted for proteasome subcomplexes following native PAGE with anti-Rpt1 (top part) and anti β5 (the 20S CP section). Proteasome subunits (β5 and Rpt1), k-48 linked ubiquitinated proteins and GAPDH (loading control) were also immunoblotted after SDS-PAGE. (B) Densitometry of (A) presented as a ratio of 26S to 20S proteasome. (C) Hydrolysis of Suc-LLVY-AMC by 20S proteasome treated with different concentrations of TCH-165, TCH-013 or TCH-165. (D) HEK293T cells treated with the vehicle, TCH-165 (10 and 30 μM), TCH-013 (10 and 30 μM) or TCH-023 (10 and 30 μM) for 24h were immunoblotted for proteasome subcomplexes following native PAGE, with anti- β5 antibody.

To further evaluate the relationship between 20S activation and 26S assembly, three imidazolines with different potency in the 20S peptide assay (Fig. 2.11C) were assessed for their abilities to interfere with 26S assembly in HEK29T cells. As shown in Fig. 2.11D, the potencies

of these imidazolines directly correlates with inhibition of 26S assembly. This further supports the hypothesis that decreased levels of 26S might be as a result of TCH-165 competing with the 19S for binding in the alpha ring of the 20S proteasome, because the inactive analogue was consistently found to be weakly bound in the  $\alpha$ -ring (*in silico* docking).

### **2.2.8 TCH-165 forms a hybrid with single capped 20S proteasome**

Considering the reduction in K-48 ubiquitinated proteins at  $\leq 10 \mu\text{M}$  TCH-165 (comparing lane 1-3 of Fig. 2.11A), where there is still a remnant of single and double capped 20S, I was curious to find out if TCH-165 can form a hybrid with single capped 20S (TCH165-20S-19S) that could contribute to the enhanced clearance of ubiquitinated proteins. Unfortunately, *in vitro* proteasome purification cannot completely separate single and double capped 20S. Thus, to test this hypothesis, individual proteasome subcomplexes were obtained by resolving untreated HEK293T cell lysate on a native gel and an in-gel proteasome activation assayed performed with TCH-165, as shown in Fig. 2.12A. Each gel was split into two halves and exposed to the vehicle or 20  $\mu\text{M}$  TCH-165 containing buffer, with or without  $\text{MgCl}_2/\text{ATP}$ . In the presence of  $\text{MgCl}_2/\text{ATP}$  (Fig. 2.12B), all proteasome subcomplexes can hydrolyze the CT-L peptide substrate, Suc-LLVY-AMC. Under this condition, only the activity of free 20S is significantly affected by TCH-165. In the absence of  $\text{MgCl}_2/\text{ATP}$ , the double capped 20S (19S-20S-19S) cannot hydrolyze substrates (Fig. 2.12C), since ATP is required for 20S gate opening. However, peptide substrate can still be degraded by the single capped 20S (19S-20S), and this was found to be enhanced by about 50% in the presence of TCH-165. Note that, in the absence of  $\text{MgCl}_2/\text{ATP}$  the activity of the 26S complexes is relatively low. Thus, by the time the 26S activity became detectable, the 20S activity for both vehicle and TCH-165 were already saturated. Therefore, the effect of TCH-165 on 20S is not very apparent in Fig. 2.12C. Western blot analysis

using anti- $\beta 5$  indicates equal loading for the proteasome subcomplexes (Fig. 2.12D). These data suggest that TCH-165 is likely to boost the activity of both free and single capped 20S proteasome in the cell.

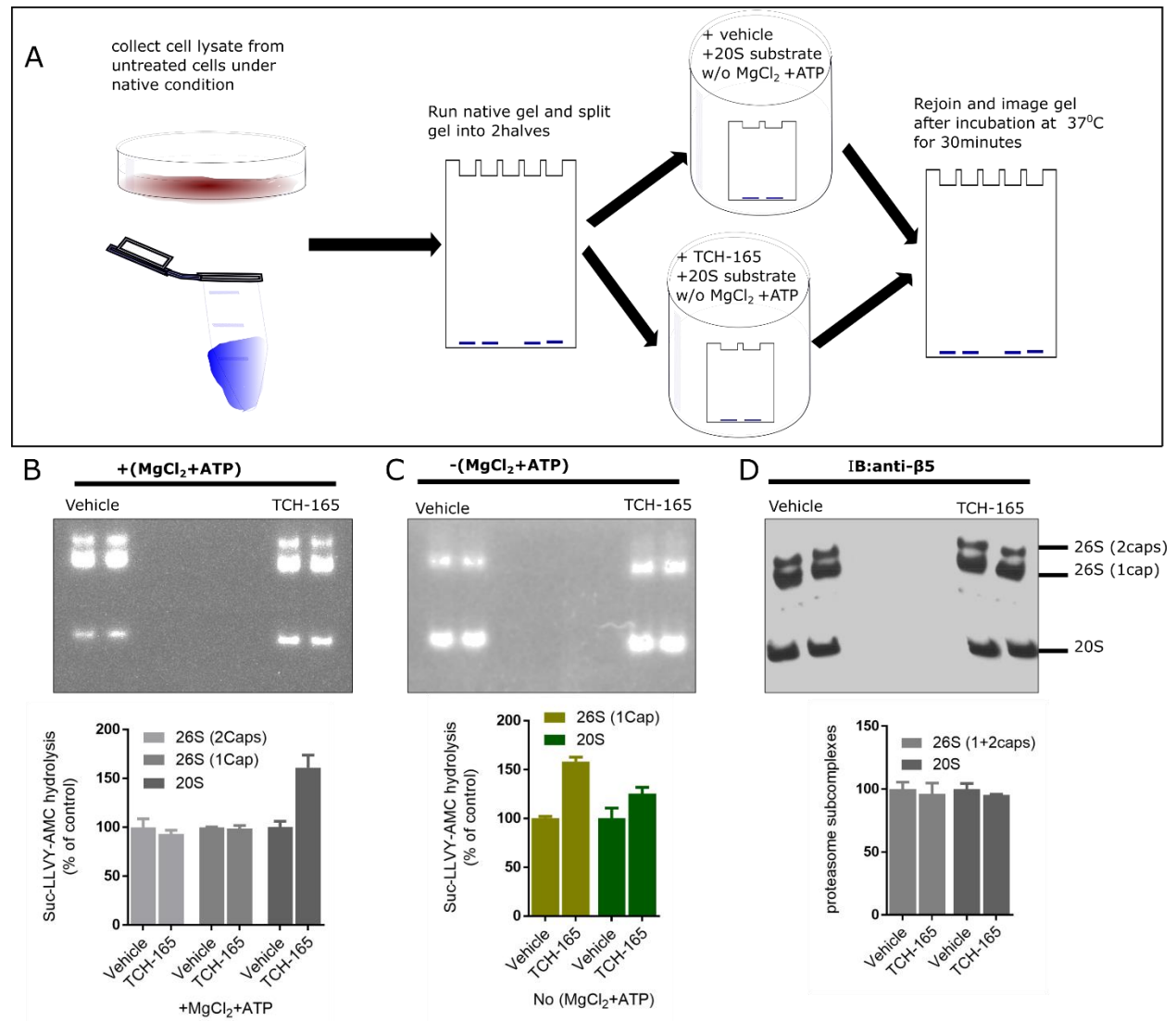


**Figure 2.12: In-gel activation of single capped 20S proteasome: (A)** Schematic of experimental setup. **(B)** Proteasome native gel and densitometry showing activity of different proteasome subcomplexes following in-gel exposure to vehicle or TCH-165 (20  $\mu M$ ) and Suc-LLVY-AMC, with and **(C)** without  $MgCl_2$ /ATP. **(D)** Immunoblot with anti- $\beta 5$  (a 20S subunit) and densitometry showing equal loading of samples.



### 2.2.9 Imidazolines do not induce oxidative stress in cells

Under conditions of oxidative stress, the 26S disassembles into its 19S and 20S subcomplexes.<sup>261</sup> The 20S is more stable under oxidative stress, and is therefore responsible for the clearance of oxidatively damaged proteins.<sup>124,262</sup> To ensure that the activity of imidazolines on 26S proteasome assembly were directly linked to interaction with the 20S, the production of reactive oxygen species (ROS) following treatment with imidazolines or menadione (a redox cycler, as positive control) was quantified using 2',7'-dichlorofluorescein diacetate. Unlike menadione, neither TCH-165 nor TCH-023 significantly changed cellular ROS levels (Fig. 2.13).

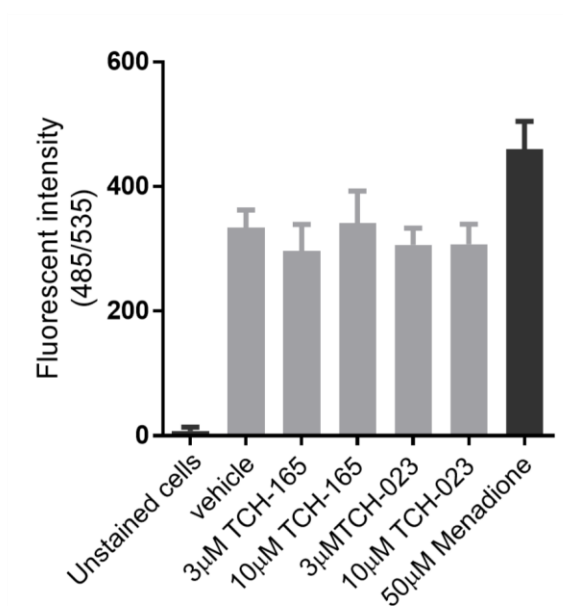


**Figure 2.13: Imidazolines do not induce oxidative stress in cells.** U-87 MG cells were treated with the indicated compounds for 12h and 2',7'-dichlorofluorescein diacetate (DCFDA) added at 2x final concentration (50 µM final) in medium. Cells were incubated for a further 45 minutes under cell culture conditions and fluorescence taken at 485/535 nm.

### 2.2.10 TCH-165 is effective against established and primary cancer cells

The parent imidazoline, TCH-013 was previously reported to be effective in different cancer cell lines and in a tumor model of multiple myeloma.<sup>234</sup> Thus, the efficacy of the optimized analogue was tested in different cancer cell lines. TCH-165 was found to be effective against CCR-CEM and RPMI-8226 as well as U-87 MG cells with low single digit micromolar potency (Fig. 2.14A and B). Interestingly, the Active Concentration at which TCH-165 doubles (200%) proteasome activity was similar to the effective concentration (CC<sub>50</sub>) of TCH-165 (1-3 $\mu$ M) against these cancer cells.

One of the biggest challenges with multiple myeloma (MM) treatment is the fact that most patients are inherently resistant to bortezomib (refractory),<sup>230</sup> the standard of care. Therefore, overcoming intrinsic resistance as well as bortezomib-induced resistance is a critical component of new therapeutic approaches targeting MM. In this effort, we collaborated with Dr. Daniel Isaac, Dr. Omar Alkharabsheh, and Dr. Anas Al-Janadi at the MSU Breslin Cancer Center who provided me with bone marrow aspirates from newly diagnosed and bortezomib refractory (intrinsic resistance to bortezomib) patients. MM cells were then isolated from these samples by CD138+ enrichment and evaluated for vulnerability to TCH-165 treatment. Consistently, and unlike the cells from a newly diagnosed patient, cells from the refractory patient was insensitive to bortezomib treatment (Fig. 2.14D and E). However, TCH-165 was effective against both primary samples, although with lower potency against the refractory patient (Fig. 2.14C and E). Additional samples from larger population groups will need to be considered to determine whether activation of the 20S proteasome is effective in refractory patients, in general, and whether this efficacy is related to c-Myc degradation.

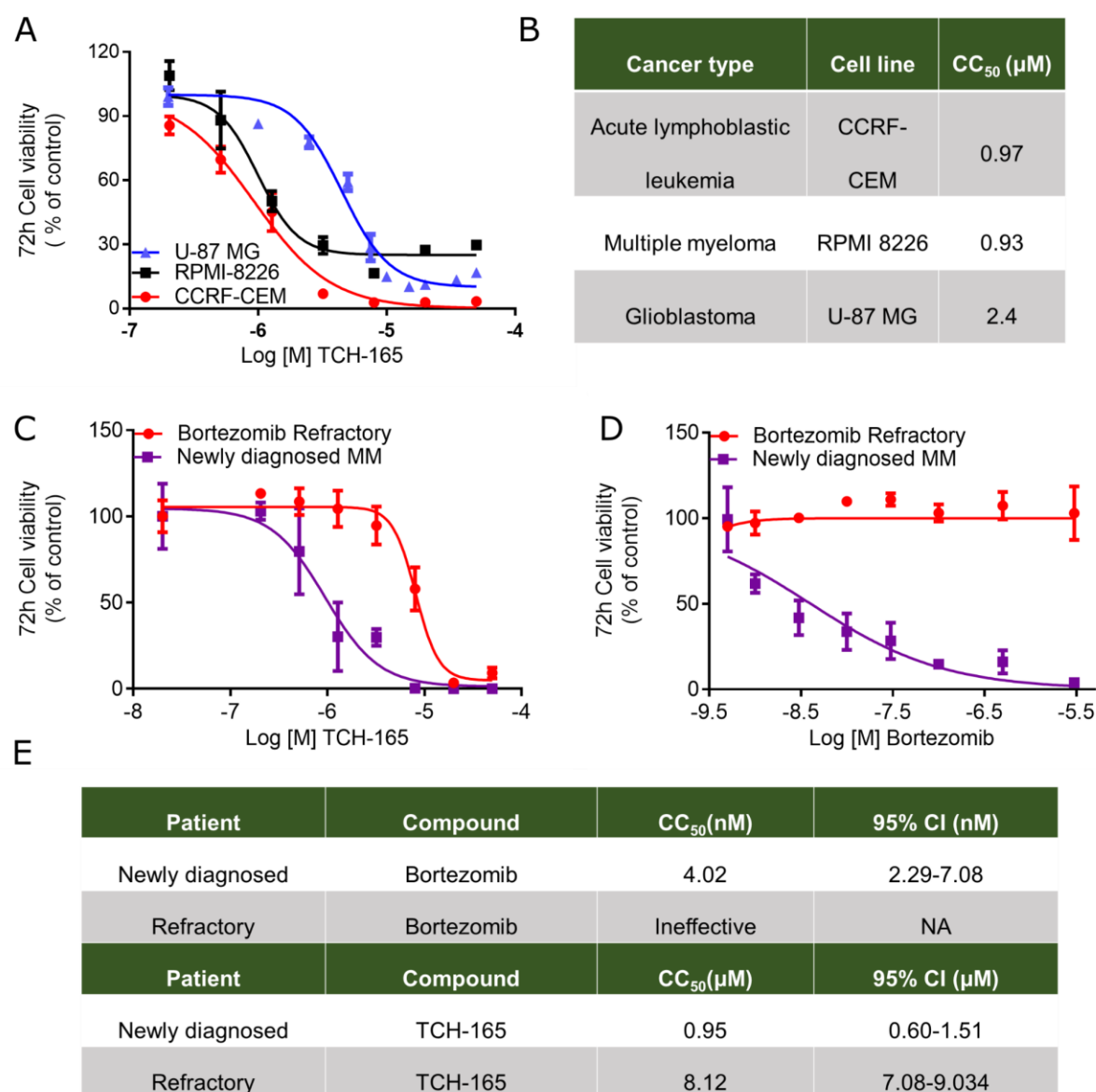


**Figure 2.14: TCH-165 is effective against established and primary cancer cells.** (A) CEM, RPMI or U-87 MG cells were treated with different concentrations of TCH-165 for 72h and assayed for viability by measuring ATP content. (B) Concentrations of TCH-165 required to inhibit cell proliferation by 50% (CC<sub>50</sub>) in CEM, RPMI and U-87MG cells. (C) Same as A for cells obtained from multiple myeloma patients. (D) same as C with bortezomib (E) Same as B for the primary cells.

## 2.3 Conclusions

In summary, TCH-165 was found to induce an opened-gate, active 20S conformation. This proteolytically hyperactive 20S proteasome CPs translates into enhanced degradation of intrinsically disordered proteins (IDPs), but not structured proteins, in biochemical and cellular assays. Furthermore, this active 20S conformation failed to assemble into 26S complex, probably due to competition with the 19S cap as predicted by *in silico* docking and supported by biochemical assays. In cells, the clearance of ubiquitinated proteins was largely maintained at a concentration of TCH-165 ( $\leq 10 \mu\text{M}$ ) sufficient for enhanced clearance of IDPs. This implies that the activity of the 20S proteasome could be boosted without inhibiting 26S-mediated proteolysis. From this work, the following contributions were made:

1. Demonstration of a clearer understanding of how imidazolines regulate proteasome activity.
2. Identification of new vulnerability for IDP-driven cancers and other proteostasis disorders.
3. Support for the possibility of targeting multiple myeloma through enhancement of 20S-mediated proteolysis of IDPs such as c-Myc.

## **CHAPTER THREE**

### **The Role of 20S Proteasome in Autophagy Regulation: A Small Molecule-Driven Mechanistic Investigation**

Reproduced in part with permission from **Njomen Evert** and Tepe J. Jetze. Regulation of Autophagic Flux by the 20S Proteasome. *Cell Chemical Biology* **2019**, 26, 1-12. Copyright 2019 Elsevier Ltd.

## 3.1 Introduction

### 3.1.1 Background

Cellular protein degradation is a shared affair of both the proteasome and the autophagy pathways.<sup>20,263</sup> Cross communications among components of the two pathways are crucial in keeping cellular processes in check. After establishing that the imidazoline, TCH-165, activates the 20S proteasome and can selectively control the degradation of IDPs, I wanted to assess the role of proteasome activation in autophagy-mediated proteolysis. The goal is that a clearer understanding of how regulation of one proteolytic system influences the other will provide better judgment in developing proteolysis targeted therapeutics.

The proteasome targets the degradation of mostly membrane,<sup>264,265</sup> soluble nuclear and cytosolic proteins<sup>240,260,266</sup> whereas the autophagy pathway enables cells to degrade protein complexes, protein aggregates and cellular organelles in a lysosome-dependent mechanism.<sup>267</sup> Shuttle proteins recognize ubiquitinated substrates and direct them towards either or both degradation pathways. For example, lysine-48 (K-48)-linked polyubiquitinated substrates are preferentially directed to the 26S proteasome by UB-associated (UBA)-Ub-Like (UBL) shuttling proteins, while p62/SQSTM-1 and neighbor of BRCA1 (NBR1) shuttle K-63-linked polyubiquitinated substrates to autophagic vacuoles.<sup>20</sup>

Autophagy is an intracellular lysosome-dependent degradation pathway characterized by the formation of an autophagosome.<sup>241,268,269</sup> In the initial step, an isolated membrane forms through specific autophagy effectors such as the microtubules-associated protein light chain 3 (LC3) that engulfs its targeted protein aggregates or damaged organelles. Elongation and closure of the crescent-shaped structure (phagophore) forms the autophagosome. The autophagosome then fuses with the lysosome to form the autolysosome. The fusion step is regulated by various

soluble *N*-ethylmaleimide-sensitive factor activating protein receptor (SNARE) proteins.<sup>270</sup> During this process, the Qa soluble *N*-ethylmaleimide-sensitive factor attachment protein receptor (Qa-SNARE), syntaxin 17 (STX17), is only recruited to completed autophagosome membrane (most likely from the cytosol) by immunity-related GTPase M (IRGM).<sup>271</sup> STX17 then binds to its interacting partner SNAREs, snaptosomal-associated protein 29 (SNAP29, a Qbc-SNARE) and vesicle-associated membrane protein 8 (VAMP8, an R-SNARE) and promote autophagosome-lysosome fusion (Fig. 3.1).<sup>270</sup> Components of the homotypic fusion and protein sorting (HOPS)–tethering complex, vacuolar protein sorting 33A (VPS33A), VPS16, and VPS39 also assist in autophagosome-lysosome fusion, through interactions with STX17. Upon fusion, several hydrolases act as endopeptidases under the highly acidic condition (pH 4.5-5.0) of the autolysosome to degrade the cargo.<sup>272</sup>

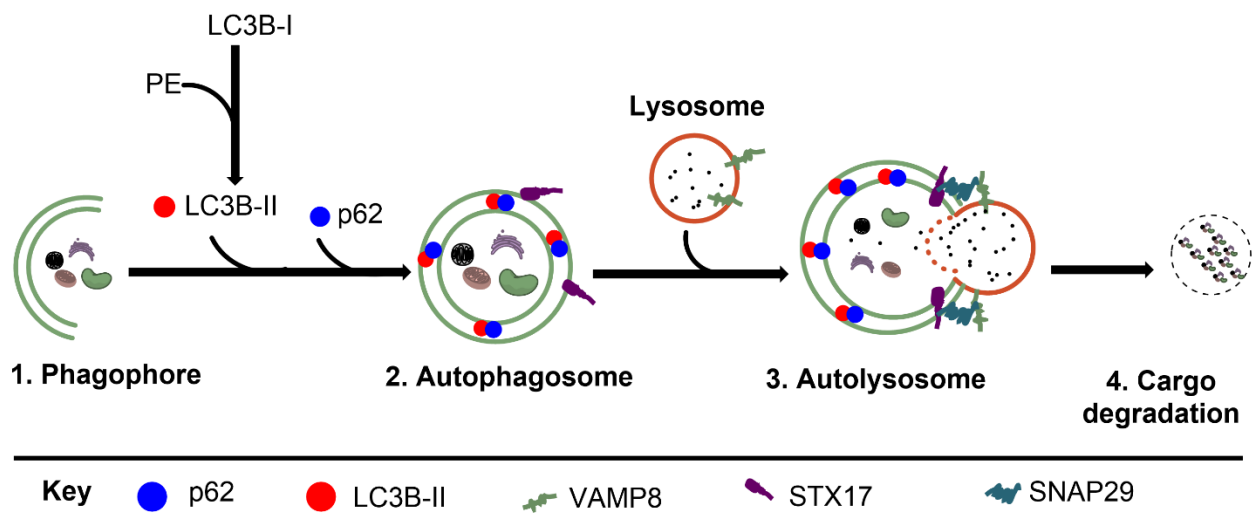


**Figure 3.1:** A simplified overview of the autophagy pathway

Current knowledge of how the proteasome cross-communicate with the autophagy pathway is limited to ubiquitinylation and 26S-dependent degradation.<sup>9,273</sup> For example, the

accumulation of ubiquitinated proteins following proteasome inhibition results in ER stress, unfolded protein response (UPR), p53 and HDAC6 signaling, with subsequent activation of downstream pathways and upregulation of autophagy (ATG) genes.<sup>274–277</sup> Activation of 26S-dependent degradation through inhibition of the de-ubiquitinase, USP14, triggers conflicting outcomes in autophagic flux.<sup>278–280</sup>

The role of the 20S proteasome in autophagy regulation is largely unexplored (Fig. 3.2B), yet, support for its relevance exists.<sup>281</sup> Specifically, the crosstalk and underlying mechanism(s) from 20S-mediated ubiquitin-independent proteolysis to autophagy is unknown.

### 3.1.2 Objective

The general goal of this chapter was to use the small molecule 20S proteasome activator, TCH-165,<sup>81</sup> as a chemical probe to decipher the role of 20S proteasome in autophagy regulation and the cellular mechanism (s) underlying the possible crosstalk.

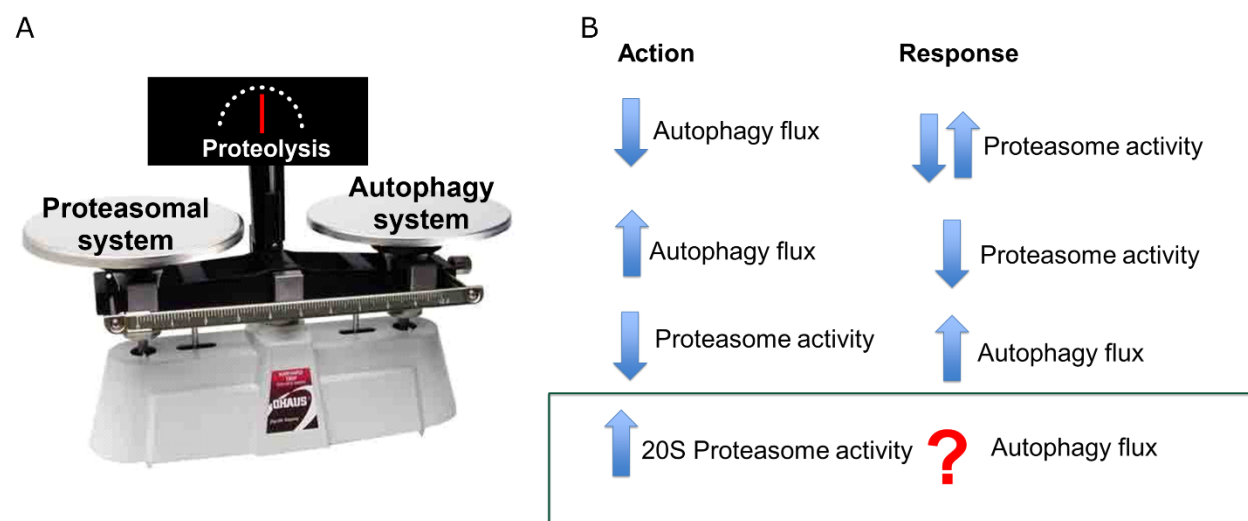


**Figure 3.2: The proteolytic arms of the proteostasis machinery. (A)** The two proteolytic systems that balance cellular protein degradation. **(B)** Characterized and uncharacterized crosstalk between the proteasome and autophagy pathways.



**Note:** The mammalian target of rapamycin, mTOR, is a negative regulator of autophagy. Thus, mTOR inhibitors such as rapamycin and torin1 act as inducers or activators of autophagy. These molecules will be used as control autophagy activators in this study. Meanwhile, molecules that interfere with acidification of the lysosome such as the v-ATPase inhibitor, Bafilomycin A (BafA) and the basic agent, chloroquine will serve as control autophagy inhibitors.

## 3.2 Results and Discussion

### 3.2.1 TCH-165 inhibits autophagy flux

During autophagosome formation, microtubule-associated protein 1 light chain 3 (LC3B-I) is converted to LC3B-II via the conjugation of phosphatidylethanolamine (PE) to the C-terminal glycine of LC3B-I (Fig.3.1). LC3B-II is then recruited to autophagosome membrane and degraded upon autolysosome formation. Thus, the turnover of the autophagosome membrane protein, LC3B-II, reflects autophagic activity.<sup>268,282</sup> To elucidate the effect of TCH-165 on autophagy flux, glioblastoma cells (U-87 MG)<sup>283</sup> were treated with the 20S proteasome activator, TCH-165, and the level of LC3B-II quantified by immunoblot and confocal microscopy. TCH-165 significantly increases the levels of LC3B-II in a concentration (Fig. 3.3A and 3.3B) and time (Fig. 3.3C and 3.3D) dependent manner.

LC3B-I displays a diffuse staining pattern within the cytoplasm, while LC3B-II appears as small punctate or dots in autophagic vacuoles (AVs).<sup>284</sup> Confocal immunofluorescence with anti-LC3B further confirmed the accumulation of LC3B positive vacuoles in cells treated with TCH-165 (10  $\mu$ M) for 16h (Fig. 3.3E and 3.3F). Furthermore, staining the cells with antibody against lysosome associated membrane protein 1 (LAMP 1) showed increase in lysosome dilation (Fig. 3.3G). Increased levels of LC3B-II and accumulation of AVs could result from upregulation in autophagosome formation (autophagy activation) or impaired downstream degradation of basal level autophagosome (autophagy inhibition)<sup>32</sup>. To distinguish between these two scenarios, accumulation of LC3B-II was measured in the presence of the late stage autophagy inhibitor, bafilomycin A1 (BafA1, a V-ATPase inhibitor).<sup>286</sup> Treatment with BafA1 or TCH-165 led to a significant increase in LC3B-II (Fig. 3.4A). As anticipated, the combination of BafA1 and

autophagy activator torin1<sup>287</sup> increases LC3B-II levels (Fig. 3.4A).

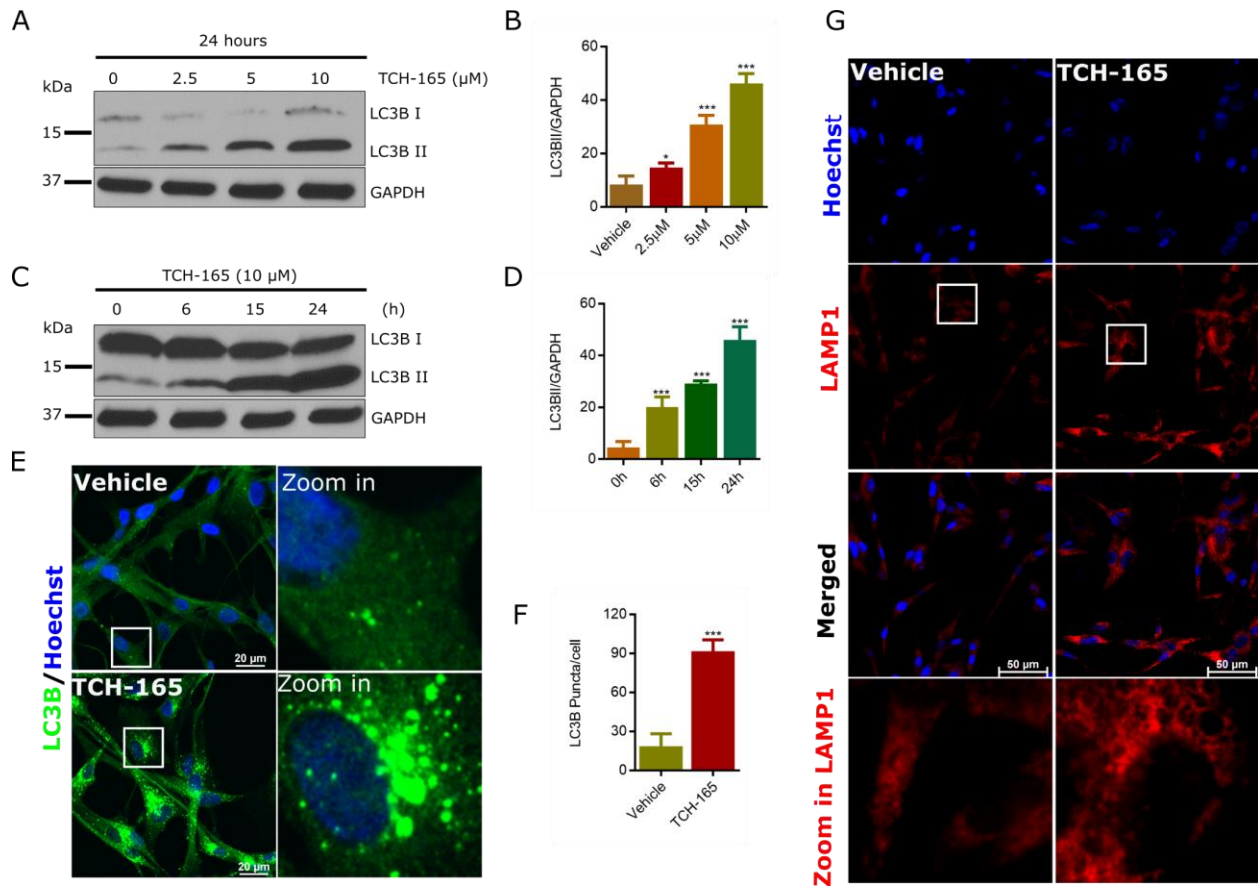


**Figure 3.3: TCH-165 induces the accumulation of LC3B-II and autophagic vacuoles.** (A) U-87 MG cells were treated with different concentrations of TCH-165 and immunoblotted for LC3B. (B) Image J quantification of (A). (C) Same as A at different time point, with GAPDH as a loading control. (D) Image J quantification of (C). (E) Immunofluorescent analysis of U-87 MG cells treated with vehicle, or TCH-165 (10 μM, 16h) using anti-LC3B /Alexa Fluor 488 (green). Blue = Hoechst (fluorescent DNA dye). (F) Mean LC3B punctae/cell for E. (G) Immunofluorescent analysis of U-87 MG cells treated with vehicle or TCH-165 (10 μM, 24h) using anti-LAMP1 antibody/Alexa Fluor 488 (pseudo red). Data are graphed as mean ± SD and were analyzed by One-Way ANOVA with Bonferroni's multiple comparison test or by unpaired student t-test (ns=not significant, \*p<0.05, \*\*p<0.01, \*\*\*p<0.001).

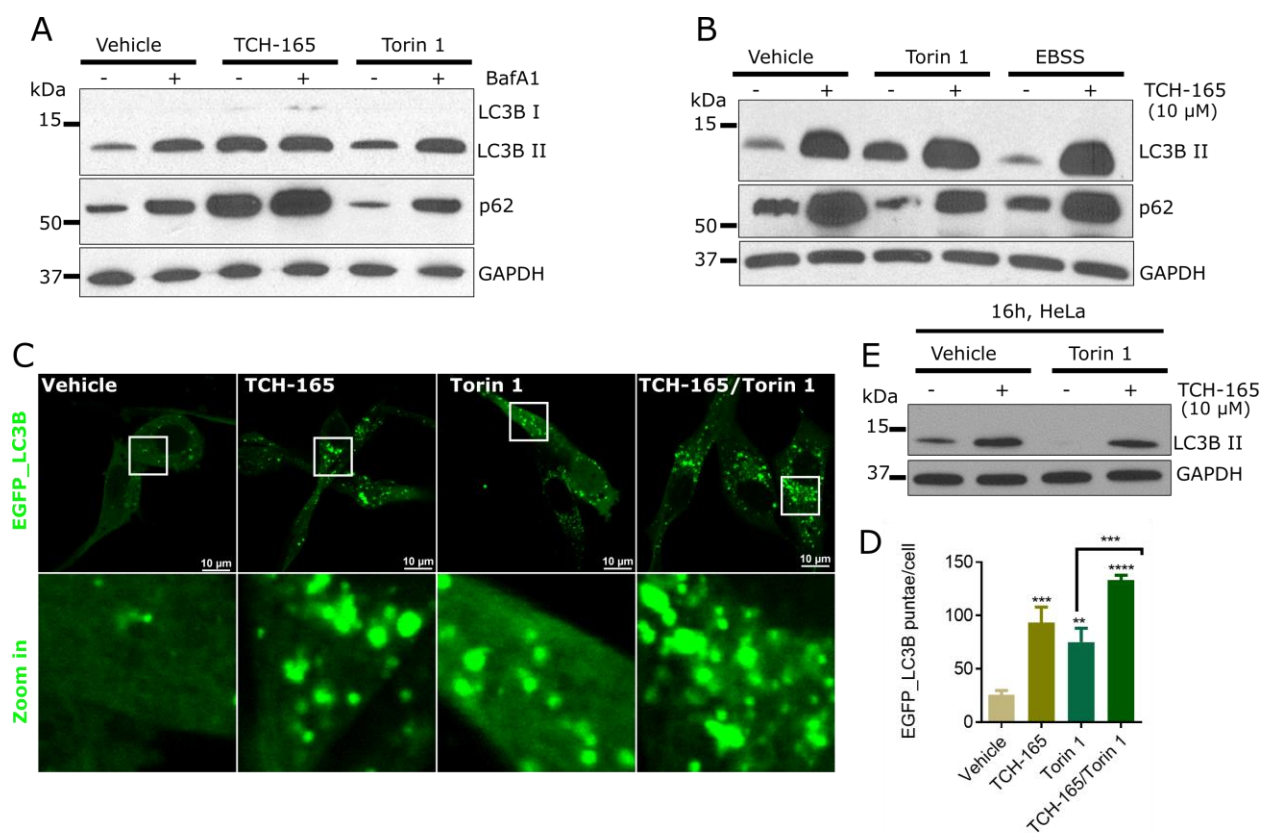


**Figure 3.4: TCH-165 inhibits autophagic flux.** (A) Immunoblot of U-87 MG cells treated with either vehicle, torin1 (500 nM) or TCH-165 (10  $\mu$ M) for 16h, followed by treatment with bafilomycin A1 (100 nM) for 4h. (B) Immunoblot of U-87 MG cells pre-treated with either vehicle or torin1 in complete medium or with vehicle in Earle's Balanced Salt Solution, EBSS (starved), for 4h, followed by TCH-165 (10  $\mu$ M) for an additional 16h. (C) live image of EGFP-LC3B in U-87 MG cells treated with either vehicle, torin1 (200 nM), TCH-165 (10  $\mu$ M) or of torin 1/ TCH-165 for 16h. (D) Quantification of C. (E) Same as A but in HeLa cells. (mean  $\pm$  SD, n=3 One-Way ANOVA with Bonferroni's multiple comparison test \* $p$ <0.05, \*\* $p$ <0.01, \*\*\* $p$ <0.001, \*\*\*\* $p$ <0.0001).

However, treatment with TCH-165 for 16h followed by BafA1 for 4h did not increase LC3B-II levels above that induced by TCH-165 alone (Fig. 3.4A), suggesting that TCH-165 inhibits autophagic flux.

To determine whether the 20S proteasome activator, TCH-165, affects late stage autophagy, the compound's ability to inhibit torin1 or starvation (Earle's balanced salt solution, EBSS) induced autophagy was evaluated. The combination of a late stage inhibitor and autophagy activators should significantly increase LC3B-II levels.<sup>285</sup> As seen in Fig. 3.4B, TCH-165 treatment of U-87 MG cells increases the accumulation of LC3B-II in both torin1 and starvation induced autophagy. Furthermore, U-87 MG cells expressing EGFP-LC3B were treated with torin1 and TCH-165 for 16h. Treatment with torin1 induced modest accumulation of AVs, while the combination of TCH-165 and torin1 significantly increased the number of AVs (Fig. 3.4C and 3.4D). This suggests that TCH-165 blocks the degradation of autophagosome induced by torin1. Similar activities were observed in HeLa cells (Fig. 3.4E).

Next, the effect of TCH-165 on the autophagy substrate, p62, was evaluated. During autophagy, p62/SQSTM1 is incorporated into autophagosome via interaction with LC3B, where it serves as a receptor for the delivery of polyubiquitinated proteins to autophagosomes.<sup>273,288</sup> As such, its clearance also serves as a measure of autophagic flux. Treatment of the U-87 MG cells with TCH-165 resulted in an increase in p62 in a concentration (Fig. 3.5A and B) and time (Fig. 3.5C and D) dependent manner. These data were further confirmed by confocal immunofluorescent imaging showing increased p62 punctate following TCH-165 treatment. The accumulated p62 was found to be co-localized with LC3B in AVs (Fig. 3.5E). This further

confirmed inhibition of autophagic flux in response to enhancement of 20S proteasome activity with TCH-165.

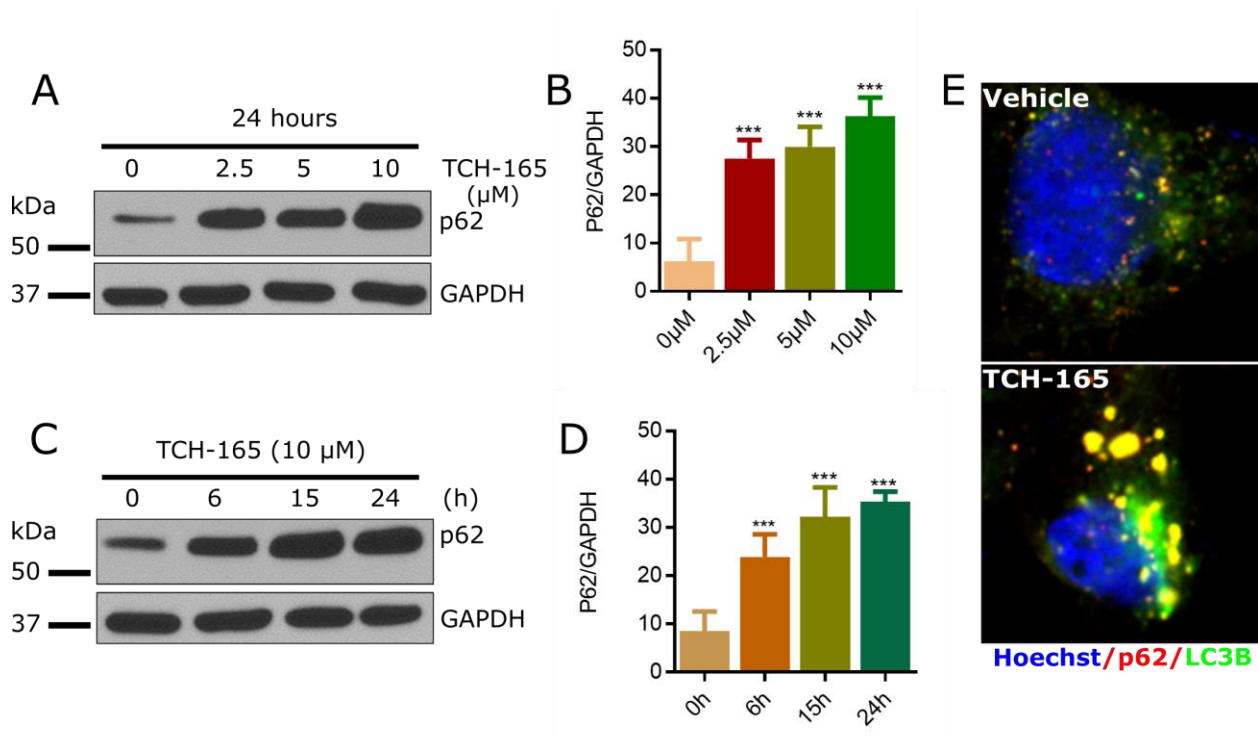


**Figure 3.5: TCH-165 induces the accumulation of p62.** (A) U-87 MG cells were treated with different concentrations of TCH-165 for 24h and immunoblotted for p62. (B) Image J quantification of A. (C) U-87 MG cells were treated with TCH-165 (10 μM) for 0, 6, 15, and 24h. and cell lysates were immunoblotted for p62. GAPDH as was used as a loading control. (D) Image J quantification of C. (E) Immunofluoresence of U-87MG cells treated with vehicle or TCH-165 (10 μM) for 24h and immunostained with LC3B specific/Alexa Fluor 488 (green) antibody, p62 specific/Alexa Fluor 594 (red) antibody and Hoechst DNA dye (blue). (n=4; mean ± SD; One-Way ANOVA with Bonferroni's multiple comparison test \*\*\*p<0.00).

### 3.2.2 TCH-165 interferes with autolysosome formation

The accumulation of LC3B-II and p62 in autophagic vacuoles suggests that TCH-165 may inhibit late stage autophagy by targeting either the lysosome and/or autophagosome-lysosome fusion. To differentiate between the two plausible target sites, tandem RFP-GFP-LC3B autophagy sensor was used to determine whether TCH-165 interferes with autolysosome formation.

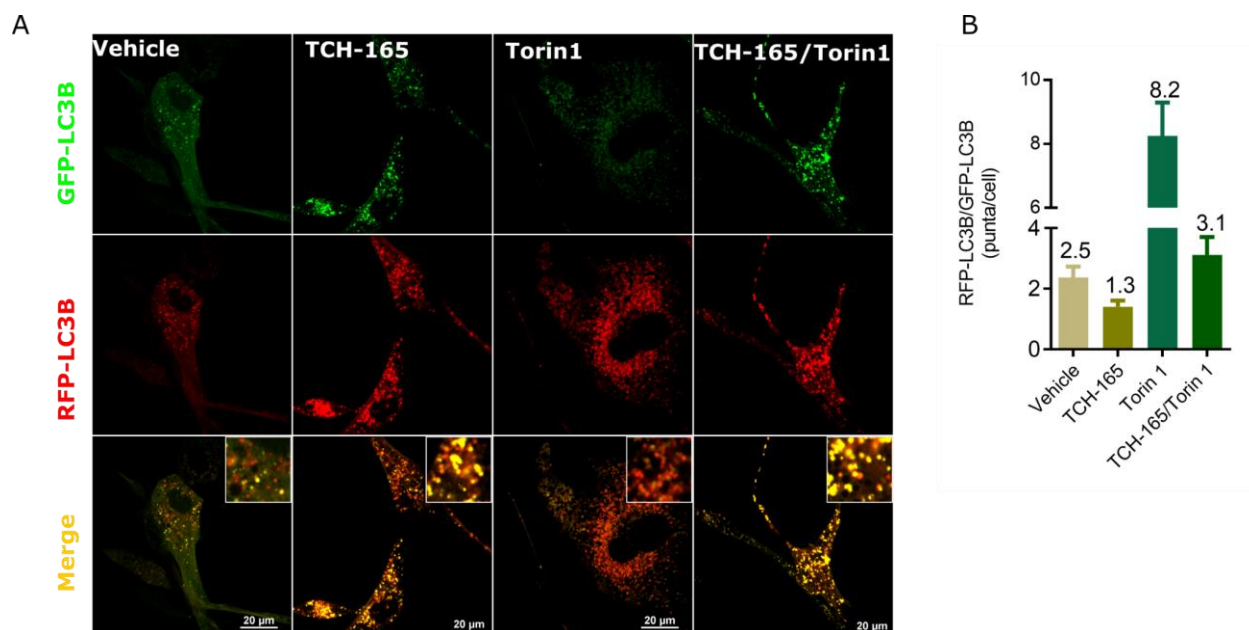


**Figure 3.6: TCH-165 interferes with autolysosome formation.** (A) U-87 MG cells were transduced with 30 particles per cell of tandem-RFP-GFP-LC3B and cultured for 24h. Cells were then incubated with either vehicle, TCH-165 (10  $\mu$ M), torin 1 (200 nM) or a combination of TCH-165 and torin1 for an additional 24h and imaged. (B) Quantification of RFP to GFP positive punctae of A.

Through the combination of an acid insensitive RFP with an acid sensitive GFP, the conversion of an autophagosome (neutral pH, indicated by yellow fluorescence in the merged channel) to an autolysosome (acidic pH, indicated by red fluorescence in the merged channel) can

be visualized by monitoring the specific loss of GFP fluorescence (increase in the ratio of RFP to GFP positive dots) upon acidification of the autophagosome following lysosomal fusion.<sup>269</sup> U-87 MG (Fig. 3.6A and 3.6B cells transiently expressing RFP-GFP-LC3B retained similar levels of GFP and RFP positive vacuoles upon TCH-165 treatment. This suggests that TCH-165 inhibits autophagy flux by interfering with autolysosome formation, a mechanism distinct from inhibition of lysosomal hydrolases (No GFP signal). Consistent with torin 1 promoting autophagy flux, torin 1 treated samples had significant increase in RFP to GFP punctae, which was reduced in the presence of TCH-165 (Fig. 3.6A).

However, GFP and RFP positive punctae could also represent de-acidified autolysosome,<sup>289</sup> as seen with agents that modify lysosomal pH such as chloroquine and BafA. Thus, to distinguish inhibition of autolysosome formation from lysosome de-acidification, changes in lysosomal pH using the acidotropic dye, lysotracker red in cells expressing GFP-LAMP1 was assessed. Unlike BafA1, which neutralizes the lysosome and reduces lysotracker red fluorescence, TCH-165 or torin 1 did not reduce lysotracker red signal. Consistent with dilation of the lysosome seen in Fig. 3.3G, TCH-165 treatment results in a slight increase in red fluorescence (Fig. 3.7A and 3.7B).

Cathepsin D maturation is sensitive to changes in lysosomal pH that might not be detectable by lysotracker red. Accordingly, the lack of perturbation of lysosomal pH was confirmed by measuring cathepsin D and E activity in cells treated with TCH-165 for 24h. Unlike chloroquine which alters lysosomal pH, or pepstatin A which directly inhibits cathepsin activity, TCH-165 did not affect cathepsin D activity (Fig. 3.7C). Consistently, immunofluorescence of LC3B and LAMP1 showed a lack of co-localization between the autophagosome and the lysosome in TCH-165 samples (Fig. 3.8). These data, collectively, suggest that the 20S proteasome regulates



autophagy flux at the autolysosome stage, through a mechanism that does not involve neutralization of lysosomal pH.

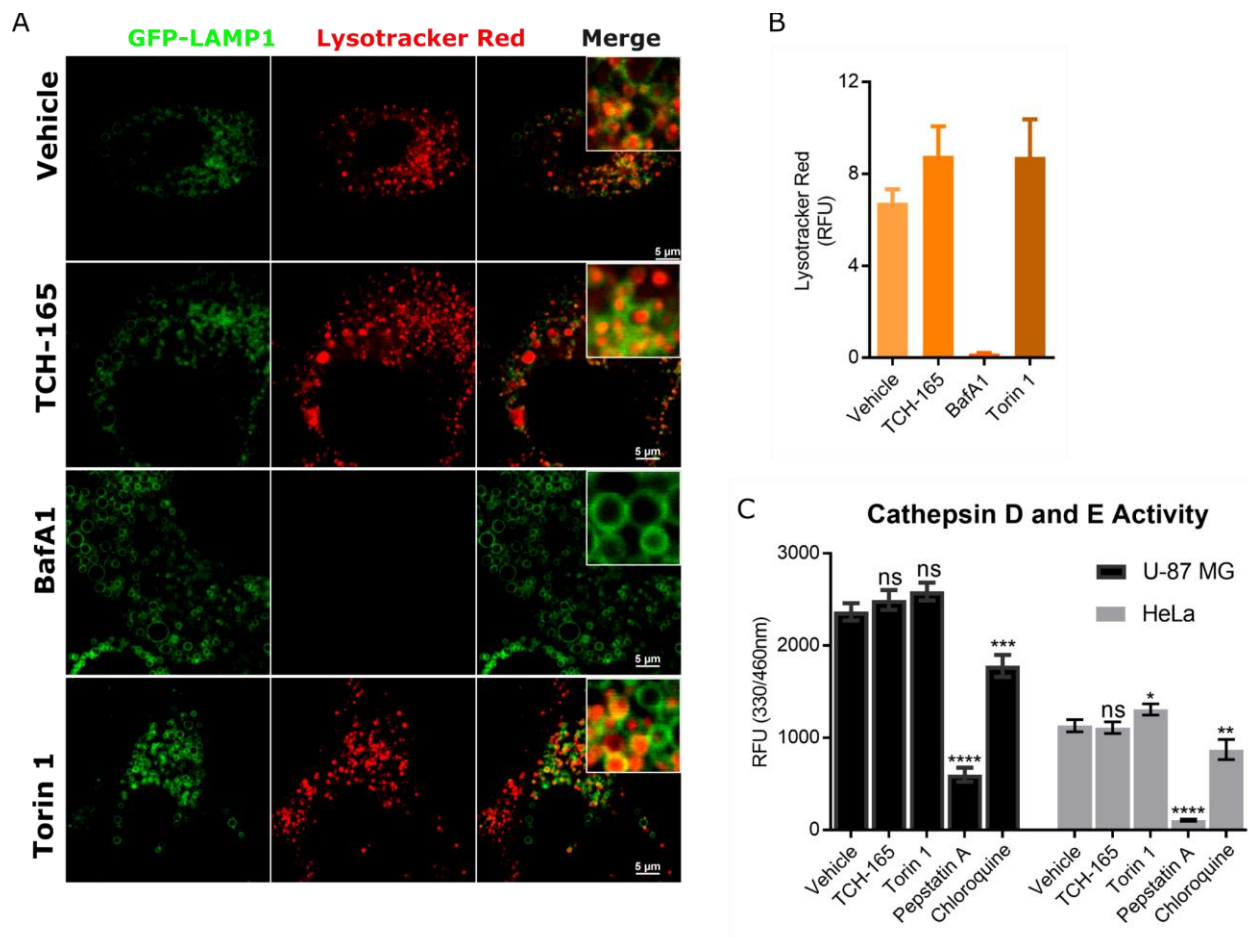


**Figure 3.7: TCH-165 does not affect lysosomal pH.** (A) U-87 MG cells were transduced with 30 particles per cell of CellLight® Lysosomes-GFP (GFP-LAMP1) and cultured for 24h. Cells were treated with vehicle, TCH-165 (10  $\mu$ M), torin 1(100 nM) or Bafilomycin A1 (50 nM) for 16h. Cells were stained with 50nM lysotracker red and imaged (B) Mean fluorescence of lysotracker red from U-87 MG cells treated with vehicle, TCH-165 (10  $\mu$ M), torin 1(100 nM) or Bafilomycin A1 (50 nM) for 16h. (C) Cathepsin D and E activity in cell lysates from U-87 MG or HeLa Cells treated with vehicle, TCH-165 (10  $\mu$ M), torin 1 (100 nM), chloroquine (100  $\mu$ M) or pepstatin A (5  $\mu$ M) for 24h.

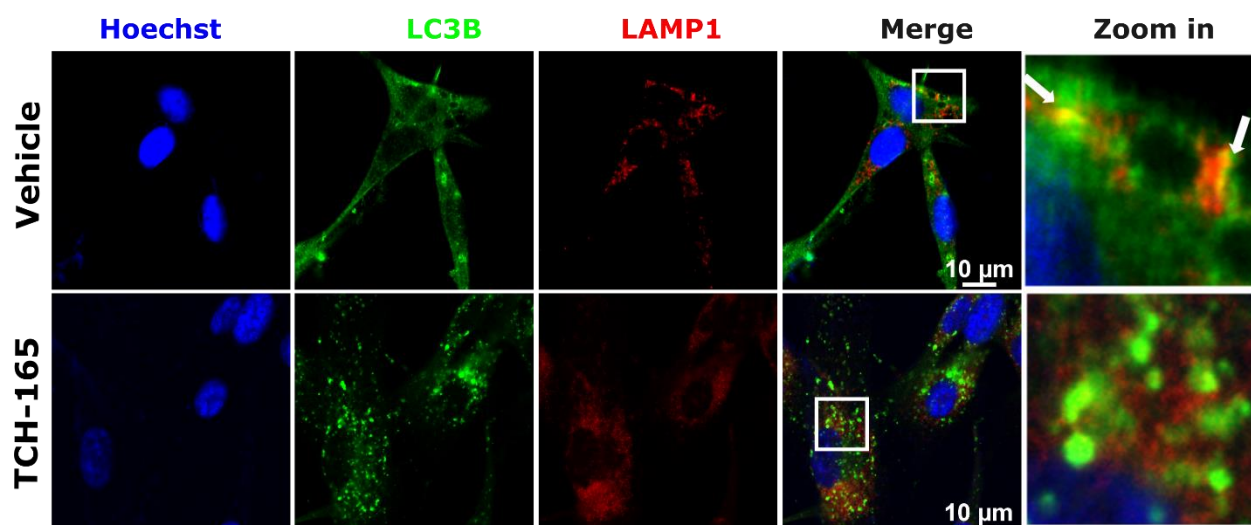


**Figure 3.8: TCH-165 inhibits autophagosome-lysosome fusion.** U-87 MG cells were treated with either vehicle or TCH-165 (10  $\mu$ M) for 24h and immunostained with rabbit anti-LC3B specific/Alexa Fluor 488 (green) antibody, mouse anti-LAMP1 specific/Alexa Fluor 594 (red) antibody and Hoechst DNA dye (blue). White arrows indicate colocalization of AVs with the lysosome (autolysosome), only present in vehicle control.

### 3.2.3 TCH-165 links the 20S proteasome as a negative regulator of autophagy flux

To elucidate the mechanism by which TCH-165 inhibits autophagic flux, the different SNAREs and HOP proteins involved in autophagosome-lysosome fusion were evaluated to identify those that are potential 20S substrates. For this, predictor of natural disorder region (PONDR) was used to identify the degree of disorder in these proteins.<sup>64</sup>

These predictive calculations indicated that at least three of these proteins have a minimum of 40% overall disorder, with SNAP29 (87.6%) being almost completely disordered (Table 1) and thus was anticipated to be a plausible 20S proteasome substrate. Therefore, the cellular degradation of these proteins was evaluated. HeLa cells were treated with vehicle or torin1, with or without TCH-165.

**Table 1:** PONDR VSL2 prediction of disorder in autophagosome-lysosome fusion proteins

<b>Proteins involve in autophagosome-lysosome fusion</b>	<b>% Disorder with PONDR VSL2 (longest disorder)</b>
Synaptosomal-associated protein 29 (SNAP29)	87.6 (109)
Syntaxin-17 (STX17)	41.4(46)
Vesicle-associated membrane protein 8 (VAMP8)	65.0(62)
Vacuolar protein sorting-associated protein 33A (VPS33A)	13.9(33)
Vacuolar protein sorting-associated protein 16 homolog (VPS16)	17.4(50)
Vam6/Vps39-like protein (VPS39)	16.3(33)

Interestingly, TCH-165 significantly reduced the protein levels of SNAP29 and STX17, but not VAMP8. However, VAMP8 was significantly reduced in torin1 treatment, but accumulated when torin1 was combined with TCH-165 (Fig. 3.9A). These observations suggest that unlike SNAP29 and STX17, VAMP8 is likely an autophagy substrate. This data is consistent with previous studies by others,<sup>290</sup> illustrating induction of VAMP8 degradation by rapamycin. Similar results were obtained in HEK293T and RPMI-8226 cells (Fig.3.9B), suggesting that the observed effect is not cell type dependent.

Next, I determined whether the changes in STX17 and SNAP29 were occurring post-translationally and at the level of the proteasome. Protein synthesis was pulsed with cycloheximide in the presence of vehicle, TCH-165, bortezomib (BTZ; proteasome inhibitor) or a combination of TCH-165 and BTZ for 8h. Immunoblot analyses indicated a significant increase in the degradation of SNAP29 and STX17 in TCH-165 treated sample, which was blocked by BTZ (Fig. 3.9C-E). These observations suggested that the change in the protein levels of SNAP29 and STX17 were due to enhanced degradation, most likely at the level of the proteasome. To be more certain, U-87 MG cells were treated with vehicle or TCH-165 for 8h or 24h and assayed for changes in total mRNA by RT-qPCR. At 8h, no significant changes were observed in the mRNA levels of STX17,

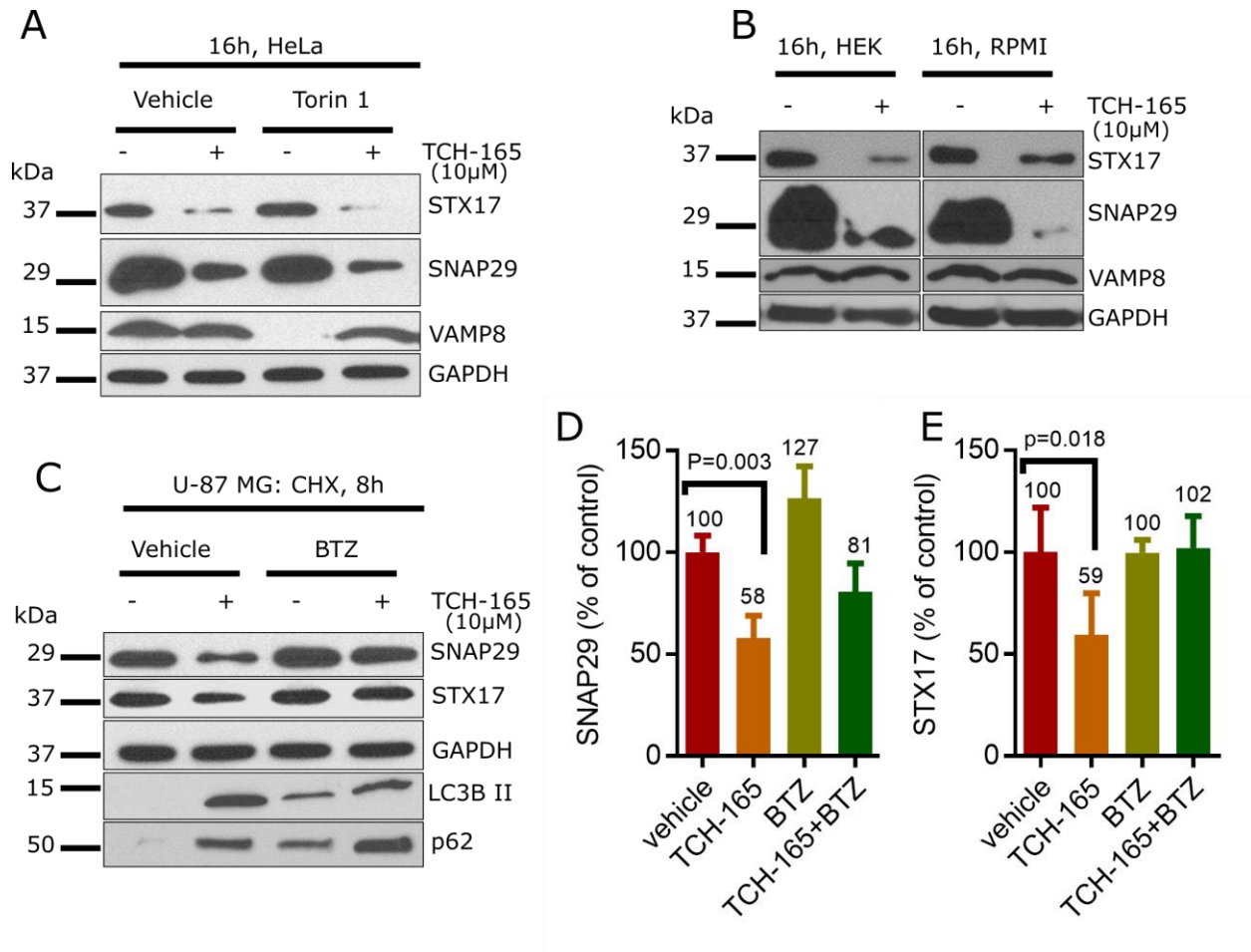


**Figure 3.9: TCH-165 stimulates proteasomal degradation of SNAP29 and STX17.** (A) HeLa cells were treated with either vehicle, torin1 (200 nM), TCH-165 (10 μM) or combinations for 16h. Cell lysates were immunoblotted for STX17, SNAP29, VAMP8 and GAPDH. (B) HEK293T or RPMI-8226 cells were treated with either vehicle or TCH-165 (10 μM) for 16h and whole cell lysates immunoblotted for STX17, SNAP29, VAMP8 and GAPDH. (C) U-87 MG cells were treated with cycloheximide (100 μg/mL) plus vehicle, TCH-165 (10 μM), bortezomib (BTZ; 5 μM) or combinations for 8h. Whole cell lysates were immunoblotted for STX17, SNAP29 and GAPDH. The degradation of SNAP29 (D) and STX17 (E) were quantified with image J software. Statistical analyses were performed on four independent experiments using unpaired t-test.

However, at 24h, the mRNA for SNAP29 and STX17 increased by about 3-fold for TCH-165 treated cells (Fig. 3.10). These increases in mRNA levels were likely a feedback response to the enhanced degradation of these proteins. The mRNA level of VAMP8 was also upregulated by 2-fold, at 24h, probably in response to accumulation of AVs. As controls, the mRNA levels of LC3B and p62 were also quantified. Both genes showed significant upregulation in mRNA at both time points (Fig. 3.10). Remarkably, changes in the mRNA of LC3B was more significant at 8h than at 24h. The upregulation of p62 and LC3B genes could also be in response to the accumulation of AVs or a general response to an exogenous stressor (TCH-165), given that these genes are components of a stress response pathway.

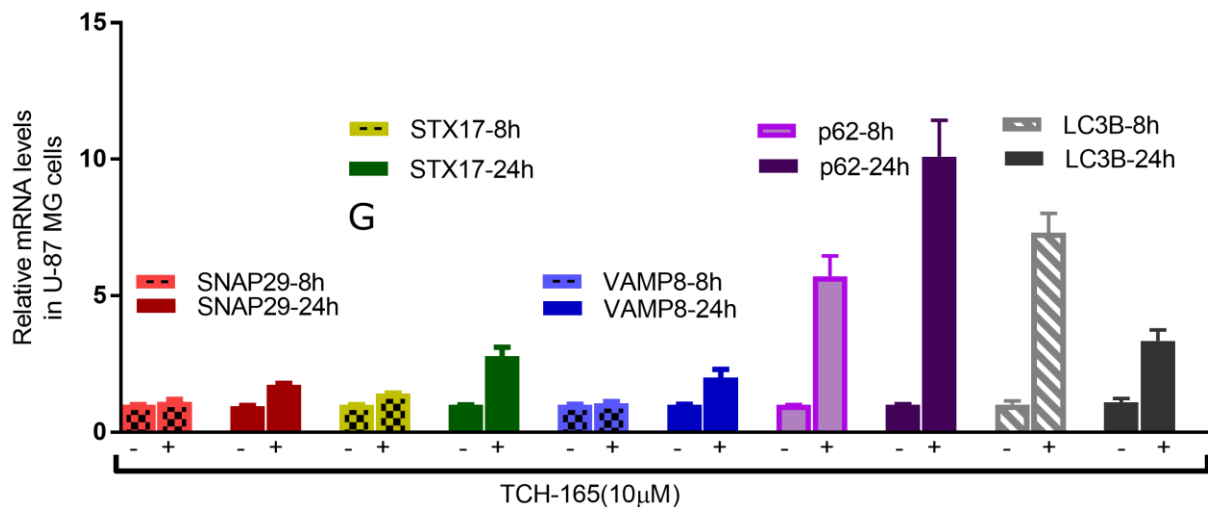


**Figure 3.10: Regulation of autophagy genes by TCH-165.** U-87 MG cells were treated with vehicle or TCH-165 (10 μM) for 8h or 24h and mRNA quantified by RT-qPCR. Data are presented as mean ± SD of two independent experiments, each ran in triplicate.

### 3.2.4 The 20S proteasome regulates autophagy via the proteolysis of SNAP29 and STX17

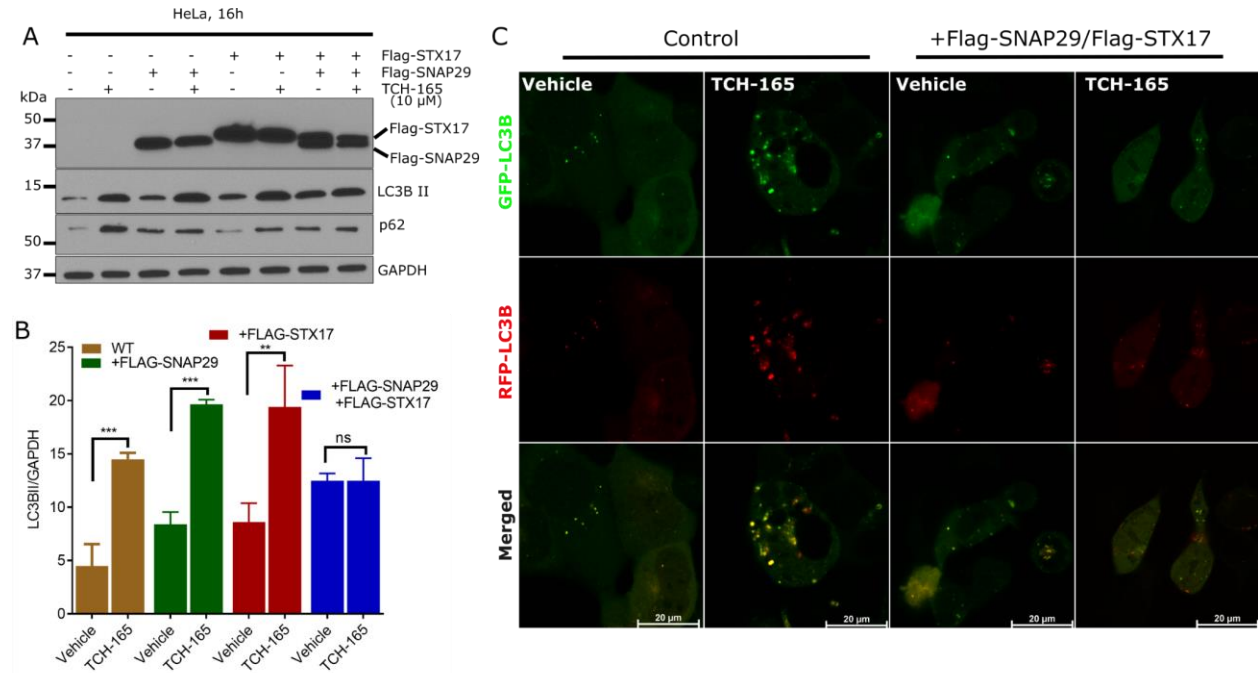


**Figure 3.11: The 20S proteasome regulates autophagy via the proteolysis of SNAP29 and STX17.** (A) Wild type HeLa cells or HeLa cells overexpressing FLAG-SNAP29, N-terminal FLAG-STX17 or both were treated with vehicle or TCH-165(10  $\mu$ M) for 16h and immunoblotted with anti-FLAG, anti-LC3B, anti-p62 and anti-GAPDH. (B) Image J quantification of LC3BII and GAPDH in A. Statistical analyses were performed on three independent experiments using unpaired t-test on GraphPad Prism7 (ns=not significant, \* $p < 0.05$ , \*\* $p < 0.01$ , \*\*\* $p < 0.001$ ). (C) HEK 293T cells were co-transfected with FLAG-SNAP29 and FLAG-STX17 for 8h. Both wild type (WT) and FLAG SNAP29/FLAG STX17 cells were further transduced with 30 particles per cell of tandem-RFP-GFP-LC3B and cultured for 24h. Cells were then incubated with either vehicle or TCH-165 (10  $\mu$ M) for an additional 16h. Live cells were imaged on a confocal microscope using with standard filter sets for GFP and RFP. In the merged images, red puncta represent autolysosomes while yellow puncta represent autophagosome.

To verify that proteasomal degradation of SNAP29 and STX17 plays a role in regulating autophagy, SNAP29, STX17 or both were overexpressed in HeLa cells and autophagic flux monitored in the presence and absence of TCH-165. Here, overexpression of the individual proteins increased LC3B-II levels, probably due to increase flux, as p62 levels went down (Fig. 3.11A and B). When cells overexpressing either SNAP29 or STX17 were treated with TCH-165, LC3B-II accumulated further. However, when both proteins were overexpressed, TCH-165 failed to significantly increase LC3B-II nor p62 levels (Fig. 3.11A and B) over the vehicle control. Furthermore, overexpression of both SNARE proteins reduced TCH-165 induced AV accumulation (Fig. 3.11C). This suggests that their (SNAP29 and STX17) production outpaced their enhanced degradation and autophagic flux was restored. Together, these data suggest that the 20S proteasome regulates autophagosome-lysosome fusion via proteolysis of the critical fusion proteins, SNAP29 and STX17.

### **3.2.5 The proteolysis of SNAP29 and STX17 are ubiquitin-independent**

Some proteins are susceptible to both ubiquitin-dependent and ubiquitin-independent proteasomal degradation.<sup>266,291</sup> To verify whether STX17 and SNAP29 belong to this group of proteins, SNAP29 and STX17 were pulled-down and probed for K-48 ubiquitin, which is the form recognized by the 26S proteasome for degradation. For this, cells expressing either Flag-SNAP29 (Fig. 3.12A) or Flag-STX17 (Fig. 3.12B) were treated with either vehicle, TCH-165, bortezomib (BTZ) or their combinations. Consistently, SNAP29 and STX17 were rapidly degraded in the presence of TCH-165 but accumulated in the presence of bortezomib, with or without TCH-165 (Fig. 3.12A and 3.12B), further implicating the proteasome as its target protease. Moreover, pull-

down with anti-Flag revealed free SNAP29 and STX17, but not their ubiquitin conjugates upon immunoblotting with anti-K-48.

Although ubiquitin-independent degradation is primarily mediated by the 20S, ubiquitin-independent degradation by the 26S proteasome cannot necessarily be excluded yet. Therefore, to determine the possible involvement of the 26S proteasome in the degradation of SNAP29 and STX17, siRNA knockdown of the 19S cap of the 26S proteasome was used. Knockdown of the 19S PSDM2 (Rpn1, Fig. 3.12C) subunit has been validated by others in the determination of 19S-dependent degradation of proteins.<sup>292</sup> For this study, HeLa cells were transfected with either control siRNA or Rpn1 siRNA for 72h and then treated with either vehicle or TCH-165 for 16h. Immunoblot revealed significant stabilization of SNAP29 in vehicle control of Rpn1 knockdown sample (Fig. 3.12D). However, under the knockdown condition, the degradation of SNAP29 was still enhanced by TCH-165 (Fig. 3.12D). This suggests that although the 26S proteasome may contribute in the degradation of SNAP29, the 20S is primarily responsible for its proteolysis. Surprisingly, STX17 which is less disordered than SNAP29 was not stabilized in the Rpn1 knockdown/vehicle control. It thus appears that STX17 is primarily degraded by the 20S proteasome. Furthermore, Rpn1 knockdown/TCH-165 treatment showed a more robust enhanced degradation of STX17 compared to control siRNA/TCH-165 sample. This is consistent with an increasing pool (with Rpn1 knockdown) of activated (upon TCH-165 exposure) 20S proteasome. Consistent with the role of STX17 in autophagy flux, LC3B II accumulated more in Rpn1 knockdown/TCH-165 compared to control siRNA/TCH-165. Predictably, Rpn1 knockdown (26S inhibition) lead to p62 accumulation compared to the control siRNA.



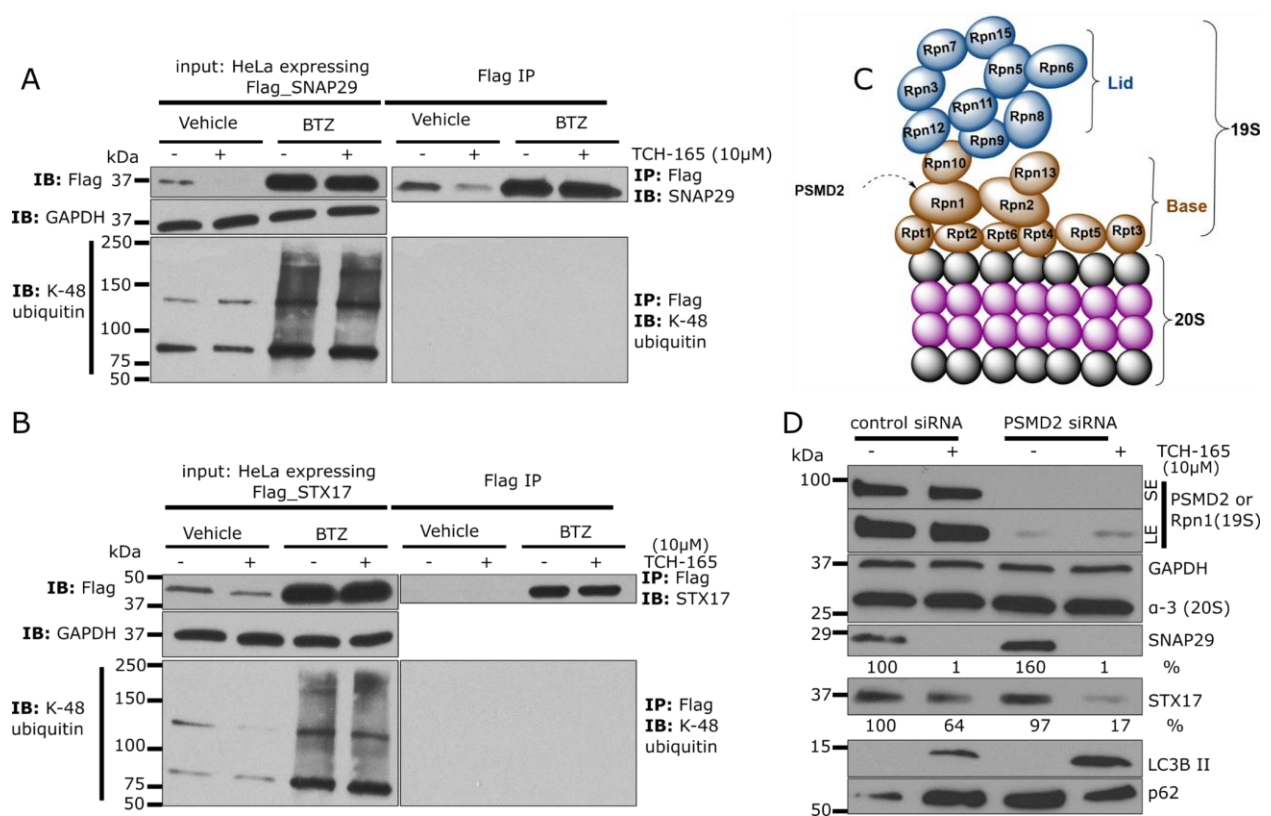


**Figure 3.12: The proteolysis of SNAP29 and STX17 are ubiquitin-independent.** (A) HeLa cells expressing N-terminal FLAG-SNAP29 were pretreated with either vehicle or bortezomib (20 μM) for 2h, followed by treatment with vehicle or TCH-165 (10 μM) for 16h. Whole cell lysates were immunoprobed with anti-Flag, anti-GAPDH or anti-K-48 ubiquitin (left column). Samples were also immunoprecipitated (IP) with anti-Flag and immunoblotted (IB) with anti-SNAP29 or anti-K-48 ubiquitin (right column). (B) Same as in C, except with cells expressing N-terminal FLAG-STX17. (C) Cartoon of the 19S showing the knockdown subunit. (D) HeLa cells were transfected with either control siRNA or PSMD2 (Rpn1) siRNA for 72h, followed by treatment with vehicle or TCH-165 for 16h. Whole cell lysate were immunoblotted for the indicated proteins. Numbers are densitometry of signal as a percentage of vehicle/control siRNA treatment. **LE**: Long exposure, **SE**: Short exposure.

### 3.2.6 SNAP29 is a substrate of the 20S proteasome

Considering that SNAP29 was stabilized following 19S knockdown (suggesting 26S-mediated degradation), its 20S-mediated proteolysis was confirmed by an *in vitro* biochemical assay. Recombinant SNAP29 was degraded by purified 20S proteasome, as observed by immunoblot (Fig. 3.13A) and by Coomassie staining (Fig. 3.13B). Moreover, the degradation of SNAP29 in this assay was enhanced by TCH-165 and blocked by the proteasome inhibitor, bortezomib (Fig. 3.13C). Together, these data suggest that the SNARE proteins, SNAP29 and STX17, are 20S substrates and that ubiquitin-independent 20S proteasome-mediated proteolysis of these proteins regulates, at least in part, autophagic flux.

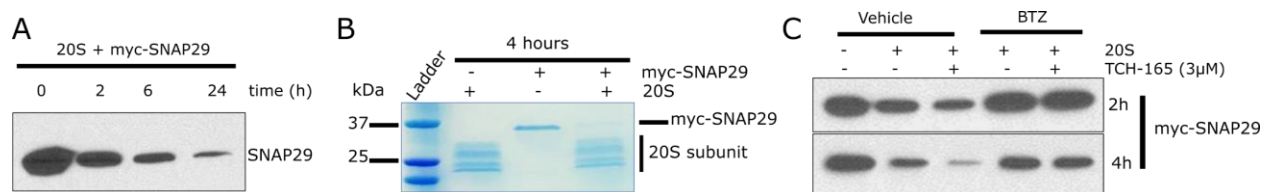


**Figure 3.13: SNAP29 is a substrate of the 20S proteasome.** (A) Purified c-myc/DDK-SNAP29 (200 nM) was degraded with 20S proteasome (20 nM) for 0h, 2h, 6h and 24h and analyzed by immunoblot with anti-SNAP29 (B) Purified c-myc/DDK-SNAP29 (200nM) was degraded with 20S proteasome (20nM) for 4h and analyzed by Coomassie instant blue staining following SDS-PAGE. (C) Purified c-myc/DDK-SNAP29 (200nM) was degraded with 20S proteasome (20nM) treated with vehicle, TCH-165 (3 μM), bortezomib (5 μM), or combinations, for 2h and 4h and analyzed by immunoblot with anti-SNAP29.

### 3.2.7 SNAP29 and STX17 interact with the 20S proteasome

Predictably, pull-down experiment to verify the interaction of these proteins with the proteasome was unproductive, given that the interaction is likely weak and transient. However,

immunofluorescence of cells expressing Flag-SNAP29 or STX17 revealed significant overlap with the proteasome (Fig. 3.14A-C).

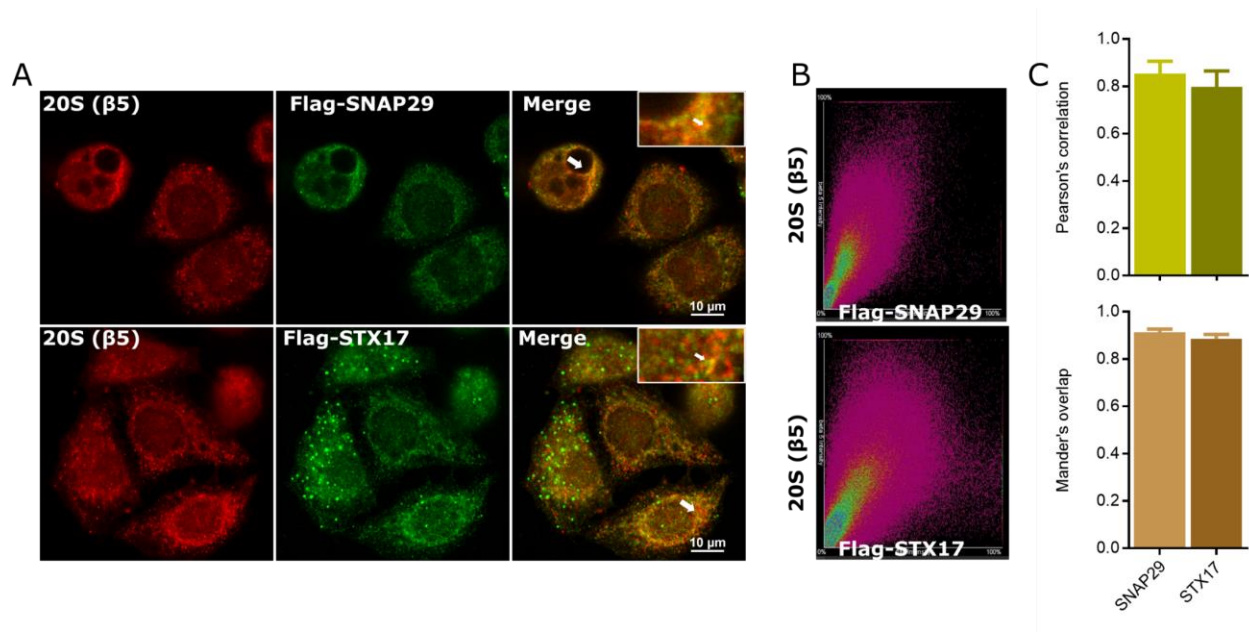


**Figure 3.14: SNAP29 and STX17 interact with the 20S proteasome.** (A) HeLa cells expressing Flag-SNAP29 or Flag-STX17 were immunostained with mouse anti-β 5/Alexa fluor 546 (red) and rabbit anti-Flag/ Alexa Fluor 488 (green) and imaged with an upright Nikon A1 confocal microscope using a 60X Plan Apo oil objective. Arrows indicate areas of colocalization visible by naked eye. (B) Sample 2-D intensity histogram for D. (C) Pearson's correlation and Mander's overlap for SNAP29/ β5 and STX17/β5 were quantified with Nikon software.

### 3.2.8 Proteasome activation by imidazolines parallel autophagy inhibition

Three different imidazoline analogues were used to determine whether 20S proteasome enhancement parallels autophagy inhibition. For this, TCH-165 (potent 20S agonist), TCH-023 (inactive analogue) and TCH-013 (weak 20S agonist) were used (Fig. 3.15A).<sup>81,234</sup> Indeed, the ability of these molecules to enhance 20S-mediated proteolysis of the peptide substrate, Suc-

LLVY-AMC (Fig. 3.15B), directly correlates with the degradation of SNAP29, STX17, and the accumulation of autophagic substrates; LC3B-II and p62 (Fig. 3.15C).

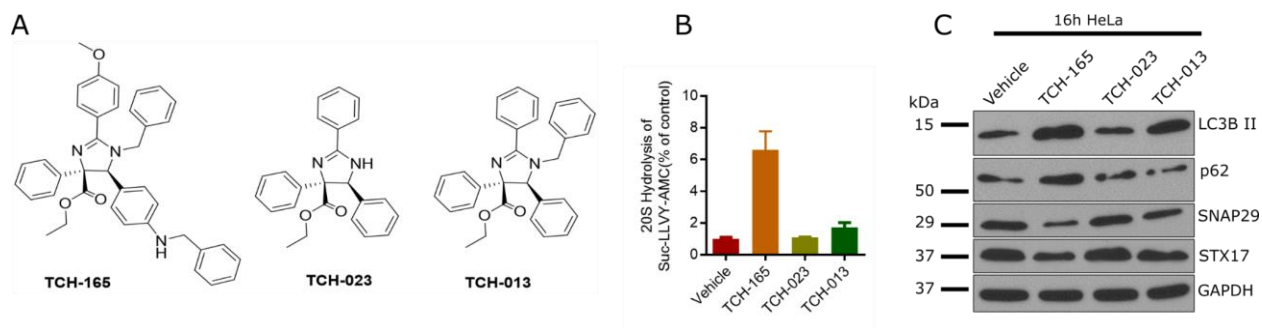


**Figure 3.15: Autophagy inhibition parallels proteasome activation by imidazolines.** (A) Chemical structures of imidazolines TCH-165 (a potent 20S agonist), TCH-023 (inactive analogue) and TCH-013 (a moderate 20S agonist). (B) Degradation of the chymotrypsin-like fluorogenic peptide substrate, Suc-LLVY-AMC (10  $\mu$ M) with 20S proteasome (1 nM) treated with vehicle (control) or 10  $\mu$ M of TCH-165, TCH-023 or TCH-013. Data are presented as percentage of vehicle control. (C) HeLa cells were treated with vehicle or 10  $\mu$ M of TCH-165, TCH-023 or TCH-013 and whole cell lysate immunoblotted for LC3B, p62, SNAP29, STX17 and GAPDH.

### 3.2.9 Oxidative stress does not mimic the effect of TCH-165 on autophagy

Under conditions of oxidative stress, there is an equilibrium shift that favors 20S-mediated proteolysis of oxidized proteins.<sup>124</sup> Thus, enhanced degradation of SNAP29 and STX17 were investigated following induction of oxidative stress with hydrogen peroxide ( $H_2O_2$ ). Here, treatment of HeLa cells with 50  $\mu$ M  $H_2O_2$  significantly reduces the level of assembled 26S proteasome (Fig. 3.16A), with a corresponding increase in oxidized proteins (Fig. 3.16B). TCH-165 (at 10  $\mu$ M) also reduced the level of 26S in HeLa cells (Fig. 3.16A).

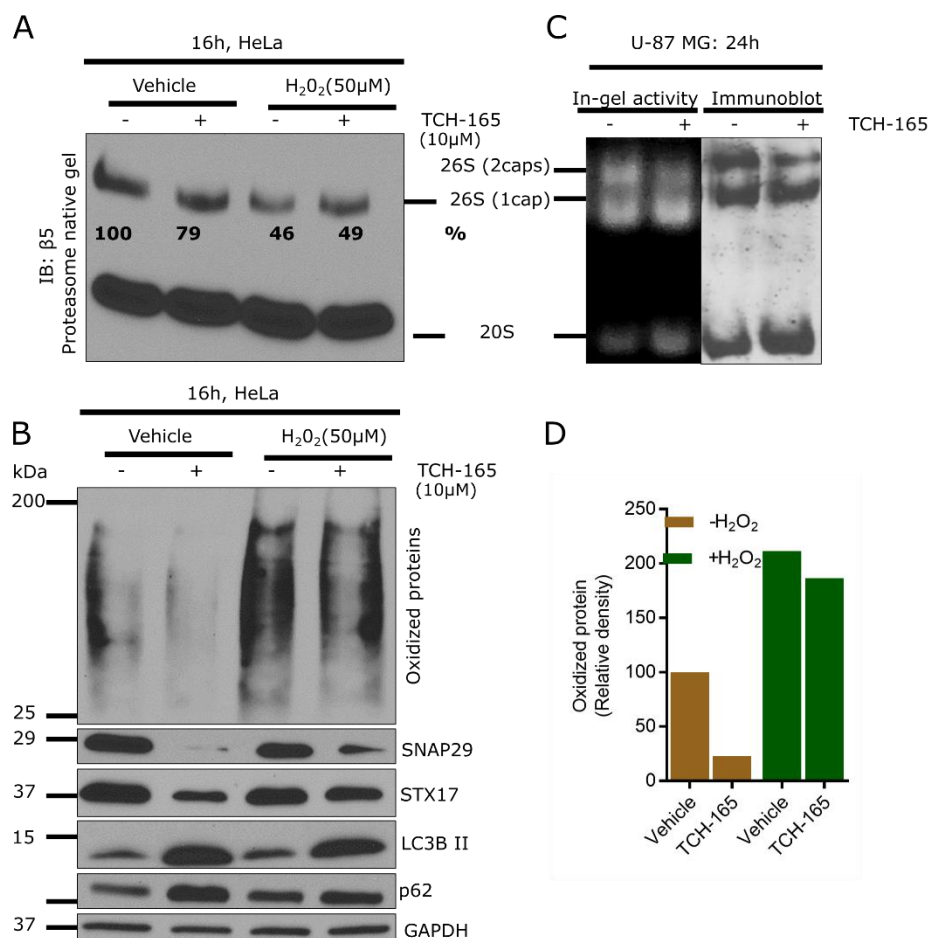


**Figure 3.16: Activity of TCH-165 under condition of oxidative stress.** (A) HeLa cells were treated with either vehicle, TCH-165 (10 μM), hydrogen peroxide (H<sub>2</sub>O<sub>2</sub>; 50 μM) or combinations for 16h. Samples were either immunoblotted under native conditions for proteasome subcomplexes **or** (B) derivatized with DNPH for oxidized proteins (top panel, and D) or immunoblotted for the indicated proteins (bottom panels). (C) Proteasome native gel for U-87 MG cells treated with vehicle or TCH-165 (10 μM) for 24h and exposed to 20S CT-L substrate (Suc-LLVY-AMC) to check for activity (left) and immunoblotted (right) to check for changes in proteasome subcomplexes.

Consistent with the observation in HEK cells (chapter 2) and U-87 MG cells (Fig. 3.16C), a significant amount of single capped 20S was maintained. However, the degradation of SNAP29

and STX17, as well as changes in autophagy markers, LC3BII and p62, were not as robust following oxidative damage, compared to TCH-165 treatment (Fig. 3.16B). Consistent with 20S activation and the role of 20S in the degradation of oxidatively damaged proteins<sup>125,144</sup>, TCH-165 was able to enhance the degradation of oxidized proteins under basal conditions (Fig. 3.16B, lane 2). The combination of TCH-165 with H<sub>2</sub>O<sub>2</sub> resulted in milder effects on the degradation of oxidized and SNARE proteins, and the accumulation of LC3BII and p62 (Fig. 3.16B, lane 4, and Fig. 3.16D), compared to TCH-165 treatment only. This observation is most likely due to increase in proteasomal load (oxidized proteins) as a result of exposure to H<sub>2</sub>O<sub>2</sub>.

Collectively, the TCH-165 was used to implicate the 20S proteasome as a key regulator of autophagy flux. A schematic of the proposed signaling pathways consistent with these findings is depicted in Fig. 3.17

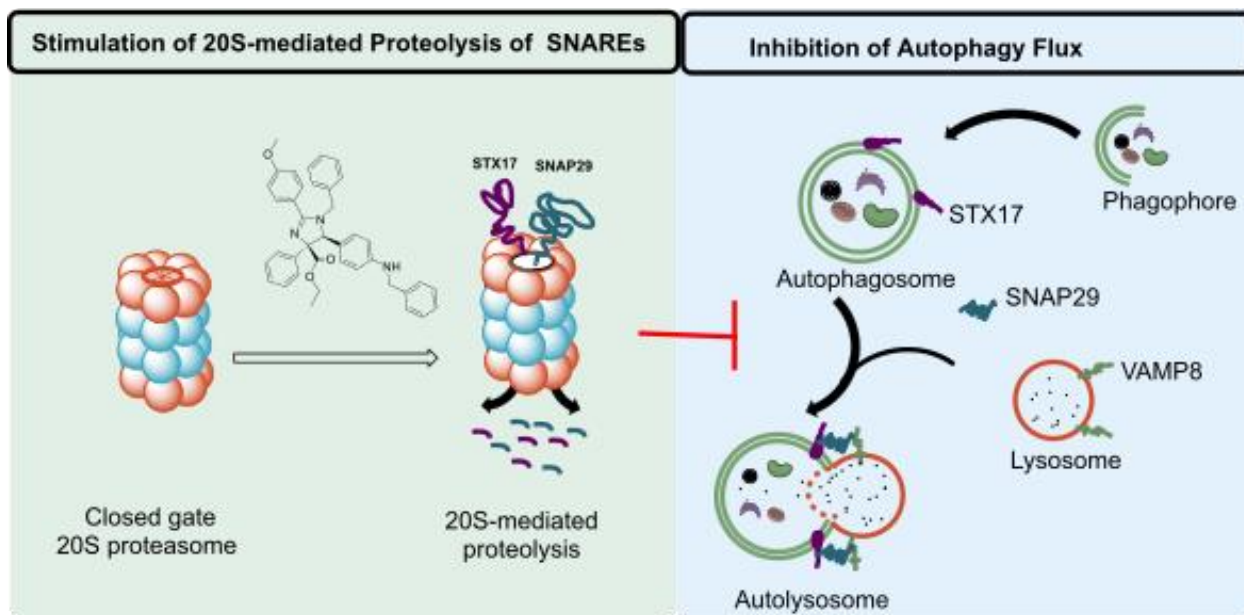


**Figure 3.17: 20S proteasome mediated regulation of autophagic flux.** Summary of the crosstalk from ubiquitin-independent pathway to the autophagy pathway

### 3.3 Conclusions

Although many of the proteins involved in the autophagosome-lysosome fusion process are membrane-bound, SNAP29, is a cytosolic and highly disordered (87%) protein and therefore a likely candidate for unremitting 20S proteasome regulation.<sup>54,214</sup> STX17 does not appear as a typical 20S substrate as it is commonly thought of as a membrane associated protein. However, the relative susceptibility of disordered proteins to 20S-mediated proteolysis is dictated by their level of disorder, protein sequence, cellular compartmentalization and proteolytic accessibility.<sup>54,73,77,214,215</sup> Due to the poor hydrophobic nature of STX17's membrane binding domain, a good fraction of STX17 are cytosolic and are only incorporated into the membrane of completed autophagosomes.<sup>270–272,293</sup> Furthermore, STX17 is recycled after autolysosome formation instead of being degraded like other autophagosome membrane proteins such as LC3B-II and p62.<sup>293</sup> These observations in part suggest that STX17 is degraded through a non-lysosomal pathway. Moreover, the lack of their (SNAP29 and STX17) degradation following autophagy induction with mTOR inhibitors, as observed here and by others<sup>290</sup> further suggests a non-lysosomal mechanism of degradation.

In conclusion, this study presents a novel mechanism of crosstalk between proteasome and autophagy pathway that is regulated by ubiquitin-independent, 20S proteasome-mediated degradation of SNAP29 and STX17. The following contributions were made through this study:

1. Identification of a new mechanism of proteasome-autophagy crosstalk.
2. Identification of new target (20S activation) for autophagy-associated chemoresistance.

## CHAPTER FOUR

### The Identification of New Scaffolds for Proteasome Activation and the Development of Assays for Hit Validation

Reproduced in part with permission from \*Corey L. Jones, \***Evert Njomen**, Benita Sjögren, Thomas S. Dexheimer and Jetze J. Tepe. Small Molecule Enhancement of 20S Proteasome Activity Targets Intrinsically Disordered Proteins. *ACS Chemical Biology* **2017**, 12(9): 2240-2247. Copyright 2017 American Chemical Society.



## 4.1 Introduction

### 4.1.1 Background

Despite the literature being flooded with numerous studies demonstrating the clinical relevance of 20S proteasome activation in neurodegeneration<sup>5,132,135,162</sup> and other proteostasis disorders,<sup>1,4,219</sup> very few molecules have been identified as direct or indirect enhancers of the ubiquitin-independent proteasome degradation pathway. Several of the few 20S proteasome agonists in literature, including detergents such as sodium dodecyl sulfate (SDS),<sup>98</sup> oleuropein,<sup>151</sup> and betulinic acid,<sup>152</sup> are disputed as *bona fide* 20S agonists, since their activities do not translate under more physiologically relevant conditions.<sup>155</sup> The rareness of such *bona fide* 20S agonist and the initial revelations from working with imidazolines (drug-like scaffold) led to an effort to discover and characterize new direct enhancers of 20S proteasome activity.

One of the challenges slowing the discovery of small molecule 20S proteasome activators is the lack of appropriate assays that can identify true 20S agonist from an initial screen. Canonical proteasome activity assays that are amenable to medium- (500-10,000 compounds) and high- (10,000-100,000 compounds) throughput screening (HTS) often employ non-physiologically relevant peptide substrates specific to each proteasome catalytic site (CT-L: Suc-LLVY-AMC, Tryp-L: Boc-LRR-AMC, and Casp-L: Z-LLE-AMC).<sup>27,238</sup> The small size of these peptides allows them to navigate the narrow gate of latent 20S proteasome, resulting in high and varying background proteasome activity. Furthermore, even this so-called standard assay is not standard as different labs use different substrate to enzyme ratios, as well as different buffer systems. Moreover, detergent-like molecules that can relax this narrow 20S gate just enough to increase peptide substrate accessibility to the catalytic core appear as positive hits in these peptide assays. These non-*bona fide* agonists fail in assays that utilize more physiologically relevant protein

substrates.<sup>155,216</sup> These limitations results in ambiguous comparison of potency for proteasome agonists, from batch to batch and from lab to lab. Furthermore, these primary screens employ purified 20S and fluorogenic peptides specific to just one 20S catalytic site, thereby ignoring the allosteric interactions among the three catalytic sites that drive protein degradation.<sup>239</sup> As such, stimulators of the other catalytic sites as well as molecules that act upstream of the proteasome are also missed.

To close this gap in proteostasis drug discovery, two types of IDPs ( $\alpha$ -synuclein and ODC) in conjunction with the AlphaLISA assay have been introduced for the screening of proteasome activators with protein targets, at the cellular level.

AlphaLISA (Amplified Luminescent Proximity Homogeneous Assay) is an adaptable bead-based proximity assay developed to measure analytes in biochemical, cellular and clinical samples in a homogenous manner.<sup>294</sup> A donor and an acceptor beads are brought to proximity by conjugated antibodies targeting either ends of the analyte (protein). Excitation of the donor bead releases singlet oxygen species which travel over a short distance (~200 nm) to excite the acceptor bead. This results in a cascade of reaction and subsequent emission of chemiluminescent signal that is directly proportional to the amount of analyte present.

In the case of analytes which are proteasome substrates, activation of the proteasome in biochemical or cellular assays is expected to enhance the degradation of these proteins, resulting in a decrease in the number of donor and acceptor beads brought to proximity. Thus, proteasome activation can be quantified by measuring the drop in alpha signal (Fig. 4.1).

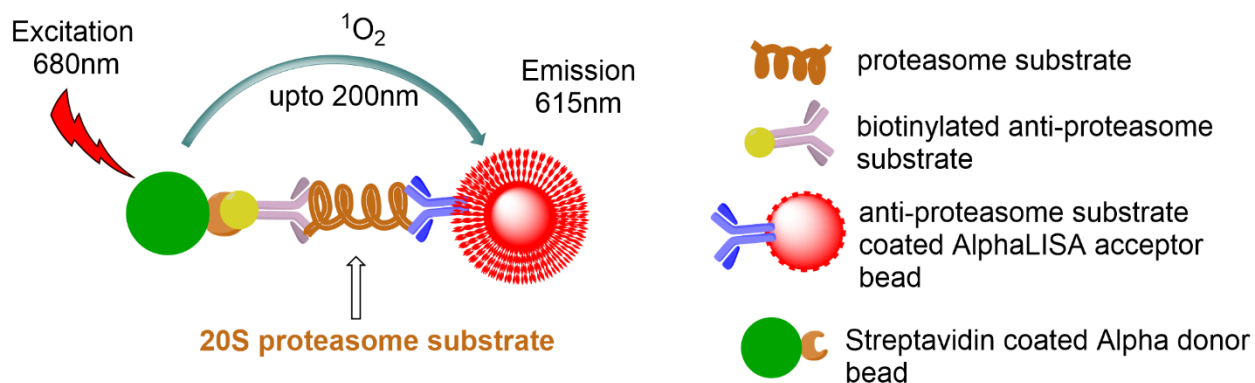


**Figure 4.1:** Principle of proteasome AlphaLISA assay

#### 4.1.2 Objective

The overall goal of this project was to explore the robustness of 20S proteasome activation, through identification of new scaffolds and the development of assay (s) for basic proof-of-concept.

### 4.2 Results and Discussion

#### 4.2.1 Phenothiazines are small molecule activators of 20S proteasome

While I was still trying to understand the mechanism of action of imidazolines, and with the initial findings that there could be non-detergent small molecule 20S activators, we decided to look for new chemical scaffolds capable of enhancing 20S activity. To minimize the chances of adding more non drug-like 20S activators in the literature, we turned to libraries of clinical drugs. Using the purified 20S proteasome and the chymotrypsin-like (CT-L) peptide substrate (Suc-LLVY-AMC), Thomas S. Dexheimer (MSU assay development and drug repurposing core, ADDRC) and I screened the NIH Clinical Collection (727compounds) and Prestwick (1280 compounds) libraries using our on campus high throughput facility. The compounds were deemed inactive if the 20S activity was  $\leq 2$  fold (at 10  $\mu\text{M}$  concentration tested). In this screen, chlorpromazine and its analogues, among other neuroleptic agents, were found to robustly

stimulate the 20S proteasome (Fig. 4.2A). The EC<sub>50</sub> values were determined from the concentration–response curve with fresh stocks of the compounds (Fig. 4.2B). Counter-screen in the absence of AMC substrate was used to eliminate compounds with intrinsic fluorescent properties.

Unlike the imidazolines that enhance all three proteasome catalytic activities, the phenothiazines could only stimulate the CT-L 20S proteasome activity, as illustrated with chlorpromazine (Fig. 4.2C). This suggested that these new scaffolds regulate 20S activity through a mechanism distinct from that of imidazolines,<sup>81</sup> and thus, worthy of further characterization. To confirm the *bona fide* nature of chlorpromazine (CPZ) as 20S agonist, its ability to enhance 20S-mediated proteolysis of  $\alpha$ -synuclein was evaluated. As shown in Fig. 4.2D, CPZ significantly enhanced the degradation of  $\alpha$ -synuclein, an IDP. Furthermore, CPZ was able to enhance 20S-mediated proteolysis of GFP-ODC in HEK293T cells (Fig. 4.2E) and tau (Fig. 4.2F) in U-87 MG cells. Excitingly, the degradation of the structured protein, GAPDH (normally not degraded by the 20S) in these assays were not induced by CPZ. These observations suggest that CPZ can selectively target IDPs for 20S degradation. Coincidentally, methylene blue, a structural analogue of chlorpromazine has been demonstrated to reduce the levels of amyloid beta (A $\beta$ ) and rescues early cognitive deficit by increasing proteasome activity in a mouse model of AD.<sup>154</sup> These data support the robustness and therapeutic potential of chlorpromazine and other phenothiazines as proteasome activators in AD therapy.

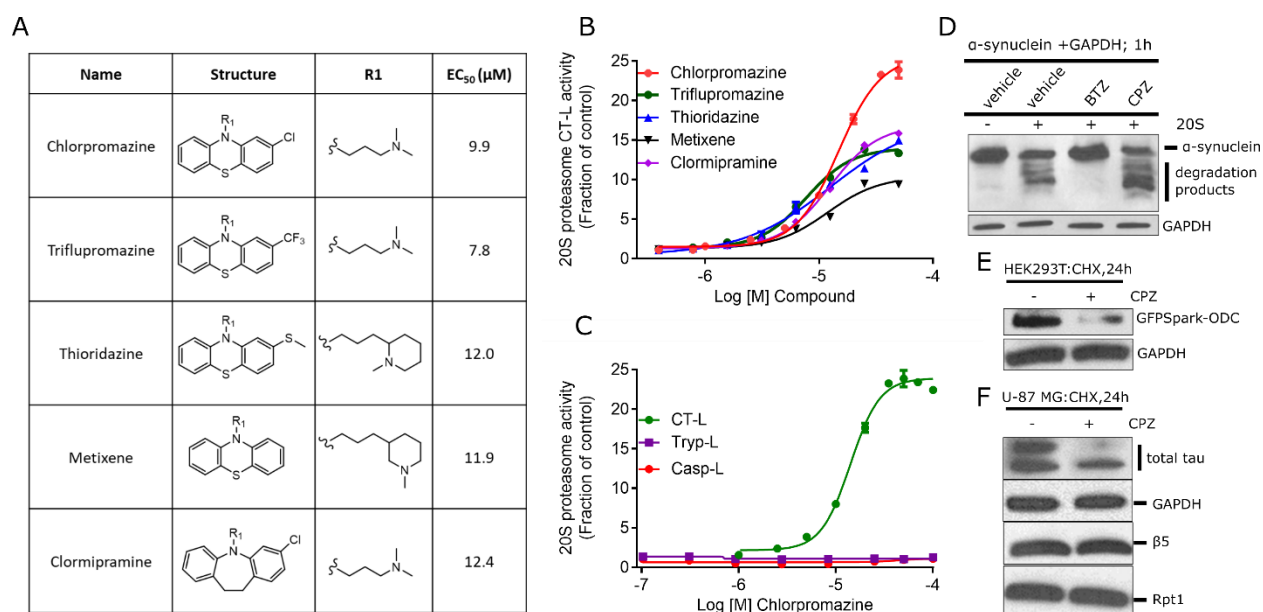


**Figure 4.2: Phenothiazines are small molecule activators of the 20S proteasome. (A)** Structure of phenothiazines and their EC<sub>50</sub> values for enhancement of 20S proteasome chymotrypsin-like (CT-L) activity and **(B)** concentration-response curves. **(C)** Concentration-response curves of chlorpromazine for 20S chymotrypsin-like (CT-L), trypsin-like (Tryp-L) and caspase-like (Casp-L) sites. **(D)** Western blot of a mixture of  $\alpha$ -synuclein ( $\alpha$ -syn) and GAPDH in the presence of purified 20S proteasome with vehicle or chlorpromazine (CPZ, 10μM) for 1h. **(E)** HEK293T cells stably expressing ODC-GFPspark were treated with 20 μg/mL of cycloheximide, in combination with either vehicle (-) or CPZ (30μM) for 24h. ODC-GFPspark degradation was monitored by immunoblot of cell lysates with GFP antibody. **(F)** Glioblastoma (U-87 MG) cells were treated with 20 μg/mL of cycloheximide, in combination with vehicle, or chlorpromazine (CPZ, 30 μM) for 24h. Tau degradation was monitored by immunoblot of cell lysates. Structured proteins (GAPDH) and proteasome subunits (β5 and Rpt1) were probed with corresponding antibodies.

#### 4.2.2 The D2R antagonist, chlorpromazine can be repurposed as 20S agonist

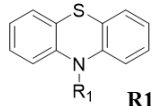
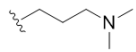
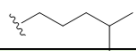
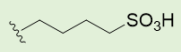
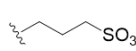
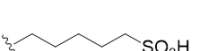
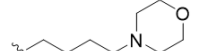
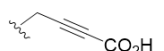
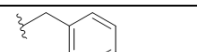
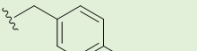
Chlorpromazine (CPZ) and other phenothiazines were first introduced in the market in the 1950s for their antipsychotic properties, resulting from antagonism at the dopamine D2 receptor (D2R).<sup>295,296</sup> Thus, to improve target selectivity, an SAR was undertaken with CPZ as the lead compound, to reduce D2R binding and maintain or improve 20S proteasome activating potential. The D2R activity of CPZ requires a three carbon linker with a terminal amine in the R1 position (Table 2).<sup>296</sup> Thus, our initial approach was to alter the length of this carbon chain and substitute this terminal amine with other functionalities. The synthesis portion of this work was undertaken by Dr. Corey Jones. The synthesized analogues were tested for 20S activation and supplemented by data on dopamine D2 receptor binding provided by Dr. Benita Sjögren (Table 2).

Consistent with literature reports, replacement of the tertiary nitrogen with a carbon to form **1** led to loss of dopamine receptor binding<sup>32</sup> as well as proteasome activating activity (Table 2). This highlighted the significance of a heteroatom in this position for proteasome activation. Accordingly, the sulfonate analogue, **2**, with four carbon linkers in the R1 position showed enhancement of proteasome activity with no DR2 inhibition. To test the specificity of this analogue, the three- (compound **3**) and five-carbon (compound **4**) sulfonate analogues were prepared and tested. Failure of these analogues to stimulate 20S activity suggested that the activity of **2** results from specific interactions with the 20S proteasome. Next, extension of the chain length with a terminal morpholine (**5**) consistently reduces D2R binding and only modestly enhanced 20S activity. Elimination of the nitrogen in the chain (compound **1–4**, **6–8**) effectively reduced the compounds' affinity for D2R to physiologically irrelevant concentrations (Table 2,  $K_i \geq 250 \mu\text{M}$ ). The benzoic acid derivative **7** enhances 20S activity at relatively low concentration ( $\text{EC}_{50}$ ,  $6.4 \mu\text{M}$ ) but exhibited a partial agonist-like behavior, with only 2–3-fold maximum response. The methyl

ester **8** nicely enhanced 20S activity with much better potency (~10-fold maximum activity over vehicle control).

Interestingly, and unlike CPZ (Fig. 4.2C), the two best analogues; sulfonate analogue **2** (Fig. 4.3A), and the methyl ester analogue **8** (Fig. 4.3C) stimulated all three proteasome catalytic sites. Although gate-opening is a common mechanism of 20S activation, chlorpromazine and synthesized analogues appear to induce 20S conformational changes that stretch to the catalytic pockets by different degrees and may or may not involve gate-opening. Compound **2** was also able to enhance 20S-mediated proteolysis of  $\alpha$ -synuclein in a biochemical assay (Fig. 4.3B). Unlike the sulfonate analogue **2**, the methyl ester **8** displayed a classical saturation curve (Fig. 4.3D).

**Table 2:** SAR of chlorpromazine analogues for proteasome activation and antagonism of D2R.

 <b>R1=</b>		20S Proteasome		Dopamine D2R	
		EC <sub>50</sub> ( $\mu$ M)	Maximum Response	Inhibition (%)	K <sub>i</sub> ( $\mu$ M)
CPZ		9.9	20	77.9	0.48
1		0.4	1.6 (inactive)	0	>250
2		6.3	8	4.5	>250
3		19.5 (inactive)	3.4	-	-
4		24.1 (inactive)	3.5	-	-
5		8.9	4.2	74.5	2.97
6		>25	-	2	>250
7		6.4	2.3	1	>250
8		15.6	10.2	2	>250

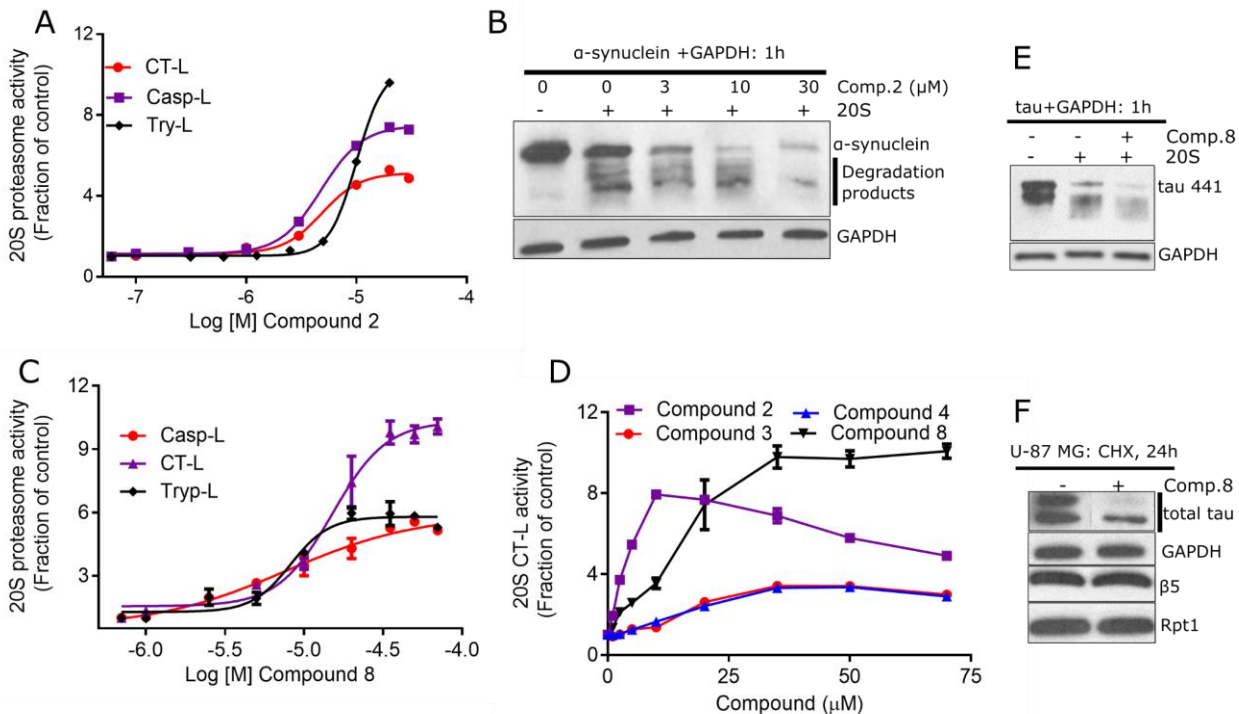


**Figure 4.3: The D2R antagonist, chlorpromazine can be repurposed as 20S agonist.** (A) Concentration-response curves of **2** for 20S CT-L, Tryp-L and Casp-L sites. (B) Western blot of a mixture of  $\alpha$ -synuclein ( $\alpha$ -syn) and GAPDH in the presence of purified 20S proteasome with vehicle different concentrations of **2**, for 1h. (C) Concentration-response curves of **8** for 20S (CT-L), (Tryp-L) and (Casp-L) sites. (D) Comparison of concentration-response curves of **2**, **3**, **4** and **8** for 20S CT-L activity and “SDS-like behavior”. (E) Western blot of a mixture of tau and GAPDH in the presence of purified 20S proteasome with/without **8** (30  $\mu$ M) for 1h. (F) Glioblastoma (U-87 MG) cells were treated with 20  $\mu$ g/mL of cycloheximide, in combination with/without **8** for 24h. Tau degradation was monitored by immunoblot of cell lysates. Structured proteins (GAPDH) and proteasome subunits ( $\beta$ 5 and Rpt1) were probed with corresponding antibodies.



Next, the ability of **8** to enhance 20S mediated proteolysis of tau in biochemical and cellular assays were evaluated. Compared to vehicle, **8** significantly enhanced the degradation of purified tau 441 (Fig. 4.3F) and total tau in U-87 MG cells (**Fig.4.3G**). Consistent with the activity of the parent compounds (CPZ), **8** did not induce the degradation of structured proteins (GAPDH and  $\beta$ -actin). Furthermore, no changes were observed in the level of 19S (Rpt1) and 20S( $\beta$ -5) subunits (Fig.4.3F). Collectively, these studies provide a simple proof-of-concept and the potential of small molecule 20S agonists as *in vitro* tools and, as an attractive approach in targeting proteostasis disorders.

#### **4.2.3 Quantification of 20S proteasome activity by alpha synuclein AlphaLISA technology**

To overcome the challenges associated with the discovery of proteasome activators (section 4.1.1), the AlphaLISA assay was amended for biochemical quantification of proteasome activity. Alpha synuclein AlphaLISA assay has already been developed and optimized by PerkinElmer for quantification of  $\alpha$ -synuclein in serum and other samples (Fig. 4.4A). The goal was to first evaluate this system in a biochemical assay and then transition into a cellular model expressing alpha synuclein.<sup>297,298</sup>

Thus, to test the practicability of using this kit to screen for proteasome activators, TCH-165, a 20S agonist from chapter 2 and epoxomicin (proteasome inhibitor) were used in a biochemical  $\alpha$ -synuclein degradation assay. The 20S proteasome was treated with vehicle, TCH-165 or epoxomicin and then exposed to  $\alpha$ -synuclein for 2h. Aliquots of assay mixture were transferred into 384-well plate and assayed using  $\alpha$ -synuclein alphaLISA kit. As anticipated, TCH-165 treated samples showed a significant reduction in the amount of  $\alpha$ -synuclein while epoxomicin treatment inhibited  $\alpha$ -synuclein degradation (Fig. 4.4B). Furthermore, the combination of  $\alpha$ -synuclein and TCH-165 only did not significantly reduce  $\alpha$ -synuclein alpha signal, confirming that

the change in the proteasome/ $\alpha$ -synuclein/TCH-165 sample is due to enhanced proteasomal degradation. Next, the  $EC_{50}$  of TCH-165 for the degradation of  $\alpha$ -synuclein was determined in a concentration-response assay to be  $17.5 \pm 3.5 \mu\text{M}$ , depending on whether degradation was carried out for 2h or 4h (Fig. 4.4C).

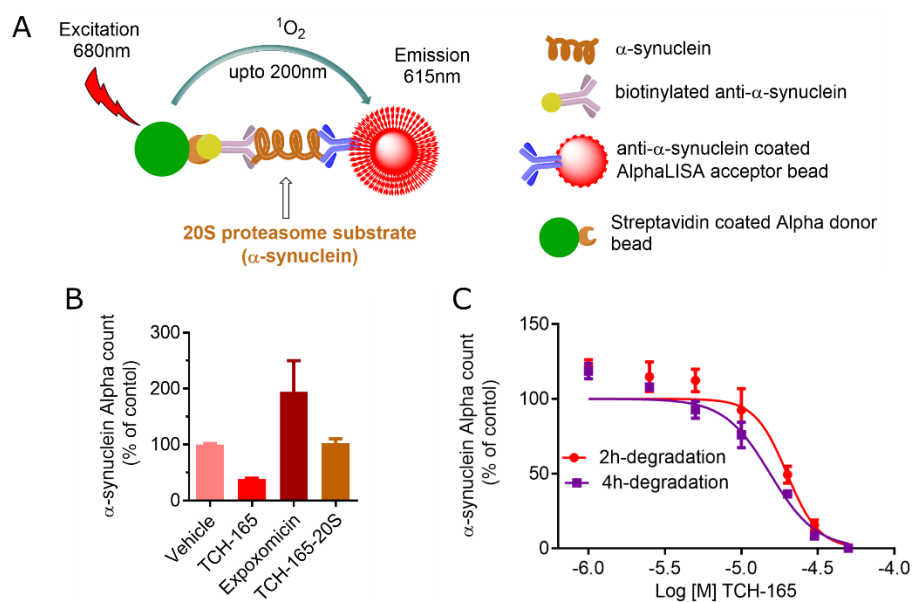


**Figure 4.4: Quantification of 20S proteasome activity by alpha synuclein AlphaLISA technology.** (A) Schematic of alpha synuclein proteasome AlphaLISA assay. (B) AlphaLISA quantification of 20S-mediated degradation of  $\alpha$ -synuclein in the presence of vehicle (DMSO), proteasome activator (TCH-165,  $10\mu\text{M}$ ), or proteasome inhibitor (epoxomicin,  $1\mu\text{M}$ ) (C) AlphaLISA determination of  $EC_{50}$  of TCH-165 for the degradation of  $\alpha$ -synuclein.

The assay was performed in two major steps; (1) Degradation of  $\alpha$ -synuclein with 20S in a  $50 \mu\text{L}$  reaction and (2) transfer of aliquots ( $5 \mu\text{L}$ ) into 384-well plate for AlphaLISA assay. When step one was performed in 96-well plate (to increase workflow and amenability to large scale testing), instead of  $1\text{mL}$  Eppendorf tube,  $\alpha$ -synuclein was found to significantly bind to the degradation plate. Pre-coating of the plate with bovine serum albumin (BSA) or casein abrogated

binding to the plate but also inhibited 20S-mediated proteolysis. This limitation precluded further optimization of the biochemical version of the assay.

In SH-SY5Y cells (a neuroblastoma cell line), endogenous  $\alpha$ -synuclein could not be detected by the AlphaLISA kit, up to 50,000 cells/well of 384-well plate. This was most likely due to limitation in the sensitivity of assay, because  $\alpha$ -synuclein could be detected when concentrated cell lysate was used. Overexpression of  $\alpha$ -synuclein to reach a detectable level inevitably resulted in toxicity. This suggested that a conditional expression system such as a Tet off (tetracycline-inducible expression) system is required. Given that I was towards the end of my program, I decided to evaluate this concept using the GFPspark-ODC expression system that I had developed in chapter 2.

#### **4.2.4 Quantification of 20S proteasome activity by GFPspark-ODC AlphaLISA in cells**

To do this, the GFPspark-ODC construct previously shown to be degraded by the 20S proteasome (Fig. 4.5A) was used. First, cell lysates from HEK cells stably expressing GFP-ODC was used to detect the GFPspark-ODC fusion protein by AlphaLISA (Fig. 4.5B), to make sure that the antibody was compatible with the assay kit. As presented in Fig. 4.5C, AlphaLISA signal was directly proportional to the microgram of protein in the cell lysate, until the hook point is reached.

Hook's phenomenon occurs when the amount of analyte (GFPspark-ODC) is greater than the bead capacity. At this point, the excess analyte starts disrupting stable interaction, resulting in signal reduction. To eliminate the cell lysis and transfer step, a more homogenous mix and read protocol in which cells are directly lysed in the 384-well AlphaLISA assay plate was developed.

First, cell numbers required for significant signal (S) to background (B) ratio below the hook's point was assayed. HEK293T cells stably expressing GFPspark-ODC were seeded at different densities per well of a 384-well plate. After 12h of culture, cells were directly lysed in

the assay plate and incubated with biotinylated anti-ODC and GFP acceptor bead, followed by incubation with streptavidin donor bead. Fig. 4.5D demonstrates direct correlation in cell density (amount of GFPspark-ODC) and alpha signal. Omission of biotinylated ODC antibody or the donor bead resulted in a background signal that was not dependent on cell number. This signal was used as a background/negative control. Next, 10,000 cells were seeded per well of a 384-well plate and the activity of different proteasome modulators tested after 24h treatment.

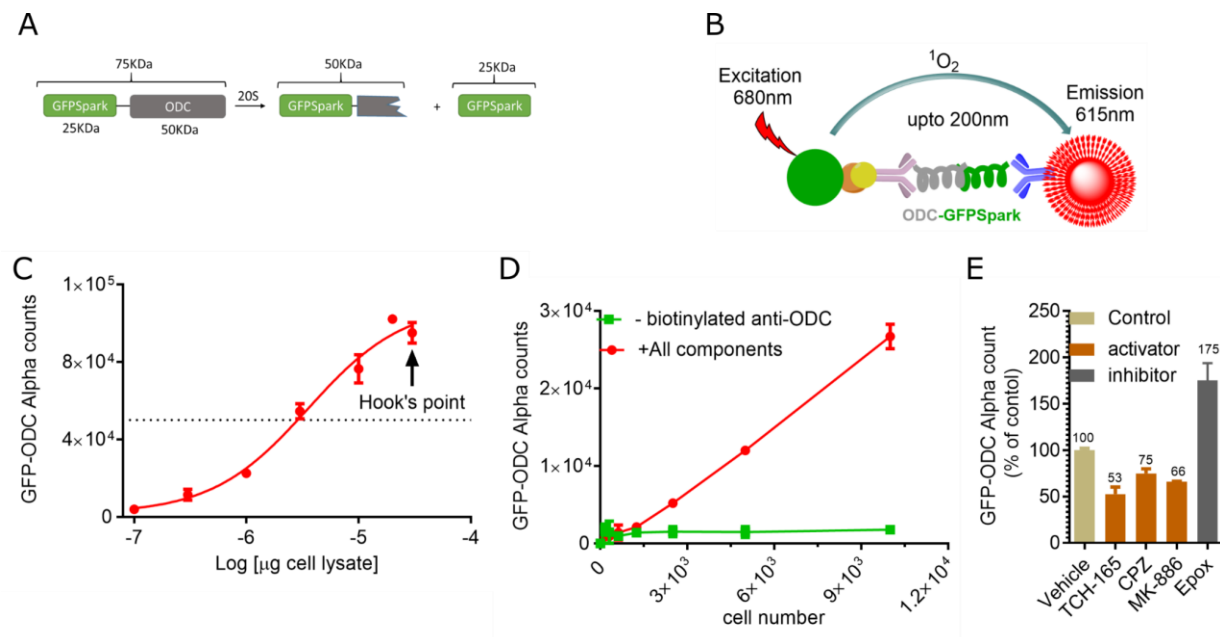


**Figure 4.5: Quantification of 20S proteasome activity by GFPspark-ODC AlphaLISA in cell culture. (A)** Schematic of GFPspark-ODC degradation by the 20S proteasome. **(B)** Schematic of GFPspark-ODC ALphaLISA assay. **(C)** Concentration-response of GFPspark-ODC in microgram of cell lysate. **(D)** Concentration-response of GFPspark-ODC signal with cell number in HEK293T cells stably expressing GFPspark-ODC. **(E)** HEK293T cells stably expressing GFPspark-ODC were seeded at a density of 10,000cells/well. Cells were then treated with vehicle, 10  $\mu$ M proteasome activators or 1  $\mu$ M proteasome inhibitor, epoxomicin for 24h. GFPspark-ODC was quantified by AlphaLISA, under condition # 2(see figure 4.6C).

As shown in Fig. 4.5E, this assay could distinguish proteasome activators from proteasome inhibitors, in a cellular system. However, for cells stably expressing GFPspark-ODC, the signal to background ratio of only 10-fold with 10,000 cells gives a very narrow working window with activators. Going above this cell number would be too crowded for 384-well plate. Thus, cell number titration was repeated with HEK293T cells transiently expressing GFPspark-ODC as described above (Fig. 4.6A). An increasing S/B ratio was observed with increasing cell number per well, until the Hook's point was reached. A significant S/B ratio (~25fold) was observed at 500 cells/well. Using this condition, the proteasome activator (TCH-165) and proteasome inhibitor (bortezomib) yielded expected activities as shown in Fig. 4.6B.

AlphaLISA is a cost ineffective assay. Thus, to cut down on reagents, HEK cells transiently expressing GFP-ODC were seeded in 384-well plate at a density of 1000 cells/well and AlphaLISA performed with ten different reagent combinations. As shown in Fig. 4.6C, cutting down on reagent maintained the S/B ratio above ten. However, the reduction in signal relative to the standard condition (condition #2 Fig. 4.6C) with reduced antibody and/or beads suggested I was working in the hook's region. To stay within the linear range of the assay, different cell numbers were re-titrated against reagent condition #10 as shown in Fig. 4.6D. While this condition appeared to be below the hooks point and gave significant S/B ratio, an initial attempt to determine the Z-factor of the assay invalidated this assay condition (high S/N).

Thus far, condition number **2** with 500-1000 cells/well under our transfection condition appears to be most appropriate for 20S activator screening. Although, further evaluation of the assay quality (Z-factor) under this condition is needed for use on a high throughput scale, this system presents the first cellular assay that would allow for direct screening of proteasome activators with a protein substrate.

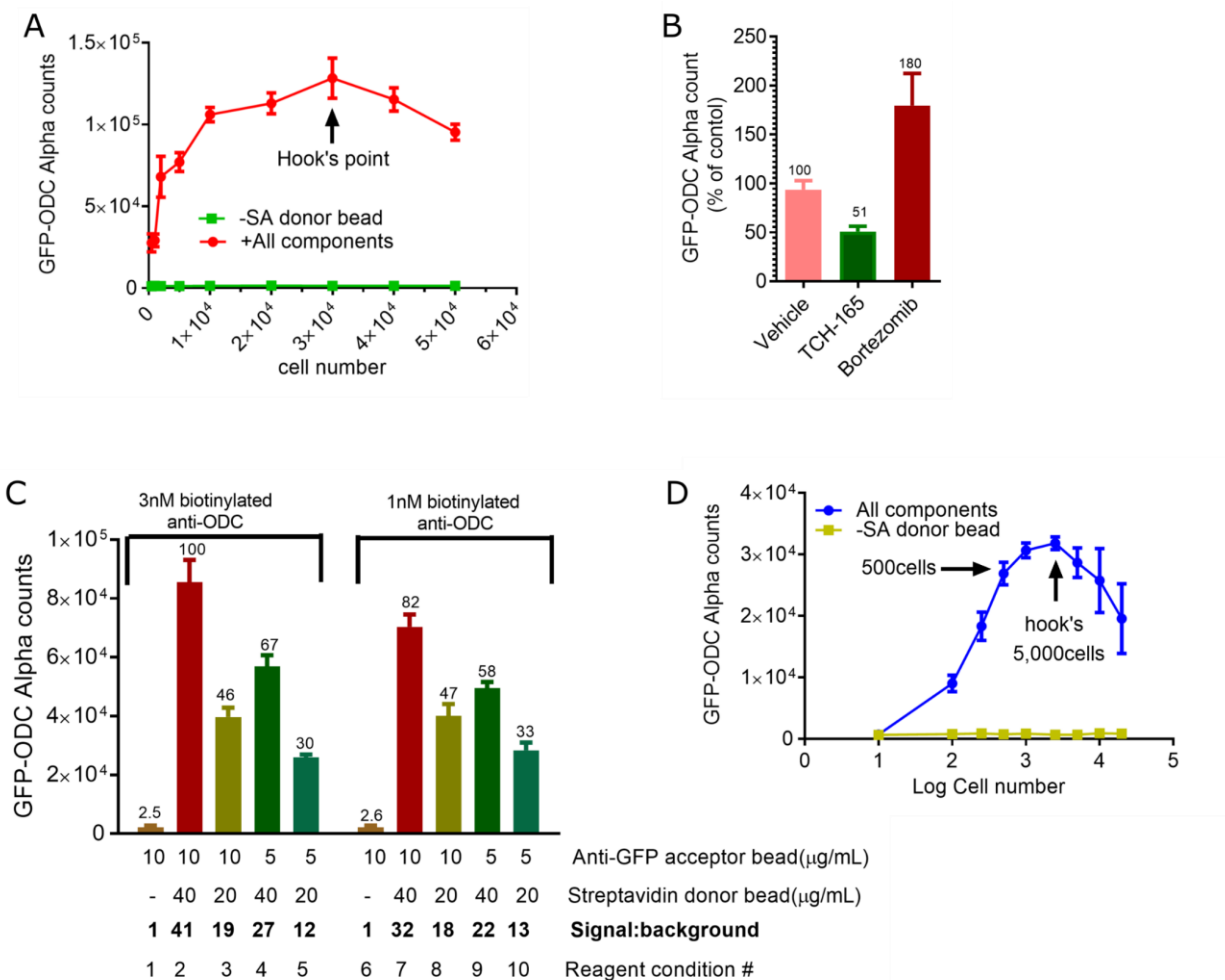


**Figure 4.6: Optimization of GFPspark-ODC assay.** (A) Concentration response of GFPspark-ODC signal with cell number in HEK293T cells transiently transfected with GFPspark-ODC. (B) HEK293T cells transiently transfected with GFP-ODC were seeded at a density of 500 cells/well for 12h. Cells were then treated with either vehicle, 10  $\mu$ M TCH-165 (20S activator), or 1  $\mu$ M Bortezomib (proteasome inhibitor) for 12h, and assayed for GFP-ODC by AlphaLISA, under condition #2. (C) Determination of optimal reagent concentration for detection of GFPspark-ODC in HEK293T cells (1000 cells/well) transiently expressing GFPspark-ODC. (D) same as C under condition number 10. Error bars represent mean  $\pm$  SD of triplicate of a single experiment.

Furthermore, the assay can be amended to any protein that is degraded by the 20S proteasome. As such, researchers interested in studying proteasome activators with respect to a specific disease could modify this assay using proteasome substrates that are associated with the disease of interest. For example,  $\alpha$ -synuclein for Parkinson's disease and c-Myc for multiple myeloma.

This assay is primarily limited by cost and the need to optimize cell numbers for every condition that changes protein expression or the use of a new batch or source of antibodies. Furthermore, multiplexing with a cell viability assay will be necessary to eliminate false positives.

#### **4.3 Conclusions**

More drug-like small molecule proteasome activators are likely available than thought. Better assays, which have been introduced here will be required to explore this field further. In neurodegeneration, proteasome activators are expected to protect the neurons from proteotoxicity. In cancer, these same molecules are expected to induce apoptosis through enhanced degradation of cancer driving IDPs. Therefore, as we move beyond basic proof-of-concept, it would be crucial to start exploring the clinical relevance of these molecules in the appropriate cell model. For example, neuroblastoma cells cannot unambiguously predict the neuroprotective as well as the anti-cancer efficacy of proteasome activators. In other words neuroprotective activities would be better assessed in primary neurons exposed to or overexpressing typical culprits such as amyloid- $\beta$  oligomer, polyglutamine tails or  $\alpha$ -synuclein.

## **CHAPTER FIVE**

### **Imidazolines as Anti-Mycobacterial Agent: CRISPRi/dCas9-Driven Target Validation**



## 5.1 Introduction

### 5.1.1 Background

In previous chapters, the regulation of human proteasome as a therapeutic strategy in non-infectious proteostasis disorders such as cancer and neurodegeneration were studied. To further expand on the therapeutic potential of proteasome regulation, imidazolines were explored on *Mycobacterium tuberculosis*, since this bacterium is one of the few infectious pathogens that relies on the proteasome for growth and survival in the host.

Tuberculosis (TB) is an infectious, air-borne disease caused by the bacillus *Mycobacterium tuberculosis* (*Mtb*) with the lungs as primary target organ.<sup>299,300</sup> Generally, only a relatively small proportion of people infected with *Mtb* develop TB. However, TB remains a major global health problem, responsible for ill health among millions of people each year.<sup>301,302</sup> TB causes about 1.5 million deaths a year, with about 10 million new cases in 2017, ranking it the number one leading cause of death from an infectious disease worldwide. The success of *Mtb* as a human pathogen resides in its ability to adapt to the host immune microenvironment.<sup>303–307</sup> This persistent nature lengthens treatment for new cases of drug-susceptible TB to 6-9 months with a regimen of four first-line drugs: isoniazid, rifampicin, ethambutol and pyrazinamide. Meanwhile, treatment for multidrug-resistant TB (MDR-TB), defined as resistance to isoniazid and rifampicin is longer (~20 months), and requires more expensive and more toxic drugs, with low treatment success rates.<sup>308,309</sup> Drug resistance is attributed in part to the long treatment period, as most patients will often get intolerant and stop treatment.<sup>310</sup> Therefore, targeting mechanisms that enable *Mtb* to persist is key to limiting latent tuberculosis, and improving treatment success for both new TB and MDR-TB cases.

Upon inhalation through the airways, *Mtb* is sequestered into alveolar macrophages that reside within the lungs.<sup>311</sup> While inside the macrophages, *Mtb* resides within the mycobacterial phagosomes, thereby avoiding lysosomal killing. Macrophages harboring mycobacteria can remain within the lungs of the infected host or spread to other organs in the body. For most healthy individuals, the immune system controls the infection by *Mtb* such that TB disease does not develop. However, about 10% of infected individuals eventually develop TB. While *Mtb* can stay viable in phagosome for years, infected macrophages produce immune modulators that coordinate the formation of granuloma (Fig. 5.1) around infected macrophages, leaving the *Mtb* in a non-replicative persistent state that is not easily accessible to nutrient and drugs.<sup>312,313</sup> *Mtb*-induced upregulation of matrix metalloproteinase eventually results in digestion of collagen around the granuloma, leasing *Mtb* to cause more infection (Fig. 5.1).<sup>314,315</sup>

Among the host's pool of antimicrobial effector is nitric oxide (NO), produced by activated macrophages. NO is believed to kill *Mtb* by forming highly reactive nitrogen intermediates (RNI) that crosses the bacterial cell wall to combine with reactive oxygen species (ROS) causing oxidative damage to *Mtb* proteins, lipids and DNA.<sup>304,316</sup> The ability to escape NO toxicity has been attributed in part to the presence of proteasome in *Mtb* that help combat biochemical damages to biomolecules.<sup>317,318</sup> Mutagenesis of *prcA* (gene that codes for 20S  $\alpha$ -subunits) and *prcB* (gene that codes for 20S  $\beta$ -subunits) have demonstrated that the proteasome is essential for optimal *in vitro* growth of *Mtb*.<sup>319</sup> Furthermore, conditional knockdown of *prcA* and *prcB*<sup>320</sup> or inactivation of proteasome-associated proteins *mpa* and *pafA*,<sup>321</sup> were found to reduced *Mtb* persistence and virulence in mice, respectively. These findings in mice, suggest that the *Mtb* proteasome is vital for pathogenicity.

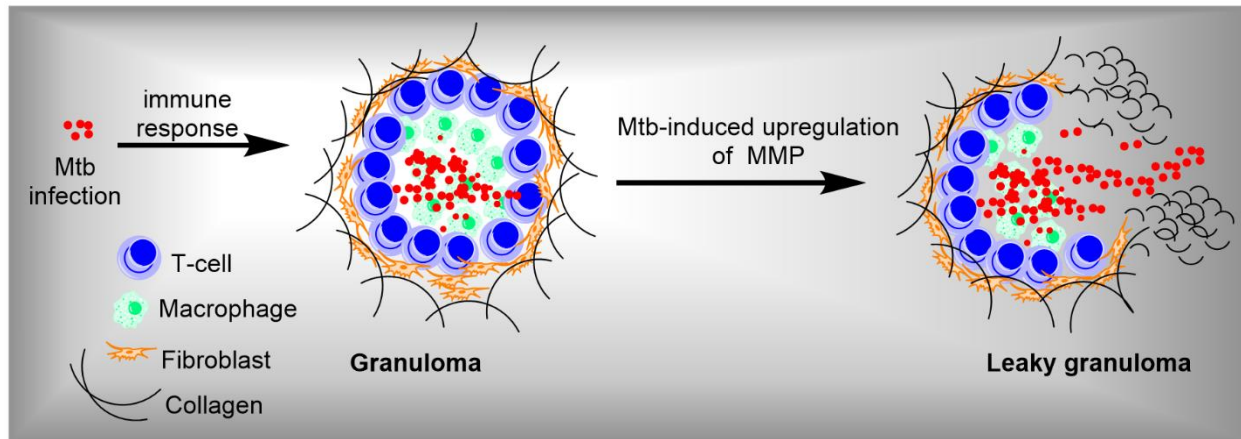


**Figure 5.1: The granuloma of *Mycobacterium tuberculosis*.** The host immune mechanism against TB infection.

The *Mycobacterium tuberculosis* 20S proteasome (*Mtb*20S) has a similar structural assembly to the eukaryotic proteasome.<sup>322</sup> The two inner  $\beta$ -rings carry the proteolytic active sites and the two outer  $\alpha$ -rings enable contact with the ATPase partners. However, unlike the eukaryotic proteasome, the bacterial 20S particle consists of homoheptameric  $\alpha$ - and  $\beta$ -rings coded by the *prcAB* gene located on an operon with *pup* (prokaryotic ubiquitin-like protein).<sup>323,324</sup> The  $\alpha$ -rings also create docking sites for the Mpa (Mycobacterial proteasome associated ATPase) cap, which is analogous to the eukaryotic 19S cap.<sup>325,326</sup> The Mpa cap is a homohexameric ring structure that caps the 20S proteasome core and interacts with the prokaryotic ubiquitin-like protein, Pup, through a hydrophobic interface. Recruitment of substrates to the mycobacterial proteasome pathway occurs in a manner analogous to ubiquitin proteasome pathway in eukaryotes. A small protein, Pup, encoded directly upstream of the *PrcAB* (Fig. 5.2A) is covalently attached to lysine residues of substrate proteins through its C-terminus.<sup>327</sup> This degron targets the substrate protein for degradation through the ATP dependent proteasome pathway. Substrate pupylation is carried

out by *PafA*, which mimics the activities of eukaryotic ubiquitin ligases; E1, E2, and E3 (Fig. 5.2B).

Limited proteasome activity reduces *Mtb* persistence. Thus, *Mtb* proteasome has emerged as a new target for the development of anti-TB chemotherapy. So far, only few of these *Mtb* proteasome inhibitors have been identified.<sup>328–330</sup> In a high throughput screening, the Abramovitch lab identified TCH-156 as an inhibitor of *Mtb* growth with EC<sub>50</sub> of ~7  $\mu$ M.

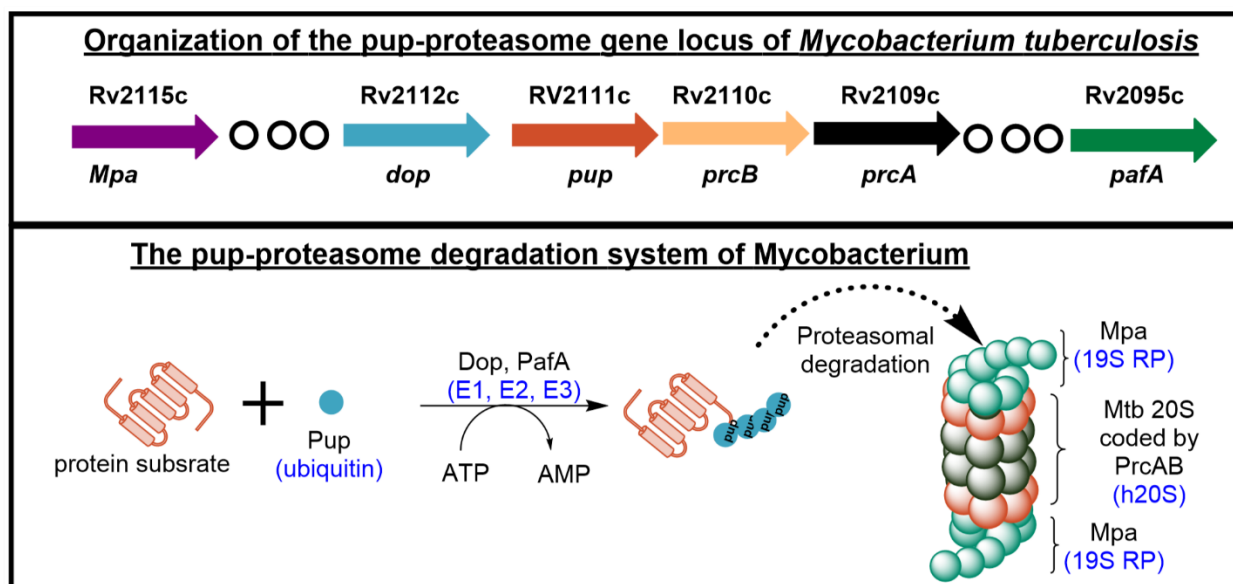


**Figure 5.2: The *Mycobacterium tuberculosis* pup-proteasome system.** (A) The proteasomal subunit genes *prcB* and *prcA* and the preceding *pup* gene are organized in an operon. The proteasomal ATPase *Mpa* is encoded by a separate gene located further upstream. The gene for the deamidase/depupylase *Dop* is usually found directly upstream of *pup*, whereas the gene for the Pup-ligase *PafA* is located further downstream. (B) The pup-proteasome system in *Mtb*. Protein substrates are tagged with pup which is then recognized, unfolded and threaded by the *Mpa* cap into the 20S core for degradation. Labels in blue represent analogous system in eukaryotes.

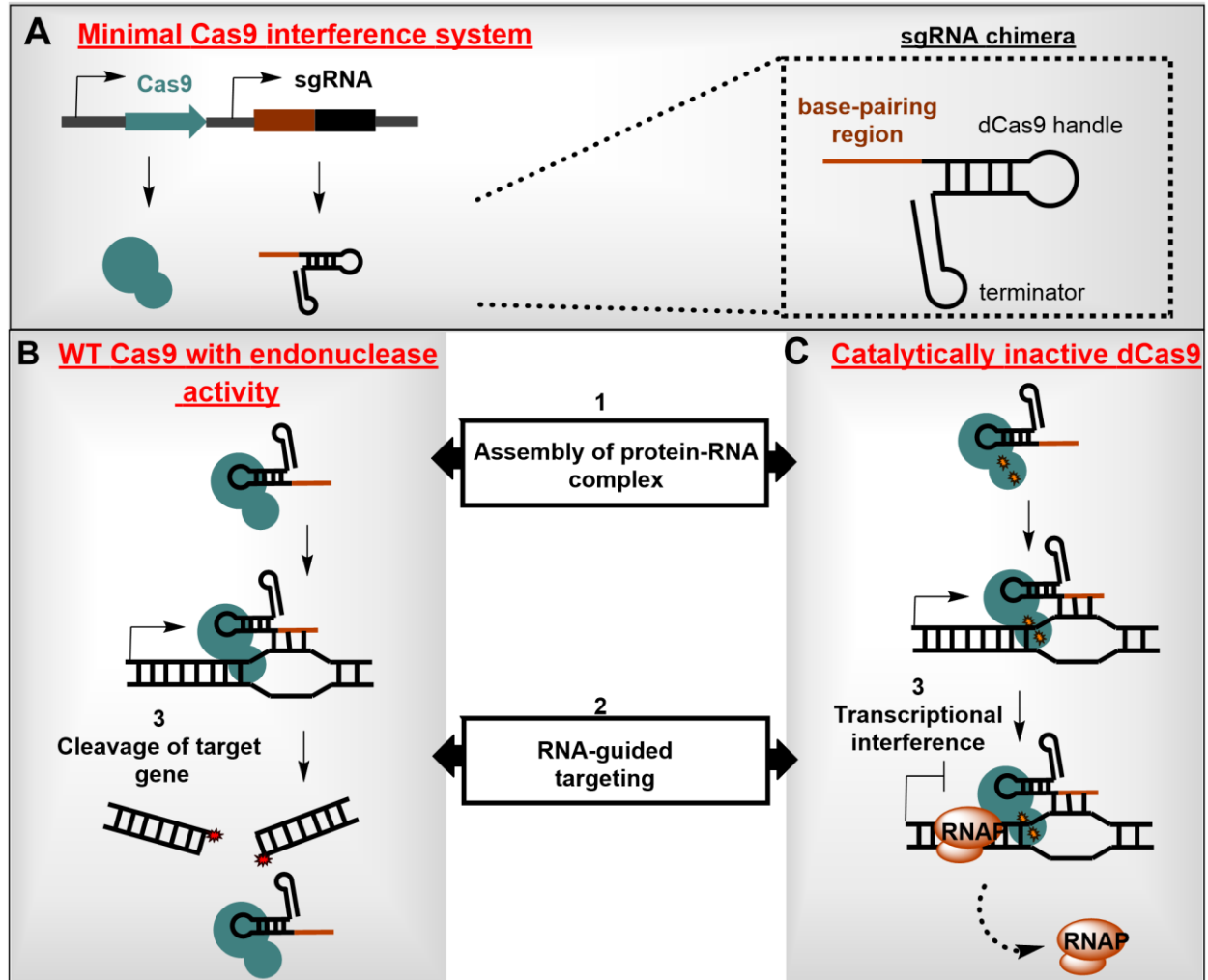


**Figure 5.3: CRISPR interference system.** (A) The minimal transcription interference system of Cas9 (B) The wild-type (WT) Cas9 protein binds to the sgRNA and forms a protein-RNA complex. The complex binds to specific DNA targets by Watson-Crick base pairing between the sgRNA and the target DNA. The DNA is then cleaved by the nuclease activity of the Cas9 protein. (C) In the case of dead-Cas9 (dCas9, dCas9- sgRNA is still formed and bound to specific DNA target. When the binding occurs on the protein-coding region, it blocks RNA polymerase (RNAP) and transcript elongation. Adapted from [Lei S. Qi et al<sup>331</sup>](#)

Given that imidazolines such as TCH-156 had earlier been identified as allosteric modulators of the human proteasome,<sup>81,234,235</sup> we speculated that the anti-mycobacterium activity of TCH-156 was related to the regulation of *Mtb* proteasome. However, the *Mtb*20S is structurally distinct from that of the human proteasome. An SAR to improve potency and reduce host toxicity would require target validation by biochemical and genetic approaches such as CRISPRi/dCas9.

CRISPR-Cas (clustered regularly interspaced short palindromic repeats–CRISPR associated proteins) is an adaptive immune system in bacteria and archaea that uses small RNAs to target and cleave foreign nucleic acid in a sequence-specific manner.<sup>332–334</sup> The most studied system is the type IIA system from *Streptococcus pyogenes*, where a single nuclease, Cas9 and two small RNAs, a CRISPR RNA (crRNA) and a partially complementary trans-activating crRNA (tracrRNA), are necessary and sufficient for RNA-guided silencing of foreign DNA. This dual RNA system has been simplified by fusing the crRNA and tracrRNA to generate a chimeric single guide RNA (sgRNA)(Fig. 5.3A).<sup>335</sup>

Targeting specificity is determined by both Watson–Crick base pairing of the sgRNA and target DNA as well as a short DNA motif (protospacer adjacent motif, PAM) within the target DNA sequence.<sup>334</sup> Wild-type CRISPR-Cas9 system (Fig. 5.3B) has been repurposed for transcriptional repression (CRISPR interference or CRISPRi) by inactivating Cas9 nuclease, through point mutations within its HNH and RuvC nuclease domains. Thus, co-expression of the nuclease-dead Cas9 protein (dCas9) with an sgRNA designed with 20 complementary nucleotides to the target gene juxtaposed to an appropriate PAM yields specific silencing of the gene of interest (Fig. 5.3C).<sup>331,335</sup> The dCas9 sgRNA complex represses target gene transcription by blocking RNA polymerase from the target promoter, by causing a steric block to transcription elongation, or by interfering with transcription factor binding. When targeting the promoter, sgRNAs specific for

either the template or non-template strand can be used, whereas an elongation block is most effective when targeting the non-template strand. The *Streptococcus pyogenes* CRISPRi/dCas9 system has been extensively characterized in model bacteria; *Escherichia coli* and *Bacillus subtilis*. In these organisms, up to 300-fold gene repression has been achieved. However, in *Mtb*, the *Streptococcus pyogenes* Cas9-based CRISPRi system is of restricted utility due to relatively weak knockdown efficiency and proteotoxicity.<sup>336</sup> Rock *et al*<sup>337</sup> addressed these limitations by developing a more robust CRISPRi/dCas9 system that utilizes an efficacious Cas9 protein from *Streptococcus thermophilus* (dCas9<sub>Sth1</sub>). The CRISPRi/dCas9 from *Streptococcus thermophilus* achieved 20- to 100-fold knockdown of endogenous gene expression with minimal proteotoxicity. The published PAM consensus for Sth1 Cas9 (5'-NNAGAAW-3') was also expanded upon. The efficiency of this system was also determined by PAM sequence used. In contrast to other CRISPRi systems, dCas9<sub>Sth1</sub>-mediated gene knockdown system of Rock *et al* is robust when targeted far from the transcriptional start site, thereby allowing high-resolution dissection of gene function in the context of bacterial operons. In this system, gene silencing is effective when targeting either the template or non-template strand of the gene promoter, or the non-template strand of the gene 5' untranslated region (UTR) and ORF.

### **5.1.2 Objective**

The overall goal of this project was to validate the *Mtb* proteasome as a target for the anti-mycobacterium activity of imidazoline TCH-156.

## 5.2 Results and Discussion

### 5.2.1 Imidazolines inhibit *Mycobacterium tuberculosis* growth

In a medium throughput screening by Dr. Abramovitch lab (MSU), some imidazolines were identified to inhibit *Mtb* growth. This growth inhibition was enhanced in the presence of nitric oxide by about two-fold (Fig. 5.4). Given that the ability of *Mtb* to escape NO toxicity has been attributed in part to the presence of proteasome in *Mtb* that degrades oxidatively damaged proteins<sup>7</sup>, a study was undertaken to validate the *Mtb* proteasome as a target for this anti-mycobacterium activity.

### 5.2. Imidazolines inhibit the proteasome of *Mycobacterium tuberculosis* in the presence of sodium dodecyl sulfate

Habitually, activity assays for eukaryotic proteasome usually include low concentration of detergent (e.g 0.02% SDS) in the assay buffer. This detergent helps open the gate into the latent 20S which is then inhibited by the drug being tested. Eukaryotic 20S is mostly latent and activation with SDS results in about 10-12fold increase in activity. Although the activity of *Mtb* proteasome is only enhanced by about 50% (1.5fold) under this SDS condition, this tradition of incorporating SDS in proteasome inhibition assay has been inherited in the *Mtb* proteasome inhibition assay.

To find out if these imidazolines inhibited *Mtb* growth by targeting the proteasome, three active (TCH-156, TCH-196, TCH-118) and three inactive (TCH-099, TCH-044, TCH-034) compounds (Fig. 5.5A) from the *Mtb* growth assay were tested for their ability to inhibit purified *Mtb*20S proteasome. For this experiment, the AMC-labelled fluorogenic peptide assay was used. A concentration-response testing of these compounds with SDS buffer showed proteasome inhibition by the three active compounds, in addition to two of the inactive molecules (Fig. 5.5B and 5.5C). However, exclusion of SDS from the assay buffer resulted in no activity of the



compound against *Mtb*20S (Fig. 5.5B). Because imidazolines inhibit human proteasome by interfering with 19S-20S interaction, the activity of these compounds was investigated in the presence of 30 molar excess of Mpa (an ATPase analogue of 19S).

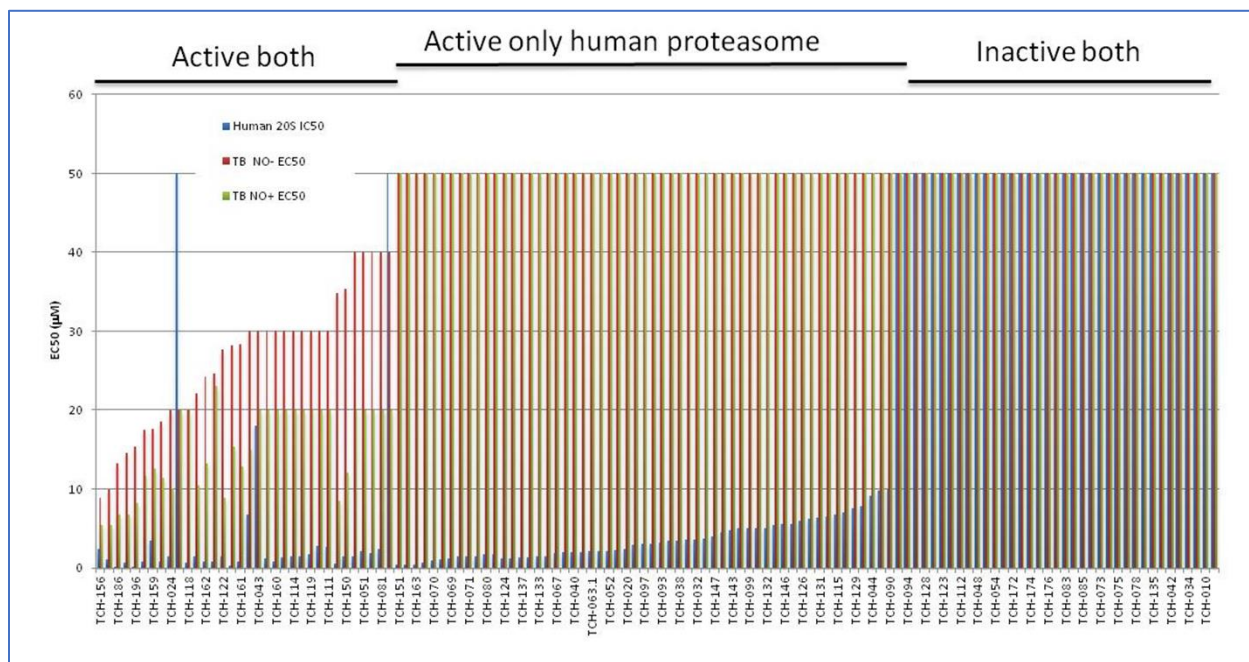


**Figure 5.4: SAR of imidazolines against human 20S proteasome and growth of *Mycobacterium tuberculosis*.** EC<sub>50</sub> of imidazolines in inhibiting *Mtb* growth with (green) or without (red) nitric oxide (NO) and in inhibiting human proteasome in SDS assay (blue). Courtesy of Dr. Abramovitch's lab.

Unlike human 20S that is activated by up to 4-fold by the 19S, the activity of *Mtb* 20S is only enhanced by about 15-20% (1.2fold) by Mpa. This is consistent with cryo-EM data showing very weak *in vitro* interaction between the protein complexes (Mpa-20S).<sup>338</sup> Just like with the SDS free buffer, these compounds had no activity on Mpa activated 20S proteasome (Fig. 5.5B).

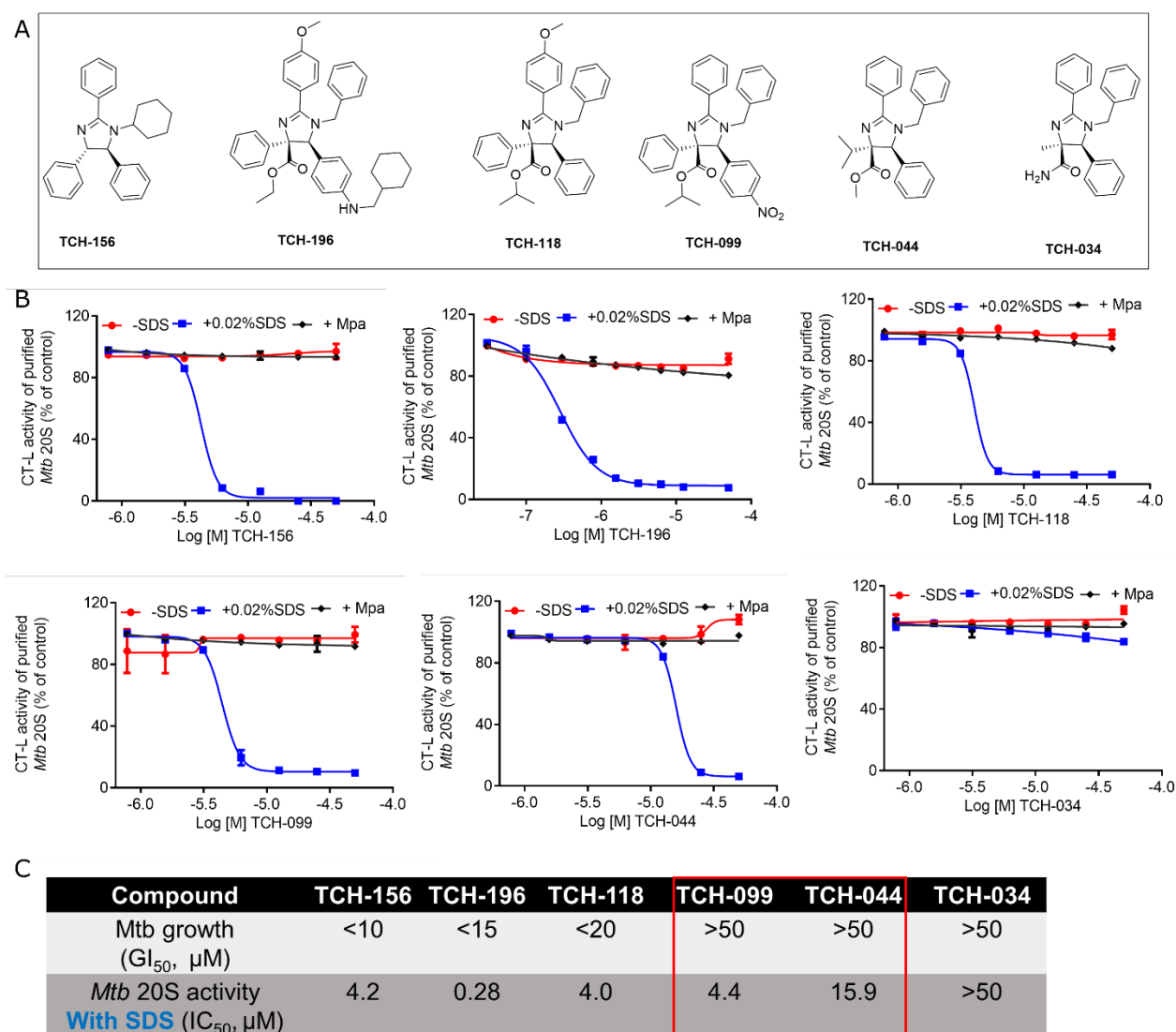


**Figure 5.5: *In vitro* activity of imidazolines in purified *Mycobacterium tuberculosis* proteasome assay. (A)** Structure of active (TCH-156, TCH-196), weakly active (TCH-118) and inactive (TCH-044, TCH-034) imidazolines as per *Mtb* growth assay (see Fig.5.4). **(B)** Four-parameter concentration-response plot for the hydrolysis of Suc-LLVY-AMC by *Mtb*20S without (red) or with (blue) 0.02% SDS or with 30-fold molar excess (150nM) Mpa (black). **(C)** EC<sub>50</sub> of the indicated imidazolines in inhibiting *Mtb* growth and in inhibiting *Mtb* proteasome in SDS buffer.

While the inconsistency in the cellular and *in vitro* activities of TCH-099 and TCH-044 could be due to other factors such as poor uptake/efflux by *Mtb* or metabolic instability (Fig. 5.5C, red box), the fact that these molecules only inhibit the *Mtb* proteasome under a non-physiological condition (*in vitro* SDS proteasome assay), warranted further validation of the *Mtb* proteasome as the target for the anti-mycobacterial activity of imidazolines.

### 5.2.3 CRISPRi/dcas9 knockdown of proteasome-related genes decreases proteasome activity in *Mycobacterium smegmatis*

Due to the complexity of working with *Mycobacterium tuberculosis* (slow growth and safety), we first evaluated this system in the non-virulence species *Mycobacterium smegmatis* (*Msmeg*). Using the method of Jeremy Rock et al<sup>20</sup>, anhydrous tetracycline (ATC)-inducible, catalytically inactive Cas9 (dCas9) fusion proteins guided by gene-specific sgRNAs were used to repress (CRISPRi) transcription of proteasome target genes. The experimental setup is shown in Fig. 5.6.

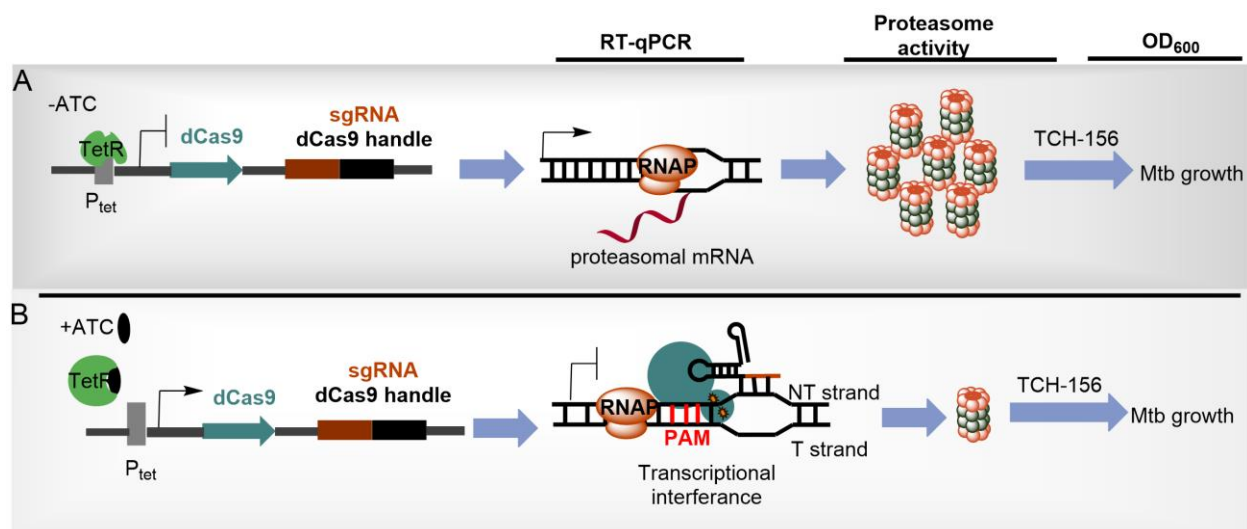


**Figure 5.6: CRISPRi/dcas9 system under the control of anhydrotetracycline (ATC)-inducible promoter (P<sub>Tet</sub>). (A) Basal system (B) Proteasome knockdown system.**

First, the gene sequences for PrcA (MSMEG\_3894), PrcB (MSMEG\_3895), Pup (pup) PafA (MSMEG\_3890), and Mpa (MSMEG\_3902) were obtained from tubercuList-TB gene (SmeigmaList-DNA sequence). From the repertoire of functional PAM reported by Rock, sgRNAs were designed with PAMS claimed to have the highest gene repression efficiency (Table 12, experimental section). The sgRNA for *Msmeg* were then cloned into the *Msmeg* CRISPRi plasmid backbone, PLJR962 and transformed into *Msmeg*. In the presence of ATC, co-expression of the sgRNA and the *dcas9* protein is expected to repress gene expression.

To check for gene knockdown, *Msmeg* with the target sgRNA were cultured with or without ATC and gene repression quantified by RT-qPCR of isolated RNA. Additional control included the PLJR962 vector with no sgRNA. At 100 ng/mL of ATC (as used by Rock *et al*) 17-100-fold repression was achieved. Doubling the concentration of ATC increased gene repression by up to 480-fold for Mpa. However, no repression was observed for pafA at both concentrations of ATC tested (Fig. 5.7A and 5.7C).

To find out if these hypomorphs influenced the pup-proteasome pathway, *Msmeg* cell lysates from cells treated with or without ATC for 48h were assayed for proteasome activity using the CT-L substrate (Suc-LLVY-AMC). Although about the same degree of gene knockdown was obtained for PrcA and PrcB, PrcA hypomorph had the highest fold decrease (22fold) in proteasome activity. Knockdown of Mpa had no effect on proteasome activity (Fig. 5.7B and 5.7C). This was not surprising, since small peptides such as Suc-LLVY-AMC can be degraded by the 20S without the need for a regulatory cap (Mpa). This also suggests that knock down of Mpa does not have a feedback effect that modulate 20S (PrcAB) transcription/translation. Interestingly, pafA which showed no change in mRNA had about 4-fold decrease in proteasome activity (Fig. 5.7C), probably due to the time difference for mRNA(14h) and proteasome assay (48h). Since PafA is

further downstream of the other proteasome gene (Fig. 5.2A), this is less likely to be a polar effect; a phenomenon whereby any gene in an operon downstream of the sgRNA binding site could also be silenced. As expected, the PLJR962 control plasmid had the same proteasome activity with/without ATC.

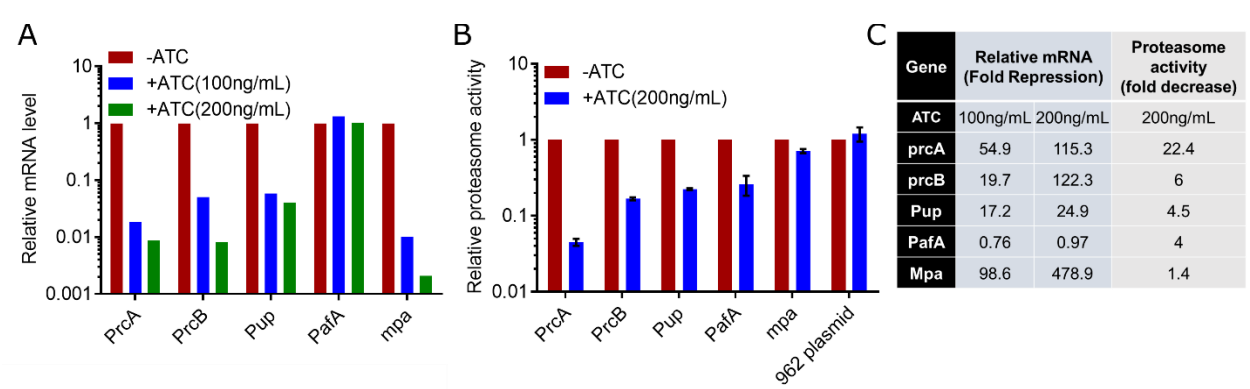


**Figure 5.7: CRISPRi/dcas9 knockdown of proteasomal genes in *Mycobacterium smegmatis*.**

(A) Fold change in mRNA (isolated after 14h treatment with or without ATC) was quantified by RT-qPCR of cDNA and normalized to the house keeping gene, sigA. (B) Hydrolysis of Suc-LLVY-AMC in *M. smegmatis* cell lysate from cells treated with or without ATC (200ng/mL) for 48h. Non-ATC samples were set to one and ATC samples expressed as a fraction of non-ATC sample for each gene. Data are means of triplicate from a single experiment.

### 5.2.4 CRISPRi/dcas9 knockdown of proteasome-related genes does not sensitize

#### *Mycobacterium smegmatis* to imidazolines

Target knockdown is expected to reduce the effective concentration of a drug as fewer targets are now available for binding. Thus, we anticipated that knock down of proteasome genes would sensitize *Msmeg* to killing by TCH-156. However, unlike the *Mtb*, knockdown of

proteasome in *Msmeg* has no effect on its growth, under normal growth condition, with sufficient nutrient.<sup>339</sup>

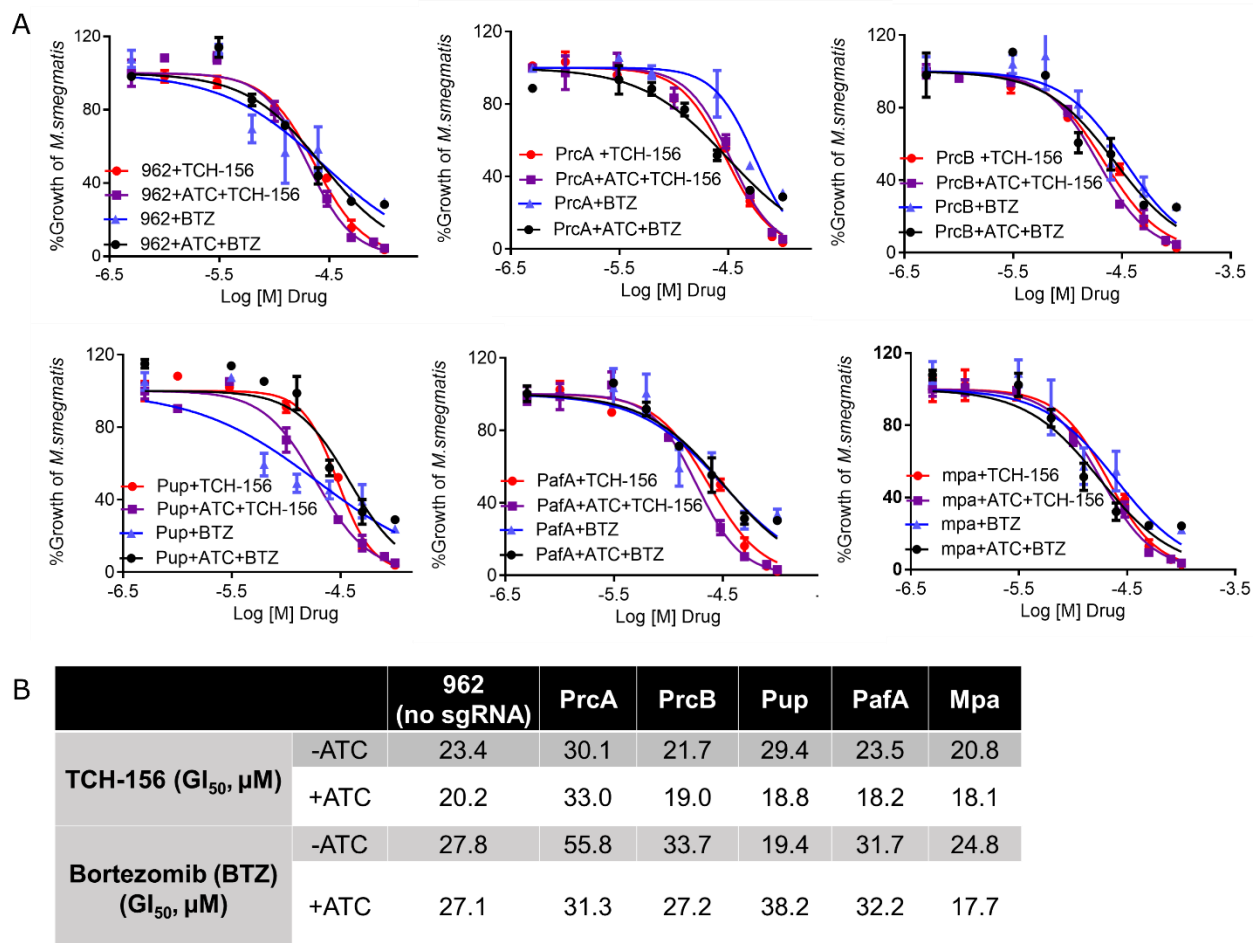


**Figure 5.8: Effect of CRISPRi/dcas9 knockdown of pup-proteasome genes on the growth of *Mycobacterium smegmatis*.** (A) Growth inhibition curves of *M smegmatis* for each proteasomal gene. Cells were cultured with or without ATC (200ng/mL) for 4days. OD<sub>600</sub> was taken, and vehicle control (–ATC) treatment set as maximum growth while streptomycin (100 $\mu$ g/mL) set as minimum. (B) EC<sub>50</sub> table for the growth of *M smegmatis* in the presence of TCH-156 or Bortezomib (BTZ) for each proteasomal gene, with or without ATC (200 ng/mL).

Consistently, when the growth of *Msmeg* was measured at different concentrations of TCH-156, with or without ATC, by measuring OD<sub>600</sub> after 4-day culture, *Msmeg* was very resistant to

TCH-156, with EC<sub>50</sub> of control sgRNA around 20  $\mu$ M (Fig. 5.8B about 3fold lower potency compared to *Mtb*, Fig. 5.4). Furthermore, gene knockdown did not appear to sensitize the cells to TCH-156 for most genes.

Consistently, even the marketed proteasome inhibitor, bortezomib was not very effective at killing these cells. The most surprising observation was the significant deviation in EC<sub>50</sub> of bortezomib for the different sgRNA, in the absence of ATC (Fig. 5.8B). This could not be explained by leaky expression of the sgRNA, since the same pattern was not observed with TCH-156. Collectively, this data confirms the use of CRISPRi/dcas9 as a conditional knockdown system in mycobacterium, supporting further evaluation of the sgRNAs in *Mycobacterium tuberculosis*.

Accordingly, sgRNAs targeting different *Mtb* proteasome genes were designed (Table 11) and cloned into the PLJR965 *Mtb* CRISPRi plasmid backbone. This was then handed to Dr. Uma Shankar (a postdoctoral associate in Dr. Abramovitch's lab) who ran similar experiments in the *Mtb* system. Based on his data, and in addition to RNAseq experiments he ran, *Mtb* appears to be sensitized to TCH-156 following proteasome knockdown. However, other important genes which may or may not be proteasome related appear to contribute to the anti-mycobacterium activity of TCH-156.

### 5.3 Conclusions

In all, the *Mtb* proteasome represents another exciting, yet, even more challenging target in the expedition for anti-TB drugs. Success in this area will be highly determined by selective targeting of the *Mtb* proteasome over the human proteasome. Current study provides exciting data for such endeavor.

Autophagy is a component of the human innate immune system that protects against intracellular microbes including *Mycobacterium tuberculosis*.<sup>340,341</sup> After demonstrating that activation of the human proteasome by imidazolines inhibits autophagy (chapter 3), it became a question of concern as to whether imidazolines might exacerbate TB infection by inhibiting autophagy in the host (human) system. Indeed, autophagy activation has been found to protect against active TB,<sup>342</sup> as well as enhances the replication of *Mtb* in HIV co-infected macrophages.<sup>343</sup> These complex outcomes make it difficult to predict the role of autophagy inhibition on the prognosis of TB infection. However, as a prerequisite to further explore the use of imidazolines as anti-mycobacterial agent in animal model of TB, the lead molecule must be more selective for *Mtb* proteasome. This by default eliminates this concern.



**CHAPTER SIX**  
**Summary and Overall Conclusion**

## 6.1 Summary

Following the discovery of the ubiquitin-proteasome system in the late 1980s, an initial suggestion that the proteasome could be inhibited as a means of targeting cancer was perceived as a taboo in the drug discovery community.<sup>344</sup> How can an enzyme that regulates the degradation of key proteins in almost all the cellular pathways be inhibited without consequences? The 2003 FDA approval of bortezomib, a proteasome inhibitor, for the treatment of multiple myeloma (MM) wiped away this skepticism.<sup>225</sup> Today, the proteasome is not only a therapeutic target for cancer,<sup>16,168</sup> but an exciting research area for numerous proteostasis disorders such as neurodegenerative diseases,<sup>5,18</sup> diabetes,<sup>58,345</sup> cardiovascular diseases,<sup>11,57</sup> as well as infectious diseases such as tuberculosis (TB)<sup>317,328</sup> and malaria.<sup>346</sup>

After more than three decades since the discovery of the proteasome, there is still so much to be known about this exquisite enzyme. Proteolysis by the proteasome could be 20S- or 26S-mediated and may or may not be ubiquitin-dependent. My PhD research has been focused on the discovery and characterization of small molecules that allow for the decoding of ubiquitin-independent-20S-mediated proteolysis and its role in the regulation of autophagy (a second protein degradation pathway), with the hope of finding new vulnerabilities for proteostasis drug discovery. In this endeavor, the following contributions were made:

1. Imidazolines were clearly characterized as small molecule activators of the 20S proteasome.

**Njomen, E.;** Osmulski, P. A.; Jones, C. L.; Gaczynska, M.; Tepe, J. J. Small Molecule Modulation of Proteasome Assembly. *Biochemistry* **2018**, 57 (28), 4214–4224. <https://doi.org/10.1021/acs.biochem.8b00579>.

2. The activation of the 20S proteasome by imidazolines was found to enhance the degradation of intrinsically disordered proteins (IDPs) associated with poor prognosis in multiple myeloma and glioblastoma multiforme. This observation presents a new therapeutic vulnerability for IDP-driven cancers and other proteostasis disorders.

**Njomen, E.;** Benham, V.; Lansdell, T. A.; Bernard, M.; Yang, Y.; Isaac, D.; Alkharabsheh, O.; Al-Janadi, A.; Bailie, M.; Bernard, J.; Yuzbasiyan-Gurkan, V; and Tepe, J.J. 20S proteasome enhancement targets the intrinsically disordered c-Myc and induces *in vivo* anti-tumor efficacy.

***Cancer Research 2019-in preparation***

3. Using imidazolines as a chemical probe, the 20S proteasome was demonstrated to be a negative regulator of autophagic flux. Autophagy regulation by the 20S proteasome involves the degradation of two key SNARE proteins; SNAP29 and STX17.
4. Inhibition of autophagy through enhancement of 20S proteasome activity provides a new vulnerability that can be taken advantage of in autophagy-associated chemoresistance.

**Njomen, E.;** Tepe, J. J. Regulation of Autophagic Flux by the 20S Proteasome. *Cell Chemical Biology* **2019**. <https://doi.org/10.1016/j.chembiol.2019.07.002>.

5. Using high throughput screening, new small molecule scaffolds for the enhancement of proteasome activity were identified and serve as the basis for a few projects in the lab.

**Jones, C. L\*.; Njomen, E.\*;** Sjögren, B.; Dexheimer, T. S.; Tepe, J. J. Small Molecule Enhancement of 20S Proteasome Activity Targets Intrinsically Disordered Proteins. *ACS Chem. Biol.* **2017**, 12 (9), 2240–2247. **\*Equal contributions.**

6. As a new research area, several *in vitro* assays were developed along the way, to further the discovery and validation of proteasome activators.

7. Using CRISPRi/dCas9, the anti-mycobacterial activity of imidazolines was found to be proteasome related, but not exclusively proteasome mediated.
8. These findings and the state of the field of proteasome activation have been summarized in a perspective review for quick reference.

**Njomen, E.;** Tepe, J. J. Proteasome Activation as a New Therapeutic Approach to Target Proteotoxic Disorders. *J. Med. Chem.* **2019**. <https://doi.org/10.1021/acs.jmedchem.9b00101>.

## **6.2 Overall conclusion**

Just like any new field, the concept of proteasome activation has also prompted a lot of apprehensions such as tumor causing potential and effect on other proteolytic pathways. These concerns have been discussed in the above review. It is also important to keep in mind that the physiological outcome of proteasome activation will depend largely on the mechanism employed and how “specific” it is to the proteasome network. Most of all, this field is still at its infant stage with positive outcomes so far. Therefore, the next few years should gleam some light on some of these concerns as we move toward efficacy validation in different animal models of diseases under consideration.

**CHAPTER SEVEN**  
**Materials and Methods**

## 7.1 Materials

### 7.1.1 Key resource tables

**Table 3:** Antibodies

Reagent or Resources	Source	Catalogue number
K48-linkage specific polyubiquitin	Cell Signaling Technology	4289
Ubiquitin (P4D1) Mouse mAb	Cell Signaling Technology	3936
c-Fos (9F6) Rabbit mAb	Cell Signaling Technology	2250
c-Myc (D84C12) Rabbit mAb	Cell Signaling Technology	5605
GAPDH (0411) HRP mouse mAb	Santa Cruz Biotechnology	sc-47724
Tau antibody (H-150)	Santa Cruz Biotechnology	sc-5587
$\alpha$ -synuclein antibody (C-20)	Santa Cruz Biotechnology	sc-7011-R
Proteasome 19S Rpt1/S7 subunit monoclonal antibody (MSS1-104)	Enzo Life Sciences	BML-PW8825
GFP Antibody (B-2) HRP	Santa Cruz Biotechnology	sc-9996 HRP
anti-mouse IgG (H+L), F(ab') <sub>2</sub> Fragment (Alexa Fluor 594 conjugate)	Cell Signaling Technology	8890
LC3B (D11) XP rabbit mAb	Cell Signaling Technology	3868
SQSTM1/p62 (D5L7G) mouse mAb	Cell Signaling Technology	88588
SQSTM1/P62 (D5E2) rabbit mAb	Cell Signaling Technology	8025
LAMP1 (D2D11) XP rabbit mAb	Cell Signaling Technology	9091
LAMP1 (D4O1S) mouse mAb	Cell Signaling Technology	15665
SNAP29 (D-8) mouse mAb	Santa Cruz Biotechnology	sc-390801
STX17 rabbit pAb	Abcam	ab116113
VAMP8 rabbit pAb	Cell Signaling Technology	13060
20S proteasome $\alpha$ -3 (A-9) mouse mAb	Santa Cruz Biotechnology	sc-166205
20S proteasome $\beta$ -5 (A-10) mouse mAb	Santa Cruz Biotechnology	sc-393931
PSMD2 (A-11) mouse mAb	Santa Cruz Biotechnology	sc-271775
GAPDH (0411) HRP mouse mAb	Santa Cruz Biotechnology	sc-47724
FLAG (D6W5B) rabbit mAb	Cell Signaling Technology	14793
Goat anti-rabbit IgG HRP-linked	Cell Signaling Technology	7074
Horse anti-mouse IgG HRP-linked	Cell Signaling Technology	7076
anti-rabbit IgG (H+L), F(ab') <sub>2</sub> Fragment (Alexa Fluor 488 Conjugate)	Cell Signaling Technology	4412
anti-mouse IgG (H+L), F(ab') <sub>2</sub> Fragment (Alexa Fluor 594 conjugate)	Cell Signaling Technology	8890
Donkey anti-Mouse IgG (H+L) Highly Cross-Adsorbed Secondary Antibody, Alexa Fluor 546	Thermo Fisher Scientific	A10036
Biotin conjugated ODC1 pAb	Epigentek	A56670-050
Anti-GFP AlphaLISA acceptor bead	PerkinElmer	AL133C
GFP Antibody (B-2) HRP	Santa Cruz Biotechnology	sc-9996 HRP

**Table 4:** Peptides and recombinant proteins

Reagent or Resources	Source	Catalogue number
Human 20S proteasomes	BostonBiochem	E-360
20S Immunoproteasome	BostonBiochem	E-370
26S Proteasome	BostonBiochem	E-365
19S Proteasome	BostonBiochem	E-366
Proteasome 20S ( <i>Saccharomyces cerevisiae</i> )	Enzo Life Sciences	BML-PW8775
Recombinant human SNAP29 with c-Myc tag	Origene	TP302179
Human tau441 full length protein	Abcam	ab84700
Human a-synuclein full length protein	Abcam	ab51189
Recombinant human GAPDH protein	Abcam	ab77109
Lysozyme	ThermoFisher Scientific	89833
3X FLAG Peptide	APExBIO	A6001
Cathepsin D & E substrate (fluorogenic)	Enzo Life Sciences	BML-P145-0001
N-Succinyl-Leu-Leu-Val-Tyr-7-amido-4-methylcoumarin (Suc-LLVY-AMC)	BostonBiochem	S-280
Z-Leu-Leu-Glu-7-amido-4-methylcoumarin (Z-LLE-AMC)	BostonBiochem	S-230
Boc-Leu-Arg-Arg-7-amido-4-methylcoumarin (Boc-LRR-AMC)	BostonBiochem	S-300

**Table 5:** Cell lines, cell culture and transfection reagents

Reagent or Resources	Source	Catalogue number
U-87 MG cells	ATCC	HTB-14
RPMI 8226	ATCC	CRM-CCL-155
CCRF-CEM	ATCC	CCL-119
HEK293T	Dr. Benita Sjögren	NA
HeLa	ATCC	CCL-2
RPMI-1640 Medium	ATCC	ATCC® 30-2001
DMEM medium	ThermoFisher Scientific	11965092
Fetal Bovine Serum	Sigma Aldrich	F2442
Penicillin-Streptomycin	ThermoFisher Scientific	15140122
Hgromycin B	Sigma Aldrich	H3274
Sinofection transfection reagent	Sino Biological	STF02

**Table 6:** Oligonucleotides and recombinant DNA

Reagent or Resources	Source	Catalogue number
SNAP29 (NM_004782.3) Primers F_GTGCTGCAACAGTGCATTAG R_CCTATGGAGGCTGTGGATATTT	Integrated DNA Technology	N/A (custom made)
STX17 (NM_017919.2) Primers F_GGGTCATCCATTCTCCTTTACC R_GCTGGACACTCAGTAAGGAATC	Integrated DNA Technology	N/A (custom made)
VAMP8 (NM_003761.4) Primers F_CATCTCCGCAACAAGACAGA R_CTTACAGTTCTTCCACCAGAA	Integrated DNA Technology	N/A (custom made)
P62 (NM_003900.4) Primers F_CTCTGGACACCATCCAGTATTC R_TGCAATTCTACGCAAGCTTAAC	Integrated DNA Technology	N/A (custom made)
LC3B (NM_022818.4) Primers F_CATCACAGTTGGCACAAACG R_GACTTTGGGTGTGGTTCTCTTA	Integrated DNA Technology	N/A (custom made)
GAPDH (NM_002046.6) Primers F_CAGCCTCAAGATCATCAGCA R_GTCATGAGTCCTTCCACGATAC	Integrated DNA Technology	N/A (custom made)
PSMD2 siRNA (h)	Santa Cruz Biotechnology	sc-62900
SignalSilence <sup>®</sup> Control siRNA (Unconjugated)	Cell Signaling Technology	6568
Ornithine Decarboxylase/ODC1 cDNA ORF Clone, Human, N-GFPspark <sup>®</sup> tag	Sino Biological	HG18052-ANG
Premo Autophagy Tandem Sensor RFP- GFP-LC3B	ThermoFisher Scientific	P36239
CellLight <sup>™</sup> Lysosomes-GFP, BacMam 2.0	ThermoFisher Scientific	C10507
N-FLAG-SNAP29	Noboru Mizushima <i>et al</i> <sup>270</sup> , 2012. Addgene plasmid	45915
N-FLAG-STX17	Noboru Mizushima <i>et al</i> <sup>270</sup> , 2012. Addgene plasmid	45911
EGFP-LC3B	Karla Kirkegaard <i>et al</i> <sup>347</sup> , 2005. Addgene plasmid	11546
<i>M tb</i> PLJR965 CRISPRi backbone plasmids	Sarah M. Fortune	N/A
<i>M. smeg</i> PLJR962 CRISPRi backbone plasmids	Sarah M. Fortune	N/A
His-tag Mpa plasmid: NP 216631.1 Pet- 20b(+)	GenScript	N/A
T7-prcAB-His6 plasmid	C Nathan/R Abramovitch	N/A



**Table 7:** Bacterial strains

Reagent or Resources	Source	Catalogue number
TOP10 Chemically Competent <i>E. coli</i>	ThermoFisher Scientific	C404003
mc <sup>2</sup> 155 <i>M. smegmatis</i>		
BL21(DE3) Chemically Competent <i>E. coli</i>	ThermoFisher Scientific	C600003

**Table 8:** Critical commercial assay kits

Reagent or Resources	Source	Catalogue number
BCA assay	ThermoFisher Scientific	23225
Immunofluorescence Application Solutions Kit	Cell Signaling Technology	12727
CellTiter-Glo® Luminescent Cell Viability Assay	Promega	G7570
Whole Blood CD138 MicroBeads, human	Miltenyi Biotec	130-093-062
Alpha synuclein (human) AlphaLISA detection kit	Perkin Elmer	AL321HV
T4 DNA Ligase	New England Biolab Inc.	M0202M
T4 Polynucleotide Kinase	New England Biolab Inc.	M0201L
BsmBI restriction enzyme kit	New England Biolab Inc.	R0580S
RNeasy Mini Kit	QIAGEN	74104
RNeasy MinElute Cleanup Kit	QIAGEN	74204
TURBO DNase-free kit	ThermoFisher Scientific	AM1907
iTaq universal SYBR green Supermix	Bio-Rad	172-5120
iScript™ cDNA Synthesis Kit	Bio-Rad	1708891

**Table 9:** Other chemicals and reagents

Reagent or Resources	Source	Catalogue number
TCH-165, TCH-023, TCH-013	Tepe lab	NA
Bortezomib	Cayman Chemical	10008822
Epoxomicin	Cayman Chemical	10007806
Cycloheximide	Cell Signaling Technology	2112
MK-886	Cayman Chemical	21753
Chloroquine	Cell Signaling Technology	14774
Torin 1	Cell Signaling Technology	14379
Bafilomycin A1	Sigma Aldrich	B1793
Pepstatin A (synthetic)	Enzo Life Sciences	ALX-260-085-M005
leupeptin	Sigma Aldrich	L2884
IPTG	GOLDBIO	I2481C
PMSF	ThermoFisher Scientific	36978
LB agar	Sigma-Aldrich	L3027
LB Broth	Sigma-Aldrich	L7275
Middlebrook 7H9 broth		
Carbenicillin	Sigma-Aldrich	C1389
Chloramphenicol	Sigma-Aldrich	C0378
Proaffinity IMAC Ni-charged resin	Bio-Rad	1560131
Chlorpromazine hydrochloride	Sigma Aldrich	C8138
Triflupromazine hydrochloride	Sigma Aldrich	1686003
Sigmafast inhibitor cocktail	Sigma Aldrich	S8820
Adenosine 5'-triphosphate magnesium salt	Sigma Aldrich	A9187
Adenosine 5'-diphosphate sodium salt	Sigma Aldrich	A2754
LysoTracker red	ThermoFisher Scientific	L7528
TRIzol Reagent	ThermoFisher Scientific	15596026
Pierce™ Protein A/G Magnetic Beads	ThermoFisher Scientific	88802
Alpha screen streptavidin donor beads	PerkinElmer	6760002S
AlphaLISA lysis buffer	PerkinElmer	AL003F
Immunoassay buffer	PerkinElmer	AL000C
Mini-PROTEAN® TGX™ Precast Gels	Bio-Rad	4561094
Immun-Blot® PVDF Membrane	Bio-Rad	1620177
Clarity™ Western ECL Substrate	Bio-Rad	1705060
Rhinohide™ Polyacrylamide Gel Strengthener Concentrate	ThermoFisher Scientific	R33400
TEMED	Sigma Aldrich	T7024
30% Acrylamide/Bis Solution, 37.5:1	Bio-Rad	1610158

## **7.2 Methods**

### **7.2.1 Cell culture**

Human embryonic kidney cells (HEK293T), HeLa and glioblastoma cells (U-87 MG) were maintained in Dulbecco's Modified Eagle's Medium (DMEM) supplemented with 10% Fetal Bovine Serum, and 100 U/mL Penicillin/Streptomycin, at 37°C with 5% CO<sub>2</sub>. RPMI and CCRF-CEM cells were maintained in RPMI medium supplemented with 10% Fetal Bovine Serum, and 100 U/mL Penicillin/Streptomycin, at 37°C with 5% CO<sub>2</sub>.

### **7.2.2 Isolation and culture of primary multiple myeloma cells**

Bone marrow aspirates were received from Dr. Isaac Daniel. WBCs were separated from RBCs by ficoll density gradient. Multiple myeloma cells were then isolated from WBCs using human CD138<sup>+</sup> affinity magnetic beads. Cells were cryopreserved in 10% DMSO in FBS. Revived cells were maintained in RPMI medium with 10% FBS for 10 days.

### **7.2.3 Cell viability assay**

Primary or established cells (10,000) were seeded per well of 96-well plate in 100 µL medium and treated with TCH-165 or Bortezomib for 72h. Cells were equilibrated to RT and CellTiter-Glo solution (100 µL) added and incubated with shaking for 10 minutes at RT. Assay plate was then allowed to equilibrate for 5 minutes at RT and luminescent readings taken on a SpectraMax M5<sup>e</sup>. For cytotoxicity reversibility assay, viability was performed as above, following treatment and washing as detailed in the legends. Data are presented as a percentage of the vehicle control for each experimental condition, after background subtraction.

### **7.2.4 Transient and stable transfections**

**Transient transfection with GFP-ODC:** HEK293T cells were seeded at a density of  $2.5 \times 10^6$  cells in a 100 mm plate overnight. DNA (2.5µg of GFPSpark-ODC plasmid) was mixed

with 2 mL of serum free-DMEM medium. Sinofection transfection reagent (30  $\mu$ L) was also mixed with 2 mL of serum free medium in a separate vial. The separate mixtures were combined and allowed to sit at RT for 20 minutes. The mixture was then added to HEK 293T cells in a 100 mm dish and allowed to incubate for 4h at 37°C, 5% CO<sub>2</sub>, in a tissue culture incubator. The transfection medium was replaced with fresh complete culture medium (with 10% FBS) and cultured for a further 48h. Cells were then trypsinized and seeded for 12h in complete medium, prior to treatment or use in AlphaLISA.

**Generation of GFPSpark-ODC HEK293T stable cell lines:** HEK 293T cells were seeded at a density of  $1 \times 10^5$  cells/mL in a 24-well plate overnight. DNA (1  $\mu$ g of GFPSpark-ODC plasmid) was mixed with 250  $\mu$ L of serum free-DMEM medium. Sinofection transfection reagent (5  $\mu$ L) was also mixed with 250  $\mu$ L of serum free medium in a separate vial. The separate mixtures were combined and allowed to sit at RT for 15 minutes. The mixture was then added to HEK 293T cells in a 24-well plate and allowed to incubate for 4h at 37°C, 5% CO<sub>2</sub>, in a tissue culture incubator. The transfection medium was replaced with fresh complete culture medium (with 10% FBS). Three days later, cells were trypsinized and re-suspended in hygromycin (100  $\mu$ g/mL) selection medium. Survived clones were picked and expanded in hygromycin selection medium for six weeks. After three passages, stable expression was confirmed by confocal fluorescent imaging, using standard filters for GFP.

**Transient transfection with autophagy-associated proteins and siRNA:** BacMam plamids (Premo Autophagy Tandem Sensor RFP-GFP-LC3B and CellLight™ Lysosomes-GFP, BacMam 2.0) were directly added to cells in cover glass chamber 16h or 24h before treatment. For other transfections, the following protocol was followed. For plasmid transfection, plasmid to transfection reagent (sinofection reagent) was maintained at ratio of 1:6 ( $\mu$ g: $\mu$ L). For siRNA

transfection, a ratio of 2.5:1 (nM:  $\mu$ L) was used. Flag-SNAP29 and FLAGSTX17 were used at concentrations of 5  $\mu$ g/million cells for overexpression experiments to ameliorate the effect of TCH-165 and at 2  $\mu$ g/million cells for all other experiments. PSMD2 siRNA and control siRNA were used at concentrations of 250 nM. HeLa or U-87 MG cells were seeded at a density of 1 million in 60 mm or 2.5 million in 100 mm dish overnight. Plasmids or oligonucleotides were mixed with 1 mL of serum free-DMEM medium. Sinofection transfection reagent was also mixed with 1 mL of serum free medium in a separate vial. The separate mixtures were combined and allowed to sit at RT for 15 minutes. For 60 mm dish, the mixture was directly added to the cells. For 100 mm dish, the mixture was further diluted with 2 mL medium before adding to cells, to cover the entire surface area. After incubating for 4h at 37°C, 5% CO<sub>2</sub> in a tissue culture incubator, fresh medium (4 mL for 60 mm and 10 mL for 100 mm dish) with 10%FBS was then added and allowed to culture. For Flag-SNAP29 and or STX-17 transfection, cells were cultured for a further 20h, then split into 60 mm dish each and cultured for 8h before treatment (at 32h post-transfection).For EGFP-LC3B, cells were cultured for a further 24h then split into cover glass chamber and cultured for 24h before treatment (at 48h post-transfection). For siRNA knockdown, cells were cultured for a further 48h then split into 60 mm dish each and cultured for 24h before treatment (at 72h post-transfection).

### **7.2.5 Immunoprecipitation**

HeLa cells transiently transfected with Flag-SNAP29 (2  $\mu$ g, plasmid) or Flag STX17 (2  $\mu$ g, plasmid) in 60 mm dish (see transient transfection above) were pretreated with vehicle or bortezomib(20  $\mu$ M) for 2h, followed by treatment with vehicle or TCH-165 (10  $\mu$ M) for a further 16h. Cells were washed 2x with chilled DPBS buffer and scrapped with 200  $\mu$ L of lysis buffer (50 mM Tris-HCl pH 7.5, 150 mM NaCl, 1 mM EDTA, 1% Triton X-100, 1 mM PMSF, 1 mM

Na<sub>3</sub>VO<sub>4</sub>, 1x sigmafast protease inhibitor cocktail). Cells were completely lysed by sonication. Lysates were clarified by spinning at 14,000g for 20 minutes and supernatant collected into new tubes. Total protein was quantified by bicinchoninic acid (BCA) assay following standard protocol. Samples were normalized with lysis buffer to 0.5 mg/mL with lysis buffer. Lysates (200 µL or 100 µg) were mixed with 4 µL of Flag antibody (Cell Signaling Technology: 14793) and incubated at 4°C overnight with shaking. Pre-washed Pierce Protein A/G Magnetic Beads (25 µL or 0.25 mg) was then added and incubated at RT with shaking for 1h. Beads were collected with magnetic stand and washed 4x with 1 mL of lysis buffer. Flag-tagged proteins were eluted by shaking beads overnight at 4°C with 200 µL of 4 mg/mL 3x flag peptide in 50 mM Tris-HCl pH 7.5, 150 mM NaCl. Samples were collected with magnetic stand and boiled with 5x SDS buffer and blotted for SNAP29, STX17, and K-48 ubiquitin. Input lysates were also immunoblotted for Flag, K-48 ubiquitin, LC3B, P62, and GAPDH as above.

#### **7.2.6 Immunoblot**

Wild type or transfected cells at 70-80% confluency was treated with test compounds at the reported concentrations and time as indicated in figure legends. Samples meant for immunoblot only were washed 3x with warm DPBS buffer and scrapped with chilled RIPA buffer supplemented with protease inhibitor cocktail. Samples were briefly sonicated, spun and supernatant assayed for total protein with bicinchoninic acid (BCA) assay. Normalized and boiled samples, or boiled samples from purified protein degradation assay were resolved on 4-20% or 12% (for ≤ 20kDa) Tris-glycine SDS-PAGE and blotted onto a PVDF membrane. Membranes were blocked in 5% non-fat milk in TBST buffer for 60 minutes at RT. Membranes were then incubated with primary antibody in 2% non-fat milk TBST buffer, overnight at 4°C. Membranes were then washed 5x for 5 minutes each and incubated in secondary antibody at RT for 60 minutes.

Membranes were washed again as above and developed with ECL clarity reagent. Images were captured with Hyblot films. All primary antibodies were used at a dilution of 1:1000, except for SNAP29 (1:2000),  $\alpha$ -synuclein (1:4000) and STX17 (1:500). Goat anti-rabbit HRP and Goat anti-mouse HRP were also used at 1:1000 while anti-GAPDH-HRP was used at a dilution of 1:2000.

#### **7.2.7 Oxyblot: Protein carbonyl quantification**

HeLa cells at 70% confluency in 100 mm dish were treated with vehicle, TCH-165 (10  $\mu$ M), H<sub>2</sub>O<sub>2</sub> (50  $\mu$ M), or a combination of TCH-165 (10  $\mu$ M) and H<sub>2</sub>O<sub>2</sub> (50  $\mu$ M) for 16h. Cells were washed with warm DPBS and collected by trypsinization. Pellets were washed 3x with chilled DPBS buffer and split into two parts. One part was used for proteasome native gel as previously reported (see below) and the second half lysed by sonication in RIPA buffer supplemented with sigmafast protease inhibitor cocktail and used for oxyblot. Lysates were clarified by spinning at 14,000g for 20 minutes and supernatant collected into new tubes. Total protein was quantified by bicinchoninic acid (BCA) assay following standard protocol. Samples were normalized with lysis buffer to 2 mg/mL with lysis buffer. One-part cell lysate (20  $\mu$ L) was mixed with one part 12% SDS (20  $\mu$ L) and incubated at RT for 10 minutes. Two parts (40  $\mu$ L) 20 mM DNPH (2, 4-Dinitrophenylhydrazine) solution in 10% TFA was then added, mixed and incubated at RT for 20 minutes. Reaction was then quenched with 1.5 part (35  $\mu$ L) 2 M Tris/30% glycerol. Samples were resolved on 4-20% Tris/glycine gel at 4 °C, blotted onto PVDF membrane and probed with mouse anti DNP (1:1000) and anti-mouse HRP (1:1000). Underivatized lysates were boiled with SDS buffer and immunoblotted as above.

### **7.2.8 siRNA gene knockdown**

HeLa cells were transfected with control and PSMD2 siRNA as described under transient transfection. Post-transfection (72h), cells were treated with either vehicle or TCH-165 (10  $\mu$ M) for 16h. Samples were collected and immunoblotted as described under immunoblot.

### **7.2.9 Quantitative real time polymerase chain reaction (qRT-PCR)**

Glioblastoma (U-87 MG) cells were treated with either vehicle or TCH-165 (10  $\mu$ M) for 8h or 24h. Total mRNA was isolated by Trizol extraction and purified on a RNeasy column. Residual contaminating genomic DNA was digested with TURBO DNase and samples were cleaned with RNA clean-up columns. The cDNA was prepared from 200 ng of mRNA with random hexamers using iScript cDNA synthesis kit as per manufacturer instructions. cDNA (2  $\mu$ L of PCR product) levels were then measured by quantitative real-time PCR (qRT-PCR) with 500 nM of forward and reverse primers each, using iTaq universal SYBR Green supermix on a Viia7 lightCycler (Applied Biosystems). Signals were normalized to that of GAPDH and quantified by the  $\Delta\Delta C_t$  method. Data are means  $\pm$  SD of two independent experiments each ran in triplicates.

### **7.2.10 Purified 20S proteasome activity assay and high throughput screening**

Activity assays were carried out in a 200  $\mu$ L reaction volume. Different concentrations of test compounds (1  $\mu$ L) were added to a black flat/clear bottom 96-well plate containing 1nM of either human constitutive 20S proteasome, immunoproteasome (i20S), 26S proteasome, *Mtb* 20S proteasome or yeast proteasome in assay buffer (50 mM Tris-HCl pH 7.5) and allowed to sit for 10 minutes at RT. Fluorogenic substrates (10  $\mu$ L of 20x stock in assay buffer) were then added and the enzymatic activity measured at 37°C on a SpectraMax M5e spectrometer by measuring change in fluorescence unit per minute for 1h at 380/460 nm. Medium throughput screening (MTS) was carried out in 384-well plates as described above, with the following exceptions. Single



concentration of compounds (10 $\mu$ M; 150nL of 2mM) were dispensed into 384-well plate containing 25 $\mu$ L enzyme solution, followed by 5 $\mu$ L of 6x substrate working solution (Suc-LLVY-AMC diluted in assay buffer), using automated liquid dispensers. Enzymatic activity was measured at 37°C on a BioTek plate reader by measuring change in fluorescence unit per minute for 1h at 380/460 nm. The relative fluorescence units for the vehicle (DMSO) control was set at 100% and the ratio of drug-treated sample to that of vehicle control was used to calculate fold change in enzymatic activity. Fold activity was plotted as a function of drug concentration, using GraphPad Prism 5. The fluorogenic substrates used were Suc-LLVY-AMC (CT-L activity, 10 $\mu$ M for human and yeast and 40  $\mu$ M for *Mtb20S*), Z-LLE-AMC (Casp-L activity, 10 $\mu$ M), Boc-LRR-AMC (T-L activity, 20 $\mu$ M). Magnesium chloride (5 mM) and ATP (2.5 mM) were included in assays containing 26S proteasome.

#### **7.2.11 Proteasome activity in cell lysates from treated cells**

HEK293T cells were grown in T-75 flask to about 80% confluency. Cells were treated with vehicle, TCH-165 (10  $\mu$ M) and epoxomicin (1  $\mu$ M) for 12h. Cells were trypsinized and washed 2x with PBS buffer (pH7.4). Cells were resuspended in 500  $\mu$ L of lysis buffer (20 mM Tris-HCl, 5 mM MgCl<sub>2</sub>, 1 mM ATP, 0.5 mM EDTA, 1 mM DTT, 10% glycerol) and lysed by sonication. Samples were clarified for 20 minutes at 14,000g. Supernatant was assayed for total protein using bicinchoninic acid assay (BCA assay) and normalized to 1 mg/mL (*Note: DTT is added after BCA assay, since it interferes with the assay*). Samples were diluted to 0.036  $\mu$ g/ $\mu$ L in assay buffer (20 mM Tris-HCl, 5 mM MgCl<sub>2</sub>, 1 mM ATP, 1 mM DTT) and 140  $\mu$ L (5  $\mu$ g total protein) of the diluted samples transferred into three wells of a black, clear-bottom 96-well plate. Substrate (10  $\mu$ L of Suc-LLVY-AMC) in assay buffer was added to a final concentration of 25  $\mu$ M. Kinetic readings

were taken every 5 minutes at 37°C, at 380/460 nm for 1h. Epoxomicin treatment was set to zero and vehicle control set to 100%.

#### **7.2.12 Cathepsin D and E activity**

U-87 MG or HeLa cells at ~70% confluency in 100 mm dish were treated with vehicle, TCH-165 (10  $\mu$ M), Torin 1(100 nM), Pepstatin A (5  $\mu$ M) or Chloroquine (100  $\mu$ M) for 24h. Cells were washed 2x with chilled DPBS buffer and scrapped with 500  $\mu$ L of lysis buffer (100 mM NaCl, 100 mM NaOAc, 1 mM EDTA, 1% Triton X-100, pH 5.0) into an Eppendorf tube. Cells were then lysed by rocking the tubes on a shaker for 1h at 4°C. Lysates were clarified by spinning at 14,000g for 20 minutes and supernatant collected into new tubes. Total protein was quantified by bicinchoninic acid (BCA) assay following standard protocol. Samples were normalized with lysis buffer to 1 mg/mL, and then diluted to 0.1 mg/mL in assay buffer (100 mM NaCl, 100 mM NaOAc, pH 5.0). Each sample (100  $\mu$ L or 10  $\mu$ g) was transferred into quadruplicate well of a black-clear bottom 96 well plate. Cathepsin D and E substrate (BML-P145-0001, Mca-Gly-Lys-Pro-Ile-Leu-Phe-Phe-Arg-Leu-Lys (Dnp)-D-Arg-NH<sub>2</sub> [Mca= (7-methoxycoumarin-4-yl)acetyl; Dnp=dinitrophenyl]) was then diluted in assay buffer and 50  $\mu$ L added to the wells to a final concentration of 20  $\mu$ M. Plate was incubated at 37°C for 1h and fluorescence reading taken at 330/460 nm on a SpectraMax M5<sup>e</sup>. Data are presented as means  $\pm$  SD of three independent experiments.

#### **7.2.13 Proteasome-mediated degradation of IDPs in biochemical assays**

**Degradation of  $\alpha$ -synuclein:** Digestion of  $\alpha$ -synuclein was carried out in a 50  $\mu$ L reaction volume made of 20 mM HEPES pH 7.4, 2 mM EDTA, 1 mM EGTA, 0.5  $\mu$ M purified  $\alpha$ -synuclein, 0.5  $\mu$ M GAPDH, and 15 nM purified human 20S proteasome. Briefly, 20S proteasome was diluted to 17 nM in the reaction buffer. Test compounds or vehicle (1  $\mu$ L of 50x stock) were added to 44

μL of 17 nM 20S and incubated at RT for 20 minutes. The substrate (5 μL of 5 μM GAPDH/ α-synuclein mixture) was then added to the reaction mixture and incubated at 37°C for 1h. The reactions were quenched with concentrated SDS- loading buffer. After boiling for 5 minutes, samples were resolved on a 4-20% Tris-glycine SDS-PAGE and immunoblotted with rabbit polyclonal anti α-synuclein IgG (1:4000) and goat anti-rabbit HRP (1:5000)/ anti-GAPDH-HRP. Blots were developed with ECL western reagent and imaged with x-ray film. EDTA and EGTA were excluded from 20S degradation buffer and supplemented with magnesium chloride (5 mM) and ATP (2.5 mM).

**Degradation of tau441:** Tau degradation was carried out in the same way as α-synuclein with the exceptions that tau and GAPDH were used at final concentrations of 0.1 μM.

**Degradation of SNAP29-c-Myc/DDK:** Digestion of SNAP29-c-Myc/DDK was carried out in a 50 μL reaction volume made of 20 mM HEPES pH 7.4, 2 mM EDTA, 1 mM EGTA, 200 nM SNAP29, 20 nM purified human 20S proteasome with or without the test compounds. Briefly, 20S proteasome was diluted to 23 nM in the reaction buffer. Test compounds or vehicle (1 μL of 50x stock) were added to 44 μL of 23 nM 20S and incubated at RT for 20 minutes. The substrate (5 μL of 2 μM SNAP29-c-Myc/DDK) was then added to the reaction mixture and incubated at 37°C and 10 uL aliquot was taken out and mixed with 2x SDS loading buffer, at the indicated time. Samples were boiled and immunoblotted.

#### **7.2.14 Proteasome-mediated degradation of IDPs in cells**

**Degradation of GFPSpark-ODC in HEK293T cells:** HEK293T cells stably expressing GFPSpark-ODC were seeded in T-75 flask, in hygromycin selection medium two days prior to treatment, such that cells were about 80% confluent at the time of treatment. Cells were incubated with fresh medium (no hygromycin) with or without 50 μg/mL of cycloheximide, in combination

with either vehicle, bortezomib (3  $\mu$ M) or TCH165 (3 and 10  $\mu$ M) for 24h. GFPSpark-ODC degradation was monitored by immunoblot of cell lysates with GFP antibody.

**Degradation of c-Fos in U-87 MG cells:** U-87 MG cells were grown to approximately 80% confluency in a 100 mm dish. Cells were treated with vehicle, TCH-165 (3, 10, 30  $\mu$ M) or epoxomicin (100 nM) without or with cycloheximide (50  $\mu$ g/mL) for 8h. Cells were washed 2x with warm PBS buffer and scrapped into chilled RIPA buffer supplemented with sigmafast protease inhibitor cocktail. Total protein was quantified by bicinchoninic acid assay (BCA assay), normalized to 2 mg/mL and boiled with 5x SDS loading buffer. Equal amounts of lysates were resolved on a 4-20% Tris/glycine gel and transferred to a PVDF membrane. Membrane was probed with anti c-Fos and anti-GAPDH antibodies.

**Degradation of c-Myc in RPMI and CEM cells:** CEM or RPMI cells were grown to approximately 80% confluency in a T-75 flask. Cells were treated with either vehicle or TCH-165 at the indicated concentrations, for 4h. In experiments involving bortezomibs, cells were pretreated with bortezomib (5  $\mu$ M) for 1h before adding TCH-165 or vehicle for a further 4h. Cells were pelleted and washed with chilled PBS buffer (2x) and resuspended in chilled RIPA buffer supplemented with sigmafast protease inhibitor cocktail. Total protein was quantified by bicinchoninic acid assay (BCA assay), normalized to 2 mg/mL and boiled with 5x SDS loading buffer. Equal amounts of lysates (30  $\mu$ g) were resolved on a 4-20% Tris/glycine gel and transferred to a PVDF membrane. Membrane was probed with anti c-Myc and anti-GAPDH antibodies.

#### **7.2.15 Proteasome AlphaLISA assays**

**Detection of GFP-ODC in HEK-293T cell lysates by AlphaLISA:** Cells stably expressing GFP-ODC were lysed in AlphaLISA lysis buffer and total protein quantified by BCA method. Lysate was diluted in 1x AlphaLISA immunoassay buffer to 10x the desired final

concentrations. Samples (5  $\mu$ L) were transferred into replicate wells of white solid-bottom 384-well plate. Anti GFP acceptor bead (10  $\mu$ g/mL final) and biotinylated anti-ODC (3 nM or 0.47  $\mu$ g/mL final) at 5x final concentrations were each added in 10  $\mu$ L. Samples were incubated at RT for 1h. Donor bead (25  $\mu$ L) at 2x final concentration (40  $\mu$ g/mL final) was added and incubated for a further 30 minutes. Alpha signal was measured using BioTek plate reader equipped with Alpha filter. Data are presented as mean  $\pm$  SD of 2 replicates of a single experiment.

**GFP-ODC AlphaLISA: Reagent optimization:** HEK293T cells transiently expressing GFP-ODC were seeded at a density of 500 cells/well in a 384-well plate in 20  $\mu$ L of DMEM medium for 12h. Cells were lysed with 5  $\mu$ L of 5x lysis buffer and AlphaLISA performed with different combinations of beads and antibody as above.

**GFP-ODC AlphaLISA: Cell number Optimization:** HEK293T cells transiently expressing GFP-ODC were seeded at different densities (500-50,000cells/well) in a 384-well plate in 20  $\mu$ L of DMEM medium for 12h. AlphaLISA lysis buffer (5  $\mu$ L of 5x stock) was added to each well and incubated on a shaker (400rpm) for 30 minutes. A mixture (5  $\mu$ L of 10x working solution) of biotinylated anti-ODC (3 nM or 0.47  $\mu$ g/mL final) and anti-GFP acceptor beads (10  $\mu$ g/mL final) in 1x immunoassay buffer was added to each well and incubated at RT for 1h. Streptavidin donor bead (20  $\mu$ L of 2.5x, 40  $\mu$ g/mL final) was then added and incubated for a further 30 minutes. Alpha signal was measured as above. Data are presented as mean  $\pm$  SD of triplicate of a single experiment.

**AlphaLISA quantification of proteasome-mediated degradation of GFPspark-ODC in cell culture:** HEK293T cells transiently (500 cells/well) or stably expressing GFP-ODC (10,000cells/well) were seeded in a 384 well plate in 10  $\mu$ L of DMEM medium for 12h. Compounds were diluted to 2x the desired final concentration in culture medium and 10 $\mu$ L added

to cells. Cells were allowed to culture for a further 12h or 24h. AlphaLISA lysis buffer (5  $\mu$ L of 5x) was added to each well and incubated on a shaker (400rpm) for 30 minutes. A mixture (5 $\mu$ L of 10x working solution) of biotinylated anti-ODC (3 nM or 0.47  $\mu$ g/mL final) and anti-GFP acceptor beads (10  $\mu$ g/mL final) in 1x immunoassay buffer was added to each well and incubated at RT for 1h. Streptavidin donor bead (20  $\mu$ L of 2.5x, 40  $\mu$ g/mL final) was then added and incubated for a further 30 minutes. Alpha signal was measured using BioTek plate reader equipped with Alpha filter. All activators were tested at 10  $\mu$ M while the proteasome inhibitor was tested at 1  $\mu$ M. Data are presented as mean  $\pm$  SD of triplicate of a single experiment.

**AlphaLISA quantification of 20S proteasome-mediated degradation of  $\alpha$ -synuclein:**

Human constitutive 20S proteasome (15 nM) in assay buffer (20 mM Tris/HCl, 100 mM NaCl pH 7.4) was treated with either vehicle, TCH-165 or epoxomicin (1  $\mu$ M) for 10 minutes at RT.  $\alpha$ -synuclein (5  $\mu$ L) was then added to a final concentration of 10 ng/mL in a 50  $\mu$ L reaction mixture. Additional control included buffer with TCH-165 and  $\alpha$ -synuclein only. Samples were incubated at 37°C and 5  $\mu$ L aliquots transferred into 384-well assay plate at 2h and 4h. Samples were kept on ice to slow down further degradation. A 20  $\mu$ L mixture of anti-  $\alpha$ -synuclein acceptor bead (10  $\mu$ g/mL final) and  $\alpha$ -synuclein antibody (1 nM final, targeting one end of the protein) was then added to each well and incubated at RT for 1h. To the mixture was added 25  $\mu$ L of donor beads (40  $\mu$ g/mL, final) and incubated for a further 30 minutes. Alpha sign was read as above. Buffer only control was set to zero and vehicle control set to 100%. Data are presented as mean  $\pm$  SD of 3 independent experiments. EC<sub>50</sub> was determined by fitting the data into a four-parameter sigmoidal dose-response plot using Graphpad Prism5.

### 7.2.16 Proteasome native gel and in-gel activity assays

**Native lysis buffer:** 50 mM Tris-HCl (pH 8.0), 2 mM Na<sub>2</sub>ATP, 5 mM MgCl<sub>2</sub>, 0.5 mM EDTA, 0.05% Triton X-100 and 10% glycerol.

**5x native sample buffer:** 250 mM Tris-HCl pH 8.0, 50% glycerol, 150 µg/mL xylene cyanol

**5x TBE running buffer:** 450 mM Tris, 450 mM boric acid, 2.5 mM EDTA.

**Table 10:** Proteasome native gel composition

Reagent	3% stacking gel	4% resolving gel	5% gel resolving gel
5x TBE	2 mL	4 mL	4 mL
Rhinohide	2 mL	3 mL	2 mL
30% Acrylamide:Bis acrylamide (37.5:1)	1 mL	2.7 mL	3.34 mL
4% Glycerol in water	6 mL	10 mL	10 mL
500 mM Mg <sup>2+</sup> -ATP	50 µL	100 µL	100 µL
TEMED	20 µL	20 µL	20 µL
10% APS (Ammonium persulfate)	200 µL	200 µL	200 µL
This is enough for 4 gels in a 1.5 mm spacer plate, poured as 2.5 cm of 5%, 3 cm of 4% and 0.5 cm of 3% below the comb. Make sure the comb thickness matches the spacer plate.			

**Native gel:** Cells were treated with either vehicle, TCH165, TCH-013, TCH-023, or H<sub>2</sub>O<sub>2</sub> at the concentrations and time indicated under each figure legend. Cells were trypsinized and washed three times with chilled phosphate-buffered saline (PBS). Cell pellets were homogenized in native lysis buffer using acid-washed glass beads. Total protein was quantified by a bicinchoninic acid (BCA) assay. Lysates were mixed with 5x native loading buffer (1x final, see above for composition) and equal amounts of lysates (30 µg) resolved on a 3%–4%–5% (stacking–resolving–resolving) Tris-borate-EDTA (TBE) gel supplemented with Rhinohide polyacrylamide gel strengthener (see table above), for 3h at 150 V, at 4°C

**In gel activity assay:** To check for activation of single capped 20S (19S-20S), HEK cells were lysed by vortexing (30sec, 2x) with glass beads in lysis buffer over a 20 minutes time period.

Homogenate was cleared at 14000g for 20 minutes and total protein quantified by BCA to be 1.9 mg/mL. Lysate was mixed with 5x native loading buffer to a final concentration of 1.5 mg/mL. Lysate (40µL, 60µg) was loaded into a freshly prepared 3-4-5% native gel and resolved for 3h at 150V, at 4°C. The gel was split into two halves and incubated in assay buffer (50 mM Tris-HCl pH 7.4) with DMSO or with TCH-165 (20 µM) for 1h. Buffer was replaced with new assay buffer containing either DMSO or TCH-165 (20 µM) supplemented with 10 µM Suc-LLVY-AMC, with or without 2 mM Na<sub>2</sub>ATP and 5 mM MgCl<sub>2</sub>. Gels were incubated at 37°C for 30 min, then joint together on a filter and image taken with Alpha imager at 365 nm. Gels were then immunoblotted with anti-β5. Note-TCH-165 solubility was better when added from a 5 mM stock than from 10 mM stock. Proteasome gels from cells treated with drug were only incubated with substrate without the compound.

**Immunoblot of native gel:** Gels from native gels or in-gel activity assays were washed 3x with water and incubated in chilled 1% SDS in transfer buffer for 10 minutes. Gel was then rinsed 3x with water and blotted onto a PVDF membrane for 3h at 100 V at 4°C. Proteasome subcomplexes were probed with anti-β5 or Rpt1 antibody. Lysates used for 26S assembly were also boiled with reducing/denaturing SDS loading buffer and immunoblotted for k-48-linked ubiquitin, 20S β5 subunit, 19S Rpt1 subunit and GAPDH as indicated under immunoblot.

#### **7.2.17 Confocal immunofluorescence**

All reagents used for sample staining, except for methanol were from the immunofluorescence application solutions kit (Cell Signaling Technology cat# 12727). U87-MG or HeLa cells were plated in complete medium at 2.5x10<sup>5</sup> cells/well of a four-chamber glass slide overnight. Fresh medium (500 µL) containing the test compound was added and allowed to incubate for the desire time under cell culture conditions. Cells were washed with chilled



immunofluorescent (IF) wash buffer (1x PBS, pH 8.0) and fixed with methanol at -20°C for 10 minutes. Cells were then washed 2x with IF wash buffer and incubated in blocking buffer (1x PBS, 5% normal goat serum, 0.3% Triton X-100 pH 8.0) for 60 minutes at RT. Blocking buffer was replaced with primary antibody diluted in dilution buffer (1x PBS, 1% BSA, 0.3% Triton X-100 pH 8.0) overnight (1:200) at 4°C. Primary antibody was washed off 3x and incubated in anti-rabbit Alexa Fluor 488 (1:500) and/or anti-mouse Alexa Fluor 594 for 60 minutes in the dark, at RT. Secondary antibodies were then washed off (3x) and nuclei stained with Hoechst (4 µg/mL) at RT, for 20 minutes. DNA dye was rinsed off and slides mounted in Prolong Gold and allowed to cure overnight at RT, in the dark. Slides were sealed with nail polish, and LC3B, Flag, proteasome beta 5, LAMP1 and/or p62 puncta or fluorescence detected with a 60x Plan Apo oil objective on a Nikon C2+ or Nikon A1 confocal laser scanning microscope. For Flag SNAP29 or Flag-STX17 co-staining with proteasome  $\beta$ 5, untreated cells were fixed with 4% paraformaldehyde at RT for 10 minutes, and immunostained as above with rabbit anti-Flag/ Alexa Fluor 488 and mouse anti- $\beta$ 5/ Alexa Fluor 546.

#### **7.2.18 Confocal live imaging**

**Autophagosome-lysosome fusion:** U-87MG or HEK293 cells cultured on cover glass slide were transduced with 30 particles per cell of tandem-RFP-GFP-LC3B and cultured for 24h. Cells were then incubated with either vehicle, TCH-165 (10 µM), chloroquine (100 µM) leupeptin A (200 µM), torin 1 (100 nM), or combination of torin 1 and TCH-165 for a further 24h. Cells were imaged on an upright Nikon A1 confocal microscope using a 60x Plan Apo oil objective with standard filter sets for GFP and RFP.

**EGFP-LC3B puncta:** U-87 MG cells were transiently transfected with EGFP-LC3B (2 µg/1 million cells) using sinofection reagent as described above. Cells were then split at 24h post-

transfection and seeded on cover glass slide for a further 24h. Cells were then treated with either vehicle, TCH-165 (10  $\mu$ M), torin 1 (200 nM), or combination of torin 1 and TCH-165 for a further 16h and imaged as above with GFP filter.

**Perturbation of lysosomal pH:** U-87 MG cells were seeded in a four-chamber cover glass overnight. Cells were treated with either vehicle, TCH-165 (10  $\mu$ M) Bafilomycin A1 (50 nM) or Torin1 (100 nM) for 16h. Culture medium was replaced with fresh medium containing 50 nM LysoTracker red and allowed to incubate for 15 minutes under cell culture conditions. Cells were then imaged on an upright Nikon A1 confocal microscope using a 60x Plan Apo oil objective with an excitation and emission wavelengths of 560 nm and 570-620 nm, respectively. For co-staining with LAMP1, Cells were transduced with 30 particles per cell of CellLight™ Lysosomes-GFP, BacMam 2.0 and cultured for 24h, before treatment and lysotracker red staining.

#### 7.2.19 Bacterial culture

*M. smegmatis* were grown at 37°C in Middlebrook 7H9 broth or 7H10 plates supplemented with 0.5% glycerol, 0.05% Tween 80, 1 $\times$  oleic albumin dextrose catalase (OADC) and kanamycin (25 $\mu$ g/mL) with or without anhydrous tetracycline (ATC; 100ng/mL and 200ng/mL).

#### 7.2.20 Affinity purification of *Mtb* 20S proteasome

The *Mtb* 20S was purified by affinity chromatography from a T7-prcAB-His6 plasmid (from Dr Carl Nathan) transformed into *E. coli* BL21(DE3) (glycerol stock was a gift from Dr. Abramovitch's lab). Briefly, Luria-Bertani (LB) broth containing 50  $\mu$ g/mL of chloramphenicol was inoculated with the glycerol stock. Cells were grown to OD<sub>600</sub> 0.5 and proteasome expression induced with 0.2 mM isopropyl  $\beta$ -D-1-thiogalactopyranoside (IPTG) for 20h at 37°C. Pellets (10g) from 3L of culture was obtained by centrifugation and resuspended in 80mL of lysis buffer (50mM phosphate buffer, 300 mM NaCl, 10% glycerol, 10 mM imidazole, 100  $\mu$ g/mL PMSF, 500  $\mu$ g/mL

lysozyme). The homogenate was allowed to shake (200rpm) at 37°C for 30min, and then chilled on ice for 15min before sonication (1min x 3 at 80% pulse). The lysate was centrifuged at 18000g for 20min. The collected supernatant(70mL) was mixed with 3mL of prewashed Ni-charged resin and allowed to shake for 10min at 4°C. The mixture was then loaded onto a chromatography column. The flow through was collected and column washed 2x with 3mL of washed buffer (50 mM phosphate buffer, 300 mM NaCl, 10% glycerol, 2 0mM imidazole). The proteasome was eluted by stepwise gradient of imidazole (25 mM, 50 mM, 75 mM, 100 mM, 250 mM) in 3 mL of equilibration buffer (50 mM phosphate buffer, 300 mM NaCl, 10% glycerol). The 75 mM fraction and above were confirmed to contain 20S with minimal contamination, by Coomassie gel. These fractions were combined and concentrated on a 100kDa cutoff filter, thereby removing free alpha and beta subunits. The concentrate was further cleaned by gel filtration chromatography on a Superdex-200 column with 50 mM HEPES buffer. The collected fraction was concentrated and assayed for total protein by BCA method (2.4 mg). Activity of the enzyme was checked by quantifying the hydrolysis of Suc-LLVY-AMC. The *Mtb*20S is very sensitive to freeze thaw cycle. Storage at 4°C for 4-6weeks did not appear to affect activity. Long term storage with 50% glycerol at -80°C maintains activity for more than a year.

#### **7.2.21 Affinity purification of mycobacterium proteasome-associated ATPase (Mpa)**

The gene sequence of mycobacterium proteasome associated ATPase (H37Rv strain; NP 216631.1) was cloned into NdeI/BamHI restriction sites of pET-20b (+) vector with a C-terminal his-tag, by GenScript. The received plasmid was transformed into chemically competent *BL21 E. coli* cells. Transformed clones were selected with 100µg/mL of carbenicillin and glycerol stock prepared from this. LB broth containing 100µg/mL of carbenicillin was inoculated with the glycerol stock. Cells were grown to OD<sub>600</sub> 0.53 and Mpa expression induced with 0.2mM isopropyl

$\beta$ -D-1-thiogalactopyranoside (IPTG) for 13h at 30°C. Mpa was purified by Ni-resin as with 20S above. Mpa was eluted in  $\geq 200$  mM imidazole and concentrated on a 30 kDa cutoff filter. Following gel filtration, the enzyme was stored in 50 mM HEPES, 150 mM NaCl 1mM DTT at 80°C.

#### **7.2.22 Design of single guide RNA (sgRNA)**

sgRNAs were designed to target the open reading frame (ORF) of proteasome and proteasome-associated genes. Gene silencing is more effective when targeting the ORF on the non-template strand.<sup>337</sup> This means that when targeting the ORF, PAMs must be located on the template strand. Thus, for each gene, the coding or non-template strand was obtained from SmegmaList-DNA sequence (for *M. smegmatis*) or TubercuList-TB ( for *M. tuberculosis*) genes which are now found in a single database called mycobrowser (<https://mycobrowser.epfl.ch/>). The reverse and/or complement DNA sequences (template strand) for each gene were then obtained with a software at <http://arep.med.harvard.edu/labgc/adnan/projects/Utilities/revcomp.html>. Starting with the strongest PAM, three top PAMs (based Rock *et al*'s<sup>337</sup> classification) were identified for each gene by manually searching the repertoire of functional PAM from the strongest. If the strongest was not found for that gene, then I would move to the next strongest and continue searching until 3 PAMs were identified for each gene. Next, the sgRNA targeting sequence of 20-25 nucleotides (nt) immediately 5' to the PAM is extracted. The length variability is as a result of the fact that transcription initiates most efficiently with an "A" or "G", hence the sgRNA is extracted to be at least 20nt and begins with an "A" or "G" and may sometimes require slightly longer sgRNA sequences. Forward and reverse primers were then designed from the sgRNA. The forward primary is the sgRNA and the reverse primer is the reverse complement. To regenerate the sgRNA

and dCas9 handle sequences, 5'-GGGA-3' and 5'-AAAC-3' were added to the forward and reverse primers, respectively (Table 12).

**Table 11:** sgRNAs for mycobacterium proteasome and proteasome-related genes. Fold repression (FR) for the PAMs indicated are based on Rock et al's study.<sup>337</sup> The sgRNAs corresponding to the yellow highlighted FR were the ones used in this study.

<i>Mycobacterium tuberculosis</i>	FR	5'-3'(sgRNA-PAM) (extracted from the template strand)	Forward primer 5'-3'(sgRNA)	Reverse primer 5'-3' (complement of sgRNA)
<i>M. tuberculosis</i> H37Rv Rv2109 <i>cprcA</i>	120	GCGCCGTGGCCG GTTGGCATCGAG AAC	GGGAGCGCCGTGG CCGGTTGGCAT	AAACATGCCAA CCGGCCACGGC GC
	110	GCCTGCTCAGGC GAGATGAAATAC GGAAA	GGGAGCCTGCTCA GGCGAGATGAAAT	AAACATTTCAT CTCGCCTGAGC AGGC
	51	AGGGCGGAGCCG GTGATGCGCCGG AAC	GGGAAGGGCGGAG CCGGTGATGCG	AAACCGCATCA CCGGCTCCGCC CT
<i>M. tuberculosis</i> H37Rv Rv2110 <i>cprcB</i>	53	ACGCATGAATGT CGTAGCCCCGCA GCAA	GGGAACGCATGAA TGTCGTAGCCCG	AAACCGGGCTA CGACATTCATG CGT
	42	GCCCGCCAGCAA CGGCAACGCCAG CAG	GGGAGCCCCGCCAG CAACGGCAACG	AAACCGTTGCC GTTGCTGGCGG GC
	38	GCAACTCCGGCG CCTGGCGGCGCA GGAA	GGGAGCAACTCCG GCGCCTGGCGGC	AAACGCCGCCA GGCGCCGGAGT TGC
<i>M. tuberculosis</i> H37Rv Rv2097 <i>cprfa</i>	145	ATACAGGCGCGC ACCGTTACGCAG GAAG	GGGAATACAGGCG CGCACCGTTACG	AAACCGTAACG GTGCGCGCCTG TAT
	110	ATGGCGCGGATC GGGTTATCCAGG GAAA	GGGAATGGCGCGG ATCGGGTTATCC	AAACGGATAAC CCGATCCGCGC CAT
	84	GAGCGCCGCGGT GCCACCTTGAGC AT	GGGAGAGCGCCGC GGTGCCACCT	AAACAGGTGG GCACCGCGGCG CTC

Table 11 (cont'd)

<i>Mycobacterium tuberculosis</i>	FR	5'-3'(sgRNA-PAM) (extracted from the template strand)	Forward primer 5'-3'(sgRNA)	Reverse primer 5'-3' (complement of sgRNA)
<i>M. tuberculosis</i> H37Rv Rv2115 <i>c mpa</i>	145	GACGCCTTCTCGC GGGCCCCGTTGGA AG	GGGAGACGCCTTCT CGCGGGCCCCG	AAACCGGGCCCC GCGAGAAGGC GTC
	120	AGATCGTCGGCG TGCACCGGCAAG AAC	GGGAAGATCGTCG GCGTGCACCGG	AAACCCGGTGC ACGCCGACGAT CT
	110	ACCACCGTGGTCT CGACGTCCGAGG AAA	GGGAACCACCGTG GTCTCGACGTC	AAACGACGTCG AGACCACGGTG GT
<i>M. tuberculosis</i> H37Rv Rv2111 <i>c pup</i>	42	GAGGACGTCGTC GATTTCGTCGAGC AG	GGGAGAGGACGTC GTCGATTTCGT	AAACACGAAAT CGACGACGTCC TC
	25	GAAGTCCTCGGC GTTCTCCTCGAGG AC	GGGAGAAGTCCTC GGCGTTCTCCT	AAACAGGAGA ACGCCGAGGAC TTC
<i>Mycobacterium smegmatis</i>		sgRNA	Forward primer	Reverse primer
<i>prcA</i> <i>M. smegmatis</i> MC2-155   MSMEG_3894	145	GCCTGTTCGGGCG ATATGAAGTACG GGAAG	GGGAGCCTGTTCG GGCGATATGAAGT A	AAACTACTTCA TATCGCCCGAA CAGGC
	64	GCCCCGGCGTGGC CGGCCCGCGTCG AGGAT	GGGAGCCCCGGCGT GGCCGGCCCCGCGT	AAACACGCGG GCCGGCCACGC CGGGC
	51	AGCGCCGCGCCG GTGATCCGGCGG AAC	GGGAAGCGCCGCG CCGGTGATCCG	AAACCGGATCA CCGGCGCGGGC CT
<i>prcB</i> <i>M. smegmatis</i> MC2-155   MSMEG_3895	120	GCCTGCCTGCTGA GCAGTTCGGAGA AC	GGGAGCCTGCCTG CTGAGCAGTTC	AAACGAACTGC TCAGCAGGCAG GC
	42	ATCGTCGAGGTC GTAGCCCACCAG CAG	GGGAATCGTCGAG GTCGTAGCCCA	AAACTGGGCTA CGACCTCGACG AT
	24	GTCGGGCCCCGAA AGTGTCGGTACG GGAG	GGGAGTCGGGCCC GAAAGTGTCGGT	AAACACCGACA CTTTCGGGCCC GAC

Table 11 (cont'd)

<i>Mycobacterium smegmatis</i>	FR	5'-3'(sgRNA-PAM) (extracted from the template strand)	Forward primer 5'-3'(sgRNA)	Reverse primer 5'-3' (complement of sgRNA)
<i>PafA</i> <i>M. smegmatis</i> MC2-155   MSMEG_3890	120	GCCTGCCTGCTGA GCAGTTCGGAGA AC	GGGAGCCTGCCTG CTGAGCAGTTC	AAACGAACTGC TCAGCAGGCAG GC
	51	GCCAGCCGGTTG ACCTTGCCGCGG AAC	GGGAGCCAGCCGG TTGACCTTGCC	AAACGGCAAG GTCAACCGGCT GGC
	42	ATCGTCGAGGTC GTAGCCCACCAG CAG	GGGAATCGTCGAG GTCGTAGCCCA	AAACTGGGCTA CGACCTCGACG AT
<i>Mpa</i> <i>M. smegmatis</i> MC2-155   MSMEG_3902	145	GAGGCCTTCTCGC GCGCACGCTGGA AG	GGGAGAGGCCTTC TCGCGCGCACG	AAACCGTGCGC GCGAGAAGGC CTC
	110	ACCCCGCTCCGGC GAAACCCTCGGG AAA	GGGAACCCCGCTC CGGCGAAACCCT	AAACAGGGTTT CGCCGGAGCGG GGT
	84	ACCGCGTTTTTCCA ACTGCTCGCGCA GCAT	GGGAACCGCGTTTT CCAAGTCTCGC	AAACGCGAGC AGTTGGAAAAC GCGGT
<i>Pup</i> <i>M. smegmatis</i> MC2-155   pup	42	GAGGACGTCGTC GATCTCATCCAGC AG	GGGAGAGGACGTC GTCGATCTCAT	AAACATGAGAT CGACGACGTCC TC
	25	GCTCCTGGCCGGC AGCCGAAGCACC GGGGAG	GGGAGCTCCTGGC CGGCAGCCGAAGC AC	AAACGTGCTTC GGCTGCCGGCC AGGAGC

### 7.2.23 Plasmid construction and cloning

The *M. smegmatis* (PLJR962) and *M. tuberculosis* (PLJR965) CRISPRi backbone plasmids were obtained from Sarah M. Fortune lab, amplified in *E. coli* and purified by miniprep. The CRISPRi backbones have BsmBI restriction sites immediately 5' to the sgRNA scaffold sequence. To clone sgRNA targeting sequences, sgRNA targeting oligos (forward and reverse primers) were annealed and ligated into the BsmBI-digested CRISPRi vector backbone. Plasmids were amplified in *E. coli*, purified and sequenced to confirm insertion. Confirmed clones were

transformed into *M. smegmatis* or *M. tuberculosis* by electroporation. Transformed *M. smegmatis* colonies were selected on kanamycin (25µg/mL) 7H9 plate and use for downstream experiments.

**Plasmid digestion (40 µL reaction scale):** A mixture of 1 µg plasmid (4.7 µL), 4 µL buffer, 0.4 µL 100xBSA, 1.5µL BsmBI, 29.3 µL nuclease free water was prepared and incubated at 55°C for 1.5h. An additional 1µL of BsmBI was added and incubated for a further 2h at 55°C. The reaction mixture was then mixed with 8µL of 6x loading buffer with gel red and resolved on a 0.8% agarose gel. The cut plasmid was visualized by UV-lamp and cut into a tube. The plasmid was then extracted using gel extraction kit.

**Primer phosphorylation/annealing (24 µL reaction scale):** A mixture of 6 µL 100 µM forward primer, 6 µL 100 µM reverse primer, 2 µL 10x polynucleotide kinase (PNK) buffer, 1 µL PNK, 2 µL 10 mM ATP, 3 µL nuclease free water was prepared and incubated at 37°C for 1h. To anneal the primers, 4 µL of annealing buffer (50 mM Tris pH7.5, 50 mM NaCl, 1 mM EDTA) was then added to the mixture and boiled at 95°C on a heating block for 10 minutes. The heating block was turned off and allowed to cool to RT. **Note:** The cooling needs to occur at a rate of about 0.1°C/sec, which means the samples must be left in the heating block to gradually cool down.

**Ligation (30 µL reaction scale):** Ligation was carried out on a 30 µL reaction scale at 4°C overnight (16h). The ligation mixture consisted of 12 µL of annealed primers, 3.3 µL gel purified CRISPRi backbone (50 ng), 3 µL 10xT4 buffer, 1 µL T4 ligase, and 10.7 µL nuclease free water. Control was setup without primer.

**Transformation:** The ligated plasmid (10 µL) was mixed with 20 µL of E-coli TOPO10 competent cells and allowed to sit on ice for 10minutes. Cells were heat shocked at 42°C for 30sec. and then rested on ice for 2minutes. Medium (200µL of SOC) was then added to each sample and shook at 37°C for 1h. The culture was then plated on a kanamycin (25µg/mL) agar plate. Individual



colonies were inoculated, cultured, miniprep and sequenced (Genewiz). Desired clones were transformed into mc<sup>2</sup>155 *M. smegmatis* by electroporation.

#### **7.2.24 Bacterial mRNA isolation and quantification**

For each sample, cultures were grown to log phase and then diluted to OD 0.2 with or without 200 ng/mL anhydrous tetracyclin (ATC), to maintain the cultures in the log phase, and to induce CRISPR interference of gene expression (for ATC samples). Target knockdown proceeded for 14h. Cells from each culture were harvested by centrifugation, resuspended in 1 mL of TRIzol and disrupted by bead beating using Zirconia Silica beads at 6.0M/s for 2 minutes. Chloroform (0.2 mL) was added to each sample and vortexed for 15sec to mix. Samples were incubated for 5 min at RT and then centrifuged at 10,000rpm for 15 min at 4°C. The colorless upper aqueous phase containing RNA (~800 µL) was transferred into 1.5mL RNAase-free tube and 500 µL of absolute ethanol added and immediately mixed by inverting 5x. The RNA was isolated by RNA miniprep and residual contaminating genomic DNA was digested with TURBO DNase. Samples were cleaned with RNA clean-up columns. The cDNA was prepared from 200 ng RNA with random hexamers as per manufacturer instructions. Quantification of cDNA were done by quantitative real-time PCR (qRT-PCR) on a Viia7 light cycler (Applied Biosystems) using iTaq Universal SYBR Green Supermix. All qPCR primer pairs were validated by melt curve and amplicon sequencing. Signals were normalized to the housekeeping sigA transcript *M. smegmatis* (Ms2758) and quantified by the  $\Delta\Delta C_t$  method. Data are means of three replicates.

#### **7.2.25 Proteasome activity in *Mycobacterium smegmatis* cell lysate**

*M. smegmatis* at 0.1 OD<sub>600</sub> were cultured in 7H9 broth with kanamycin (25 µg/mL) with or with ATC (200 ng/mL) for 48h. Cells were pelleted and lyzed by vortexing with Zirconium beads in 50 mM Tris/HCl pH7.4, 10% glycerol, 0.5 mM EDTA. Lysates were clarified and total

protein quantified by bicinchoninic acid assay (BCA). Lysate (10 µg/well) was assayed for proteasome activity in 50mM Tris/HCl pH7.4 with or without 2.5 mM ATP/5 mM MgCl<sub>2</sub> by measuring fluorescence emission of AMC at 380/440 nm after 1h incubation with 40 µM Suc-LLVY-AMC at 37°C.

#### **7.2.26 *Mycobacterium smegmatis* growth inhibition**

To measure the GI<sub>50</sub> of TCH-156, *M. smegmatis* culture was grown to log phase and diluted to 0.05 OD<sub>600</sub>. Culture (198 µL) was transferred into a sterile clear bottom, black 96-well plate and 2mL of the test compound at 100x final concentration added to it. For background control, 100µg/mL of streptomycin (to kill the cells) was used.

#### **7.2.27 Quantification and statistical analysis**

Data are presented as mean ± standard deviation (SD). For each figure, the number of replicates is indicated in the figure legends. Statistical analysis was only performed on experiments with three or more n (biological replicates for cellular experiments or individual experiment for biochemical assays). Western blots and immunofluorescence (total fluorescence or puncta) quantification were performed with imageJ and colocalization (Mander's overlap and pearson's correlation) with Nikon software. For total fluorescence/colocalization, measurements were taken from an entire field of view. For puncta or AVs, mean puncta for an entire field of view per cell number in that field was used for each experiment. statistical analysis was performed with GraphPad Prism 7 software. Unpaired Student's t-test was used for two samples while one-way analysis of variance with post hoc Bonferroni test was used for multiple comparisons of means. Effect was considered significant for \*p<0.05, \*\*p<0.01, \*\*\*p<0.001, \*\*\*\*p<0.0001.

**AFM imaging (By Dr. Pawel A. Osmulski and Dr. Maria Gaczynska)<sup>81</sup>**  
**D2R Binding Assay (by Dr. Benita Sjögren)<sup>153</sup>**

## **APPENDICES**

## APPENDIX A: Copyright permission letter for chapter 1

6/22/2019

Rightslink® by Copyright Clearance Center



RightsLink®

Home

Account  
Info

Help



ACS Publications  
Most Trusted. Most Cited. Most Read.

Title:

Proteasome Activation as a New  
Therapeutic Approach To Target  
Proteotoxic Disorders

Logged in as:

Evert Njomen

LOGOUT

Author:

Evert Njomen, Jetze J. Tepe

Publication:

Journal of Medicinal Chemistry

Publisher:

American Chemical Society

Date:

Mar 1, 2019

Copyright © 2019, American Chemical Society

### Quick Price Estimate

Permission for this particular request is granted for print and electronic formats, and translations, at no charge. Figures and tables may be modified. Appropriate credit should be given. Please print this page for your records and provide a copy to your publisher. Requests for up to 4 figures require only this record. Five or more figures will generate a printout of additional terms and conditions. Appropriate credit should read: "Reprinted with permission from {COMPLETE REFERENCE CITATION}. Copyright {YEAR} American Chemical Society." Insert appropriate information in place of the capitalized words.

I would like to... ?

reuse in a Thesis/Dissertation ▼

Requestor Type ?

Author (original work) ▼

Portion ?

make a selection ▼

Format ?

Print and Electronic ▼

Select your currency

USD - \$ ▼

Quick Price

Click Quick Price

This service provides permission for reuse only. If you do not have a copy of the article you are using, you may copy and paste the content and reuse according to the terms of your agreement. Please be advised that obtaining the content you license is a separate transaction not involving Rightslink.

QUICK PRICE

CONTINUE

To request permission for a type of use not listed, please contact [the publisher](#) directly.

## APPENDIX B: Copyright permission letter for chapter 2

6/22/2019

Rightslink® by Copyright Clearance Center



RightsLink®

Home

Account  
Info

Help



ACS Publications  
Most Trusted. Most Cited. Most Read.

**Title:** Small Molecule Modulation of  
Proteasome Assembly

**Author:** Evert Njomen, Pawel A.  
Osmulski, Corey L. Jones, et al

**Publication:** Biochemistry

**Publisher:** American Chemical Society

**Date:** Jul 1, 2018

Copyright © 2018, American Chemical Society

Logged in as:  
Evert Njomen

LOGOUT

### Quick Price Estimate

Permission for this particular request is granted for print and electronic formats, and translations, at no charge. Figures and tables may be modified. Appropriate credit should be given. Please print this page for your records and provide a copy to your publisher. Requests for up to 4 figures require only this record. Five or more figures will generate a printout of additional terms and conditions. Appropriate credit should read: "Reprinted with permission from {COMPLETE REFERENCE CITATION}. Copyright {YEAR} American Chemical Society." Insert appropriate information in place of the capitalized words.

I would like to... ?

reuse in a Thesis/Dissertation ▼

Requestor Type ?

Author (original work) ▼

Portion ?

make a selection ▼

Format ?

Print and Electronic ▼

Select your currency

USD - \$ ▼

Quick Price

Click Quick Price

This service provides permission for reuse only. If you do not have a copy of the article you are using, you may copy and paste the content and reuse according to the terms of your agreement. Please be advised that obtaining the content you license is a separate transaction not involving Rightslink.

QUICK PRICE

CONTINUE

To request permission for a type of use not listed, please contact [the publisher](#) directly.

## APPENDIX C: Copyright permission letter for chapter 3

7/23/2019

Rightslink® by Copyright Clearance Center



RightsLink®

Home

Account  
Info

Help



**Title:** Regulation of Autophagic Flux by the 20S Proteasome

**Author:** Evert Njomen, Jetze J. Tepe

**Publication:** Cell Chemical Biology

**Publisher:** Elsevier

**Date:** Available online 18 July 2019

© 2019 Elsevier Ltd.

Logged in as:  
Evert Njomen

Account #:  
3001473180

LOGOUT

Please note that, as the author of this Elsevier article, you retain the right to include it in a thesis or dissertation, provided it is not published commercially. Permission is not required, but please ensure that you reference the journal as the original source. For more information on this and on your other retained rights, please visit: <https://www.elsevier.com/about/our-business/policies/copyright#Author-rights>

BACK

CLOSE WINDOW

Copyright © 2019 Copyright Clearance Center, Inc. All Rights Reserved. [Privacy statement](#). [Terms and Conditions](#).  
Comments? We would like to hear from you. E-mail us at [customer@copyright.com](mailto:customer@copyright.com)

## APPENDIX D: Copyright permission letter for chapter 4

6/22/2019

Rightslink® by Copyright Clearance Center



RightsLink®

Home

Account  
Info

Help



ACS Publications  
Most Trusted. Most Cited. Most Read.

Title:

Small Molecule Enhancement of  
20S Proteasome Activity Targets  
Intrinsically Disordered Proteins

Author:

Corey L. Jones, Evert Njomen,  
Benita Sjögren, et al

Publication: ACS Chemical Biology

Publisher: American Chemical Society

Date: Sep 1, 2017

Copyright © 2017, American Chemical Society

Logged in as:

Evert Njomen

LOGOUT

### Quick Price Estimate

Permission for this particular request is granted for print and electronic formats, and translations, at no charge. Figures and tables may be modified. Appropriate credit should be given. Please print this page for your records and provide a copy to your publisher. Requests for up to 4 figures require only this record. Five or more figures will generate a printout of additional terms and conditions. Appropriate credit should read: "Reprinted with permission from {COMPLETE REFERENCE CITATION}. Copyright {YEAR} American Chemical Society." Insert appropriate information in place of the capitalized words.

I would like to... ?

reuse in a Thesis/Dissertation ▼

Requestor Type ?

Author (original work) ▼

Field is required.

Portion ?

make a selection ▼

Format ?

Print and Electronic ▼

Select your currency

USD - \$ ▼

Quick Price

Click Quick Price

This service provides permission for reuse only. If you do not have a copy of the article you are using, you may copy and paste the content and reuse according to the terms of your agreement. Please be advised that obtaining the content you license is a separate transaction not involving Rightslink.

QUICK PRICE

CONTINUE

## REFERENCES



## REFERENCES

- (1) Balch, W. E.; Morimoto, R. I.; Dillin, A.; Kelly, J. W. Adapting Proteostasis for Disease Intervention. *Science* **2008**, *319* (5865), 916–919.
- (2) First Aid for a Damaged Proteome. *Nature Chemical Biology* **2014**, *10* (11), 869. <https://doi.org/10.1038/nchembio.1684>.
- (3) Niforou, K.; Cheimonidou, C.; Trougakos, I. P. Molecular Chaperones and Proteostasis Regulation during Redox Imbalance. *Redox Biology* **2014**, *2*, 323–332. <https://doi.org/10.1016/j.redox.2014.01.017>.
- (4) Korovila, I.; Hugo, M.; Castro, J. P.; Weber, D.; Höhn, A.; Grune, T.; Jung, T. Proteostasis, Oxidative Stress and Aging. *Redox Biology* **2017**, *13*, 550–567. <https://doi.org/10.1016/j.redox.2017.07.008>.
- (5) Tanaka, K.; Matsuda, N. Proteostasis and Neurodegeneration: The Roles of Proteasomal Degradation and Autophagy. *Biochimica et Biophysica Acta (BBA) - Molecular Cell Research* **2014**, *1843* (1), 197–204. <https://doi.org/10.1016/j.bbamcr.2013.03.012>.
- (6) Hetz, C.; Glimcher, L. H. Protein Homeostasis Networks in Physiology and Disease. *Current Opinion Cell Biology* **2011**, *23* (2), 123–125.
- (7) Frydman, J. Folding of Newly Translated Proteins in Vivo: The Role of Molecular Chaperones. *Annual Review of Biochemistry* **2001**, *70*, 603–647.
- (8) Douglas, P. M.; Summers, D. W.; Cyr, D. M. Molecular Chaperones Antagonize Proteotoxicity by Differentially Modulating Protein Aggregation Pathways. *Prion* **2009**, *3* (2), 51–58.
- (9) Ji, C. H.; Kwon, Y. T. Crosstalk and Interplay between the Ubiquitin-Proteasome System and Autophagy. *Molecular Cells* **2017**, *40* (7), 441–449. <https://doi.org/10.14348/molcells.2017.0115>.
- (10) Korolchuk, V. I.; Mansilla, A.; Menzies, F. M.; Rubinsztein, D. C. Autophagy Inhibition Compromises Degradation of Ubiquitin-Proteasome Pathway Substrates. *Molecular Cell* **2009**, *33* (4), 517–527. <https://doi.org/10.1016/j.molcel.2009.01.021>.
- (11) Zheng, Q.; Su, H.; Tian, Z.; Wang, X. Proteasome Malfunction Activates Macroautophagy in the Heart. *American Journal of Cardiovascular Diseases* **2011**, *1* (3), 214–226.
- (12) Halliwell, B.; Isacson, O.; Jenner, P.; McNaught, K. S. P.; Olanow, C. W. Failure of the Ubiquitin-Proteasome System in Parkinson's Disease. *Nature Reviews Neuroscience* **2001**, *2* (8), 589+.

- (13) Saez, I.; Vilchez, D. The Mechanistic Links Between Proteasome Activity, Aging and Age-Related Diseases. *Current Genomics* **2014**, *15* (1), 38–51. <https://doi.org/10.2174/138920291501140306113344>.
- (14) Calamini, B.; Morimoto, R. I. Protein Homeostasis as a Therapeutic Target for Diseases of Protein Conformation. *Current Topics in Medicinal Chemistry* **2012**, *12* (22), 2623–2640.
- (15) Voges, D.; Zwickl, P.; Baumeister, W. The 26S Proteasome: A Molecular Machine Designed for Controlled Proteolysis. *Annual Review of Biochemistry* **1999**, *68* (1), 1015–1068. <https://doi.org/10.1146/annurev.biochem.68.1.1015>.
- (16) Voorhees, P. M.; Dees, E. C.; O’Neil, B.; Orlowski, R. Z. The Proteasome as a Target for Cancer Therapy. *Clinical Cancer Research* **2003**, *9* (17), 6316–6325.
- (17) Ostrowska, H. The Ubiquitin-Proteasome System: A Novel Target for Anticancer and Anti-Inflammatory Drug Research. *Cellular and Molecular Biology Letters* **2008**, *13* (3), 353–365. <https://doi.org/10.2478/s11658-008-0008-7>.
- (18) Biophysics Demasi, M. and Faria, B. F. Activation of the Ubiquitin-Proteasome System: Implications for Neurodegeneration, Aging, and Tumorigenesis. *Journal of Neurology and Neuromedicine* **2017**, *2* (8), 1–4.
- (19) Opattova, A.; Cente, M.; Novak, M.; Filipcik, P. The Ubiquitin Proteasome System as a Potential Therapeutic Target for Treatment of Neurodegenerative Diseases. *General Physiology and Biophysics* **2015**, *34* (4), 337–352. [https://doi.org/10.4149/gpb\\_2015024](https://doi.org/10.4149/gpb_2015024).
- (20) Cohen-Kaplan, V.; Livneh, I.; Avni, N.; Cohen-Rosenzweig, C.; Ciechanover, A. The Ubiquitin-Proteasome System and Autophagy: Coordinated and Independent Activities. *International Journal of Biochemistry and Cell Biology* **2016**, *79*, 403–418. <https://doi.org/10.1016/j.biocel.2016.07.019>.
- (21) Shang, F.; Taylor, A. Ubiquitin-Proteasome Pathway and Cellular Responses to Oxidative Stress. *Free Radical Biology and Medicine* **2011**, *51* (1), 5–16. <https://doi.org/10.1016/j.freeradbiomed.2011.03.031>.
- (22) Yoshimura, T.; Kameyama, K.; Takagi, T.; Ikai, A.; Tokunaga, F.; Koide, T.; Tanahashi, N.; Tamura, T.; Cejka, Z.; Baumeister, W. Molecular Characterization of the “26S” Proteasome Complex from Rat Liver. *Journal of Structural Biology* **1993**, *111* (3), 200–211.
- (23) Xie, Y. Structure, Assembly and Homeostatic Regulation of the 26S Proteasome. *Journal of Molecular Cell Biology* **2010**, *2* (6), 308–317. <https://doi.org/10.1093/jmcb/mjq030>.
- (24) Huang, X.; Luan, B.; Wu, J.; Shi, Y. An Atomic Structure of the Human 26S Proteasome. *Nature Structural & Molecular Biology* **2016**, *23* (9), 778–785. <https://doi.org/10.1038/nsmb.3273>.

- (25) da Fonseca, P. C. A.; Morris, E. P. Structure of the Human 26S Proteasome: Subunit Radial Displacements Open the Gate into the Proteolytic Core. *Journal of Biological Chemistry* **2008**, 283 (34), 23305–23314. <https://doi.org/10.1074/jbc.M802716200>.
- (26) Tanaka, K.; Yoshimura, T.; Kumatori, A.; Ichihara, A.; Ikai, A.; Nishigai, M.; Kameyama, K.; Takagi, T. Proteasomes (Multi-Protease Complexes) as 20 S Ring-Shaped Particles in a Variety of Eukaryotic Cells. *Journal of Biological Chemistry*. **1988**, 263 (31), 16209–16217.
- (27) Groll, M.; Heinemeyer, W.; Jäger, S.; Ullrich, T.; Bochtler, M.; Wolf, D. H.; Huber, R. The Catalytic Sites of 20S Proteasomes and Their Role in Subunit Maturation: A Mutational and Crystallographic Study. *Proceedings of the National Academy of Sciences of the United States of America* **1999**, 96 (20), 10976–10983. <https://doi.org/10.1073/pnas.96.20.10976>.
- (28) Unno, M.; Mizushima, T.; Morimoto, Y.; Tomisugi, Y.; Tanaka, K.; Yasuoka, N.; Tsukihara, T. The Structure of the Mammalian 20S Proteasome at 2.75 Å Resolution. *Structure* **2002**, 10 (5), 609–618. [https://doi.org/10.1016/S0969-2126\(02\)00748-7](https://doi.org/10.1016/S0969-2126(02)00748-7).
- (29) Groll, M.; Bochtler, M.; Brandstetter, H.; Clausen, T.; Huber, R. Molecular Machines for Protein Degradation. *Chembiochem* **2005**, 6 (2), 222–256. <https://doi.org/10.1002/cbic.200400313>.
- (30) Ustrell, V.; Hoffman, L.; Pratt, G.; Rechsteiner, M. PA200, a Nuclear Proteasome Activator Involved in DNA Repair. *European Molecular Biology Organization Journal* **2002**, 21 (13), 3516–3525. <https://doi.org/10.1093/emboj/cdf333>.
- (31) Stadtmueller, B. M.; Hill, C. P. Proteasome Activators. *Molecular Cell* **2011**, 41 (1), 8–19. <https://doi.org/10.1016/j.molcel.2010.12.020>.
- (32) Sadre-Bazzaz, K.; Whitby, F. G.; Robinson, H.; Formosa, T.; Hill, C. P. Structure of a Blm10 Complex Reveals Common Mechanisms for Proteasome Binding and Gate Opening. *Mol. Cell* **2010**, 37 (5), 728–735. <https://doi.org/10.1016/j.molcel.2010.02.002>.
- (33) Whitby, F. G.; Masters, E. I.; Kramer, L.; Knowlton, J. R.; Yao, Y.; Wang, C. C.; Hill, C. P. Structural Basis for the Activation of 20S Proteasomes by 11S Regulators. *Nature* **2000**, 408 (6808), 115–120. <https://doi.org/10.1038/35040607>.
- (34) Lander, G. C.; Estrin, E.; Matyskiela, M. E.; Bashore, C.; Nogales, E.; Martin, A. Complete Subunit Architecture of the Proteasome Regulatory Particle. *Nature* **2012**, 482 (7384), 186–191. <https://doi.org/10.1038/nature10774>.
- (35) Rabl, J.; Smith, D. M.; Yu, Y.; Chang, S.-C.; Goldberg, A. L.; Cheng, Y. Mechanism of Gate Opening in the 20S Proteasome by the Proteasomal ATPases. *Molecular Cell* **2008**, 30 (3), 360–368. <https://doi.org/10.1016/j.molcel.2008.03.004>.
- (36) Smith, D. M.; Chang, S.-C.; Park, S.; Finley, D.; Cheng, Y.; Goldberg, A. L. Docking of the Proteasomal ATPases' Carboxyl Termini in the 20S Proteasome's Alpha Ring Opens

the Gate for Substrate Entry. *Molecular Cell* **2007**, 27 (5), 731–744.  
<https://doi.org/10.1016/j.molcel.2007.06.033>.

- (37) Chu-Ping, M.; Vu, J. H.; Proske, R. J.; Slaughter, C. A.; DeMartino, G. N. Identification, Purification, and Characterization of a High Molecular Weight, ATP-Dependent Activator (PA700) of the 20 S Proteasome. *Journal of Biological Chemistry* **1994**, 269 (5), 3539–3547.
- (38) Xie, Y.; Varshavsky, A. RPN4 Is a Ligand, Substrate, and Transcriptional Regulator of the 26S Proteasome: A Negative Feedback Circuit. *Proceedings of the National Academy of Sciences of the United States of America* **2001**, 98 (6), 3056–3061.  
<https://doi.org/10.1073/pnas.071022298>.
- (39) Wang, X.; Xu, H.; Ju, D.; Xie, Y. Disruption of Rpn4-Induced Proteasome Expression in *Saccharomyces Cerevisiae* Reduces Cell Viability Under Stressed Conditions. *Genetics* **2008**, 180 (4), 1945–1953. <https://doi.org/10.1534/genetics.108.094524>.
- (40) Sharon, M.; Taverner, T.; Ambroggio, X. I.; Deshaies, R. J.; Robinson, C. V. Structural Organization of the 19S Proteasome Lid: Insights from MS of Intact Complexes. *PLoS Biology*. **2006**, 4 (8), e267. <https://doi.org/10.1371/journal.pbio.0040267>.
- (41) Ehlinger, A.; Walters, K. J. Structural Insights into Proteasome Activation by the 19S Regulatory Particle. *Biochemistry* **2013**, 52 (21). <https://doi.org/10.1021/bi400417a>.
- (42) Verma, R.; Aravind, L.; Oania, R.; McDonald, W. H.; Yates, J. R.; Koonin, E. V.; Deshaies, R. J. Role of Rpn11 Metalloprotease in Deubiquitination and Degradation by the 26S Proteasome. *Science* **2002**, 298 (5593), 611–615.  
<https://doi.org/10.1126/science.1075898>.
- (43) Yao, T.; Cohen, R. E. A Cryptic Protease Couples Deubiquitination and Degradation by the Proteasome. *Nature* **2002**, 419 (6905), 403–407. <https://doi.org/10.1038/nature01071>.
- (44) Lee, M. J.; Lee, B.-H.; Hanna, J.; King, R. W.; Finley, D. Trimming of Ubiquitin Chains by Proteasome-Associated Deubiquitinating Enzymes. *Molecular and Cellular Proteomics* **2011**, 10 (5). <https://doi.org/10.1074/mcp.R110.003871>.
- (45) Basler, M.; Kirk, C. J.; Groettrup, M. The Immunoproteasome in Antigen Processing and Other Immunological Functions. *Current Opinion in Immunology* **2013**, 25 (1), 74–80.  
<https://doi.org/10.1016/j.coi.2012.11.004>.
- (46) Huber, E. M.; Basler, M.; Schwab, R.; Heinemeyer, W.; Kirk, C. J.; Groettrup, M.; Groll, M. Immuno- and Constitutive Proteasome Crystal Structures Reveal Differences in Substrate and Inhibitor Specificity. *Cell* **2012**, 148 (4), 727–738.  
<https://doi.org/10.1016/j.cell.2011.12.030>.
- (47) Sijts, A. J. A. M.; Standera, S.; Toes, R. E. M.; Ruppert, T.; Beekman, N. J. C. M.; Van, V.; Ossendorp, F. A.; Melief, C. J. M.; Kloetzel, P. M. MHC Class I Antigen Processing of an Adenovirus CTL Epitope Is Linked to the Levels of Immunoproteasomes in

- Infected Cells. *Journal of Immunology* **2000**, *164* (9), 4500–4506.  
<https://doi.org/10.4049/jimmunol.164.9.4500>.
- (48) Toes, R. E. M.; Nussbaum, A. K.; Degermann, S.; Schirle, M.; Emmerich, N. P. N.; Kraft, M.; Laplace, C.; Zwinderman, A.; Dick, T. P.; Müller, J.; et al. Discrete Cleavage Motifs of Constitutive and Immunoproteasomes Revealed by Quantitative Analysis of Cleavage Products. *Journal of Experimental Medicine* **2001**, *194* (1), 1–12.  
<https://doi.org/10.1084/jem.194.1.1>.
  - (49) Aki, M.; Shimbara, N.; Takashina, M.; Akiyama, K.; Kagawa, S.; Tamura, T.; Tanahashi, N.; Yoshimura, T.; Tanaka, K.; Ichihara, A. Interferon-Gamma Induces Different Subunit Organizations and Functional Diversity of Proteasomes. *Journal of Biochemistry* **1994**, *115* (2), 257–269.
  - (50) McCarthy, M. K.; Weinberg, J. B. The Immunoproteasome and Viral Infection: A Complex Regulator of Inflammation. *Frontier in Microbiology* **2015**, *6*.  
<https://doi.org/10.3389/fmicb.2015.00021>.
  - (51) Murata, S.; Sasaki, K.; Kishimoto, T.; Niwa, S.; Hayashi, H.; Takahama, Y.; Tanaka, K. Regulation of CD8+ T Cell Development by Thymus-Specific Proteasomes. *Science* **2007**, *316* (5829), 1349–1353. <https://doi.org/10.1126/science.1141915>.
  - (52) Chondrogianni, N.; Gonos, E. S. Proteasome Function Determines Cellular Homeostasis and the Rate of Aging. *Advances in Experimental Medicine and Biology* **2010**, *694*, 38–46.
  - (53) Varshavsky, A. Regulated Protein Degradation. *Trends in Biochemical Sciences* **2005**, *30* (6), 283–286. <https://doi.org/10.1016/j.tibs.2005.04.005>.
  - (54) Asher, G.; Reuven, N.; Shaul, Y. 20S Proteasomes and Protein Degradation “by Default.” *Bioessays* **2006**, *28* (8), 844–849. <https://doi.org/10.1002/bies.20447>.
  - (55) Uversky, V. N. A Decade and a Half of Protein Intrinsic Disorder: Biology Still Waits for Physics. *Protein Science* **2013**, *22* (6), 693–724. <https://doi.org/10.1002/pro.2261>.
  - (56) Dunker, A. K.; Brown, C. J.; Lawson, J. D.; Iakoucheva, L. M.; Obradović, Z. Intrinsic Disorder and Protein Function. *Biochemistry* **2002**, *41* (21), 6573–6582.  
<https://doi.org/10.1021/bi012159+>.
  - (57) Cheng, Y.; LeGall, T.; Oldfield, C. J.; Dunker, A. K.; Uversky, V. N. Abundance of Intrinsic Disorder in Protein Associated with Cardiovascular Disease. *Biochemistry* **2006**, *45* (35), 10448–10460. <https://doi.org/10.1021/bi060981d>.
  - (58) Du, Z.; Uversky, V. N. A Comprehensive Survey of the Roles of Highly Disordered Proteins in Type 2 Diabetes. *International Journal of Molecular Sciences* **2017**, *18* (10).  
<https://doi.org/10.3390/ijms18102010>.

- (59) Uversky, V. N.; Oldfield, C. J.; Dunker, A. K. Intrinsically Disordered Proteins in Human Diseases: Introducing the D2 Concept. *Annual Review of Biophysics* **2008**, *37*, 215–246. <https://doi.org/10.1146/annurev.biophys.37.032807.125924>.
- (60) Williams, R. M.; Obradovi, Z.; Mathura, V.; Braun, W.; Garner, E. C.; Young, J.; Takayama, S.; Brown, C. J.; Dunker, A. K. The Protein Non-Folding Problem: Amino Acid Determinants of Intrinsic Order and Disorder. *Pacific Symposium on Biocomputing* **2001**, 89–100.
- (61) Romero, P.; Obradovic, Z.; Li, X.; Garner, E. C.; Brown, C. J.; Dunker, A. K. Sequence Complexity of Disordered Protein. *Proteins* **2001**, *42* (1), 38–48.
- (62) Garner, null; Cannon, null; Romero, null; Obradovic, null; Dunker, null. Predicting Disordered Regions from Amino Acid Sequence: Common Themes Despite Differing Structural Characterization. *Genome Inform Ser Workshop Genome Inform* **1998**, *9*, 201–213.
- (63) Dunker, A. K.; Garner, E.; Guilliot, S.; Romero, P.; Albrecht, K.; Hart, J.; Obradovic, Z.; Kissinger, C.; Villafranca, J. E. Protein Disorder and the Evolution of Molecular Recognition: Theory, Predictions and Observations. *Pacific Symposium on Biocomputing* **1998**, 473–484.
- (64) Xue, B.; Dunbrack, R. L.; Williams, R. W.; Dunker, A. K.; Uversky, V. N. PONDR-FIT: A Meta-Predictor of Intrinsically Disordered Amino Acids. *Biochimica et Biophysica Acta* **2010**, *1804* (4), 996–1010. <https://doi.org/10.1016/j.bbapap.2010.01.011>.
- (65) Mészáros, B.; Erdos, G.; Dosztányi, Z. IUPred2A: Context-Dependent Prediction of Protein Disorder as a Function of Redox State and Protein Binding. *Nucleic Acids Research* **2018**, *46* (W1), W329–W337. <https://doi.org/10.1093/nar/gky384>.
- (66) Hanson, J.; Paliwal, K.; Zhou, Y. Accurate Single-Sequence Prediction of Protein Intrinsic Disorder by an Ensemble of Deep Recurrent and Convolutional Architectures. *Journal of Chemical Information and Modeling* **2018**, *58* (11), 2369–2376. <https://doi.org/10.1021/acs.jcim.8b00636>.
- (67) Goda, N.; Shimizu, K.; Kuwahara, Y.; Tenno, T.; Noguchi, T.; Ikegami, T.; Ota, M.; Hiroaki, H. A Method for Systematic Assessment of Intrinsically Disordered Protein Regions by NMR. *International Journal of Molecular Sciences* **2015**, *16* (7), 15743–15760. <https://doi.org/10.3390/ijms160715743>.
- (68) Kumagai, P. S.; Araujo, A. P. U.; Lopes, J. L. S. Going Deep into Protein Secondary Structure with Synchrotron Radiation Circular Dichroism Spectroscopy. *Biophysical Reviews* **2017**, *9* (5), 517–527. <https://doi.org/10.1007/s12551-017-0314-2>.
- (69) Na, J.-H.; Lee, W.-K.; Yu, Y. G. How Do We Study the Dynamic Structure of Unstructured Proteins: A Case Study on Nopp140 as an Example of a Large, Intrinsically

Disordered Protein *International Journal of Molecular Sciences* **2018**, *19* (2).  
<https://doi.org/10.3390/ijms19020381>.

- (70) Haynes, C.; Oldfield, C. J.; Ji, F.; Klitgord, N.; Cusick, M. E.; Radivojac, P.; Uversky, V. N.; Vidal, M.; Iakoucheva, L. M. Intrinsic Disorder Is a Common Feature of Hub Proteins from Four Eukaryotic Interactomes. *PLoS Computational Biology* **2006**, *2* (8).  
<https://doi.org/10.1371/journal.pcbi.0020100>.
- (71) Singh, G. P.; Ganapathi, M.; Dash, D. Role of Intrinsic Disorder in Transient Interactions of Hub Proteins. *Proteins: Structure, Function, and Bioinformatics* **2007**, *66* (4), 761–765. <https://doi.org/10.1002/prot.21281>.
- (72) Wright, P. E.; Dyson, H. J. Intrinsically Disordered Proteins in Cellular Signaling and Regulation. *Nature Reviews Molecular and Cell Biology* **2015**, *16* (1), 18–29.  
<https://doi.org/10.1038/nrm3920>.
- (73) Biran, A.; Myers, N.; Adler, J.; Broennimann, K.; Reuven, N.; Shaul, Y. A 20S Proteasome Receptor for Degradation of Intrinsically Disordered Proteins. *bioRxiv* **2017**, 210898. <https://doi.org/10.1101/210898>.
- (74) Uversky, V. N. Intrinsically Disordered Proteins and Their (Disordered) Proteomes in Neurodegenerative Disorders. *Frontiers in Aging Neuroscience* **2015**, *7*.  
<https://doi.org/10.3389/fnagi.2015.00018>.
- (75) Alvarez-Castelao, B.; Goethals, M.; Vandekerckhove, J.; Castaño, J. G. Mechanism of Cleavage of Alpha-Synuclein by the 20S Proteasome and Modulation of Its Degradation by the RedOx State of the N-Terminal Methionines. *Biochimica et Biophysica Acta (BBA) - Molecular Cell Research* **2014**, *1843* (2), 352–365.  
<https://doi.org/10.1016/j.bbamcr.2013.11.018>.
- (76) Asher, G.; Bercovich, Z.; Tsvetkov, P.; Shaul, Y.; Kahana, C. 20S Proteasomal Degradation of Ornithine Decarboxylase Is Regulated by NQO1. *Molecular Cell* **2005**, *17* (5), 645–655. <https://doi.org/10.1016/j.molcel.2005.01.020>.
- (77) Tsvetkov, P.; Reuven, N.; Shaul, Y. The Nanny Model for IDPs. *Nature Chemical Biology* **2009**, *5*, 778–781. <https://doi.org/10.1038/nchembio.233>.
- (78) Liu, Z.; Huang, Y. Advantages of Proteins Being Disordered. *Protein Science* **2014**, *23* (5), 539–550. <https://doi.org/10.1002/pro.2443>.
- (79) Waxman, L.; Fagan, J. M.; Goldberg, A. L. Demonstration of Two Distinct High Molecular Weight Proteases in Rabbit Reticulocytes, One of Which Degrades Ubiquitin Conjugates. *Journal of Biological Chemistry* **1987**, *262* (6), 2451–2457.
- (80) Ben-Nissan, G.; Sharon, M. Regulating the 20S Proteasome Ubiquitin-Independent Degradation Pathway. *Biomolecules* **2014**, *4* (3), 862–884.  
<https://doi.org/10.3390/biom4030862>.

- (81) Njomen, E.; Osmulski, P. A.; Jones, C. L.; Gaczynska, M.; Tepe, J. J. Small Molecule Modulation of Proteasome Assembly. *Biochemistry* **2018**, *57* (28), 4214–4224. <https://doi.org/10.1021/acs.biochem.8b00579>.
- (82) Baugh, J. M.; Viktorova, E. G.; Pilipenko, E. V. Proteasomes Can Degrade a Significant Proportion of Cellular Proteins Independent of Ubiquitination. *Journal of Molecular Biology* **2009**, *386* (3), 814–827. <https://doi.org/10.1016/j.jmb.2008.12.081>.
- (83) Etlinger, J. D.; Goldberg, A. L. A Soluble ATP-Dependent Proteolytic System Responsible for the Degradation of Abnormal Proteins in Reticulocytes. *Proceedings of the National Academy of Sciences of the United States of America* **1977**, *74* (1), 54–58.
- (84) Ciechanover, A.; Heller, H.; Elias, S.; Haas, A. L.; Hershko, A. ATP-Dependent Conjugation of Reticulocyte Proteins with the Polypeptide Required for Protein Degradation. *Proc. Natl. Acad. Sci. U.S.A.* **1980**, *77* (3), 1365–1368.
- (85) Komander, D.; Rape, M. The Ubiquitin Code. *Annual Reviews of Biochemistry* **2012**, *81* (1), 203–229. <https://doi.org/10.1146/annurev-biochem-060310-170328>.
- (86) Vijay-Kumar, S.; Bugg, C. E.; Cook, W. J. Structure of Ubiquitin Refined at 1.8Å resolution. *Journal of Molecular Biology* **1987**, *194* (3), 531–544. [https://doi.org/10.1016/0022-2836\(87\)90679-6](https://doi.org/10.1016/0022-2836(87)90679-6).
- (87) Saeki, Y. Ubiquitin Recognition by the Proteasome. *Biochemistry* **2017**, *161* (2), 113–124. <https://doi.org/10.1093/jb/mvw091>.
- (88) Song, L.; Luo, Z.-Q. Post-Translational Regulation of Ubiquitin Signaling. *Cell Biology* **2019**, *218* (6), 1776–1786. <https://doi.org/10.1083/jcb.201902074>.
- (89) Wickliffe, K. E.; Williamson, A.; Meyer, H.-J.; Kelly, A.; Rape, M. K11-Linked Ubiquitin Chains as Novel Regulators of Cell Division. *Trends in Cell Biology* **2011**, *21* (11), 656–663. <https://doi.org/10.1016/j.tcb.2011.08.008>.
- (90) Birsa, N.; Norkett, R.; Wauer, T.; Mevissen, T. E. T.; Wu, H.-C.; Foltynie, T.; Bhatia, K.; Hirst, W. D.; Komander, D.; Plun-Favreau, H.; et al. Lysine 27 Ubiquitination of the Mitochondrial Transport Protein Miro Is Dependent on Serine 65 of the Parkin Ubiquitin Ligase. *Journal of Biological Chemistry* **2014**, *289* (21), 14569–14582. <https://doi.org/10.1074/jbc.M114.563031>.
- (91) Yuan, W.-C.; Lee, Y.-R.; Lin, S.-Y.; Chang, L.-Y.; Tan, Y. P.; Hung, C.-C.; Kuo, J.-C.; Liu, C.-H.; Lin, M.-Y.; Xu, M.; et al. K33-Linked Polyubiquitination of Coronin 7 by Cul3-KLHL20 Ubiquitin E3 Ligase Regulates Protein Trafficking. *Molecular Cell* **2014**, *54* (4), 586–600. <https://doi.org/10.1016/j.molcel.2014.03.035>.
- (92) Kraft, C.; Peter, M.; Hofmann, K. Selective Autophagy: Ubiquitin-Mediated Recognition and Beyond. *Nat Cell Biol* **2010**, *12* (9), 836–841. <https://doi.org/10.1038/ncb0910-836>.



- (93) Hershko, A.; Ciechanover, A. The Ubiquitin System. *Annual Review of Biochemistry* **1998**, *67* (1), 425–479. <https://doi.org/10.1146/annurev.biochem.67.1.425>.
- (94) Pickart, C. M. Mechanisms Underlying Ubiquitination. *Annual Review of Biochemistry* **2001**, *70* (1), 503–533. <https://doi.org/10.1146/annurev.biochem.70.1.503>.
- (95) Weissman, A. M. Ubiquitin and Proteasomes: Themes and Variations on Ubiquitylation. *Nature Reviews Molecular Cell Biology* **2001**, *2* (3), 169–178. <https://doi.org/10.1038/35056563>.
- (96) Pickering, Andrew. M.; Davies, Kelvin. J. A. Degradation of Damaged Proteins - The Main Function of the 20S Proteasome. *Progress in Molecular Biology and Translational Science* **2012**, *109*, 227–248. <https://doi.org/10.1016/B978-0-12-397863-9.00006-7>.
- (97) Erales, J.; Coffino, P. Ubiquitin-Independent Proteasomal Degradation. *Biochimica et Biophysica Acta* **2014**, *1843* (1). <https://doi.org/10.1016/j.bbamcr.2013.05.008>.
- (98) Tanaka, K.; Yoshimura, T.; Ichihara, A. Role of Substrate in Reversible Activation of Proteasomes (Multi-Protease Complexes) by Sodium Dodecyl Sulfate. *Journal of Biochemistry* **1989**, *106* (3), 495–500. <https://doi.org/10.1093/oxfordjournals.jbchem.a122880>.
- (99) Geng, F.; Wenzel, S.; Tansey, W. P. Ubiquitin and Proteasomes in Transcription. *Annual Review of Biochemistry* **2012**, *81*, 177–201. <https://doi.org/10.1146/annurev-biochem-052110-120012>.
- (100) Tsvetkov, P.; Adler, J.; Myers, N.; Biran, A.; Reuven, N.; Shaul, Y. Oncogenic Addiction to High 26S Proteasome Level. *Cell Death & Disease* **2018**, *9* (7), 773. <https://doi.org/10.1038/s41419-018-0806-4>.
- (101) Anderson, K. C.; Carrasco, R. D. Pathogenesis of Myeloma. *Annual Review of Pathology* **2011**, *6*, 249–274. <https://doi.org/10.1146/annurev-pathol-011110-130249>.
- (102) Chiang, M. Y.; Stadtmauer, E. A. NF-KappaB, IL-6 and Myeloma Cell Growth: Making the Connection. *Cancer Biology and Therapy* **2004**, *3* (10), 1018–1020.
- (103) Anderson, K. C.; Alsina, M.; Bensinger, W.; Biermann, J. S.; Chanan-Khan, A.; Cohen, A. D.; Devine, S.; Djulbegovic, B.; Faber, E. A.; Gasparetto, C.; et al. Multiple Myeloma. *Journal of the National Comprehensive Cancer Network* **2011**, *9* (10), 1146–1183.
- (104) Suraweera, A.; Münch, C.; Hanssum, A.; Bertolotti, A. Failure of Amino Acid Homeostasis Causes Cell Death Following Proteasome Inhibition. *Molecular Cell* **2012**, *48* (2), 242–253. <https://doi.org/10.1016/j.molcel.2012.08.003>.
- (105) Kumar, D.; Sharma, N.; Giri, R. Therapeutic Interventions of Cancers Using Intrinsically Disordered Proteins as Drug Targets: C-Myc as Model System. *Cancer Informatics* **2017**, *16*, 1176935117699408. <https://doi.org/10.1177/1176935117699408>.

- (106) Holien, T.; Våtsveen, T. K.; Hella, H.; Waage, A.; Sundan, A. Addiction to C-MYC in Multiple Myeloma. *Blood* **2012**, *120* (12), 2450–2453. <https://doi.org/10.1182/blood-2011-08-371567>.
- (107) Shaffer, A. L.; Emre, N. C. T.; Lamy, L.; Ngo, V. N.; Wright, G. N.; Xiao, W.; Powell, J. G.; Dave, S.; Yu, X.; Zhao, H.; et al. IRF4 Addiction in Multiple Myeloma. *Nature* **2008**, *454*, 226–231. <https://doi.org/10.1038/nature07064>.
- (108) Holien, T.; Misund, K.; Olsen, O. E.; Baranowska, K. A.; Buene, G.; Børset, M.; Waage, A.; Sundan, A. MYC Amplifications in Myeloma Cell Lines: Correlation with MYC-Inhibitor Efficacy. *Oncotarget* **2015**, *6* (26), 22698–22705.
- (109) Miller, D. M.; Thomas, S. D.; Islam, A.; Muench, D.; Sedoris, K. C-Myc and Cancer Metabolism. *Clinical Cancer Research* **2012**, *18* (20), 5546–5553. <https://doi.org/10.1158/1078-0432.CCR-12-0977>.
- (110) Allen, A.; Gill, K.; Hoehn, D.; Sulis, M.; Bhagat, G.; Alobeid, B. C-Myc Protein Expression in B-Cell Acute Lymphoblastic Leukemia, Prognostic Significance? *Leukemia Research* **2014**, *38* (9), 1061–1066. <https://doi.org/10.1016/j.leukres.2014.06.022>.
- (111) Liu, Z.-G.; Jiang, G.; Tang, J.; Wang, H.; Feng, G.; Chen, F.; Tu, Z.; Liu, G.; Zhao, Y.; Peng, M.-J.; et al. C-Fos over-Expression Promotes Radioresistance and Predicts Poor Prognosis in Malignant Glioma. *Oncotarget* **2016**, *7* (40), 65946–65956. <https://doi.org/10.18632/oncotarget.11779>.
- (112) Silvestre, D. C.; Gil, G. A.; Tomasini, N.; Bussolino, D. F.; Caputto, B. L. Growth of Peripheral and Central Nervous System Tumors Is Supported by Cytoplasmic C-Fos in Humans and Mice. *PLoS ONE* **2010**, *5* (3), e9544. <https://doi.org/10.1371/journal.pone.0009544>.
- (113) Urbańska, K.; Sokołowska, J.; Szmids, M.; Sysa, P. Glioblastoma Multiforme – an Overview. *Contemporary Oncology (Pozn)* **2014**, *18* (5), 307–312. <https://doi.org/10.5114/wo.2014.40559>.
- (114) Ray-Chaudhury, A. Pathology of Glioblastoma Multiforme. In *Glioblastoma: Molecular Mechanisms of Pathogenesis and Current Therapeutic Strategies*; Ray, S. K., Ed.; Springer New York: New York, NY, 2010; pp 77–84. [https://doi.org/10.1007/978-1-4419-0410-2\\_3](https://doi.org/10.1007/978-1-4419-0410-2_3).
- (115) Holland, E. C. Glioblastoma Multiforme: The Terminator. *Proceedings of the National Academy of Sciences of the United States of America* **2000**, *97* (12), 6242–6244.
- (116) Mangiola, A.; Maira, G.; De Bonis, P.; Porso, M.; Pettorini, B.; Sabatino, G.; Anile, C. Glioblastoma Multiforme in the Elderly: A Therapeutic Challenge. *Journal of Neurooncology* **2006**, *76* (2), 159–163. <https://doi.org/10.1007/s11060-005-4711-1>.

- (117) Shergalis, A.; Bankhead, A.; Luesakul, U.; Muangsin, N.; Neamati, N. Current Challenges and Opportunities in Treating Glioblastoma. *Pharmacological Reviews* **2018**, 70 (3), 412–445. <https://doi.org/10.1124/pr.117.014944>.
- (118) Caputto, B. L.; Cardozo Gizzi, A. M.; Gil, G. A. C-Fos: An AP-1 Transcription Factor with an Additional Cytoplasmic, Non-Genomic Lipid Synthesis Activation Capacity. *Biochimica et Biophysica Acta (BBA) - Molecular and Cell Biology of Lipids* **2014**, 1841 (9), 1241–1246. <https://doi.org/10.1016/j.bbalip.2014.05.007>.
- (119) Grune, T. Oxidative Stress, Aging and the Proteasomal System. *Biogerontology* **2000**, 1 (1), 31–40.
- (120) Jung, T.; Grune, T. The Proteasome and Its Role in the Degradation of Oxidized Proteins. *IUBMB Life* **2008**, 60 (11), 743–752. <https://doi.org/10.1002/iub.114>.
- (121) Grune, T.; Reinheckel, T.; Davies, K. J. Degradation of Oxidized Proteins in Mammalian Cells. *The FASEB Journal* **1997**, 11 (7), 526–534. <https://doi.org/10.1096/fasebj.11.7.9212076>.
- (122) Sitte, N.; Merker, K.; Grune, T. Proteasome-Dependent Degradation of Oxidized Proteins in MRC-5 Fibroblasts. *FEBS Letters* **1998**, 440 (3), 399–402. [https://doi.org/10.1016/S0014-5793\(98\)01495-1](https://doi.org/10.1016/S0014-5793(98)01495-1).
- (123) Breusing, N.; Arndt, J.; Voss, P.; Bresgen, N.; Wiswedel, I.; Gardemann, A.; Siems, W.; Grune, T. Inverse Correlation of Protein Oxidation and Proteasome Activity in Liver and Lung. *Mechanisms of Ageing and Development* **2009**, 130 (11–12), 748–753. <https://doi.org/10.1016/j.mad.2009.09.004>.
- (124) Reinheckel, T.; Sitte, N.; Ullrich, O.; Kuckelkorn, U.; Davies, K. J.; Grune, T. Comparative Resistance of the 20S and 26S Proteasome to Oxidative Stress. *Biochemistry Journal* **1998**, 335 (Pt 3), 637–642.
- (125) Wang, X.; Yen, J.; Kaiser, P.; Huang, L. Regulation of the 26S Proteasome Complex During Oxidative Stress. *Science Signal* **2010**, 3 (151), ra88. <https://doi.org/10.1126/scisignal.2001232>.
- (126) Saez, I.; Vilchez, D. The Mechanistic Links Between Proteasome Activity, Aging and Age-Related Diseases. *Current Genomics* **2014**, 15 (1), 38–51. <https://doi.org/10.2174/138920291501140306113344>.
- (127) Lam, Y. A.; Pickart, C. M.; Alban, A.; Landon, M.; Jamieson, C.; Ramage, R.; Mayer, R. J.; Layfield, R. Inhibition of the Ubiquitin-Proteasome System in Alzheimer's Disease. *Proceedings of the National Academy of Sciences of the United States of America* **2000**, 97 (18), 9902–9906. <https://doi.org/10.1073/pnas.170173897>.
- (128) Ross, C. A.; Poirier, M. A. Protein Aggregation and Neurodegenerative Disease. *Published online: 01 July 2004; | doi:10.1038/nm1066* **2004**, 10, S10–S17. <https://doi.org/10.1038/nm1066>.

- (129) Soto, C. Unfolding the Role of Protein Misfolding in Neurodegenerative Diseases. *Nat Rev Neurosci* **2003**, 4 (1), 49–60. <https://doi.org/10.1038/nrn1007>.
- (130) Keller, J. N.; Hanni, K. B.; Markesbery, W. R. Impaired Proteasome Function in Alzheimer's Disease. *Journal of Neurochemistry* **2000**, 75 (1), 436–439. <https://doi.org/10.1046/j.1471-4159.2000.0750436.x>.
- (131) Tofaris, G. K.; Layfield, R.; Spillantini, M. G. Alpha-Synuclein Metabolism and Aggregation Is Linked to Ubiquitin-Independent Degradation by the Proteasome. *FEBS Letters* **2001**, 509 (1), 22–26.
- (132) Bedford, L.; Hay, D.; Devoy, A.; Paine, S.; Powe, D. G.; Seth, R.; Gray, T.; Topham, I.; Fone, K.; Rezvani, N.; et al. Depletion of 26S Proteasomes in Mouse Brain Neurons Causes Neurodegeneration and Lewy-like Inclusions Resembling Human Pale Bodies. *Journal of Neuroscience* **2008**, 28 (33), 8189–8198. <https://doi.org/10.1523/JNEUROSCI.2218-08.2008>.
- (133) Liu, Y.; Hettinger, C. L.; Zhang, D.; Rezvani, K.; Wang, X.; Wang, H. The Proteasome Function Reporter GFPu Accumulates in Young Brains of the APP<sup>swe</sup>/PS1<sup>dE9</sup> Alzheimer's Disease Mouse Model. *Cellular and Molecular Neurobiology* **2014**, 34 (3), 315–322. <https://doi.org/10.1007/s10571-013-0022-9>.
- (134) Zabel, C.; Nguyen, H. P.; Hin, S. C.; Hartl, D.; Mao, L.; Klose, J. Proteasome and Oxidative Phosphorylation Changes May Explain Why Aging Is a Risk Factor for Neurodegenerative Disorders. *Journal of Proteomics* **2010**, 73 (11), 2230–2238. <https://doi.org/10.1016/j.jprot.2010.08.008>.
- (135) Vigouroux, S.; Briand, M.; Briand, Y. Linkage between the Proteasome Pathway and Neurodegenerative Diseases and Aging. *Molecular Neurobiology*. **2004**, 30 (2), 201–221. <https://doi.org/10.1385/MN:30:2:201>.
- (136) Tomaru, U.; Takahashi, S.; Ishizu, A.; Miyatake, Y.; Gohda, A.; Suzuki, S.; Ono, A.; Ohara, J.; Baba, T.; Murata, S.; et al. Decreased Proteasomal Activity Causes Age-Related Phenotypes and Promotes the Development of Metabolic Abnormalities. *American Journal of Pathology* **2012**, 180 (3), 963–972. <https://doi.org/10.1016/j.ajpath.2011.11.012>.
- (137) Opoku-Nsiah, K. A.; Gestwicki, J. E. Aim for the Core: Suitability of the Ubiquitin-Independent 20S Proteasome as a Drug Target in Neurodegeneration. *Translational Research* **2018**, 198, 48–57. <https://doi.org/10.1016/j.trsl.2018.05.002>.
- (138) Coleman, R. A.; Trader, D. J. All About the Core: A Therapeutic Strategy to Prevent Protein Accumulation with Proteasome Core Particle Stimulators. *ACS Pharmacology and Translational Science* **2018**, 1 (2), 140–142. <https://doi.org/10.1021/acsptsci.8b00042>.
- (139) Perry, G.; Friedman, R.; Shaw, G.; Chau, V. Ubiquitin Is Detected in Neurofibrillary Tangles and Senile Plaque Neurites of Alzheimer Disease Brains. *Proceedings of the*

*National Academy of Sciences of the United States of America* **1987**, 84 (9), 3033–3036.  
<https://doi.org/10.1073/pnas.84.9.3033>.

- (140) Gillette, T. G.; Kumar, B.; Thompson, D.; Slaughter, C. A.; DeMartino, G. N. Differential Roles of the COOH Termini of AAA Subunits of PA700 (19 S Regulator) in Asymmetric Assembly and Activation of the 26 S Proteasome. *Journal of Biological Chemistry* **2008**, 283 (46), 31813–31822. <https://doi.org/10.1074/jbc.M805935200>.
- (141) Gaczynska, M.; Osmulski, P. A.; Gao, Y.; Post, M. J.; Simons, M. Proline- and Arginine-Rich Peptides Constitute a Novel Class of Allosteric Inhibitors of Proteasome Activity. *Biochemistry* **2003**, 42 (29), 8663–8670. <https://doi.org/10.1021/bi034784f>.
- (142) Anbanandam, A.; Albarado, D. C.; Tirziu, D. C.; Simons, M.; Veeraraghavan, S. Molecular Basis for Proline- and Arginine-Rich Peptide Inhibition of Proteasome. *Journal of Molecular Biology* **2008**, 384 (1), 219–227. <https://doi.org/10.1016/j.jmb.2008.09.021>.
- (143) Giżyńska, M.; Witkowska, J.; Karpowicz, P.; Rostankowski, R.; Chocron, E. S.; Pickering, A. M.; Osmulski, P.; Gaczynska, M.; Jankowska, E. Proline- and Arginine-Rich Peptides as Flexible Allosteric Modulators of Human Proteasome Activity. *Journal of Medicinal Chemistry* **2018**. <https://doi.org/10.1021/acs.jmedchem.8b01025>.
- (144) Dal Vechio, F. H.; Cerqueira, F.; Augusto, O.; Lopes, R.; Demasi, M. Peptides That Activate the 20S Proteasome by Gate Opening Increased Oxidized Protein Removal and Reduced Protein Aggregation. *Free Radical Biology and Medicine*. **2014**, 67, 304–313. <https://doi.org/10.1016/j.freeradbiomed.2013.11.017>.
- (145) Kisselev, A. F.; Kaganovich, D.; Goldberg, A. L. Binding of Hydrophobic Peptides to Several Non-Catalytic Sites Promotes Peptide Hydrolysis by All Active Sites of 20 S Proteasomes. Evidence for Peptide-Induced Channel Opening in the Alpha-Rings. *Journal of Biological Chemistry* **2002**, 277 (25), 22260–22270. <https://doi.org/10.1074/jbc.M112360200>.
- (146) Micale, N.; Scarbaci, K.; Troiano, V.; Ettari, R.; Grasso, S.; Zappalà, M. Peptide-Based Proteasome Inhibitors in Anticancer Drug Design. *Medicinal Research Reviews* **2014**, 34 (5), 1001–1069. <https://doi.org/10.1002/med.21312>.
- (147) Otvos, L.; Wade, J. D. Current Challenges in Peptide-Based Drug Discovery. *Frontiers in Chemistry* **2014**, 2. <https://doi.org/10.3389/fchem.2014.00062>.
- (148) Tanaka, K.; Yoshimura, T.; Kumatori, A.; Ichihara, A.; Ikai, A.; Nishigai, M.; Kameyama, K.; Takagi, T. Proteasomes (Multi-Protease Complexes) as 20 S Ring-Shaped Particles in a Variety of Eukaryotic Cells. *Journal of Biological Chemistry* **1988**, 263 (31), 16209–16217.
- (149) Mena, I. R. de; Mahillo, E.; Arribas, J.; Castaño, J. G. Kinetic Mechanism of Activation by Cardiolipin (Diphosphatidylglycerol) of the Rat Liver Multicatalytic Proteinase. *Biochemical Journal* **1993**, 296 (1), 93–97. <https://doi.org/10.1042/bj2960093>.

- (150) Watanabe, N.; Yamada, S. Activation of 20S Proteasomes from Spinach Leaves by Fatty Acids. *Plant Cell Physiology* **1996**, 37 (2), 147–151.
- (151) Katsiki, M.; Chondrogianni, N.; Chinou, I.; Rivett, A. J.; Gonos, E. S. The Olive Constituent Oleuropein Exhibits Proteasome Stimulatory Properties In Vitro and Confers Life Span Extension of Human Embryonic Fibroblasts. *Rejuvenation Research* **2007**, 10 (2), 157–172. <https://doi.org/10.1089/rej.2006.0513>.
- (152) Huang, L.; Ho, P.; Chen, C.-H. Activation and Inhibition of Proteasomes by Betulinic Acid and Its Derivatives. *FEBS Letters* **2007**, 581 (25), 4955–4959. <https://doi.org/10.1016/j.febslet.2007.09.031>.
- (153) Jones, C. L.; Njomen, E.; Sjögren, B.; Dexheimer, T. S.; Tepe, J. J. Small Molecule Enhancement of 20S Proteasome Activity Targets Intrinsically Disordered Proteins. *ACS Chem. Biol.* **2017**, 12 (9), 2240–2247. <https://doi.org/10.1021/acscchembio.7b00489>.
- (154) Medina, D. X.; Caccamo, A.; Oddo, S. Methylene Blue Reduces A $\beta$  Levels and Rescues Early Cognitive Deficit by Increasing Proteasome Activity. *Brain Pathology* **2011**, 21 (2), 140–149. <https://doi.org/10.1111/j.1750-3639.2010.00430.x>.
- (155) Trader, D. J.; Simanski, S.; Dickson, P.; Kodadek, T. Establishment of a Suite of Assays That Support the Discovery of Proteasome Stimulators. *Biochimica et Biophysica Acta General Subjects* **2017**, 1861 (4), 892–899. <https://doi.org/10.1016/j.bbagen.2017.01.003>.
- (156) Coleman, R. A.; Trader, D. J. Development and Application of a Sensitive Peptide Reporter to Discover 20S Proteasome Stimulators. *ACS Combinatorial Science* **2018**, 20 (5), 269–276. <https://doi.org/10.1021/acscombsci.7b00193>.
- (157) Guo, X.; Huang, X.; Chen, M. J. Reversible Phosphorylation of the 26S Proteasome. *Protein Cell* **2017**, 8 (4), 255–272. <https://doi.org/10.1007/s13238-017-0382-x>.
- (158) Lee, S.-H.; Park, Y.; Yoon, S. K.; Yoon, J.-B. Osmotic Stress Inhibits Proteasome by P38 MAPK-Dependent Phosphorylation. *Journal of Biological Chemistry* **2010**, 285 (53), 41280–41289. <https://doi.org/10.1074/jbc.M110.182188>.
- (159) Zhang, F.; Hu, Y.; Huang, P.; Toleman, C. A.; Paterson, A. J.; Kudlow, J. E. Proteasome Function Is Regulated by Cyclic AMP-Dependent Protein Kinase through Phosphorylation of Rpt6. *Journal of Biological Chemistry* **2007**, 282 (31), 22460–22471. <https://doi.org/10.1074/jbc.M702439200>.
- (160) Asai, M.; Tsukamoto, O.; Minamino, T.; Asanuma, H.; Fujita, M.; Asano, Y.; Takahama, H.; Sasaki, H.; Higo, S.; Asakura, M.; et al. PKA Rapidly Enhances Proteasome Assembly and Activity in in Vivo Canine Hearts. *Journal of Molecular and Cellular Cardiology*. **2009**, 46 (4), 452–462. <https://doi.org/10.1016/j.yjmcc.2008.11.001>.
- (161) Park, S.-J.; Ahmad, F.; Philp, A.; Baar, K.; Williams, T.; Luo, H.; Ke, H.; Rehmann, H.; Taussig, R.; Brown, A. L.; et al. Resveratrol Ameliorates Aging-Related Metabolic

- Phenotypes by Inhibiting CAMP Phosphodiesterases. *Cell* **2012**, *148* (3), 421–433. <https://doi.org/10.1016/j.cell.2012.01.017>.
- (162) Myeku, N.; Clelland, C. L.; Emrani, S.; Kukushkin, N. V.; Yu, W. H.; Goldberg, A. L.; Duff, K. E. Tau-Driven 26S Proteasome Impairment and Cognitive Dysfunction Can Be Prevented Early in Disease by Activating CAMP-PKA Signaling. *Nature Medicine* **2016**, *22* (1), 46–53. <https://doi.org/10.1038/nm.4011>.
  - (163) Lokireddy, S.; Kukushkin, N. V.; Goldberg, A. L. CAMP-Induced Phosphorylation of 26S Proteasomes on Rpn6/PSMD11 Enhances Their Activity and the Degradation of Misfolded Proteins. *Proceedings of the National Academy of Sciences of the United States of America* **2015**, *112* (52), E7176–E7185. <https://doi.org/10.1073/pnas.1522332112>.
  - (164) Koulich, E.; Li, X.; DeMartino, G. N. Relative Structural and Functional Roles of Multiple Deubiquitylating Proteins Associated with Mammalian 26S Proteasome. *Molecular Biology of the Cell* **2008**, *19* (3), 1072–1082. <https://doi.org/10.1091/mbc.e07-10-1040>.
  - (165) Lee, B.-H.; Lee, M. J.; Park, S.; Oh, D.-C.; Elsasser, S.; Chen, P.-C.; Gartner, C.; Dimova, N.; Hanna, J.; Gygi, S. P.; et al. Enhancement of Proteasome Activity by a Small-Molecule Inhibitor of USP14. *Nature* **2010**, *467* (7312), 179–184. <https://doi.org/10.1038/nature09299>.
  - (166) Wang, X.; Mazurkiewicz, M.; Hillert, E.-K.; Olofsson, M. H.; Pierrou, S.; Hillertz, P.; Gullbo, J.; Selvaraju, K.; Paulus, A.; Akhtar, S.; et al. The Proteasome Deubiquitinase Inhibitor VLX1570 Shows Selectivity for Ubiquitin-Specific Protease-14 and Induces Apoptosis of Multiple Myeloma Cells. *Scientific Reports* **2016**, *6*, 26979. <https://doi.org/10.1038/srep26979>.
  - (167) Tian, Z.; D’Arcy, P.; Wang, X.; Ray, A.; Tai, Y.-T.; Hu, Y.; Carrasco, R. D.; Richardson, P.; Linder, S.; Chauhan, D.; et al. A Novel Small Molecule Inhibitor of Deubiquitylating Enzyme USP14 and UCHL5 Induces Apoptosis in Multiple Myeloma and Overcomes Bortezomib Resistance. *Blood* **2014**, *123* (5), 706–716. <https://doi.org/10.1182/blood-2013-05-500033>.
  - (168) D’Arcy, P.; Brnjic, S.; Olofsson, M. H.; Fryknäs, M.; Lindsten, K.; De Cesare, M.; Perego, P.; Sadeghi, B.; Hassan, M.; Larsson, R.; et al. Inhibition of Proteasome Deubiquitinating Activity as a New Cancer Therapy. *Nature Medicine* **2011**, *17* (12), 1636–1640. <https://doi.org/10.1038/nm.2536>.
  - (169) Gaczynska, M.; Rock, K. L.; Spies, T.; Goldberg, A. L. Peptidase Activities of Proteasomes Are Differentially Regulated by the Major Histocompatibility Complex-Encoded Genes for LMP2 and LMP7. *Proceedings of the National Academy of Sciences of the United States of America* **1994**, *91* (20), 9213–9217. <https://doi.org/10.1073/pnas.91.20.9213>.

- (170) Gaczynska, M.; Goldberg, A. L.; Tanaka, K.; Hendil, K. B.; Rock, K. L. Proteasome Subunits X and Y Alter Peptidase Activities in Opposite Ways to the Interferon- $\gamma$ -Induced Subunits LMP2 and LMP7. *Journal of Biological Chemistry* **1996**, 271 (29), 17275–17280. <https://doi.org/10.1074/jbc.271.29.17275>.
- (171) Chondrogianni, N.; Tzavelas, C.; Pemberton, A. J.; Nezis, I. P.; Rivett, A. J.; Gonos, E. S. Overexpression of Proteasome B5 Assembled Subunit Increases the Amount of Proteasome and Confers Ameliorated Response to Oxidative Stress and Higher Survival Rates. *Journal of Biological Chemistry* **2005**, 280 (12), 11840–11850. <https://doi.org/10.1074/jbc.M413007200>.
- (172) Liu, Y.; Liu, X.; Zhang, T.; Luna, C.; Liton, P. B.; Gonzalez, P. Cytoprotective Effects of Proteasome B5 Subunit Overexpression in Lens Epithelial Cells. *Molecular Vision* **2007**, 13, 31–38.
- (173) Lu, L.; Song, H.-F.; Wei, J.-L.; Liu, X.-Q.; Song, W.-H.; Yan, B.-Y.; Yang, G.-J.; Li, A.; Yang, W.-L. Ameliorating Replicative Senescence of Human Bone Marrow Stromal Cells by PSMB5 Overexpression. *Biochemical and Biophysical Research Communications* **2014**, 443 (4), 1182–1188. <https://doi.org/10.1016/j.bbrc.2013.12.113>.
- (174) Moi, P.; Chan, K.; Asunis, I.; Cao, A.; Kan, Y. W. Isolation of NF-E2-Related Factor 2 (Nrf2), a NF-E2-like Basic Leucine Zipper Transcriptional Activator That Binds to the Tandem NF-E2/AP1 Repeat of the Beta-Globin Locus Control Region. *Proceedings of the National Academy of Sciences of the United States of America* **1994**, 91 (21), 9926–9930.
- (175) Nguyen, T.; Yang, C. S.; Pickett, C. B. The Pathways and Molecular Mechanisms Regulating Nrf2 Activation in Response to Chemical Stress. *Free Radical Biology and Medicine* **2004**, 37 (4), 433–441. <https://doi.org/10.1016/j.freeradbiomed.2004.04.033>.
- (176) Kwak, M.-K.; Wakabayashi, N.; Greenlaw, J. L.; Yamamoto, M.; Kensler, T. W. Antioxidants Enhance Mammalian Proteasome Expression through the Keap1-Nrf2 Signaling Pathway. *Molecular and Cellular Biology* **2003**, 23 (23), 8786–8794. <https://doi.org/10.1128/MCB.23.23.8786-8794.2003>.
- (177) Cui, Y.; Ma, S.; Zhang, C.; Li, D.; Yang, B.; Lv, P.; Xing, Q.; Huang, T.; Yang, G. L.; Cao, W.; et al. Pharmacological Activation of the Nrf2 Pathway by 3H-1, 2-Dithiole-3-Thione Is Neuroprotective in a Mouse Model of Alzheimer Disease. *Behavioral. Brain Research* **2018**, 336, 219–226. <https://doi.org/10.1016/j.bbr.2017.09.011>.
- (178) Kapeta, S.; Chondrogianni, N.; Gonos, E. S. Nuclear Erythroid Factor 2-Mediated Proteasome Activation Delays Senescence in Human Fibroblasts. *Journal of Biological Chemistry* **2010**, 285 (11), 8171–8184. <https://doi.org/10.1074/jbc.M109.031575>.
- (179) Papaevgeniou, N.; Sakellari, M.; Jha, S.; Tavernarakis, N.; Holmberg, C. I.; Gonos, E. S.; Chondrogianni, N. 18 $\alpha$ -Glycyrrhetic Acid Proteasome Activator Decelerates Aging and Alzheimer's Disease Progression in Caenorhabditis Elegans and Neuronal Cultures.



*Antioxidants and Redox Signaling* **2016**, 25 (16), 855–869.  
<https://doi.org/10.1089/ars.2015.6494>.

- (180) Jang, J.; Wang, Y.; Kim, H.-S.; Lalli, M. A.; Kosik, K. S. Nrf2, a Regulator of the Proteasome, Controls Self-Renewal and Pluripotency in Human Embryonic Stem Cells. *Stem Cells* **2014**, 32 (10), 2616–2625. <https://doi.org/10.1002/stem.1764>.
- (181) Kwak, M.-K.; Cho, J.-M.; Huang, B.; Shin, S.; Kensler, T. W. Role of Increased Expression of the Proteasome in the Protective Effects of Sulforaphane against Hydrogen Peroxide-Mediated Cytotoxicity in Murine Neuroblastoma Cells. *Free Radical Biology and Medicine* **2007**, 43 (5), 809–817.  
<https://doi.org/10.1016/j.freeradbiomed.2007.05.029>.
- (182) Förster, A.; Whitby, F. G.; Hill, C. P. The Pore of Activated 20S Proteasomes Has an Ordered 7-fold Symmetric Conformation. *European Molecular Biology Organization Journal* **2003**, 22 (17), 4356–4364. <https://doi.org/10.1093/emboj/cdg436>.
- (183) Vilchez, D.; Boyer, L.; Morante, I.; Lutz, M.; Merkwirth, C.; Joyce, D.; Spencer, B.; Page, L.; Masliah, E.; Berggren, W. T.; et al. Increased Proteasome Activity in Human Embryonic Stem Cells Is Regulated by PSMD11. *Nature* **2012**, 489 (7415), 304–308.  
<https://doi.org/10.1038/nature11468>.
- (184) Li, J.; Horak, K. M.; Su, H.; Sanbe, A.; Robbins, J.; Wang, X. Enhancement of Proteasomal Function Protects against Cardiac Proteinopathy and Ischemia/Reperfusion Injury in Mice. *Journal of Clinical Investigation* **2011**, 121 (9), 3689–3700.  
<https://doi.org/10.1172/JCI45709>.
- (185) Choi, W. H.; Poot, S. A. H. de; Lee, J. H.; Kim, J. H.; Han, D. H.; Kim, Y. K.; Finley, D.; Lee, M. J. Open-Gate Mutants of the Mammalian Proteasome Show Enhanced Ubiquitin-Conjugate Degradation. *Nature Communications* **2016**, 7, 10963.  
<https://doi.org/10.1038/ncomms10963>.
- (186) Benmohamed, R.; Arvanites, A. C.; Kim, J.; Ferrante, R. J.; Silverman, R. B.; Morimoto, R. I.; Kirsch, D. R. Identification of Compounds Protective against G93A-SOD1 Toxicity for the Treatment of Amyotrophic Lateral Sclerosis. *Amyotrophic Lateral Sclerosis* **2011**, 12 (2), 87–96. <https://doi.org/10.3109/17482968.2010.522586>.
- (187) Chen, T.; Benmohamed, R.; Kim, J.; Smith, K.; Amante, D.; Morimoto, R. I.; Kirsch, D. R.; Ferrante, R. J.; Silverman, R. B. ADME-Guided Design and Synthesis of Aryloxanyl Pyrazolone Derivatives To Block Mutant Superoxide Dismutase 1 (SOD1) Cytotoxicity and Protein Aggregation: Potential Application for the Treatment of Amyotrophic Lateral Sclerosis. *Journal of Medicinal Chemistry* **2012**, 55 (1), 515–527.  
<https://doi.org/10.1021/jm2014277>.
- (188) Chen, T.; Benmohamed, R.; Arvanites, A. C.; Ranaivo, H. R.; Morimoto, R. I.; Ferrante, R. J.; Watterson, D. M.; Kirsch, D. R.; Silverman, R. B. Arylsulfanyl Pyrazolones Block Mutant SOD1-G93A Aggregation. Potential Application for the Treatment of

- Amyotrophic Lateral Sclerosis. *Bioorganic and Medicinal Chemistry* **2011**, *19* (1), 613–622. <https://doi.org/10.1016/j.bmc.2010.10.052>.
- (189) Trippier, P. C.; Zhao, K. T.; Fox, S. G.; Schiefer, I. T.; Benmohamed, R.; Moran, J.; Kirsch, D. R.; Morimoto, R. I.; Silverman, R. B. Proteasome Activation Is a Mechanism for Pyrazolone Small Molecules Displaying Therapeutic Potential in Amyotrophic Lateral Sclerosis. *ACS Chem Neuroscience* **2014**, *5* (9), 823–829. <https://doi.org/10.1021/cn500147v>.
- (190) Leestemaker, Y.; de Jong, A.; Witting, K. F.; Penning, R.; Schuurman, K.; Rodenko, B.; Zaal, E. A.; van de Kooij, B.; Laufer, S.; Heck, A. J. R.; et al. Proteasome Activation by Small Molecules. *Cell Chemical Biology* **2017**, *24* (6), 725–736.e7. <https://doi.org/10.1016/j.chembiol.2017.05.010>.
- (191) Chondrogianni, N.; Petropoulos, I.; Franceschi, C.; Friguet, B.; Gonos, E. S. Fibroblast Cultures from Healthy Centenarians Have an Active Proteasome. *Experimental Gerontology* **2000**, *35* (6–7), 721–728.
- (192) Zinc supplementation in the elderly subjects: Effect on oxidized protein degradation and repair systems in peripheral blood lymphocytes - PDF Free Download <https://kundoc.com/pdf-zinc-supplementation-in-the-elderly-subjects-effect-on-oxidized-protein-degradat.html> (accessed Dec 21, 2018).
- (193) Rodriguez, K. A.; Edrey, Y. H.; Osmulski, P.; Gaczynska, M.; Buffenstein, R. Altered Composition of Liver Proteasome Assemblies Contributes to Enhanced Proteasome Activity in the Exceptionally Long-Lived Naked Mole-Rat. *PLoS ONE* **2012**, *7* (5), e35890. <https://doi.org/10.1371/journal.pone.0035890>.
- (194) Rodriguez, K. A.; Osmulski, P. A.; Pierce, A.; Weintraub, S. T.; Gaczynska, M.; Buffenstein, R. A Cytosolic Protein Factor from the Naked Mole-Rat Activates Proteasomes of Other Species and Protects These from Inhibition. *Biochimica et Biophysica Acta* **2014**, *1842* (11), 2060–2072. <https://doi.org/10.1016/j.bbadis.2014.07.005>.
- (195) Kapetanou, M.; Chondrogianni, N.; Petrakis, S.; Koliakos, G.; Gonos, E. S. Proteasome Activation Enhances Stemness and Lifespan of Human Mesenchymal Stem Cells. *Free Radical Biology and Medicine* **2017**, *103*, 226–235. <https://doi.org/10.1016/j.freeradbiomed.2016.12.035>.
- (196) Chondrogianni, N.; Sakellari, M.; Lefaki, M.; Papaevgeniou, N.; Gonos, E. S. Proteasome Activation Delays Aging in Vitro and in Vivo. *Free Radical Biology and Medicine* **2014**, *71*, 303–320. <https://doi.org/10.1016/j.freeradbiomed.2014.03.031>.
- (197) Chondrogianni, N.; Georgila, K.; Kourtis, N.; Tavernarakis, N.; Gonos Efstathios, S. Enhanced Proteasome Degradation Extends *Caenorhabditis Elegans* Lifespan and Alleviates Aggregation-Related Pathologies. *Free Radical Biology and Medicine* **2014**, *75 Suppl 1*, S18. <https://doi.org/10.1016/j.freeradbiomed.2014.10.632>.

- (198) Chondrogianni, N.; Gonos, E. S. Overexpression of HUMP1/POMP Proteasome Accessory Protein Enhances Proteasome-Mediated Antioxidant Defence. *Experimental Gerontology* **2007**, 42 (9), 899–903. <https://doi.org/10.1016/j.exger.2007.01.012>.
- (199) Voutetakis, K.; Delitsikou, V.; Magouritsas, M. G.; Gonos, E. S. Anti-Ageing Properties of Khelma Longevity™: Treatment of Human Fibroblasts Increases Proteasome Levels and Decreases the Levels of Oxidized Proteins. *New Biotechnology* **2017**, 38 (Pt A), 36–39. <https://doi.org/10.1016/j.nbt.2017.03.002>.
- (200) Gonos, E. Proteasome Activation Delays Aging and Protects against Proteotoxicity in Neurodegenerative Disease. *Advances in Experimental Medicine and Biology* **2015**, 821, 7. [https://doi.org/10.1007/978-3-319-08939-3\\_4](https://doi.org/10.1007/978-3-319-08939-3_4).
- (201) Chondrogianni, N.; Voutetakis, K.; Kapetanou, M.; Delitsikou, V.; Papaevgeniou, N.; Sakellari, M.; Lefaki, M.; Filippopoulou, K.; Gonos, E. S. Proteasome Activation: An Innovative Promising Approach for Delaying Aging and Retarding Age-Related Diseases. *Ageing Research Reviews* **2015**, 23, 37–55. <https://doi.org/10.1016/j.arr.2014.12.003>.
- (202) Gonos, E. Proteasome Activation as a Novel Anti-Aging Strategy. *Free Radical Biology and Medicine* **2014**, 75 Suppl 1, S7. <https://doi.org/10.1016/j.freeradbiomed.2014.10.842>.
- (203) Vilchez, D.; Morantte, I.; Liu, Z.; Douglas, P. M.; Merkwirth, C.; Rodrigues, A. P. C.; Manning, G.; Dillin, A. RPN-6 Determines C. Elegans Longevity under Proteotoxic Stress Conditions. *Nature* **2012**, 489 (7415), 263–268. <https://doi.org/10.1038/nature11315>.
- (204) Kruegel, U.; Robison, B.; Dange, T.; Kahlert, G.; Delaney, J. R.; Kotireddy, S.; Tsuchiya, M.; Tsuchiyama, S.; Murakami, C. J.; Schleit, J.; et al. Elevated Proteasome Capacity Extends Replicative Lifespan in Saccharomyces Cerevisiae. *PLoS Genetics*. **2011**, 7 (9), e1002253. <https://doi.org/10.1371/journal.pgen.1002253>.
- (205) Mayor, T.; Sharon, M.; Glickman, M. H. Tuning the Proteasome to Brighten the End of the Journey. *American Journal of Physiology-Cell Physiology* **2016**, 311 (5), C793–C804. <https://doi.org/10.1152/ajpcell.00198.2016>.
- (206) Tsvetkov, P.; Myers, N.; Moscovitz, O.; Sharon, M.; Prilusky, J.; Shaul, Y. Thermo-Resistant Intrinsically Disordered Proteins Are Efficient 20S Proteasome Substrates. *Molecular BioSystems* **2011**, 8 (1), 368–373. <https://doi.org/10.1039/C1MB05283G>.
- (207) Fishbain, S.; Inobe, T.; Israeli, E.; Chavali, S.; Yu, H.; Kago, G.; Babu, M. M.; Matouschek, A. Sequence Composition of Disordered Regions Fine-Tunes Protein Half-Life. *Nature Structural and Molecular Biology* **2015**, 22 (3), 214–221. <https://doi.org/10.1038/nsmb.2958>.
- (208) Rastogi, N.; Mishra, D. P. Therapeutic Targeting of Cancer Cell Cycle Using Proteasome Inhibitors. *Cell Division* **2012**, 7, 26. <https://doi.org/10.1186/1747-1028-7-26>.

- (209) Chen, L.; Brewer, M. D.; Guo, L.; Wang, R.; Jiang, P.; Yang, X. Enhanced Degradation of Misfolded Proteins Promotes Tumorigenesis. *Cell Report* **2017**, *18* (13), 3143–3154. <https://doi.org/10.1016/j.celrep.2017.03.010>.
- (210) Best, S. A.; De Souza, D. P.; Kersbergen, A.; Policheni, A. N.; Dayalan, S.; Tull, D.; Rathi, V.; Gray, D. H.; Ritchie, M. E.; McConville, M. J.; et al. Synergy between the KEAP1/NRF2 and PI3K Pathways Drives Non-Small-Cell Lung Cancer with an Altered Immune Microenvironment. *Cell Metabolism* **2018**, *27* (4), 935-943.e4. <https://doi.org/10.1016/j.cmet.2018.02.006>.
- (211) Solis, L. M.; Behrens, C.; Dong, W.; Suraokar, M.; Ozburn, N. C.; Moran, C. A.; Corvalan, A. H.; Biswal, S.; Swisher, S. G.; Bekele, B. N.; et al. Nrf2 and Keap1 Abnormalities in Non-Small Cell Lung Carcinoma and Association with Clinicopathologic Features. *Clinical Cancer Research* **2010**, *16* (14), 3743–3753. <https://doi.org/10.1158/1078-0432.CCR-09-3352>.
- (212) LIN, Y.; SUI, L.-C.; WU, R.-H.; MA, R.-J.; FU, H.-Y.; XU, J.-J.; QIU, X.-H.; CHEN, L. Nrf2 Inhibition Affects Cell Cycle Progression during Early Mouse Embryo Development. *Journal of Reproductive Development* **2018**, *64* (1), 49–55. <https://doi.org/10.1262/jrd.2017-042>.
- (213) Gavet, O.; Pines, J. Activation of Cyclin B1–Cdk1 Synchronizes Events in the Nucleus and the Cytoplasm at Mitosis. *The Journal of Cell Biology* **2010**, *189* (2), 247–259. <https://doi.org/10.1083/jcb.200909144>.
- (214) Tsvetkov, P.; Shaul, Y. Determination of IUP Based on Susceptibility for Degradation by Default. *Methods in Molecular Biology* **2012**, *895*, 3–18. [https://doi.org/10.1007/978-1-61779-927-3\\_1](https://doi.org/10.1007/978-1-61779-927-3_1).
- (215) Tsvetkov, P.; Asher, G.; Paz, A.; Reuven, N.; Sussman, J. L.; Silman, I.; Shaul, Y. Operational Definition of Intrinsically Unstructured Protein Sequences Based on Susceptibility to the 20S Proteasome. *Proteins* **2008**, *70* (4), 1357–1366. <https://doi.org/10.1002/prot.21614>.
- (216) Njomen, E.; Tepe, J. J. Proteasome Activation as a New Therapeutic Approach To Target Proteotoxic Disorders. *Journal of Medicinal Chemistry* **2019**. <https://doi.org/10.1021/acs.jmedchem.9b00101>.
- (217) Mitsiades, N.; Mitsiades, C. S.; Poulaki, V.; Chauhan, D.; Fanourakis, G.; Gu, X.; Bailey, C.; Joseph, M.; Libermann, T. A.; Treon, S. P.; et al. Molecular Sequelae of Proteasome Inhibition in Human Multiple Myeloma Cells. *Proceedings of the National Academy of Sciences of the United States of America* **2002**, *99* (22), 14374–14379. <https://doi.org/10.1073/pnas.202445099>.
- (218) Boland, B.; Yu, W. H.; Corti, O.; Mollereau, B.; Henriques, A.; Bezard, E.; Pastores, G. M.; Rubinsztein, D. C.; Nixon, R. A.; Duchen, M. R.; et al. Promoting the Clearance of Neurotoxic Proteins in Neurodegenerative Disorders of Ageing. *Nature Reviews Drug Discovery* **2018**, *17* (9), 660–688. <https://doi.org/10.1038/nrd.2018.109>.

- (219) Chondrogianni, N.; Voutetakis, K.; Kapetanou, M.; Delitsikou, V.; Papaevgeniou, N.; Sakellari, M.; Lefaki, M.; Filippopoulou, K.; Gonos, E. S. Proteasome Activation: An Innovative Promising Approach for Delaying Aging and Retarding Age-Related Diseases. *Ageing Research Reviews* **2015**, *23* (Pt A), 37–55. <https://doi.org/10.1016/j.arr.2014.12.003>.
- (220) Kisselev, A. F.; van der Linden, W. A.; Overkleeft, H. S. Proteasome Inhibitors: An Expanding Army Attacking a Unique Target. *Chemical Biology* **2012**, *19* (1), 99–115. <https://doi.org/10.1016/j.chembiol.2012.01.003>.
- (221) Bianchi, G.; Oliva, L.; Cascio, P.; Pengo, N.; Fontana, F.; Cerruti, F.; Orsi, A.; Pasqualetto, E.; Mezghrani, A.; Calbi, V.; et al. The Proteasome Load versus Capacity Balance Determines Apoptotic Sensitivity of Multiple Myeloma Cells to Proteasome Inhibition. *Blood* **2009**, *113* (13), 3040–3049. <https://doi.org/10.1182/blood-2008-08-172734>.
- (222) Meister, S.; Schubert, U.; Neubert, K.; Herrmann, K.; Burger, R.; Gramatzki, M.; Hahn, S.; Schreiber, S.; Wilhelm, S.; Herrmann, M.; et al. Extensive Immunoglobulin Production Sensitizes Myeloma Cells for Proteasome Inhibition. *Cancer Research* **2007**, *67* (4), 1783–1792. <https://doi.org/10.1158/0008-5472.CAN-06-2258>.
- (223) Suraweera, A.; Münch, C.; Hanssum, A.; Bertolotti, A. Failure of Amino Acid Homeostasis Causes Cell Death Following Proteasome Inhibition. *Molecular Cell* **2012**, *48* (2), 242–253. <https://doi.org/10.1016/j.molcel.2012.08.003>.
- (224) Cenci, S.; Mezghrani, A.; Cascio, P.; Bianchi, G.; Cerruti, F.; Fra, A.; Lelouard, H.; Masciarelli, S.; Mattioli, L.; Oliva, L.; et al. Progressively Impaired Proteasomal Capacity during Terminal Plasma Cell Differentiation. *European Molecular Biology Organization Journal* **2006**, *25* (5), 1104–1113. <https://doi.org/10.1038/sj.emboj.7601009>.
- (225) Kane, R. C.; Bross, P. F.; Farrell, A. T.; Pazdur, R. Velcade: U.S. FDA Approval for the Treatment of Multiple Myeloma Progressing on Prior Therapy. *Oncologist* **2003**, *8* (6), 508–513.
- (226) Kirk, C. J. Discovery and Development of Second-Generation Proteasome Inhibitors. *Seminars in Hematology* **2012**, *49* (3), 207–214. <https://doi.org/10.1053/j.seminhematol.2012.04.007>.
- (227) Kuhn, D. J.; Orlowski, R. Z.; Bjorklund, C. C. Second Generation Proteasome Inhibitors: Carfilzomib and Immunoproteasome-Specific Inhibitors (IPSI). *Curr Cancer Drug Targets* **2011**, *11* (3), 285–295.
- (228) Murray, M. Y.; Auger, M. J.; Bowles, K. M. Overcoming Bortezomib Resistance in Multiple Myeloma. *Biochemical Society Transactions* **2014**, *42* (4), 804–808. <https://doi.org/10.1042/BST20140126>.

- (229) Lü, S.; Wang, J. The Resistance Mechanisms of Proteasome Inhibitor Bortezomib. *Biomark Res* **2013**, *1*, 13. <https://doi.org/10.1186/2050-7771-1-13>.
- (230) Wu, Y.-X.; Yang, J.-H.; Saitsu, H. Bortezomib-Resistance Is Associated with Increased Levels of Proteasome Subunits and Apoptosis-Avoidance. *Oncotarget* **2016**, *7* (47), 77622–77634. <https://doi.org/10.18632/oncotarget.12731>.
- (231) Carozzi, V. A.; Renn, C. L.; Bardini, M.; Fazio, G.; Chiorazzi, A.; Meregalli, C.; Oggioni, N.; Shanks, K.; Quartu, M.; Serra, M. P.; et al. Bortezomib-Induced Painful Peripheral Neuropathy: An Electrophysiological, Behavioral, Morphological and Mechanistic Study in the Mouse. *PLoS One* **2013**, *8* (9). <https://doi.org/10.1371/journal.pone.0072995>.
- (232) Anbanandam, A.; Albarado, D. C.; Tirziu, D. C.; Simons, M.; Veeraraghavan, S. Molecular Basis for Proline- and Arginine-Rich Peptide Inhibition of Proteasome. *Journal of Molecular Biology* **2008**, *384* (1), 219–227. <https://doi.org/10.1016/j.jmb.2008.09.021>.
- (233) Ruschak, A. M.; Slassi, M.; Kay, L. E.; Schimmer, A. D. Novel Proteasome Inhibitors to Overcome Bortezomib Resistance. *Journal of the National Cancer Institute* **2011**, *103* (13), 1007–1017. <https://doi.org/10.1093/jnci/djr160>.
- (234) Lansdell, T. A.; Hurchla, M. A.; Xiang, J.; Hovde, S.; Weilbaecher, K. N.; Henry, R. W.; Tepe, J. J. Noncompetitive Modulation of the Proteasome by Imidazoline Scaffolds Overcomes Bortezomib Resistance and Delays MM Tumor Growth in Vivo. *ACS Chemical Biology* **2013**, *8* (3), 578–587. <https://doi.org/10.1021/cb300568r>.
- (235) Azevedo, L. M.; Lansdell, T. A.; Ludwig, J. R.; Mosey, R. A.; Woloch, D. K.; Cogan, D. P.; Patten, G. P.; Kuszpit, M. R.; Fisk, J. S.; Tepe, J. J. Inhibition of the Human Proteasome by Imidazoline Scaffolds. *Journal of Medicinal Chemistry* **2013**, *56* (14), 5974–5978. <https://doi.org/10.1021/jm400235r>.
- (236) Dahlmann, B.; Becher, B.; Sobek, A.; Ehlers, C.; Kopp, F.; Kuehn, L. In Vitro Activation of the 20S Proteasome. *EPD* **1993**, *47*, 274–284. <https://doi.org/10.1159/000468685>.
- (237) Kahlon, D. K.; Lansdell, T. A.; Fisk, J. S.; Hupp, C. D.; Friebe, T. L.; Hovde, S.; Jones, A. D.; Dyer, R. D.; Henry, R. W.; Tepe, J. J. Nuclear Factor-KappaB Mediated Inhibition of Cytokine Production by Imidazoline Scaffolds. *Journal of Medicinal Chemistry* **2009**, *52* (5), 1302–1309. <https://doi.org/10.1021/jm8013162>.
- (238) Kisselev, A. F.; Goldberg, A. L. Monitoring Activity and Inhibition of 26S Proteasomes with Fluorogenic Peptide Substrates. In *Methods in Enzymology*; Ubiquitin and Protein Degradation, Part A; Academic Press, 2005; Vol. 398, pp 364–378. [https://doi.org/10.1016/S0076-6879\(05\)98030-0](https://doi.org/10.1016/S0076-6879(05)98030-0).
- (239) Kisselev, A. F.; Akopian, T. N.; Castillo, V.; Goldberg, A. L. Proteasome Active Sites Allosterically Regulate Each Other, Suggesting a Cyclical Bite-Chew Mechanism for

- Protein Breakdown. *Molecular Cell* **1999**, 4 (3), 395–402. [https://doi.org/10.1016/S1097-2765\(00\)80341-X](https://doi.org/10.1016/S1097-2765(00)80341-X).
- (240) Bennett, M. C.; Bishop, J. F.; Leng, Y.; Chock, P. B.; Chase, T. N.; Mouradian, M. M. Degradation of  $\alpha$ -Synuclein by Proteasome. *Journal of Biological Chemistry* **1999**, 274 (48), 33855–33858. <https://doi.org/10.1074/jbc.274.48.33855>.
  - (241) Webb, J. L.; Ravikumar, B.; Atkins, J.; Skepper, J. N.; Rubinsztein, D. C.  $\alpha$ -Synuclein Is Degraded by Both Autophagy and the Proteasome. *Journal of Biological Chemistry* **2003**, 278 (27), 25009–25013. <https://doi.org/10.1074/jbc.M300227200>.
  - (242) David, D. C.; Layfield, R.; Serpell, L.; Narain, Y.; Goedert, M.; Spillantini, M. G. Proteasomal Degradation of Tau Protein. *Journal of Neurochemistry* **2002**, 83 (1), 176–185.
  - (243) Grune, T.; Botzen, D.; Engels, M.; Voss, P.; Kaiser, B.; Jung, T.; Grimm, S.; Ermak, G.; Davies, K. J. A. Tau Protein Degradation Is Catalyzed by the ATP/Ubiquitin-Independent 20S Proteasome under Normal Cell Conditions. *Archives of Biochemistry and Biophysics* **2010**, 500 (2), 181–188. <https://doi.org/10.1016/j.abb.2010.05.008>.
  - (244) Gaczynska, M.; Osmulski, P. A. Atomic Force Microscopy of Proteasome Assemblies. *Methods in Molecular Biology* **2011**, 736, 117–132. [https://doi.org/10.1007/978-1-61779-105-5\\_9](https://doi.org/10.1007/978-1-61779-105-5_9).
  - (245) Osmulski, P. A.; Hochstrasser, M.; Gaczynska, M. A Tetrahedral Transition State at the Active Sites of the 20S Proteasome Is Coupled to Opening of the  $\alpha$ -Ring Channel. *Structure* **2009**, 17 (8), 1137–1147. <https://doi.org/10.1016/j.str.2009.06.011>.
  - (246) Trott, O.; Olson, A. J. AutoDock Vina: Improving the Speed and Accuracy of Docking with a New Scoring Function, Efficient Optimization and Multithreading. *Journal of Computational Chemistry* **2010**, 31 (2), 455–461. <https://doi.org/10.1002/jcc.21334>.
  - (247) Dallakyan, S.; Olson, A. J. Small-Molecule Library Screening by Docking with PyRx. *Methods in Molecular Biology* **2015**, 1263, 243–250. [https://doi.org/10.1007/978-1-4939-2269-7\\_19](https://doi.org/10.1007/978-1-4939-2269-7_19).
  - (248) Schweitzer, A.; Aufderheide, A.; Rudack, T.; Beck, F.; Pfeifer, G.; Plitzko, J. M.; Sakata, E.; Schulten, K.; Förster, F.; Baumeister, W. Structure of the Human 26S Proteasome at a Resolution of 3.9 Å. *Proceedings of the National Academy of Sciences of the United States of America* **2016**, 113 (28), 7816–7821. <https://doi.org/10.1073/pnas.1608050113>.
  - (249) Smith, D. M.; Chang, S.-C.; Park, S.; Finley, D.; Cheng, Y.; Goldberg, A. L. Docking of the Proteasomal ATPases' Carboxyl Termini in the 20S Proteasome's  $\alpha$  Ring Opens the Gate for Substrate Entry. *Molecular Cell* **2007**, 27 (5), 731–744. <https://doi.org/10.1016/j.molcel.2007.06.033>.

- (250) Groll, M.; Ditzel, L.; Löwe, J.; Stock, D.; Bochtler, M.; Bartunik, H. D.; Huber, R. Structure of 20S Proteasome from Yeast at 2.4Å Resolution. *Nature* **1997**, 386 (6624), 463–471. <https://doi.org/10.1038/386463a0>.
- (251) Unno, M.; Mizushima, T.; Morimoto, Y.; Tomisugi, Y.; Tanaka, K.; Yasuoka, N.; Tsukihara, T. The Structure of the Mammalian 20S Proteasome at 2.75 Å Resolution. *Structure* **2002**, 10 (5), 609–618. [https://doi.org/10.1016/S0969-2126\(02\)00748-7](https://doi.org/10.1016/S0969-2126(02)00748-7).
- (252) Li, D.; Li, H.; Wang, T.; Pan, H.; Lin, G.; Li, H. Structural Basis for the Assembly and Gate Closure Mechanisms of the Mycobacterium Tuberculosis 20S Proteasome. *European Molecular Biology Organization Journal* **2010**, 29 (12), 2037–2047. <https://doi.org/10.1038/emboj.2010.95>.
- (253) Campbell, K. M.; Terrell, A. R.; Laybourn, P. J.; Lumb, K. J. Intrinsic Structural Disorder of the C-Terminal Activation Domain from the BZIP Transcription Factor Fos. *Biochemistry* **2000**, 39 (10), 2708–2713.
- (254) Adler, J.; Reuven, N.; Kahana, C.; Shaul, Y. C-Fos Proteasomal Degradation Is Activated by a Default Mechanism, and Its Regulation by NAD(P)H:Quinone Oxidoreductase 1 Determines c-Fos Serum Response Kinetics. *Molecular Cell Biology* **2010**, 30 (15), 3767–3778. <https://doi.org/10.1128/MCB.00899-09>.
- (255) Bossis, G.; Ferrara, P.; Acquaviva, C.; Jariel-Encontre, I.; Piechaczyk, M. C-Fos Proto-Oncoprotein Is Degraded by the Proteasome Independently of Its Own Ubiquitylation in Vivo. *Molecular Cell Biology* **2003**, 23 (20), 7425–7436. <https://doi.org/10.1128/mcb.23.20.7425-7436.2003>.
- (256) Eralles, J.; Coffino, P. Ubiquitin-Independent Proteasomal Degradation. *Biochimica et Biophysica Acta (BBA) - Molecular Cell Research* **2014**, 1843 (1), 216–221. <https://doi.org/10.1016/j.bbamcr.2013.05.008>.
- (257) Silvestre, D. C.; Gil, G. A.; Tomasini, N.; Bussolino, D. F.; Caputto, B. L. Growth of Peripheral and Central Nervous System Tumors Is Supported by Cytoplasmic C-Fos in Humans and Mice. *PLoS One* **2010**, 5 (3). <https://doi.org/10.1371/journal.pone.0009544>.
- (258) Motomura, H.; Seki, S.; Shiozawa, S.; Aikawa, Y.; Nogami, M.; Kimura, T. A Selective C-Fos/AP-1 Inhibitor Prevents Cartilage Destruction and Subsequent Osteophyte Formation. *Biochem. Biochemical and Biophysical Research Communications* **2018**, 497 (2), 756–761. <https://doi.org/10.1016/j.bbrc.2018.02.147>.
- (259) Makino, H.; Seki, S.; Yahara, Y.; Shiozawa, S.; Aikawa, Y.; Motomura, H.; Nogami, M.; Watanabe, K.; Sainoh, T.; Ito, H.; et al. A Selective Inhibition of C-Fos/Activator Protein-1 as a Potential Therapeutic Target for Intervertebral Disc Degeneration and Associated Pain. *Scientific Reports* **2017**, 7 (1), 16983. <https://doi.org/10.1038/s41598-017-17289-y>.



- (260) Gregory, M. A.; Hann, S. R. C-Myc Proteolysis by the Ubiquitin-Proteasome Pathway: Stabilization of c-Myc in Burkitt's Lymphoma Cells. *Molecular and Cellular Biology* **2000**, *20* (7), 2423–2435. <https://doi.org/10.1128/MCB.20.7.2423-2435.2000>.
- (261) Wang, X.; Chemmama, I. E.; Yu, C.; Huszagh, A.; Xu, Y.; Viner, R.; Block, S. A.; Cimermanic, P.; Rychnovsky, S. D.; Ye, Y.; et al. The Proteasome-Interacting Ecm29 Protein Disassembles the 26S Proteasome in Response to Oxidative Stress. *Journal of Biological Chemistry* **2017**, *292* (39), 16310–16320. <https://doi.org/10.1074/jbc.M117.803619>.
- (262) Aiken, C. T.; Kaake, R. M.; Wang, X.; Huang, L. Oxidative Stress-Mediated Regulation of Proteasome Complexes. *Molecular Cell Proteomics* **2011**, *10* (5). <https://doi.org/10.1074/mcp.M110.006924>.
- (263) Wang, C.; Wang, X. The Interplay between Autophagy and the Ubiquitin-Proteasome System in Cardiac Proteotoxicity. *Biochimica et Biophysica Acta* **2015**, *1852* (2), 188–194. <https://doi.org/10.1016/j.bbadis.2014.07.028>.
- (264) Avci, D.; Lemberg, M. K. Clipping or Extracting: Two Ways to Membrane Protein Degradation. *Trends in Cell Biology* **2015**, *25* (10), 611–622. <https://doi.org/10.1016/j.tcb.2015.07.003>.
- (265) Neutzner, A.; Youle, R. J.; Karbowski, M. Outer Mitochondrial Membrane Protein Degradation by the Proteasome. *Novartis Foundation Symposium* **2007**, *287*, 4–14; discussion 14–20.
- (266) Tsvetkov, P.; Reuven, N.; Shaul, Y. Ubiquitin-Independent P53 Proteasomal Degradation. *Cell Death Differentiation* **2010**, *17* (1), 103–108. <https://doi.org/10.1038/cdd.2009.67>.
- (267) Dikic, I. Proteasomal and Autophagic Degradation Systems. *Annual Review of Biochemistry* **2017**, *86* (1), 193–224. <https://doi.org/10.1146/annurev-biochem-061516-044908>.
- (268) Glick, D.; Barth, S.; Macleod, K. F. Autophagy: Cellular and Molecular Mechanisms. *Journal of Pathology* **2010**, *221* (1), 3–12. <https://doi.org/10.1002/path.2697>.
- (269) Barth, S.; Glick, D.; Macleod, K. F. Autophagy: Assays and Artifacts. *Journal of Pathology* **2010**, *221* (2), 117–124. <https://doi.org/10.1002/path.2694>.
- (270) Itakura, E.; Kishi-Itakura, C.; Mizushima, N. The Hairpin-Type Tail-Anchored SNARE Syntaxin 17 Targets to Autophagosomes for Fusion with Endosomes/Lysosomes. *Cell* **2012**, *151* (6), 1256–1269. <https://doi.org/10.1016/j.cell.2012.11.001>.
- (271) Kumar, S.; Jain, A.; Farzam, F.; Jia, J.; Gu, Y.; Choi, S. W.; Mudd, M. H.; Claude-Taupin, A.; Wester, M. J.; Lidke, K. A.; et al. Mechanism of Stx17 Recruitment to Autophagosomes via IRGM and Mammalian Atg8 Proteins. *Journal of Cell Biology* **2018**, *217* (3), 997–1013. <https://doi.org/10.1083/jcb.201708039>.

- (272) Minton, K. Membrane Dynamics: How Lysosomes SNARE Autophagosomes. *Nature Reviews Molecular Cell Biology* **2012**, *14*, 65. <https://doi.org/10.1038/nrm3506>.
- (273) Peng, H.; Yang, J.; Li, G.; You, Q.; Han, W.; Li, T.; Gao, D.; Xie, X.; Lee, B.-H.; Du, J.; et al. Ubiquitylation of P62/Sequestosome1 Activates Its Autophagy Receptor Function and Controls Selective Autophagy upon Ubiquitin Stress. *Cell Research* **2017**, *27* (5), 657–674. <https://doi.org/10.1038/cr.2017.40>.
- (274) Zhu, K.; Dunner, K.; McConkey, D. J. Proteasome Inhibitors Activate Autophagy as a Cytoprotective Response in Human Prostate Cancer Cells. *Oncogene* **2010**, *29* (3), 451–462. <https://doi.org/10.1038/onc.2009.343>.
- (275) Lee, A.-H.; Iwakoshi, N. N.; Anderson, K. C.; Glimcher, L. H. Proteasome Inhibitors Disrupt the Unfolded Protein Response in Myeloma Cells. *Proceedings of the National Academy of Sciences of the United States of America* **2003**, *100* (17), 9946–9951. <https://doi.org/10.1073/pnas.1334037100>.
- (276) Vousden, K. H.; Ryan, K. M. P53 and Metabolism. *Nature Reviews Cancer* **2009**, *9* (10), 691–700. <https://doi.org/10.1038/nrc2715>.
- (277) Pandey, U. B.; Nie, Z.; Batlevi, Y.; McCray, B. A.; Ritson, G. P.; Nedelsky, N. B.; Schwartz, S. L.; DiProspero, N. A.; Knight, M. A.; Schuldiner, O.; et al. HDAC6 Rescues Neurodegeneration and Provides an Essential Link between Autophagy and the UPS. *Nature* **2007**, *447* (7146), 859–863. <https://doi.org/10.1038/nature05853>.
- (278) Kim, E.; Park, S.; Lee, J. H.; Mun, J. Y.; Choi, W. H.; Yun, Y.; Lee, J.; Kim, J. H.; Kang, M.-J.; Lee, M. J. Dual Function of USP14 Deubiquitinase in Cellular Proteasomal Activity and Autophagic Flux. *Cell Reports* **2018**, *24* (3), 732–743. <https://doi.org/10.1016/j.celrep.2018.06.058>.
- (279) Xu, D.; Shan, B.; Sun, H.; Xiao, J.; Zhu, K.; Xie, X.; Li, X.; Liang, W.; Lu, X.; Qian, L.; et al. USP14 Regulates Autophagy by Suppressing K63 Ubiquitination of Beclin 1. *Genes Dev* **2016**, *30* (15), 1718–1730. <https://doi.org/10.1101/gad.285122.116>.
- (280) Chakraborty, J.; von Stockum, S.; Marchesan, E.; Caicci, F.; Ferrari, V.; Rakovic, A.; Klein, C.; Antonini, A.; Bubacco, L.; Ziviani, E. USP14 Inhibition Corrects an in Vivo Model of Impaired Mitophagy. *European Molecular Biology Organization Molecular Medicine* **2018**, *10* (11). <https://doi.org/10.15252/emmm.201809014>.
- (281) Gao, Z.; Gammoh, N.; Wong, P.-M.; Erdjument-Bromage, H.; Tempst, P.; Jiang, X. Processing of Autophagic Protein LC3 by the 20S Proteasome. *Autophagy* **2010**, *6* (1), 126–137.
- (282) Kaur, J.; Debnath, J. Autophagy at the Crossroads of Catabolism and Anabolism. *Nature Reviews Molecular Cell Biology* **2015**, *16* (8), 461–472. <https://doi.org/10.1038/nrm4024>.

- (283) Jiang, H.; White, E. J.; Conrad, C.; Gomez-Manzano, C.; Fueyo, J. Autophagy Pathways in Glioblastoma. *Methods in Enzymology* **2009**, *453*, 273–286. [https://doi.org/10.1016/S0076-6879\(08\)04013-5](https://doi.org/10.1016/S0076-6879(08)04013-5).
- (284) Klionsky, D. J.; Abdelmohsen, K.; Abe, A.; Abedin, M. J.; Abeliovich, H.; Acevedo Arozena, A.; Adachi, H.; Adams, C. M.; Adams, P. D.; Adeli, K.; et al. Guidelines for the Use and Interpretation of Assays for Monitoring Autophagy (3rd Edition). *Autophagy* **2016**, *12* (1), 1–222. <https://doi.org/10.1080/15548627.2015.1100356>.
- (285) Mizushima, N.; Yoshimori, T.; Levine, B. Methods in Mammalian Autophagy Research. *Cell* **2010**, *140* (3), 313–326. <https://doi.org/10.1016/j.cell.2010.01.028>.
- (286) Mauvezin, C.; Nagy, P.; Juhász, G.; Neufeld, T. P. Autophagosome-Lysosome Fusion Is Independent of V-ATPase-Mediated Acidification. *Nature Communication* **2015**, *6*, 7007. <https://doi.org/10.1038/ncomms8007>.
- (287) Zhao, J.; Zhai, B.; Gygi, S. P.; Goldberg, A. L. MTOR Inhibition Activates Overall Protein Degradation by the Ubiquitin Proteasome System as Well as by Autophagy. *Proceedings of the National Academy of Sciences of the United States of America* **2015**, *112* (52), 15790–15797. <https://doi.org/10.1073/pnas.1521919112>.
- (288) Bjørkøy, G.; Lamark, T.; Pankiv, S.; Øvervatn, A.; Brech, A.; Johansen, T. Monitoring Autophagic Degradation of P62/SQSTM1. *Methods in Enzymology* **2009**, *452*, 181–197. [https://doi.org/10.1016/S0076-6879\(08\)03612-4](https://doi.org/10.1016/S0076-6879(08)03612-4).
- (289) Homewood, C. A.; Warhurst, D. C.; Peters, W.; Baggaley, V. C. Lysosomes, PH and the Anti-Malarial Action of Chloroquine. *Nature* **1972**, *235* (5332), 50–52.
- (290) Fu, R.; Deng, Q.; Zhang, H.; Hu, X.; Li, Y.; Liu, Y.; Hu, J.; Luo, Q.; Zhang, Y.; Jiang, X.; et al. A Novel Autophagy Inhibitor Berbamine Blocks SNARE-Mediated Autophagosome-Lysosome Fusion through Upregulation of BNIP3. *Cell Death Disease* **2018**, *9* (2), 243. <https://doi.org/10.1038/s41419-018-0276-8>.
- (291) Yang, Y.; Li, C.-C. H.; Weissman, A. M. Regulating the P53 System through Ubiquitination. *Oncogene* **2004**, *23* (11), 2096–2106. <https://doi.org/10.1038/sj.onc.1207411>.
- (292) Winkler, L. L.; Hwang, J.; Kalejta, R. F. Ubiquitin-Independent Proteasomal Degradation of Tumor Suppressors by Human Cytomegalovirus Pp71 Requires the 19S Regulatory Particle. *Journal of Virology* **2013**, *87* (8), 4665–4671. <https://doi.org/10.1128/JVI.03301-12>.
- (293) Jiang, P.; Nishimura, T.; Sakamaki, Y.; Itakura, E.; Hatta, T.; Natsume, T.; Mizushima, N. The HOPS Complex Mediates Autophagosome-Lysosome Fusion through Interaction with Syntaxin 17. *Molecular Biology of the Cell* **2014**, *25* (8), 1327–1337. <https://doi.org/10.1091/mbc.E13-08-0447>.

- (294) Beaudet, L.; Rodriguez-Suarez, R.; Venne, M.-H.; Caron, M.; Bédard, J.; Brechler, V.; Parent, S.; Bielefeld-Sévigny, M. AlphaLISA Immunoassays: The No-Wash Alternative to ELISAs for Research and Drug Discovery. *Nature Methods* **2008**, *5*, A10–A11. <https://doi.org/10.1038/nmeth.f.230>.
- (295) Feinberg, A. P.; Snyder, S. H. Phenothiazine Drugs: Structure-Activity Relationships Explained by a Conformation That Mimics Dopamine. *Proceedings of the National Academy of Sciences of the United States of America* **1975**, *72* (5), 1899–1903.
- (296) Horn, A. S.; Snyder, S. H. Chlorpromazine and Dopamine: Conformational Similarities That Correlate with the Antischizophrenic Activity of Phenothiazine Drugs. *Proceedings of the National Academy of Sciences of the United States of America* **1971**, *68* (10), 2325–2328. <https://doi.org/10.1073/pnas.68.10.2325>.
- (297) Zhao, H.; Zhao, J.; Hou, J.; Wang, S.; Ding, Y.; Lu, B.; Wang, J. AlphaLISA Detection of Alpha-Synuclein in the Cerebrospinal Fluid and Its Potential Application in Parkinson's Disease Diagnosis. *Protein Cell* **2017**, *8* (9), 696–700. <https://doi.org/10.1007/s13238-017-0424-4>.
- (298) AlphaLISA h a-synuclein kit,100pts-AL321HV|PerkinElmer [//www.perkinelmer.com/product/alphalisa-h-a-synuclein-kit-100pts-al321hv](http://www.perkinelmer.com/product/alphalisa-h-a-synuclein-kit-100pts-al321hv) (accessed Jun 20, 2019).
- (299) Schluger, N. W. The Pathogenesis of Tuberculosis. *American Journal of Respiratory Cell and Molecular Biology* **2005**, *32* (4), 251–256. <https://doi.org/10.1165/rcmb.F293>.
- (300) Smith, I. Mycobacterium Tuberculosis Pathogenesis and Molecular Determinants of Virulence. *Clinical Microbiology Reviews* **2003**, *16* (3), 463–496. <https://doi.org/10.1128/CMR.16.3.463-496.2003>.
- (301) Houben, R. M. G. J.; Dodd, P. J. The Global Burden of Latent Tuberculosis Infection: A Re-Estimation Using Mathematical Modelling. *PLoS Medicine* **2016**, *13* (10), e1002152. <https://doi.org/10.1371/journal.pmed.1002152>.
- (302) WHO | Global tuberculosis report 2018 [http://www.who.int/tb/publications/global\\_report/en/](http://www.who.int/tb/publications/global_report/en/) (accessed May 30, 2019).
- (303) Flynn, J. L.; Goldstein, M. M.; Chan, J.; Triebold, K. J.; Pfeffer, K.; Lowenstein, C. J.; Schreiber, R.; Mak, T. W.; Bloom, B. R. Tumor Necrosis Factor-Alpha Is Required in the Protective Immune Response against Mycobacterium Tuberculosis in Mice. *Immunity* **1995**, *2* (6), 561–572.
- (304) Yang, C.-S.; Yuk, J.-M.; Jo, E.-K. The Role of Nitric Oxide in Mycobacterial Infections. *Immune Network* **2009**, *9* (2), 46–52. <https://doi.org/10.4110/in.2009.9.2.46>.
- (305) Balcewicz-Sablinska, M. K.; Keane, J.; Kornfeld, H.; Remold, H. G. Pathogenic Mycobacterium Tuberculosis Evades Apoptosis of Host Macrophages by Release of

- TNF-R2, Resulting in Inactivation of TNF- $\alpha$ . *The Journal of Immunology* **1998**, 161 (5), 2636–2641.
- (306) Keane, J.; Balcewicz-Sablinska, M. K.; Remold, H. G.; Chupp, G. L.; Meek, B. B.; Fenton, M. J.; Kornfeld, H. Infection by Mycobacterium Tuberculosis Promotes Human Alveolar Macrophage Apoptosis. *Infection and Immunity* **1997**, 65 (1), 298–304.
  - (307) Rojas, M.; Barrera, L. F.; Puzo, G.; Garcia, L. F. Differential Induction of Apoptosis by Virulent Mycobacterium Tuberculosis in Resistant and Susceptible Murine Macrophages: Role of Nitric Oxide and Mycobacterial Products. *The Journal of Immunology* **1997**, 159 (3), 1352–1361.
  - (308) Treatment | TB | CDC <https://www.cdc.gov/tb/topic/treatment/default.htm> (accessed May 30, 2019).
  - (309) WHO | Guidelines for treatment of tuberculosis <https://www.who.int/tb/publications/2010/9789241547833/en/> (accessed May 30, 2019).
  - (310) Drug-Resistant TB | TB | CDC <https://www.cdc.gov/tb/topic/drtb/default.htm> (accessed May 30, 2019).
  - (311) Phagosome-Lysosome Interactions in Cultured Macrophages Infected with Virulent Tubercle Bacilli. Reversal of the Usual Nonfusion Pattern and Observations on Bacterial Survival. *Journal of Experimental Medicine* **1975**, 142 (1), 1–16.
  - (312) Silva Miranda, M.; Breiman, A.; Allain, S.; Deknuydt, F.; Altare, F. The Tuberculous Granuloma: An Unsuccessful Host Defence Mechanism Providing a Safety Shelter for the Bacteria? *Clinical and Developmental Immunology* **2012**, 2012. <https://doi.org/10.1155/2012/139127>.
  - (313) Warsinske, H. C.; DiFazio, R. M.; Linderman, J. J.; Flynn, J. L.; Kirschner, D. E. Identifying Mechanisms Driving Formation of Granuloma-Associated Fibrosis during Mycobacterium Tuberculosis Infection. *Journal of Theoretical Biology* **2017**, 429, 1–17. <https://doi.org/10.1016/j.jtbi.2017.06.017>.
  - (314) Elkington, P. T.; Ugarte-Gil, C. A.; Friedland, J. S. Matrix Metalloproteinases in Tuberculosis. *European Respiratory Journal* **2011**, 38 (2), 456–464. <https://doi.org/10.1183/09031936.00015411>.
  - (315) Xu, Y.; Wang, L.; Zimmerman, M. D.; Chen, K.-Y.; Huang, L.; Fu, D.-J.; Kaya, F.; Rakhilin, N.; Nazarova, E. V.; Bu, P.; et al. Matrix Metalloproteinase Inhibitors Enhance the Efficacy of Frontline Drugs against Mycobacterium Tuberculosis. *PLOS Pathogens* **2018**, 14 (4), e1006974. <https://doi.org/10.1371/journal.ppat.1006974>.
  - (316) Chan, J.; Tanaka, K.; Carroll, D.; Flynn, J.; Bloom, B. R. Effects of Nitric Oxide Synthase Inhibitors on Murine Infection with Mycobacterium Tuberculosis. *Infection and Immunity* **1995**, 63 (2), 736–740.

- (317) Darwin, K. H.; Ehrt, S.; Gutierrez-Ramos, J.-C.; Weich, N.; Nathan, C. F. The Proteasome of Mycobacterium Tuberculosis Is Required for Resistance to Nitric Oxide. *Science* **2003**, *302* (5652), 1963–1966. <https://doi.org/10.1126/science.1091176>.
- (318) Rhee, K. Y.; Erdjument-Bromage, H.; Tempst, P.; Nathan, C. F. S-Nitroso Proteome of Mycobacterium Tuberculosis: Enzymes of Intermediary Metabolism and Antioxidant Defense. *Proceedings of the National Academy of Sciences of the United States of America* **2005**, *102* (2), 467–472. <https://doi.org/10.1073/pnas.0406133102>.
- (319) Sassetti, C. M.; Boyd, D. H.; Rubin, E. J. Genes Required for Mycobacterial Growth Defined by High Density Mutagenesis. *Mol. Microbiol.* **2003**, *48* (1), 77–84.
- (320) Gandotra, S.; Schnappinger, D.; Monteleone, M.; Hillen, W.; Ehrt, S. *In Vivo* Gene Silencing Identifies the Mycobacterium Tuberculosis Proteasome as Essential for the Bacteria to Persist in Mice. *Nature Medicine* **2007**, *13* (12), 1515–1520. <https://doi.org/10.1038/nm1683>.
- (321) Lamichhane, G.; Raghunand, T. R.; Morrison, N. E.; Woolwine, S. C.; Tyagi, S.; Kandavelou, K.; Bishai, W. R. Deletion of a Mycobacterium Tuberculosis Proteasomal ATPase Homologue Gene Produces a Slow-Growing Strain That Persists in Host Tissues. *The Journal of Infectious Diseases* **2006**, *194* (9), 1233–1240. <https://doi.org/10.1086/508288>.
- (322) Samanovic, M. I.; Li, H.; Darwin, K. H. The Pup-Proteasome System of Mycobacterium Tuberculosis. In *Regulated Proteolysis in Microorganisms*; Dougan, D. A., Ed.; Subcellular Biochemistry; Springer Netherlands: Dordrecht, 2013; pp 267–295. [https://doi.org/10.1007/978-94-007-5940-4\\_10](https://doi.org/10.1007/978-94-007-5940-4_10).
- (323) Hu, G.; Lin, G.; Wang, M.; Dick, L.; Xu, R.-M.; Nathan, C.; Li, H. Structure of the Mycobacterium Tuberculosis Proteasome and Mechanism of Inhibition by a Peptidyl Boronate. *Molecular Microbiology* **2006**, *59* (5), 1417–1428. <https://doi.org/10.1111/j.1365-2958.2005.05036.x>.
- (324) Bode, N. J.; Darwin, K. H. The Pup-Proteasome System of Mycobacteria. *Microbiology Spectrum* **2014**, *2* (5). <https://doi.org/10.1128/microbiolspec.MGM2-0008-2013>.
- (325) Darwin, K. H.; Lin, G.; Chen, Z.; Li, H.; Nathan, C. F. Characterization of a Mycobacterium Tuberculosis Proteasomal ATPase Homologue. *Molecular Microbiology* **2005**, *55* (2), 561–571. <https://doi.org/10.1111/j.1365-2958.2004.04403.x>.
- (326) Delley, C. L.; Striebel, F.; Heydenreich, F. M.; Özcelik, D.; Weber-Ban, E. Activity of the Mycobacterial Proteasomal ATPase Mpa Is Reversibly Regulated by Pupylation. *Journal of Biological Chemistry* **2012**, *287* (11), 7907–7914. <https://doi.org/10.1074/jbc.M111.331124>.
- (327) Burns, K. E.; Darwin, K. H. Pupylation: A Signal for Proteasomal Degradation in Mycobacterium Tuberculosis. *Subcellular Biochemistry* **2010**, *54*, 149–157. [https://doi.org/10.1007/978-1-4419-6676-6\\_12](https://doi.org/10.1007/978-1-4419-6676-6_12).

- (328) Lin, G.; Li, D.; Chidawanyika, T.; Nathan, C.; Li, H. Fellutamide B Is a Potent Inhibitor of the Mycobacterium Tuberculosis Proteasome. *Archives of Biochemistry and Biophysics* **2010**, *501* (2), 214–220. <https://doi.org/10.1016/j.abb.2010.06.009>.
- (329) Mehra, R.; Chib, R.; Munagala, G.; Yempalla, K. R.; Khan, I. A.; Singh, P. P.; Khan, F. G.; Nargotra, A. Discovery of New Mycobacterium Tuberculosis Proteasome Inhibitors Using a Knowledge-Based Computational Screening Approach. *Molecular Diversity* **2015**, *19* (4), 1003–1019. <https://doi.org/10.1007/s11030-015-9624-0>.
- (330) Totaro, K. A.; Barthelme, D.; Simpson, P. T.; Jiang, X.; Lin, G.; Nathan, C. F.; Sauer, R. T.; Sello, J. K. Rational Design of Selective and Bioactive Inhibitors of the Mycobacterium Tuberculosis Proteasome. *ACS Infectious Disease* **2017**, *3* (2), 176–181. <https://doi.org/10.1021/acsinfecdis.6b00172>.
- (331) Qi, L. S.; Larson, M. H.; Gilbert, L. A.; Doudna, J. A.; Weissman, J. S.; Arkin, A. P.; Lim, W. A. Repurposing CRISPR as an RNA-Guided Platform for Sequence-Specific Control of Gene Expression. *Cell* **2013**, *152* (5), 1173–1183. <https://doi.org/10.1016/j.cell.2013.02.022>.
- (332) Gasiunas, G.; Barrangou, R.; Horvath, P.; Siksnys, V. Cas9-CrRNA Ribonucleoprotein Complex Mediates Specific DNA Cleavage for Adaptive Immunity in Bacteria. *Proceedings of the National Academy of Sciences of the United States of America* **2012**, *109* (39), E2579–2586. <https://doi.org/10.1073/pnas.1208507109>.
- (333) Horvath, P.; Romero, D. A.; Coûté-Monvoisin, A.-C.; Richards, M.; Deveau, H.; Moineau, S.; Boyaval, P.; Fremaux, C.; Barrangou, R. Diversity, Activity, and Evolution of CRISPR Loci in *Streptococcus Thermophilus*. *Journal of Bacteriology* **2008**, *190* (4), 1401–1412. <https://doi.org/10.1128/JB.01415-07>.
- (334) Wright, A. V.; Nuñez, J. K.; Doudna, J. A. Biology and Applications of CRISPR Systems: Harnessing Nature’s Toolbox for Genome Engineering. *Cell* **2016**, *164* (1–2), 29–44. <https://doi.org/10.1016/j.cell.2015.12.035>.
- (335) Jinek, M.; Chylinski, K.; Fonfara, I.; Hauer, M.; Doudna, J. A.; Charpentier, E. A Programmable Dual-RNA-Guided DNA Endonuclease in Adaptive Bacterial Immunity. *Science* **2012**, *337* (6096), 816–821. <https://doi.org/10.1126/science.1225829>.
- (336) Singh, A. K.; Carette, X.; Potluri, L.-P.; Sharp, J. D.; Xu, R.; Prsic, S.; Husson, R. N. Investigating Essential Gene Function in Mycobacterium Tuberculosis Using an Efficient CRISPR Interference System. *Nucleic Acids Research* **2016**, *44* (18), e143. <https://doi.org/10.1093/nar/gkw625>.
- (337) Rock, J. M.; Hopkins, F. F.; Chavez, A.; Diallo, M.; Chase, M. R.; Gerrick, E. R.; Pritchard, J. R.; Church, G. M.; Rubin, E. J.; Sassetti, C. M.; et al. Programmable Transcriptional Repression in Mycobacteria Using an Orthogonal CRISPR Interference Platform. *Nature Microbiology* **2017**, *2*, 16274. <https://doi.org/10.1038/nmicrobiol.2016.274>.

- (338) Wang, T.; Li, H.; Lin, G.; Tang, C.; Li, D.; Nathan, C.; Darwin, K. H.; Li, H. Structural Insights on the Mycobacterium Tuberculosis Proteasomal ATPase Mpa. *Structure* **2009**, *17* (10), 1377–1385. <https://doi.org/10.1016/j.str.2009.08.010>.
- (339) Knipfer, N.; Shrader, T. E. Inactivation of the 20S Proteasome in Mycobacterium Smegmatis. *Molecular Microbiology* **1997**, *25* (2), 375–383.
- (340) Deretic, V. Autophagy in Tuberculosis. *Cold Spring Harbor Perspective in Medicine* **2014**, *4* (11). <https://doi.org/10.1101/cshperspect.a018481>.
- (341) Bradfute, S. B.; Castillo, E. F.; Arko-Mensah, J.; Chauhan, S.; Jiang, S.; Mandell, M.; Deretic, V. Autophagy as an Immune Effector against Tuberculosis. *Current Opinion in Microbiology* **2013**, *16* (3), 355–365. <https://doi.org/10.1016/j.mib.2013.05.003>.
- (342) Romagnoli, A.; Petruccioli, E.; Palucci, I.; Camassa, S.; Carata, E.; Petrone, L.; Mariano, S.; Sali, M.; Dini, L.; Girardi, E.; et al. Clinical Isolates of the Modern Mycobacterium Tuberculosis Lineage 4 Evade Host Defense in Human Macrophages through Eluding IL-1 $\beta$ -Induced Autophagy. *Cell Death & Disease* **2018**, *9* (6), 624. <https://doi.org/10.1038/s41419-018-0640-8>.
- (343) Andersson, A.-M.; Andersson, B.; Lorell, C.; Raffetseder, J.; Larsson, M.; Blomgran, R. Autophagy Induction Targeting MTORC1 Enhances *Mycobacterium Tuberculosis* Replication in HIV Co-Infected Human Macrophages. *Scientific Reports* **2016**, *6*, 28171. <https://doi.org/10.1038/srep28171>.
- (344) Esseltine, D.-L.; Mulligan, G. An Historic Perspective of Proteasome Inhibition. *Seminar in Hematology* **2012**, *49* (3), 196–206. <https://doi.org/10.1053/j.seminhematol.2012.04.009>.
- (345) Marfella, R.; D'Amico, M.; Esposito, K.; Baldi, A.; Filippo, C. D.; Siniscalchi, M.; Sasso, F. C.; Portoghese, M.; Cirillo, F.; Cacciapuoti, F.; et al. The Ubiquitin-Proteasome System and Inflammatory Activity in Diabetic Atherosclerotic Plaques: Effects of Rosiglitazone Treatment. *Diabetes* **2006**, *55* (3), 622–632. <https://doi.org/10.2337/diabetes.55.03.06.db05-0832>.
- (346) Crunkhorn, S. Antimalarials: Novel Proteasome Inhibitor Combats Malaria. *Nature Reviews Drug Discovery* **2016**, *15*, 232–233. <https://doi.org/10.1038/nrd.2016.58>.
- (347) Jackson, W. T.; Giddings, T. H.; Taylor, M. P.; Mulinyawe, S.; Rabinovitch, M.; Kopito, R. R.; Kirkegaard, K. Subversion of Cellular Autophagosomal Machinery by RNA Viruses. *PLoS Biology* **2005**, *3* (5), e156. <https://doi.org/10.1371/journal.pbio.0030156>.